RUSSIAN ACADEMY OF SCIENCE

FEDERAL AGENCY ON EDUCATION OF RUSSIAN FEDERATION

RUSSIAN NATIONAL COMMISSION FOR UNESCO

COMMITTEE ON SCIENCE AND HIGHER EDUCATION
OF THE GOVERNMENT OF SAINT PETERSBURG

COUNCIL OF RECTORS OF SAINT PETERSBURG HIGHER EDUCATION ESTABLISHMENTS

SAINT PETERSBURG STATE UNIVERSITY OF AEROSPACE INSTRUMENTATION (SUAI)

UNESCO CHAIR "DISTANCE EDUCATION IN ENGINEERING" OF SUAI

RUSSIAN SECTION OF THE INTERNATIONAL SOCIETY OF AUTOMATION

ИЗВЕСТИЯ КАФЕДРЫ UNESCO ГУАП «ДИСТАНЦИОННОЕ ИНЖЕНЕРНОЕ ОБРАЗОВАНИЕ»

Сборник статей

Выпуск 8

BULLETIN OF THE UNESCO DEPARTMENT "DISTANCE EDUCATION IN ENGINEERING" OF THE SUAI

Collection of the papers

Issue 8

РОССИЯ, САНКТ-ПЕТЕРБУРГ 2023 SAINT PETERSBURG, RUSSIA

ББК 378.1
УДК 74.58
И33

И33 Известия кафедры UNESCO ГУАП «Дистанционное инженерное образование» = Bulletin of the UNESCO department “Distance education in engineering” of the SUAI: Collection of the papers. St. Petersburg, Issue 8. – SPb.: SUAI, 2023. – 216 p.
ISBN 978-5-8088-1825-5

ISA District 12 (The International Society of Automation) and SUAI (Sain Petersburg State University of Aerospace Instrumentation) have organized the Nineteenth ISA European student pa-per competition (ESPC-2023). Papers of professors and the best students were includ-ed into this issue of the Bulletin of the UNESCO department “Distance education in engineer-ing” of the SUAI. Papers can be interesting for students, post-graduate students, professors and specialists.

ISBN 978-5-8088-1825-5

International Society of Automation
Setting the Standard for Automation™

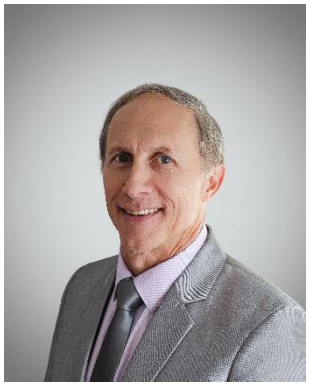

On behalf of ISA, it is my pleasure to congratulate the ISA Russia Section and the St. Petersburg State University of Aerospace Instrumentation (SUAI) on successfully completing the 2023 XIX ISA European Student Paper Competition (ESPC-2023).

I commend the students from around the world who contributed their time, knowledge, and expertise to prepare a paper. We are proud that they selected our publication. I want to acknowledge the review committee, including ISA Europe, Middle East and Africa Districts student volunteers.

Students of today are the engineers of tomorrow. Our profession sees students as future members of our profession and appreciates their interest in automation. Our society welcomes their future contributions in helping us achieve our vision of "creating a better world through automation", and our mission of "Empowering the global automation community through standards and knowledge sharing". The educators that help these students prepare for their future roles should also be commended.

Whichever career path these students choose, we hope ISA will continue to play an important role in their continuing education and professional development.

I extend my best wishes to all students and attendees in the 2023 XIX ISA European Student Paper Competition

Respectfully,

Marty Bince
2023 ISA Society President

3252 S. Miami Blvd. #102, Durham, NC 27703
PHONE: +1 919-549-8411 • FAX: +1 919-549-8288 • EMAIL: info@isa.org • www.isa.org

Setting the Standard for Automation™

I would like to extend congratulations to the ISA Russia Section, ISA District 12, and The Saint Petersburg State University of Aerospace Instrumentation (SUAI) for successfully organizing the Nineteenth ISA International Student Paper Competition.

As an educator and a member of ISA for over 50 years, I never tire of the opportunity to share with students the amazing challenges and personal rewards that a career in automation can bring. ISA is proud to have the opportunity to nurture the next generation of automation professionals.

We look forward to continuing the close relationship we have established between ISA, the Russia Section, District 12, and the SUAI. Through distance learning classes on project management and ongoing international online forums, we are developing new understandings in the technical, cultural, and personal arenas.

Congratulations to those who developed papers for this volume and to the advisory committee who had the difficult task of making paper selections.

Sincerely,

Gerald W. Cockrell

Gerald W. Cockrell
ISA Former President

Standards
Certification
Education & Training
Publishing
Conferences & Exhibits

ISA
67 Alexander Drive
P.O. Box 12277
Research Triangle Park, NC 27709
PHONE (919) 549-8411
FAX (919) 549-8288
E-MAIL info@isa.org
www.isa.org

DEVELOPMENT OF AN AUTOMATIC PORTABLE DIGITAL HEART MONITOR DESIGNED TO DETECT AND CLASSIFY ARRHYTHMIA

Akopyan Bella
Saint Petersburg State University of Aerospace Instrumentation, Saint Petersburg, Russia
E-mail: akopyan.bella@yandex.ru

Abstract. *The object of the study is a portable digital heart monitor, the subject of the study is the stages of development of this type of device. The article defines the requirements for the device. The developed block diagram of the device is presented, the selected element base is presented and described, as well as the connection diagram of the device. In the course of the study, a hardware implementation of the device was developed and the algorithms for detecting and classifying arrhythmias based on digital filtering methods used in the firmware were presented.*
Keywords: *heart monitor, microprocessor, electrocardiogram, electrocardiosignal, arrhythmia detection, detection algorithm, digital signal processing.*

Introduction

Modern electrocardiography is characterized by the widespread use of digital electrocardiographs and heart monitors with built-in algorithms for automatic processing, analysis and interpretation of electrocardiograms (ECG). In particular, such cardiac monitors are widely used for diagnosing cardiac arrhythmias.

The monitor must meet the following basic requirements:

– detect especially dangerous heart rhythm disturbances (arrhythmias) with high reliability;

– to carry out self-control from the moment of switching on during the entire period of operation of the device without interruption in the processing of the ECG;

– amplify and stabilize the ECG-, which will allow the device to immediately start working after switching on;

– perform signal processing in order to reduce the effect of interference on diagnostic results.

Thus, electronic heart monitors cover a large number of electrical circuits that perform the functions of amplifying and pre-processing the signal, analyzing it in the time or frequency domains in real time, accumulating analysis data and making a decision about an alarm, timely displaying and documenting the results of work, automating the control process. device and self-diagnosis of faults.

The task of creating a digital heart monitor is divided into two stages: the development of its hardware implementation and the development of the program operation algorithm. The main task of the software of a portable heart monitor is the current control of the subject's cardiac activity, that is, the measurement of heart rate and automatic recognition of the most pronounced cardiac arrhythmias [1].

Development of hardware implementation

Based on the requirements for the device, a block diagram of the cardiac monitor was developed, shown in Fig. 1, consisting of a control device and four blocks:

– amplification and transformation;

– information display;

– alarm notifications;

– data documentation.

Principle of operation of the device: ECG from the electrodes is fed to the input of the signal amplification and conversion unit, which performs its preliminary processing. This block limits the frequency spectrum of the input signal to improve noise immunity and samples it. It is worth noting that in some cases, the ADC can be built into the control device – in particular, if the microprocessor platform includes it.The choice of the ADC bit depth in the amplification and conversion unit is determined by the need for relatively accurate measurement of parameters and the provision of a margin over the dynamic range of the ADC to prevent information loss when exposed to interference. Acceptable ADC bit depth for both tasks is from 10 bits [2]. ADCs of this capacity are widely found in various microprocessor and microcontroller platforms.

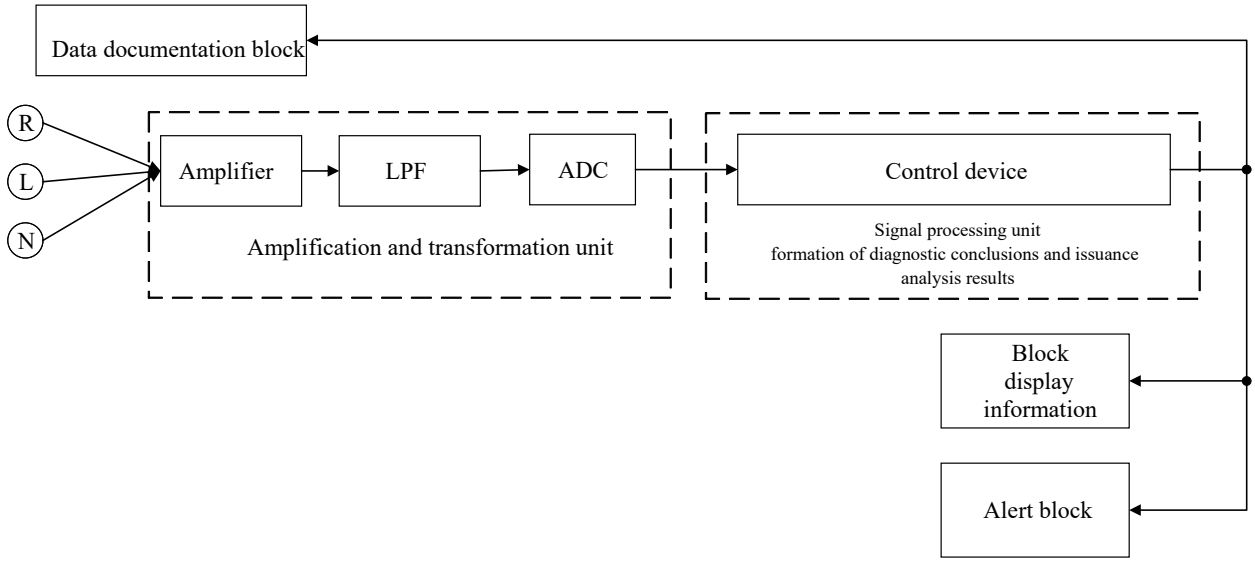

Fig. 1 – Structural diagram of a digital cardiac monitor

Reinforced and converted ECG enters the control device, the main functions of which are the digital processing of the ECG, the analysis of the processing data, the decision on the alarm and the control of the device as a whole. In accordance with the processing methods underlying the device, QRS complexes are detected and RR intervals are determined, as well as a check for heart rhythm disturbances. The received information is recorded and stored in the data documentation block. Based on these data, according to the algorithms for highlighting rhythm disturbances, appropriate diagnostic conclusions are formed and alarm alerts are generated. If it is necessary to display the received information, diagnostic conclusions about the nature of the rhythm disturbance and the ECG itself are displayed in the corresponding block.

To implement the control device, it was decided to turn to universal microprocessors. During the development, it was decided to pay attention to 32-bit MCUs, which can provide not only superior performance, but also reduce power consumption, reduce program size, and speed up software development. A high-performance 32-bit STM32F407 microcontroller with a floating point DSP function was chosen. The built-in 12-bit ADC with the possibility of using a smaller data width and the presence of a large number of timers greatly simplify the development of the device.

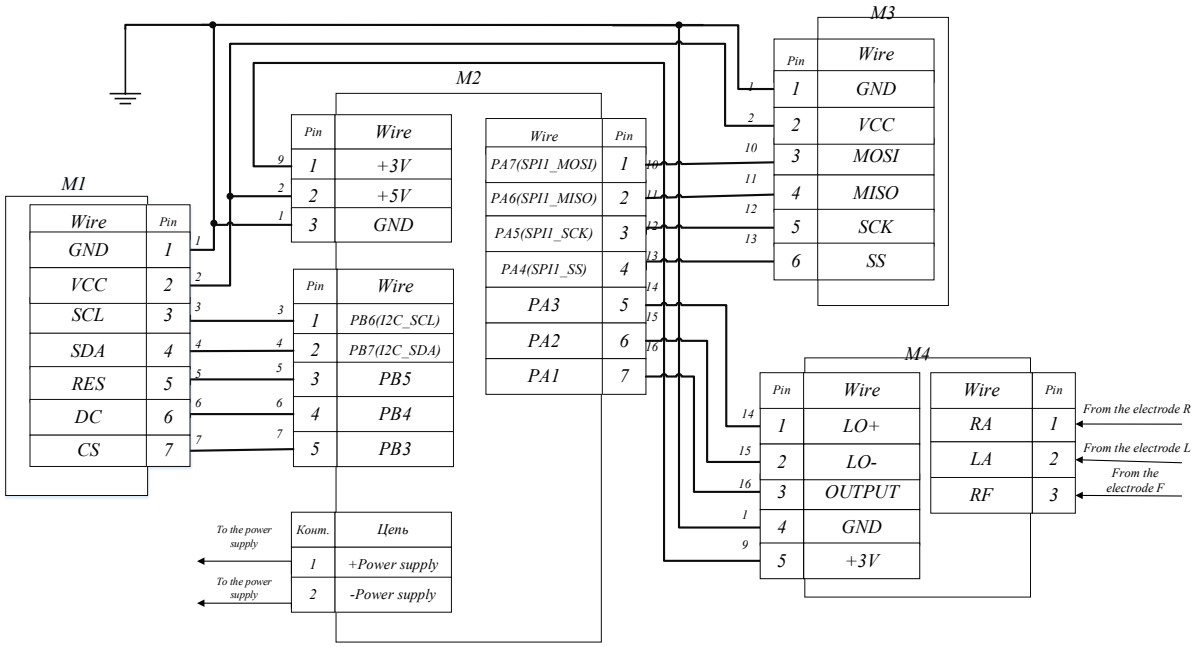

M1 – module based on OLED display, M2 – STM32F407, M3 – SD card module, M4 – AD8232 amplifier module

Fig. 2 – Connection diagram of a portable cardiac monitor

The AD8232 module [3] from Analog Devices was chosen as the amplifying unit. This module is designed to measure the electrical activity of the heart and performs the acquisition, amplification and preliminary filtering of weak ECG in conditions of strong interference.

Since during the operation of the device it becomes necessary to display the received ECG and diagnostic conclusions about the nature of the rhythm disturbance, it is advisable to use an OLED display for indication, which allows you to display not only messages, but also images.

In addition, the developed device allows you to send an alarm notification, which provides not only the display of a message about a possible violation of the rhythm, but also an audible notification (alarm) through the speaker.

An external memory (SD card) is used as the basis for the data documentation unit in order to record an electrocardiogram for the purpose of its subsequent more detailed analysis on stationary computers. In order to simplify the development of the device, it is advisable to use ready-made modules for SD memory cards connected via the SPI or SD interface as a data documentation unit. The advantage of such modules is also that there are ready-made libraries for them that need only minor changes.

Based on the block diagram, after selecting the element base, the device connection diagram was built, shown in Fig. 2.

The final efficiency of the device will also depend on a well-designed program algorithm [4].

Real-time data processing algorithm

Methods for analyzing heart rhythm disturbances are in many ways similar to methods for assessing variability [5]. But for reliable diagnosis of ECG by the methods of variability, one has to resort to long-term signal recording and delayed analysis of previously recorded ECG fragments, while the duration of arrhythmia diagnosis should not exceed several tens of seconds [5]. In this regard, there is a need for real-time arrhythmia detection algorithms.

The algorithm should also be insensitive to low noise levels in order to avoid false alarms in real conditions, and a short period of preliminary tuning of the algorithm, its adaptation to specific conditions, is allowed. [6].

The generalized principle of operation of algorithms for detecting arrhythmias by the ECG signal is shown in Fig. 3. After receiving and primary processing of the received signal, it is necessary to establish the presence of a cardiocycle in the analyzed area, after which it is required to determine whether the rhythm is normal or there is a pathology.

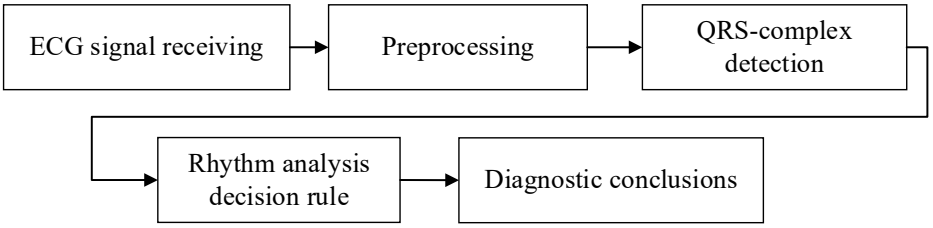

Fig. 3 – Generalized principle of operation of arrhythmia detection algorithms

1) Preprocessing of the received electrocardiosignal

The algorithm [6] based on digital filtering [7] was chosen as the electrocardiogram signal preprocessing algorithm, since it has the following advantages:

– work in real time,

– successfully cope with ECG processing under conditions of various additive interference signals [6].

First, the ECG signal is passed through a differentiating device (DU) with a cutoff frequency of 62.5 Hz, the mathematical model of which is described by the formula:

$$Y0_n = X_n - X_{n-4},\ n = 4,5\ldots N-1, \quad (1)$$

where $Y0$ is the signal at the output of the differentiator, X is the initial ECG, N is the sample size. The differentiating device neutralizes the change in signal level. The received data is then passed through a digital non-recursive LPF, the mathematical model of which is described by formula (2):

$$Y1_n = Y0_n + 4Y0_{n-1} + 6Y0_{n-2} + 4Y0_{n-3} + Y0_{n-4},\ n = 4,5\ldots N-1, \quad (2)$$

where *Y*1 is the signal at the LPF output. The received signal at the output of the digital low-pass filter is passed through a two-threshold comparison circuit: the threshold values C are equal in magnitude, but opposite in sign.

2) QRS-complex detection

A two-threshold comparison system was chosen as an algorithm for detecting QRS complexes. The signal at the output of the low-pass filter is scanned until a sample is detected, the amplitude of which exceeds the positive threshold. This sample is the beginning of the search area with a duration of 40 samples. If no other threshold crossings occur within 40 subsequent samples, then it is considered that the threshold exceeding was provoked by contour drift. Otherwise, conditions (3) are checked in turn:

$$\begin{gathered} Y1_{n+j} < -C,\ Y1_{n+k} > C \\ 0 < j < 40,\ j < k < 40. \end{gathered} \tag{3}$$

If all conditions are met, then it is assumed that a possible QRS complex has been detected.

3) Rhythm analysis. Detection of arrhythmic episodes

Methods for analyzing heart rhythm disturbances are in many ways similar to methods for assessing variability [6]. However, unlike them, rhythm detection methods must work in real time.

Obviously, the results of making a decision about rhythm disturbance directly depend on the results of the detection of QRS complexes. It should be noted that since the position of the R-wave maximum because of the operation of algorithms for detecting QRS complexes can be estimated with some deviation from the true one, it is necessary to minimize the influence of this deviation at the stage of analyzing heart rhythm disturbances. In this regard, it is advisable to use not the duration of the RR interval directly, but relative indicators based on it. In particular, heart rate variability can be judged by fluctuations in the duration of RR intervals over a short period of time [5, 7].

During the work of this stage of the analysis, the value of the current RR interval is calculated, relative indicators are determined based on the size of the interval and compared with the threshold value: if the value of the information parameter exceeds the threshold value, then a decision is made about a violation of the rhythm.

The selected parameter is based on the principle of heart rate variability SDANN [8] and uses the value of the standard deviation of RR-intervals in short intervals. The proposed information parameter S is equal to:

$$S_m = \sigma_m - \sigma_{m-1}, \tag{4}$$

where σ is a measure of the standard deviation over a sliding window with a duration of several RR intervals, and m is the number of the current window position. Based on the condition that the algorithm tuning period should not exceed a few seconds and the minimum normal heart rate is 60 beats/min, the duration of the sliding window was chosen to be 5 RR intervals.

At the same time, the structure of the decision rule itself remains the same as for Rdn: if the parameter being checked is less than the threshold value C2, then the rhythm is normal, otherwise an arrhythmia episode is recorded. The threshold C2 used in this decision rule is sqrt(0.1)≤≈0.3.

Previous studies [7-8] have shown that this algorithm is insensitive to low noise levels and is characterized by low errors of the 1st and 2nd kind.

3) Algorithm for classifying detected arrhythmic episodes. Diagnostic conclusions

Based on the generalized principle of operation of ECG express diagnostic algorithms [2, 5], it is obvious that the result of the operation of the decision-making system on the classification of cardiac arrhythmias will directly depend not only on the direct rule for classifying the detected arrhythmia, but also on the quality of the ECG processing algorithms at the stage detection of QRS complexes and analysis of rhythm disturbances. Therefore, as the basis for the developed decisive melt was chosenan algorithm for detecting arrhythmias based on digital filtering of QRS complexes with a decision rule based on measuring the difference in the standard deviation (RMS) of RR intervals on a sliding window, described in [8], which showed results suitable for practical application according to the criterion of the minimum probability of an erroneous decision.

Also, the advantage of this algorithm is that the results of its work are easier to analyze in terms of ECG signs of the considered arrhythmia. In particular, according to the number of automatically detected consecutive episodes of arrhythmias and the time relationships between them, it is possible to classify the heart rhythm into three categories:

– normal rhythm,

– single rhythm disturbances (for example, extrasystole),

– frequent rhythm disturbances (for example, atrial fibrillation, as one of the most common types of arrhythmia [10]).

Based on the analysis of the results of the algorithm operation presented in the article [11], we can distinguish the following classification criteria for the categories of signals considered in the study:

– a single atrial extrasystole corresponds to one recorded violation (interval of extrasystole coupling);

– a single ventricular extrasystole corresponds to two rhythm disturbances recorded in a row (the extrasystole coupling interval and a compensatory pause);

– atrial fibrillation correspond to three or more rhythm disturbances in a row (chaotic nature of the heart rhythm).

In accordance with these findings, the following decision rule is proposed for ECG classification depending on the recorded arrhythmic episodes. Based on the principle of the arrhythmia detection algorithm, the first five results of the decision on the state of the rhythm are part of the setup phase and do not need to be classified.

Classification of the detected rhythm disturbances is carried out by categories:

– a single episode of arrhythmia is classified as an atrial extrasystole (“ES-A” state);

– two episodes of rhythm disturbance following one after another are classified as ventricular extrasystoles (“ES-V” state);

– three consecutive episodes of arrhythmias are classified as a prolonged arrhythmic episode (“MA” state).

Otherwise, if no rhythm disturbance was recorded, the rhythm state is defined as normal (“OK” state) [12].

Conclusion

Selected and substantiated technical solutions will make it possible to create an effective portable microprocessor-based heart monitor that meets all the specified requirements. According to the results of development, articles [2, 7-9, 12] were written, the program for computers [13] was registered. Subsequently, it is planned to program the STM32F407 microcontroller in C language, debug the operation of the device and test it in real conditions. A possible option for improving such a device is to connect it to a server to form a database containing information about the patient's ECG parameters.

References:

1. Heart rate variability: standards for measurement, physiological interpretation and clinical use – Bulletin of Arrhythmology. URL: http://www.vestar.ru/atts/10480/HRV%20standards.pdf (Accessed 01.29.2023)

2. Akopyan, B.K. Microprocessor-based heart monitor. Hardware implementation / B. K. Akopyan, A. V. Gorodetskaya, O. O. Zharinov // SUAI Scientific session: collection of papers, St. Petersburg, April 08–12, 2019. Volume Part II. – St. Petersburg: St. Petersburg State University of Aerospace Instrumentation, 2019. – P. 239-242.

3. AD8232 ECG registration module, URL: hhttps:///www.alldatasheetru.com/datasheet-pdf/pdf/527942/AD/AD8232.html (date of circulation 19.02.2023)

4. M. O. Rahman etc. Internet of things based electrocardiogram monitoring system using machine learning algorithm// International Journal of Electrical and Computer Engineering No. 12(4). 2022. S. 3739-3751.

5. Friesen, GM A comparison of the noise sensitivity of nine QRS-detection algorithms/ GM Friesen, TC Jannett, MA Jadallah et al.// IEEE Transactions on biomedical engineering, vol. 37. No. 1. 1990. P. 85-97.

6. A robust open-source algorithm to detect onset and duration of QRS-complexes /W. Zong, G. B. Moody, D. Jiang// Computers in Cardiology No. 30. 2003. P. 737-740.

7. Akopyan, B. K. Review of electrocardiogram processing algorithms for decision support systems for classification of heart rate disorders / B. K. Akopyan // Processing, transmission and protection of information in computer systems '21 : International scientific conference: collection of papers, St. Petersburg, 14-22 April 2021. – St. Petersburg: St. Petersburg State University of Aerospace Instrumentation, 2021.

8. Akopyan, B. K. Development and research of quality indicators of algorithm of detection and classification of heart rate violations / B. K. Akopyan, O. O. Zharinov // Processing, transfer and protection of information in computer systems 22 : Collection of reports of the Second International Scientific Conference, Saint Petersburg, 11-15 April 2022. – St. Petersburg: St. Petersburg State University of Aerospace Instrumentation, 2022.

9. Akopyan B. Development and research of automated arrhythmic episodes detection algorithms by electrocardiographic signal// Bulletin of the UNESCO department “Distance education in engineering” of the SUAI: Collection of the papers. St. Petersburg, Issue 6.–SPb.:SUAI, 2021.

10. Kohler, B.-U. The principles of software QRS-detection/ B.-U. Köhler, C. Hennig, R. Orglmeister// IEEE Engineering in medicine and biology, no. 2. 2002. P. 42-57. Zong, W.

11. Ivanov G.G. etc. Analysis of indicators of the structure of heart rhythm variability in healthy persons according to PP- and RR-intervals // Bulletin of the RUDN University. Series: Medicine, 4, 2007. P.26-34.

12. Akopyan B. Development of the automated cardiac rhythm disorders detection and classification algorithm// Bulletin of the UNESCO department “Distance education in engineering” of the SUAI: Collection of the papers. St. Petersburg, Issue 7.–SPb.:SUAI, 2022.

13. Certificate of state registration of the computer program 2022681380 Russian Federation. Software for detecting and classifying arrhythmias by electrocardiogram signal: 2022681363 : reported. 14.11.2022 : omitted. 14.11.2022 / B. K. Akopyan, O. O. Zharinov; Applicant Federal State Autonomous Educational Institution of Higher Education "St. Petersburg State University of Aerospace Instrumentation".

SIMULATION OF AN AUTOMATED PRODUCTION LINE

Chabanenko Alexander
Saint Petersburg State University of Aerospace Instrumentation
E-mail: Chabalexandr@gmail.com

Abstract. *The object of modeling is a production line on which control and testing of gearboxes (hereinafter referred to as products) for high-power diesel engines are performed. The basis of the configuration of the line is a closed conveyor system, with the help of which the transportation of products installed on special media is carried out. An example of a miniature production line is Fig. 1.*

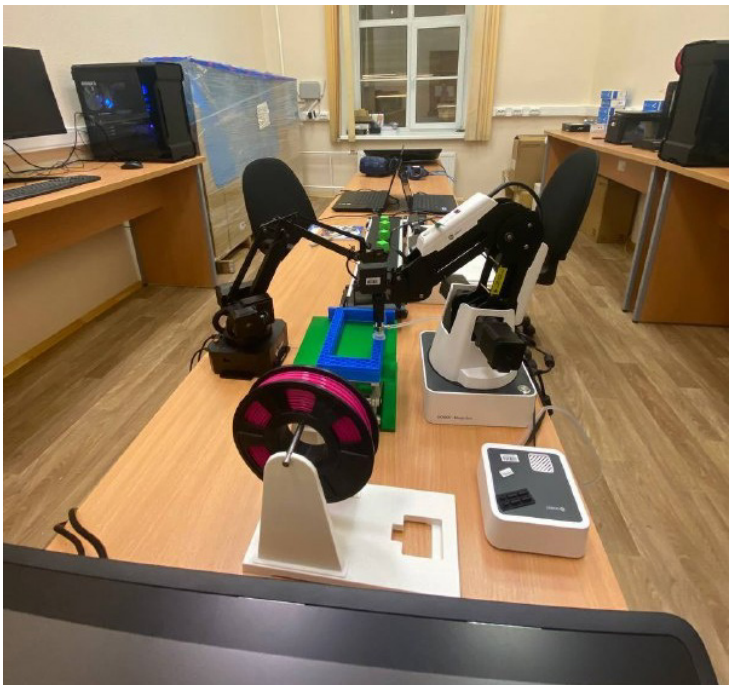

Fig. 1. Laboratorii additive technologies with miniature production line

To date, the method of simulation modeling is one of the most powerful and most effective methods for studying processes and production systems. The simulation model should reflect a large number of parameters, logic and patterns of behavior of the simulated object.

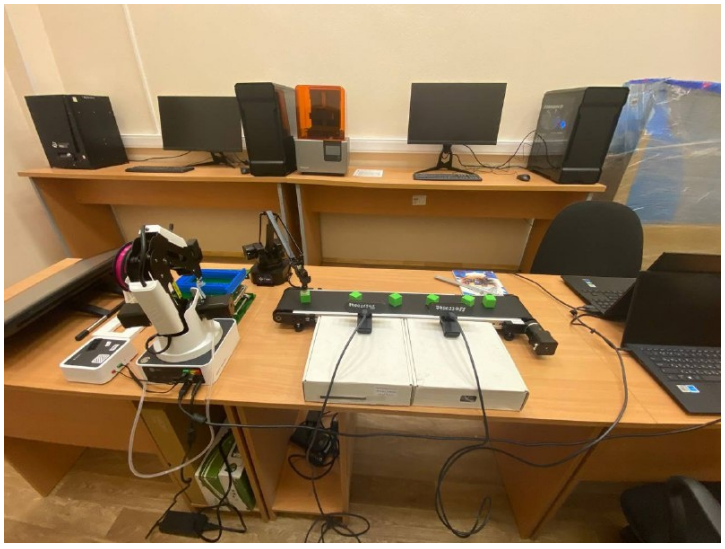

Fig. 2. Robotic manipulators

The analytical model is based on the mathematical description of the object. In the analytical model, it is necessary to go to significant simplifications and assumptions, which can lead to approximate and even unreliable results. Often the solution is presented in the form of a Laplace transform, or in the form of a system of complex integro-differential equations. It should be noted that in recent years, the possibilities of studying analytical models have increased significantly due to the rapid development and implementation of methods of computational mathematics with a numerical solution on a computer. An important advantage of analytical models in general is the ability to quickly obtain the values of the parameters of the object under study with minimal costs. When building and applying analytical models, it is important to choose only the essential parameters and discard the parameters that have little effect on the quality of the functioning of the object (system). To do this, it is necessary to have a good idea of the physical essence of the processes, the behavior of the object, in order to understand which simplifying assumptions and assumptions will have little effect on the final results. In the digital model, you can set only the basic parameters of Fig. 3.

Fig. 3. Customizing Object Models

In many cases, more detailed information about the behavior of the object, the system is required. In this case, simulation modeling is used, with the help of which the functioning of the system is described in the form of a sequence of operations on a computer. The behavior of the system is represented in the form of an algorithm, on the basis of which a computer program is developed. The essence of simulation modeling is that the process is simulated using arithmetic and logical operations in a sequence corresponding to the simulated process.

Setting up the hangar for production Fig. 4.

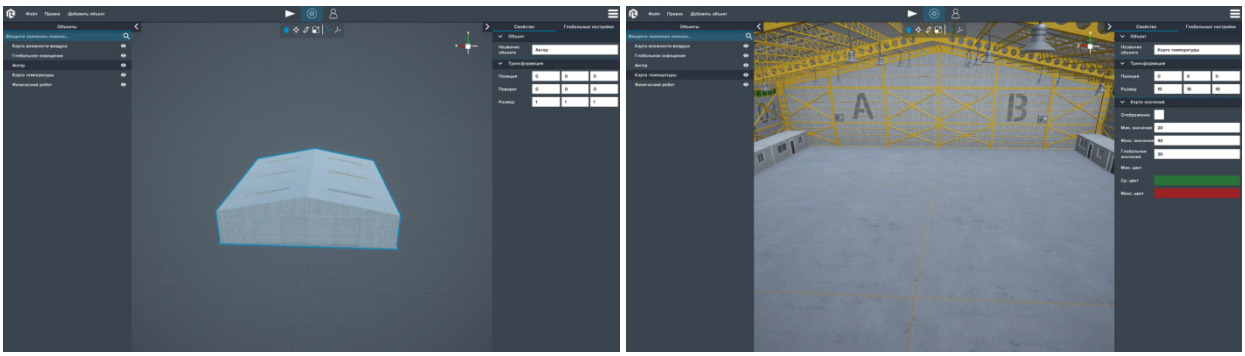

Fig. 4. Setting up a production hall in virtual reality with a temperature map

Experimental models have historically been used among the first in the conduct of tests, the study of complex systems. They give the most complete and reliable information about the object under study. In a number of industries, experimental modeling is dominant in the development of the object. For example, a mandatory stage in the development of a new aircraft design is to test its model in a wind tunnel. In fact, the whole stages of development of many types of equipment, complexes, systems have as their ultimate goal the conduct of experiments, tests of developments under appropriate operating conditions. Only on the basis of practice, testing, it is possible to finally judge the quality of the developed object. Simulation modeling allows you to reproduce the process of functioning of the system in time while preserving elementary phenomena, their logical structure and the sequence of flow through time. This allows you to obtain information about the state of the process in the future at certain points in time from the initial data. Currently, the simulation method is the most effective, and often the only method of studying complex systems at the stage of their design.

A simulation model is a dynamic model in which all processes are considered on a non-decreasing time scale. In the description of the simulation model, two components are distinguished: – A static description of the system, which is essentially a description of its structure. When developing a simulation model, it is necessary to perform structural analysis of the simulated processes. – A dynamic description of the system, or a description of the dynamics of the interactions of its elements. When compiling it, in fact, it is necessary to build a functional model of simulated dynamic processes. A distinctive feature of the simulation modeling method is the ability to describe and reproduce the interaction between various elements of the system. Thus, in order to make a simulation model, it is necessary: to represent the real system (process) as a set of interacting elements; algorithmically describe the functioning of individual elements; describe the process of interaction of various elements with each other and with the external environment. The main point in simulation modeling is the selection and description of the states of the system. A system is characterized by a set of variable states, each combination of which describes a specific state. Therefore, by changing the values of these variables, you can simulate the transition of the system from one state to another. Thus, simulation modeling is the representation of the dynamic behavior of a system by moving it from one state to another in accordance with 8 well-defined operational rules. These state changes can occur either continuously or at discrete moments in time. Simulation modeling is a dynamic reflection of changes in the state of the system over time.

The main approach to creating a simulation model on a computer is to form random variables and functions on a computer, and repeatedly reproduce them in accordance with the laws of the simulated process. As a result of the subsequent statistical processing of the obtained partial results, the final results characterizing the process of functioning of the system are obtained. The machine version of simulation modeling is called the method of statistical modeling. In a simplified form, the method of statistical modeling was known long before the advent of the computer as the MonteCarlo method, based on the manual receipt of random numbers, like the roulette of a slot machine.

Conclusion

Modeling of production systems allows you to detect and eliminate problems in advance, which will manifest themselves at the stage of commissioning and would require financial and time costs; reduce investment in production at the same productivity parameters; optimize production and choose the most rational solution from a variety of options.

References

1. Chabanenko A V, Kurlov A V 2021 Control the quality of polymers based on the model of Dzeno Journal of Physics: Conference Series
2. Chabanenko A V, Kurlov A V and Tour A C 2020 Model to improve the quality of additive production by forming competencies in training for high-tech industries *J. Phys.: Conf. Ser.* 1515 052065.
3. Chabanenko A V and Yastrebov A P 2018 Quality Assurance of Hull Elements of Radio-Electronic Equipment by Means of Control System *J. Phys.: Conf. Ser.* 1515 052065.
4. Chabanenko A V, Kurlov A V 2019 Construction of mathematical model of training and professional development of personnel support of additive production of REA IOP Conference Series: Materials Science and Engineering
5. Batkovskiy A M, Kalachikhin P A, Semenova E G, Fomina A V and Balashov V M 2018 Conficuration of enterprise networks *Entrepreneurship and Sustainability Issues* 6(1) 311–28.
6. Batkovskiy A M, Nesterov V A, S emenova E G, Sudakov V A and Fomina A V 2017 Developing intelligent decision support systems in multi-criteria problems of administrative-territorial formations infrastructure projects assessment *Journal of Applied Economic Sciences* 12(5) 1301-11.
7. Maiorov E E, Prokopenko V T, Mashek A C, Tsygankova G A, Kurlov A V, Khokhlova M V, Kirik D I and Kapralov D D 2018 Experimental study of metrological characteristics of the automated interferometric system for measuring the surface shape of diffusely reflecting objects Measurement Techniques 60(10) 1016-21.
8. Korshunov, G.I., Nazarevich, S.A., Smirnov, V.A. Fuzzy classification of technical condition at life cycle stages of responsible appointment systems (2018) CEUR Workshop Proceedings, 2258, pp. 427-437.
9. Nazarevich, S.A., Urentsev, A.V., Kurlov, V.V., Balashov, V.M., Rozhkov, N.N. Management of development of basic structures of technological systems of machine-building production (2019) IOP Conference Series: Materials Science and Engineering, 537 (4), article No. 042024.
10. Artjuhova, M.A., Balashov, V.M., Nazarevich, S.A., Smirnova, M.S. Evaluation of time to failure for radio transmitters under the radiation influence (2019) IOP Conference Series: Materials Science and Engineering, 537 (2), article No. 022016.
11. Nazarevich, S., Smirnova, M., Tushavin, V. Integral criteria for evaluation of scientific and technical research (2015) International Journal for Quality Research, 9 (3), pp. 467-480.
12. Vinnichenko, A.V., Nazarevich, S.A., Kurlov, V.V. Drifting models for evaluating the functional properties of products of innovative value (2021) Journal of Physics: Conference Series, 1889 (4), article No. 042074.
13. Vinnichenko, A.V., Nazarevich, S.A., Kurlov, V.V. Drifting models for evaluating the functional properties of products of innovative value (2021) Journal of Physics: Conference Series, 1889 (4), article No. 042074.
14. Vinnichenko, A.V., Nazarevich, S.A., Kurlov, V.V. Drifting models for evaluating the functional properties of products of innovative value (2021) Journal of Physics: Conference Series, 1889 (4), article No. 042074.
15. Artjuhova, M.A., Balashov, V.M., Semenova, E.G., Nazarevich, S.A. The quality of aerospace equipment production analysis (2019) IOP Conference Series: Materials Science and Engineering, 537 (3), article No. 032023.
16. Korshunov, G.I., Nazarevich, S.A. Parametric Models of the Product Novelty Assessment Through the Basic Structures Approach (2019) IOP Conference Series: Earth and Environmental Science, 272 (3), article No. 032142.
17. Tushavin, V.A., Semenova, E.G., Smirnova, M.S., Frolova, E.A. Comparison of qualitative assessments of employees work by randomized indicators ARPN Journal of Engineering and Applied Sciencesthis link is disabled, 2015, 10(16), pp. 7280–7287.
18. Assessment of plasticity with combined hardening for the study of deformation processes of structural materials under various modes of low-cycle loads Chabanenko Alexander Valeryevich, Rassykhaeva Maria Dmitrievna Certificate of registration of the computer program 2021619545, 11.06.2021. Application No. 2021618914 dated 11.06.2021.

RADAR SIGNALS BY THE RADIATION PATTERN OF THE RADAR RECEIVING ANTENNA

Kryachko Aleksandr F.

Abstract. *The features of the occurrence are considered and the results of the evaluation of the phase modulation of radar signals during their passage through the antenna of the radar station are presented. It is shown that with an even function of the phase distribution of the field in the antenna aperture, a phase modulation appears in the radiation pattern and the sequence of received signals, which should be taken into account when the signal is coherently accumulated. It is noted that for antennas with a common-phase or odd phase distribution of the field in the aperture in the plane coinciding with the plane of rotation of the antenna, phase changes in the main and near side lobes are manifested in the form of an abrupt phase change of 180 degrees.*
Keywords*: antenna, phase modulation, amplitude distribution, directional pattern*

Introduction

In air traffic control radar stations (radars) various design antennas are widely used, providing radiation of probing or querying high-frequency (RF) signals of radar transmitters, as well as receiving radar signals for detecting and evaluating air objects coordinates.

The characteristics of the antennas that affect the parameters of the emitted and received signals in amplitude and phase are determined not only by the design of the antennas and the wavelength of the RF signals, but also by the amplitude-phase distribution of the electromagnetic field in the antenna aperture.

The paper evaluates the influence of the amplitude-phase distribution of the field in the antenna aperture on the phase characteristics of the received radar signals resulting from the reflection of probing signals from aerial objects.

Evaluation of the phase modulation of signals by an antenna radar

In general, the antenna pattern (AP) by the electric field strength in the plane passing through the opening located on the coordinate axis x, with a linear size X and the electric axis of the antenna, can be determined by the expression [1]

$$F(\varphi)=\int_{-\frac{X}{2}}^{\frac{X}{2}} A(x)e^{j\psi(x)}e^{-\frac{2\pi}{\lambda}x\sin(\varphi)}dx, \tag{1}$$

where $A(x)$ – the amplitude distribution of the field in the antenna aperture along the x axis; $\psi(x)$ – the phase distribution of the field in the antenna aperture along the x axis; λ – the wavelength; φ – the angle of deviation of the AP direction relative to the antenna electric axis in the antenna aperture plane and the electric axis of the antenna.

For the sake of certainty, we will assume that the X-axis on the x-coordinate axis and the electric axis of the antenna lie in the horizontal plane.

After converting (1), we get

$$F(\varphi)=\int_{-\frac{X}{2}}^{\frac{X}{2}} A(x)\left\{\cos\left[\psi(x)-\frac{2\pi}{\lambda}x\times\sin(\varphi)\right]+j\sin\left[\psi(x)-\frac{2\pi}{\lambda}x\times\sin(\varphi)\right]\right\}dx=$$

$$=\int_{-X/2}^{X/2} A(x)\left\{\cos(\psi(x))\cos\left(\frac{2\pi}{\lambda}x\times\sin(\varphi)\right)+\sin(\psi(x))\sin\left(\frac{2\pi}{\lambda}x\times\sin(\varphi)\right)+\right.$$

$$\left.+j\left[\sin(\psi(x))\cos\left(\frac{2\pi}{\lambda}x\times\sin(\varphi)\right)-\cos(\psi(x))\sin\left(\frac{2\pi}{\lambda}x\times\sin(\varphi)\right)\right]\right\}dx. \tag{2}$$

Without loss of generality, we can assume that the amplitude distribution A(x) is an even function of the x coordinate relative to the phase center of the antenna, which is usually performed during the development and operation of primary and secondary radar antennas.

In this case, as follows from (2), if the phase distribution of the field in the aperture ψ(x) is an odd function of the coordinate x, then the imaginary part, as an integral within symmetric limits of the odd function of the argument x, will be zero. The antenna pattern F(φ) will be a real (positive or negative) function of the angle φ.

In this case, the square of the antenna pattern F(φ) in terms of the antenna field strength will always be non-negative.

Therefore, in a packet of pulsed radar signals reflected from the target and received by the radar antenna, phase changes between individual radar signal pulses due to the angular movement of the antenna pattern during scanning, i. e., additional phase modulation should not be expected.

The amplitude distribution of A(x) may differ from an even function, for example, when creating a special shape AP. But most often this is observed when synthesizing AP in a vertical plane, i. e. in a plane orthogonal to the scanning plane. However, a possible reason for the difference in the amplitude distribution of A(x) from an even function may be related to the peculiarities of the installation and rotation of the antenna during the radar's circular view. Such features include, in particular, the offset installation of the antenna relative to the axis of rotation, in which the phase center of the antenna is removed relative to the axis of rotation of the antenna (Fig. 1).

When the phase center is shifted relative to the axis during the rotation of the antenna, the phase center periodically moves along the direction of observation of aerial objects. This movement leads to the appearance of spurious phase and amplitude modulation of the packet of received radar signals, which can be expressed in terms of equivalent amplitude or phase modulation of the AP, including in the direction of its maximum.

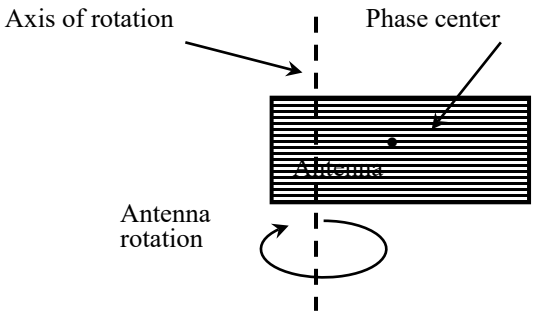

Fig 1. The displacement of the phase center of the antenna relative to the axis of rotation

In practice, mirror antennas with an irradiator are more often characterized by an even appearance ψ(x), as a result, for example, of the displacement (inaccurate installation) of the irradiator along the focal axis of the mirror or the final size of the irradiator.

Phased antenna arrays (headlights), in which there is no external irradiator, are free from this drawback.

For example, let's consider two possible cases of the phase distribution function.

A. ***Case 1***

Common-mode field distribution over the antenna aperture.

The results of calculations of the amplitude /F(φ)/ and phase ArgF(φ) radiation patterns of a typical antenna of a modern primary radar of the 23-cm range, having an antenna with a horizontal aperture size X=~7m and ψ(x)=const, taking into account (1) and (2) are shown in Fig. 2.

We believe that in the vertical plane, the antenna has a special amplitude-phase distribution of the field, which provides a cosecant AP with an increase in gain at large vertical angles. An example of a specific type of AP in the vertical plane is shown in Fig. 3

From the consideration of the amplitude /F(φ)/ and phase ArgF(φ) AP of a typical 23-cm primary radar antenna (Fig. 2), it follows:

- for radar antennas with a common-mode phase distribution of the field in the aperture in the plane coinciding with the plane of rotation of the antenna, phase changes in the main and near side lobes are manifested in the form of an abrupt phase change of 180 degrees;

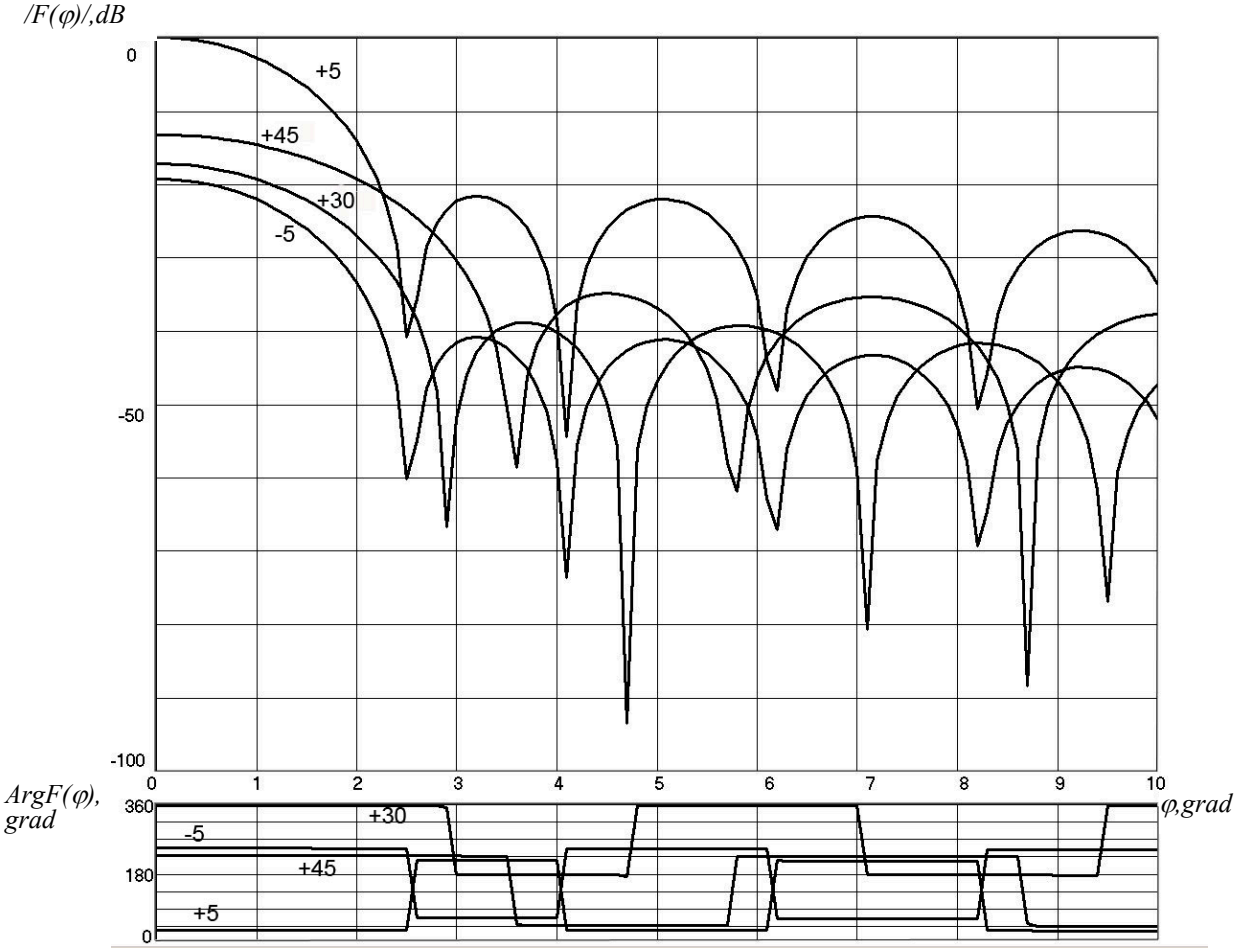

Fig 2. mplitude /F(φ)/ and phase ArgF(φ) AP of a typical primary radar antenna of the 23-cm range with a phase distribution of the form ψ(x)=const (the family of lines corresponds to different angles of the reflecting object, the amplitude distribution of the field in the antenna aperture of the form "cosine on a pedestal")

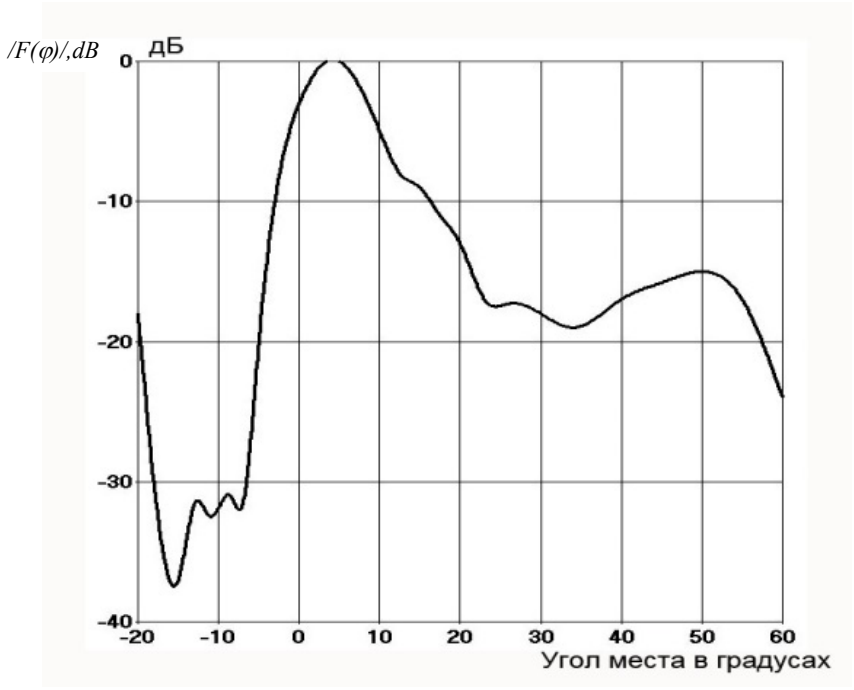

Fig 3. The amplitude AP of the antenna in the vertical plane

- the in-phase phase distribution of the field over the antenna aperture leads to deep dips in the AP;
- a constant, but significantly different phase value in the area of the main lobe of the bottom for different angles of the place, confirms the statement that with a complex (not even and not odd) amplitude-phase distribution of the field in the aperture in the scanning plane, phase modulation of the received packet of signals will necessarily be observed even in the area of the main lobe of the bottom of the antenna.

B. ***Case 2***

An even phase distribution function of the form $\psi(x)=ax^2$.

The results of calculations of the amplitude /F(φ)/ and phase ArgF(φ) antenna patterns of a typical antenna of a modern primary radar of the 23-cm range, having an antenna with a horizontal aperture size X=~7m, for an even phase distribution function $\psi(x)=ax^2$, taking into account (1) and (2) are shown in Fig. 4:

- at a=~0.03 rad/m^2 and the phase value at the edge of the aperture π/8 (Fig. 4a),
- at a=~0.06 rad/m^2 and the phase value at the edge of the aperture π/4 (Fig. 4b).

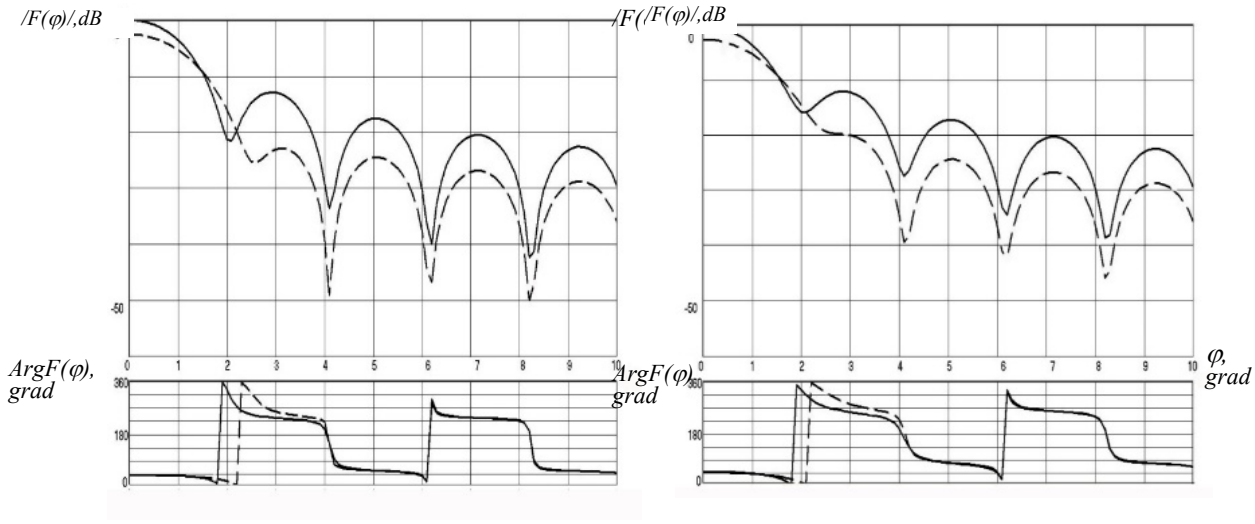

Fig 4. Amplitude /F(φ) and phase ArgF(φ) AP for an even phase distribution function of the form ψ(x) =ax^2 at the phase value at the edge of the aperture π/8 (a) and π/4 (b)

In Fig. 4, the solid lines correspond to the equilibrium amplitude field distribution in the aperture of the antenna, the dotted line shows the amplitude distribution of the field in the aperture of the antenna of the "cosine on a pedestal".

Evaluation of the amplitude and phase of the AP shown in Fig. 4, different amplitude distribution of the field shows that the use of such days during the rotation of the antenna will have amplitude and phase modulation of samples taken of radar signals.

As follows from Fig. 4, the magnitude of the amplitude and phase modulation of the signals depends on the size of the observation angle of the signal bundle in the horizontal plane formed during the rotation of the antenna.

It can be seen that for the case of Fig. 4b, within the horizontal angles from the axis to the first zero of the amplitude AP (expressed weakly), the phase AP changes by an amount of approximately 1.39 radians (80 degrees). Therefore, within the entire width (between zeros) of the AP, a signal packet with a doubled phase change of 2.78 radians, i. e. ~160 degrees, will be received in the radar.

Note that the non-phase distribution of the field over the antenna aperture leads to a decrease in the depth of dips in the radiation pattern.

Taking into account this circumstance, it becomes clear why there are often no deep bottom dips in the experimentally taken radiation patterns of the primary or secondary radar in the horizontal plane.

The quantitative value of the amplitude and phase modulation at a small range of observation angles can be estimated from the results of calculations given in Table 1, corresponding to the data in Fig. 4b. In the first column of Table 1, the horizontal angle φ of the deviation of the direction relative to the electrical axis of the antenna is given as an argument within a small range of values corresponding to the angular size of the received signal packet, in the second column – the corresponding amplitude AP on a linear scale, and in the third column – the phase AP in radians.

Table 1

Dependence of the amplitude and phase AP of the antenna on the angle □ in the horizontal plane within the value of the average angular size of the radar signal packet

Angle φ in the horizontal plane, deg.	Relative amplitude AP	Phase AP, radian
0,0	1,000	0,828
0,1	0,997	0,827
0,2	0,988	0,826
0,3	0,973	0,822
0,4	0,953	0,817
0,5	0,927	0,810
0,6	0,896	0,802
0,7	0,860	0,791
0,8	0,821	0,779
0,9	0,777	0,764
1,0	0,731	0,746
1,1	0,682	0,725
1,2	0,632	0,701
1,3	0,581	0,672
1,4	0,529	0,637
1,5	0,477	0,596
1,6	0,427	0,547
1,7	0,379	0,488
1,8	0,333	0,417
1,9	0,290	0,330
2,0	0,252	0,224
2,1	0,219	0,096
2,2	0,191	6,226
2,3	0,170	6,049
2,4	0,155	5,858
2,5	0,145	5,663
2,6	0,141	5,478
2,7	0,138	5,314
2,8	0,137	5,172
2,9	0,136	5,053
3,0	0,134	4,953

As follows from Table 1, within half the width of the radiation pattern at the level of half power (about 1 degree), the phase change of the samples of the received signals due to the influence of the phase AP will be approximately 12 degrees.

Within the sector of angles of 1.5 degrees the phase change of the samples of the received signals will increase and will be approximately 27 degrees. Within the sector up to the first zero of the AP, the phase change will be approximately 160 degrees.

The most sensitive to the distortion of the phase characteristics of the antenna output signal is the coherent processing of the received signal packet [2], which is usually performed in primary radars to increase the energy potential and Doppler filtering of signals against the background of passive interference.

Therefore, in primary radars with coherent processing, it is necessary to weaken or take into account possible changes in the phase characteristics of the samples of received signals due to the phase AP.

Research in this direction is continuing in order to determine the dependencies of the radar energy losses on the depth of the phase modulation of the received signal bundle, which in turn will allow us to

determine the permissible depth of the phase modulation, at which the phase distortions of the bundle can be ignored.

Main conclusions

1. Changes in the phase pattern of radar antennas, for example, with an even function of the phase distribution of the antenna field, lead to a change in the phase characteristics of the received signals.

2. To reduce the energy losses of the radar, as well as the correct implementation of the coherent accumulation of received radar signals, it is necessary to take into account the possible complex nature of the AP, which affects the phase characteristics of signal samples.

3. For radar antennas with a common-phase or odd phase distribution of the field in the aperture in the plane coinciding with the plane of rotation of the antenna, phase changes in the main and near side lobes are manifested in the form of an abrupt phase change of 180 degrees.

4. Smooth phase changes in the main and side lobes of the radiation pattern are possible only with even laws of phase change in the phase distribution of the field along the antenna aperture in the scanning plane.

5. The non-phase distribution of the field over the antenna aperture leads to a decrease in the depth of dips in the AP.

6. For receiving antennas in the form of headlights, due to the high repeatability of phase characteristics within the antenna aperture, the use of coherent accumulation of a packet of radar signal samples does not lead to losses even within the first zeros of the radiation pattern in the scanning plane.

7. For receiving antennas in the form of mirror reflectors with a remote irradiator, in order to prevent losses of coherent accumulation, it is required either to ensure the in-phase distribution of the field in the antenna aperture in the horizontal plane, or to take into account the phase change in the accumulated pulse packet by using a weight function complexly conjugated with the square of the AP.

References

1. Markov G.T., Sazonov D.M. *Antenny* [Antennas]. Moscow: “Energy” Publ. 1975. 528 p. (In Russian)

2. Brukhansky A.V. *Sistemy selekcii dvizhushchihsya celej* [Systems for selecting moving targets] Moscow: MAI. 1990. 15 p. [electronic resource]. (In Russian) Access mode: http://kaf401.rloc.ru/files/MTI.pdf, free.

CREATION OF 3D TERRAIN MODELS BASED ON LIDAR SURVEY

Afanaseva Victoria
Saint Petersburg State University of Aerospace Instrumentation,
Saint Petersburg, Russia
E-mail: victoria_afanaseva@mail.ru

Abstract. *The use of unmanned Earth surface monitoring systems for the collection and further processing of information is applicable in various fields of human activity, whether it is mapping the terrain or a virtual terrain model, counting the number of trees, searching for people, when planning the construction of new architectural and engineering structures, law enforcement, etc. This article will consider the process of creating 3D terrain models based on lidar surveys with an example of using them to control the environmental situation.*
Keywords*: three-dimensional terrain model, lidar, unmanned aerial systems*

Introduction

Today, an urgent task is to build a high-precision digital model (CMM) of the terrain based on data from a small-sized on-board laser system (MBLS) to monitor the environmental situation. Such tasks of environmental control may include, for example, the determination of temporary changes in the landscapes of controlled areas in dynamics. In this case, the construction of high-precision three-dimensional terrain models can be carried out according to data from the MBLS collected at the current time with archival data on which there have not been any current changes yet. The construction of multi-time digital terrain models allows you to quite clearly identify seasonal changes, for example, such as the definition of fire zones, the size of the coastal edge of rivers, lakes and other reservoirs, the scale of the formation of marshland, melting ice, snow cover and other temporary changes. The use of such an approach to build high-precision time-spaced CMCs based on complex processing of initial laser data collected from small UAVs is applicable for environmental control purposes, in particular, to identify structural changes in captured objects of various subjects, which is an important and urgent task, especially for various structures carrying out search and rescue operations, including when determination of the ice situation, as well as in the Arctic conditions.

To solve this problem, it is proposed to use UAVs with MBLS [1-2] (Fig. 1). The MBLS used includes both a lidar and a digital camera. Since lidar provides accurate information about the range, shape, size, in other words, it forms the most informative and convenient for further work with a 3D model of space consisting of many points, however, the disadvantage of lidar shooting is that it does not provide information about color, due to its monochromaticity, which is why MBLS includes I also have a digital camera.

Fig. 1. UAV with lidar installed on it

Statement of the task of constructing a high-precision digital terrain model based on data from an on-board laser system for monitoring the environmental situation

To build a high-precision digital terrain model based on data from the onboard laser system, it is necessary to collect data on the ground. It is necessary to make a flight task with the necessary parameters, the parameters are set depending on the accuracy of the desired result. If you want to get more accurate results, you need to lower the shooting height. It is worth noting that in this case, the data post-processing time also increases (Fig. 2-3).

After collecting data from the MBLS, it is necessary to process this data. Data processing is carried out in the DJI Tera program, from there a file is generated in LAS format, which is a binary file in which data records about points from lidar are stored. The resulting point cloud in binary form can be transformed into a three-dimensional model, also of a given accuracy. The conversion can take place in the Agisoft Metashape program. One of the possible formats for converting a point cloud into a three–dimensional model is FBX, this format of three-dimensional data is compatible with many types of software.

After completing the initial formation of a three-dimensional terrain model, it is necessary to save the route assignment and the received processed data. After some time, when a comparison of the situation should be carried out in order to control the environmental situation, a new three-dimensional terrain model is formed using the saved route assignment, with long-range processing.

Having received two three-dimensional models of the terrain, they can be superimposed on each other, and with the help of this, the change in terrain, the erosion of rivers, the consequences of fire and other natural disasters can be shown.

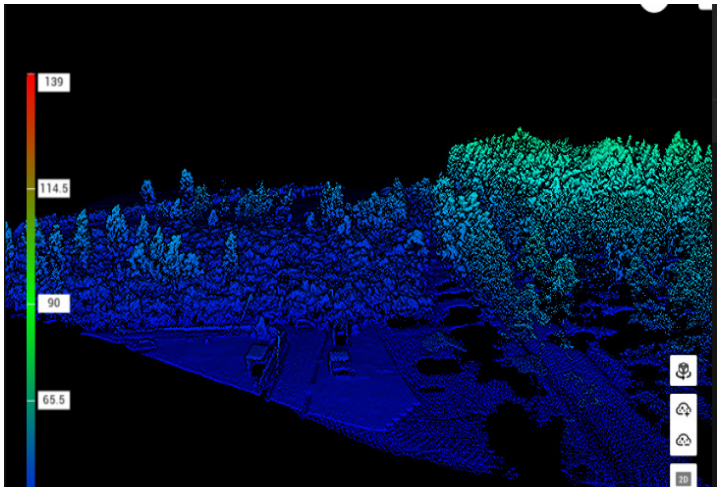

Fig. 2. Cloud of points on the scale of altitude above sea level

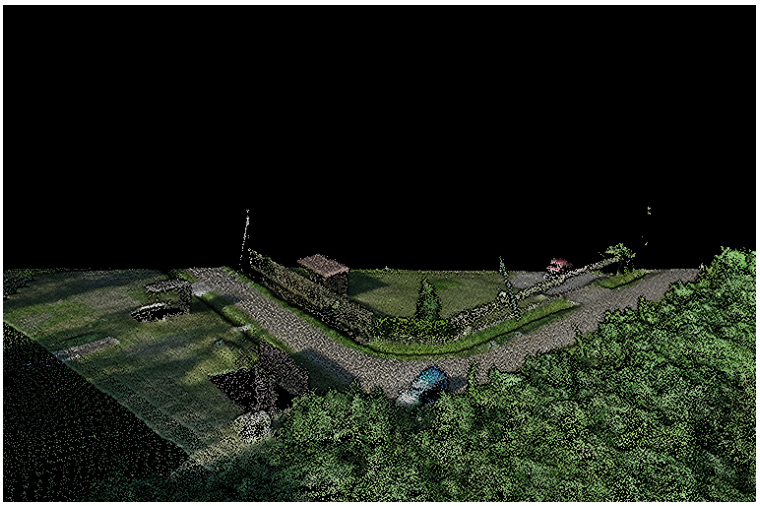

Fig. 3. Point cloud with image overlay

Results of an experimental study of two three-dimensional terrain models

For the experiment, two data collections were made in the field. The difference between the data collections was 1 week. Each collected point cloud was processed and converted into a 3D model of FBX format (Fig. 4).

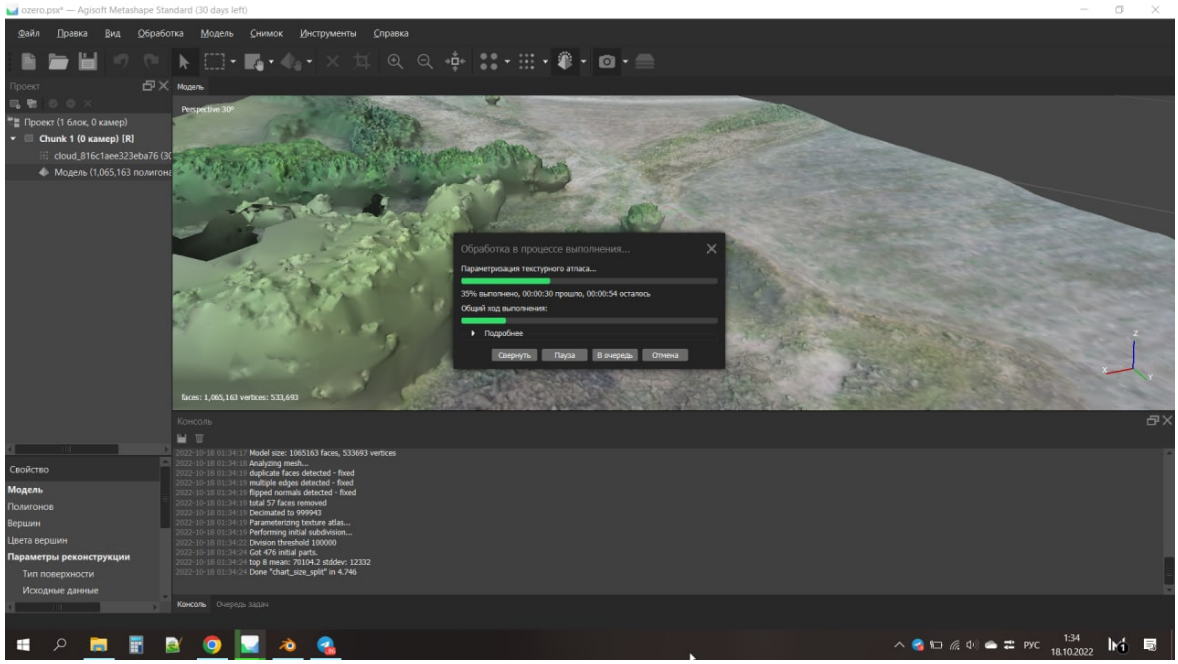

Fig. 4. Creating a 3D model

Both three-dimensional models are imported into the Blender program. Then they are superimposed on each other and changes in the relief of the earth's surface are manually tracked (Fig. 5).

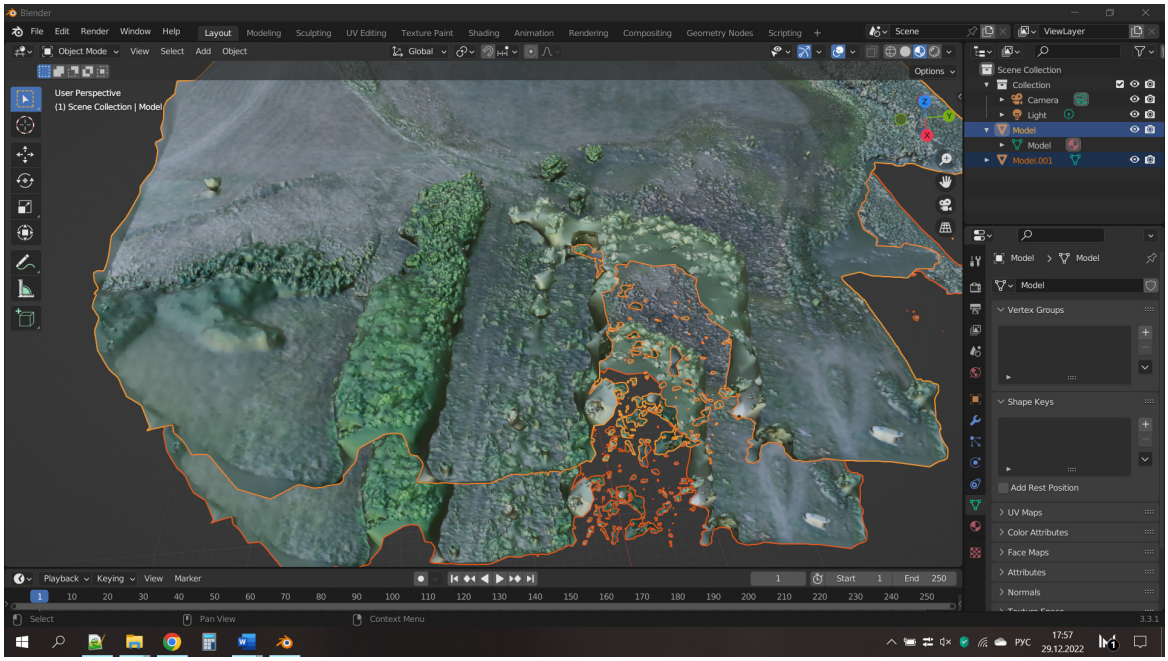

Fig. 5. Overlay of three-dimensional models

By superimposing two models, a slight difference in one of the trees appears on top of each other. In the first case, the height of the bush near the lake is about 7.6 meters, after the second shooting, the height of the bush is about 5 meters. Therefore, it is possible to draw a conclusion about the change of vegetation in a given area in one way or another (Fig. 6).

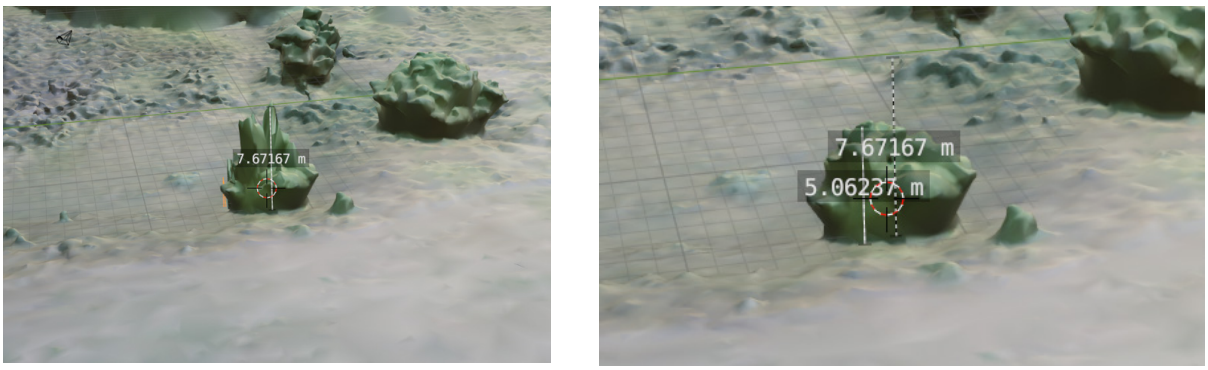

а) *б)*

Fig. 6. The difference between two three-dimensional models

Thus, an example of using a three-dimensional terrain model created using lidar data was considered.

Conclusion

Based on the results obtained, we can unequivocally say that the process of constructing a high-precision digital terrain model based on data from the onboard laser system was carried out successfully, and the quality of the resulting color point cloud is at a high level, for systems that combine location information from several heterogeneous sources is the future. The use of lidar to obtain three-dimensional terrain models is indeed becoming more and more common. Thus, it can be argued that this direction is promising and in demand today in many areas where monitoring of the Earth's surface with high detail of the observed territories is required.

Gratitude

The author expresses his sincere gratitude to his supervisor, Associate Professor V. A. Nenashev for his help and valuable advice in the preparation of this article.

Reference

1. Matrice 300 RTK platform. URL: https://www.dji.com/ru/matrice-300 (accessed 13.11.2022).
2. Zenmuse L1 module. URL: https://www.dji.com/ru/zenmuse-l1 (accessed 14.11.2022).
3. Miguel P., Girao O. 3D Object Tracking Using RGB Camera and 3D-LiDaR Data. 2016. P. 103.
4. Costa D., Vasques F., Porugal P., Aguiar A. On the Use of Cameras for the Detection of Critical Events in Sensors-Based Emergency Alerting Systems. Journal of Sensor and Actuator Networks. – Vol. 9(4). – 2020. – P. 24.
5. Lijiana Z., Zulonga L., Yingchengb L., Yanlib X., Mingb L., Zhuoleib W., Peib L., Xiaolongb L. Application and analyses of airborne LiDaR technology in topographic survey of tidal flat and coastal zone. – 2020. – P. 4.
6. Behrisch M., Leitloff J., Kurz F., Meynberg O. An airborne camera system for rapid mapping in case of disaster and mass events. Proceedings of the Earth Observation for Global Change. – 2011.– P. 6.
7. Pless S., Vollheim B., Haag M., Damma G. Infrared cameras in airborne remote sensing: IR-Imagery for photogrammetric processing at German Aerospace Center DLR, Berlin. 11th International Conference on Quantitative InfraRed Thermography. – 2012.– P. 10.
8. Verba V. S., Gavrilov K. Yu., Ilchuk A. R., Tatarsky B. G., Filatov A. A. Radar for everyone. Moscow: Technosfera, 2020. 504 p.
9. Verba V. S., Merkulov V. I., Milyakov D. A., Chernov V. S. Integrated multi-sensor complexes for monitoring the environment // Journal of radio electronics. 2015. №4 p. 15.

10. Wei P., Cagle L., Reza T., Ball J., Gafford J. LiDaR and Camera Detection Fusion in a Real-Time Industrial Multi-Sensor Collision Avoidance System. MDPI journal Electronics. – 2018.– Vol. 7(6). – P. 32.

11. Toschi I. Airborne oblique imaging: towards the hybrid era. Archives of Photogrammetry, Cartography and Remote Sensing. – 2019. – Vol. 31. – P. 21-28.

12. ПО DJI Terra. URL: https://www.dji.com/ru/dji-terra (accessed 14.11.2022).

MONT BLANC WEATHER STATION

Alfredo Gioacchino MariaPio Vecchio
Università degli Studi di Enna "Kore"
alfredogioacchinomariapio.vecchio@unikorestudent.it

ABSTRACT: *The "Mont Blanc Weather Station" is a weather station that is located on the Mont Blanc at a height of 4750 m. The main goal of the station is measuring and monitoring the weather parameters: Temperature, Air Pressure, Solar Radiation, wind direction and speed, rain, snow level, Air humidity. These parameters were sent to ARPA, organization that sponsored this project to study the weather changes, but the weather station has another goal too, that is giving weather information to the near facilities so people can enjoy their days safely.*

I. INTRODUCTION

Nowadays climate change is a very popular topic, and it refers to the variations

on different spatial-scales (regional,continental and global) and temporal-scales (decades to centuries long) of statistical parameters about climate change.

In this paper we'll focus on the studies on the Italian Alps where the temperatures are growing twice fast compared with a global average and the snow has been decreasing continuously: it's really a glaciers melting phenomenon.

This project won't give a solution to the climatic change, but it has the purpose of building a weather station located in poorly accessible environments and sending data from sensors to weather study centers allowing experts to make estimates regarding climate change in the areas of interest.

II. RELATED WORKS

The proposed software project is based on work that was ordered in 2015 by ARPA, an Italian organization and the Aosta Valley region, realized by "Hortus", an Italian company based in Milan [1].

The original project was based on the measurement of weather data and their collection into a datalogger (*CampbelScientific*) that were sent to the ARPA using a cellular connection or a satellite connection denominated Iridium.

Taking inspiration from this project, it was decided to reproduce the same scenario in the development environment "Matlab" [2], introducing additional function that were not included at the time of implementation such as regulate the access to the cableway and ski slope "Sky Way Mont Blanc", taking in consideration the **wind chill** parameter and providing to this facility also other climates parameters.

III. THE PROPOSED APPROACH

To meet those needs, the system Mont Blanc Weather Station make use of 2 types

of networks, the first network is a cable network (wired CSMA/CD ethernet) and to this network belongs the sensors, which collect the data with a specific protocol "SDI-12", that is converted in ethernet protocol [3] and a second wireless network

(802.15.4 "Zigbee"). It is composed by

controllers and actuators.

devices:

- humidity sensor: humidity range 0-100%RH, accuracy 3/-3%, voltage 7-28 vdc, 0,6 mA (Active) 50 μA(sleep) [5]
- temperature sensor: tolerance +2 C° / -2C°,temperature range -35 C° – 50 C°, current drain 100 Kohm [5]
- wind speed sensor : accuracy +0.3 / -0.3 m/s, speed range 0 – 100 m/s, temperature range -50 / 50 C° [5]
- wind direction sensor: accuracy +3 C°/ -3 C°, direction range 0° – 360°, voltage 5 – 24 vdc, current drain: 10K ohm [5]
- pressure sensor : 0.5/ -0.5 hpa, pressure range 500 – 1100 hpa, temperature range -40 C° – 60 C°, tensione 9 -28 vdc, current drain 200 μA (sleep) – 5mA (Active) [5]
- rain gauge sensor: accuracy 3% / -3%, rain range 0 – 1500 mm / h, voltage 5- 24 vdc, current drain 0,8 mA (Active) 0.007 mA (sleep) [5]

- snow level sensor: accuracy 0.2 %,snow range 0.1 m – hmax m, current drain 210 mA (Active) 14mA (sleep) [4]
- solar radiation sensor: accuracy 2.6% / -2.6%, solar radiation range 0 – 2000 w/m^2, current drain 3mA (sleep) 5mA (Active), voltage 6 – 24 vdc [6]
- controllers are devices that take care to understand all the data revealed from sensors using several fuzzy logic controllers
- actuators driven by controllers manage the lights that allow to access to the ski facility and also show the weather condition in the time interval considered
- gateway is a particular commutator node and allow to interconnect wired and wireless networks

IV. SCENARIO

This scenario has been reproduced by the development environment Matlab/Simulink and the aid of True Time [7].

The first level of development consist

in representing the revelations of the weather data though sensors. The simulation was made in the first week of January, however it's possible to extend the obtained revelations in the time,considering that the data generated through the appropriate *signal builder* take in input excel.xls files (constituted by the presence of two columns, one for the time and the second for the consideration size) build on meteorological archives of the area of interest [9].

At this level of development belongs also the choice of the *stop time* used in Simulink, the value 12,8s. The choice of this value was especially wanted, because in the xls files, used for configure the input

values of the sensors, was used a temporal scale that marks the 12 months of the year into weeks and so reduced it to this value.

The second level of development concerns the realization of the controller, which receives data detected from the sensors that arrive at the controller through the gateway.

The information received from the controller are sorted to 4 fuzzy logic controllers (figure 1):

- Windchill: this controller maps temperature and wind speed using the climate discomfort index **windchill,** measuring the temperature that we perceive on our skin for the effect of the wind[10].
- Solar Efficiency: take as input temperature and solar radiation and map them in digital output value defining the energy efficiency achieved [11].
- Scharlau Index: take as in input temperature and humidity in order to obtain as output a value on the Scharlau scale that defines the limit temperature of the air and the relative humidity beyond which a healthy man feels discomfort [12].
- Weather Alert: evaluate the presence of meteorological alert. The input parameters of this controller are: snow, rain and temperature [11].

The output value of every fuzzy logic controller is sent to the actuator.

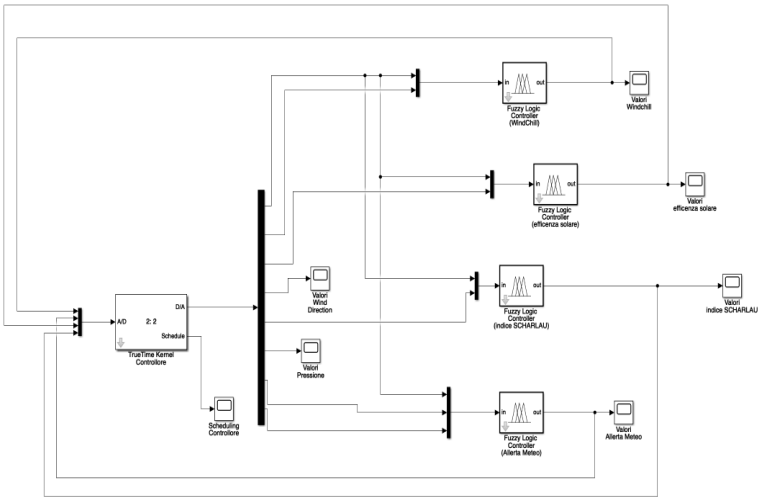

Fig. 1: from left to right we have : the controller kernel and the various fuzzy logic controller

The third level of development concerns the actuator, which receives input values from the controller and split them in two differents paths:

- one is to show in output the values received, in order to view the weather information;
- the second is to take some data from the controller and take them in input to the Stateflow Simulink, object used to model reactive instruments using state machines and flow charts. With this model is possible to simulate the way of the device that allow to the cableway and the ski slope managed by the "Sky Way Mont Blanc". Everything is visible on the screen by the indicator lights.

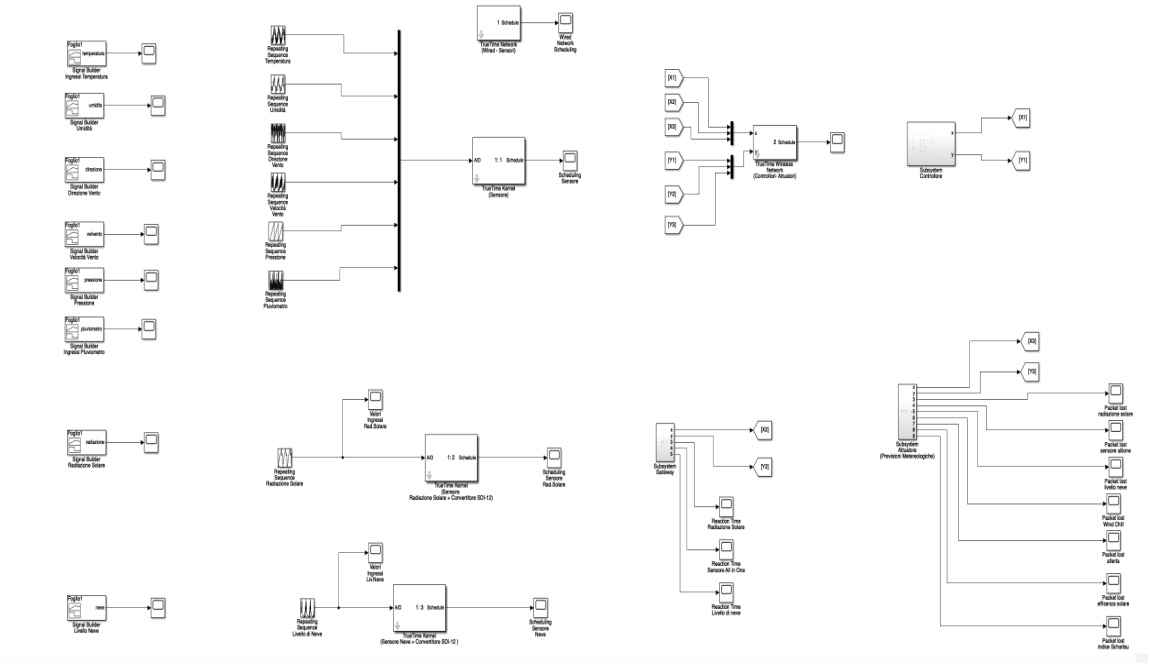

Fig. 2: from left to right we have : the sensors, wireless and wired menagers,gateway, controllers and actuators

V. PERFORMANCE EVALUATION

The performance aspect of network communication is an important topic in order to improve the whole communication system, making revelations with consequent actions aimed to optimize the whole system. The focus in this discussion is based on the three wireless nodes present in the system.

The performance analyzed concern the

Response Time, it represents the time interval between the user request and the system response, and the Packet Loss (figure 3) that is the amount of information lost in the ether.

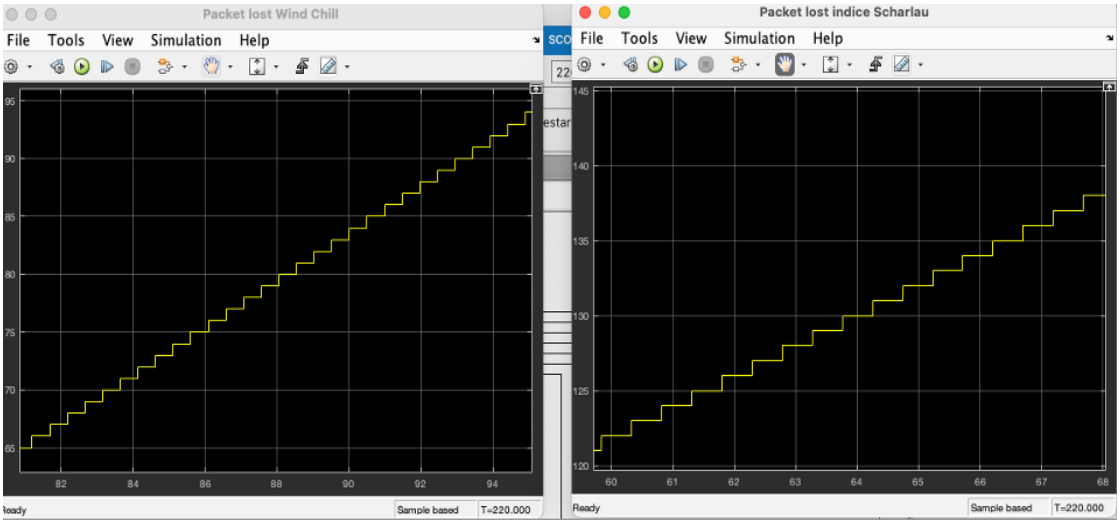

Fig. 3: on the left the windchill packet loss chart, on the right the Scharlau index packet loss chart

Given that the weather station is located at the height of 4750 m in the presence of an open space and given the studies conducted from the university of Roma “Tor Vergata”, according to which with the increasing of the height and in presence of an open space, path loss increase significantly (pathloss represents the factor of lost signal and has value in a range from 2 to 4 expressed as 1/d^a where a is a parameter related to the ambient). I used a pathloss value equal to 3.8, to generate an arguable signal. For each packet exchanged, in case the ID of the packet is different from the expected ID we can see a Packet Loss phenomenus.

We can see on the chart the presence of continuous lines that represent Lost Packets.

VI. CONCLUSIONS

The proposed solution allows us to take care about climate change, which has been a really important topic in the last years.

The project Sky Way Mont Blanc can be reproduced referring to other Italian mountains and also all over the world, focusing on the ambiental parameters of the chosen place. It’s also possible to improve the realized system by introducing 2 x 120 W solar panels in order to charge the 2 batteries of 25.3V, giving the right amount of energy to power on the weather station for a long time.

Even if the presence of the 2 solar panels would not be a good idea, because the weather station is located at 4750 m of height and solar lights could be weak to recharge the batteries; another challenge is connected to the problem of freezing the solar panels cells.

REFERENCES

1. https://hortus.it/progetti_hortus/monte-bianco/ (Hortus project weather station “Mont Blanc”)
2. Matlab Simulink documentation MathWorkshttps://it.mathworks.com/help/matlab/
3. https://www.directindustry.it/prod/kisters-hyquest-solutions/product-235669-2385784.html (converter from SDI-12 to Ethernet)
4. https://hortus.it/wp-content/uploads/prodotti_cs/doc/b_SnowVUE10.pdf (Snow Level Sensor)
5. https://s.campbellsci.com/documents/us/product-brochures/b_climavue50.pdf (All In One Sensor)
6. https://hortus.it/wp-content/uploads/prodotti_cs/doc/b_CS320.pdf (Solar Radiation Sensor)
7. TRUETIME 2.0 – Reference Manual Anton Cervin Dan Henriksson Martin Ohlin Department of Automatic Control Lund University February 2016
8. Numerical Analysis Using MATLAB and Excel Steven T. Karris ISBN 13: 9781934404041
9. https://www.meteoblue.com/it/tempo/historyclimate/climatemodelled/monte-bianco_francia_3181986 (Mont Blanc meterological history)
10. http://www.meteo.marche.it/indidisa.aspx (Wind Chill)
11. http://www.meteo.marche.it/indidisa.aspx (Scharlau Index)
12. https://www.espace-mont-blanc.com/asset/rapportclimat_ita.pdf (data used to create the fuzzy logic controller of weather alert)

APPLICATION OF GENETIC ALGORITHMS IN ROBOTICS

Badika Egor
Saint Petersburg State University of Aerospace Instrumentation, Saint Petersburg, Russia
E-mail: embadika@gmail.com

Abstract. *With the increasing demand for robotics equipment in many areas of life, engineers are faced with tasks in building complex robot movements, which are difficult to implement with classical algorithms from the point of view of programming. In such situations, it is worth using machine learning methods. The paper describes one of the ways to set the robot's movement – the use of a genetic algorithm (GA). The fields of application of this technology, its theoretical aspects are considered, as well as a study and evaluation of the quality of this technology using the example of the Half Cheetah model created by OpenAI.*

Modern robotics is aimed at implementing various types of tasks without direct human involvement. In the process of using robots, an important task is their programming, during which the technique receives the necessary algorithm of actions to solve the problem. The introduction of such technologies optimizes and improves the quality of production processes, simplifies the use of devices for various purposes, which leads to a decrease in the entry threshold for users. To date, engineers have been tasked with improving the programming of robots, one of which is to automatically determine the algorithm of actions for performing nonlinear tasks [1].

For the solution, machine learning technologies are used to simplify the programming of certain movements. Implementation is possible by two methods: the use of neural networks and the use of genetic algorithms (GA). In some tasks of controlling mobile robots, neural networks show themselves worse than genetic algorithms due to the effect of forgetting when trying to retrain the model[2] while GA works well with a minimum of information, which gives a good result in a short training time, and also combines well with other machine learning methods.[3].

Genetic algorithms are well-spread in automatic control systems: they are used to set up PID controllers [4], mechanisms for walking robots in complex environments [2], and also perform robot stabilization. [5].

This article is devoted to the study of the quality of the work performed by robots equipped with a trained genetic algorithm. The model «Half Cheetah» (cheetah) from OpenAI, whose task is to learn how to run, will be taken for analysis. [6]

Theory of genetic algorithms

A genetic algorithm is a model capable of solving problems that are not described from the point of view of algorithmics or having complex nonlinear solutions based on the basic principles of evolution and genetics [7]. In programming, this model uses several terms:

Bot, individual – is an array of data (usually two-dimensional), which are the "genes" of the bot

A population – is a set of several bots with different "genes" that perform a task.

Crossing – is the process of obtaining new types of bots from the other two.

Mutation – is a random change in certain bot genes.

Reduction – reduction of the number of bots in the population.

The reward is the value that the bot received at the end of the task. During the work of an individual, points are awarded to her for correct actions (reward) and points are deducted for incorrect actions (penalty). [8]

Fig. 1 shows the block diagram according to which the genetic algorithm is trained. The first step is to create an initial population, this happens by generating bots and filling them with a random set of data. Their number in the initial population may be greater than in subsequent populations. Bots of the original population perform a task for which they receive a reward. Next, the n best are determined, among which random two are crossed, and multiply to the size of the population. Individuals who are not among the best are removed, and a new population begins to complete the task. The model ends when the stop criterion is met, usually it is the achievement of a certain number of training epochs, however, it is possible to put a genetic algorithm to train until a certain reward value is reached.

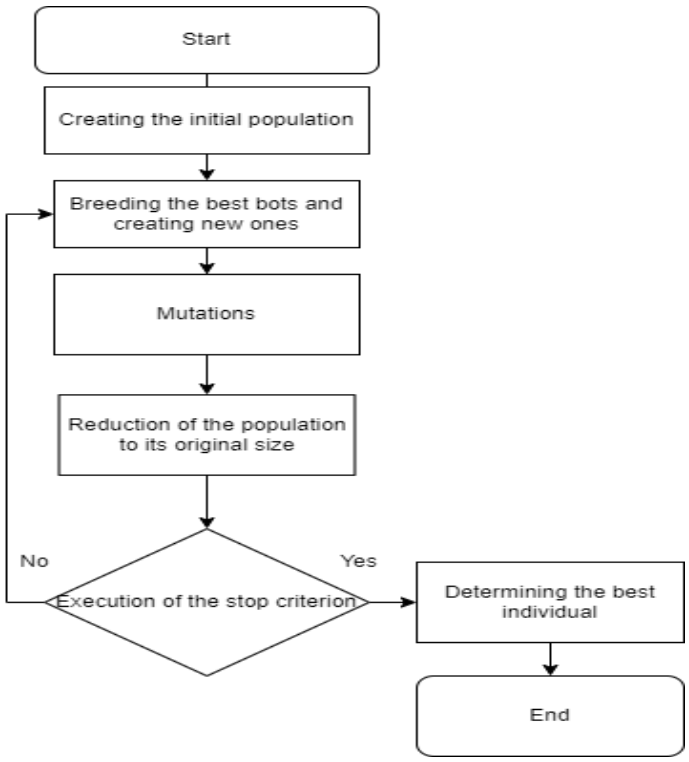

Fig. 1. Block diagram of the genetic algorithm

In the course of the study, the OpenAI environment will be used with the bot “Half Cheetah” (Fig. 2), whose task is to learn to run.

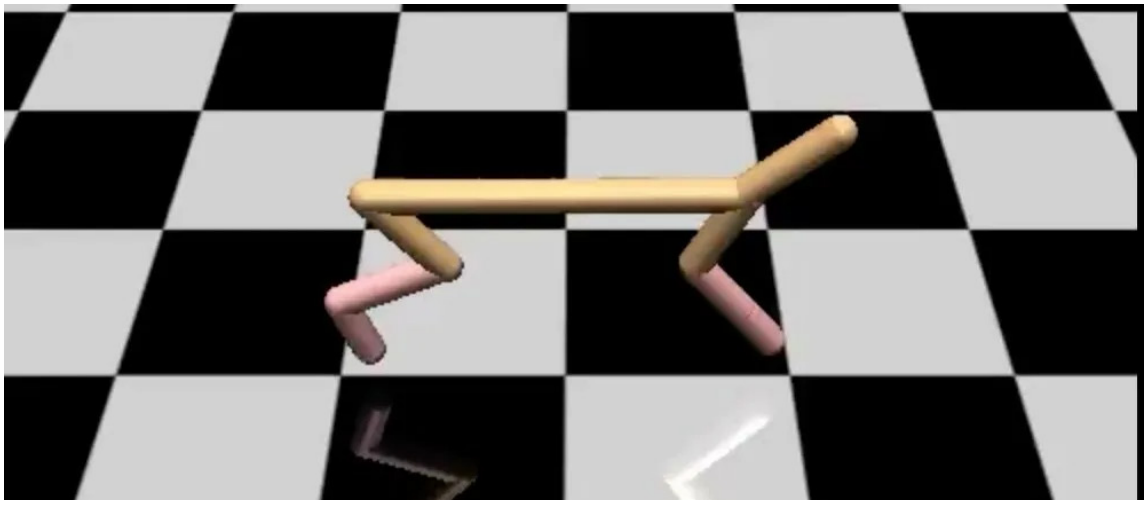

Fig. 2. Half Cheetah OpenAI

This model is well suited as an analogue of a mobile walking robot, as it has a similar structure. Let's look at the model in more detail:

During operation, each frame returns the state of the robot at the current time – a vector of 17 values of speed, rotation angles of the moving parts, the angle of rotation of the robot itself, as well as the angular velocities of the moving mechanisms of the robot (the mechanisms are located not on the thigh of the lower leg and the foot of each of the limbs). Each value belongs to an interval (-∞;+∞).

To control the robot, a vector of 6 values is used, each of which is responsible for a specific mechanism located in the limbs. Each value must be located in the interval [-1;1].

The reward consists of the speed value along the X-axis, as well as the number of actions performed at each time and belongs to the interval (-∞;+∞).

The genetic algorithm is trained by selecting such values of the bot so that when multiplying the vector of the model state by the values of the bot, the correct vector of actions is obtained. If the state vector has dimension (1,17), then in order to get the control vector (1,6), it is necessary that each bot has dimension (17,6).

Several variants of the genetic algorithm training will be used to analyze the work.

Experiment 1

In this experiment, each bot will run 50 frames and its action vector values will not be limited to the range [-1;1]. That is, the genetic algorithm must independently learn how to set actions in a given range and run at the same time.

The number of bots in the initial population is 40, in the subsequent 20, 10 bots survive in each population. Fig. 3 shows the result of 200 epochs of training. (A – reward, E – epoch)

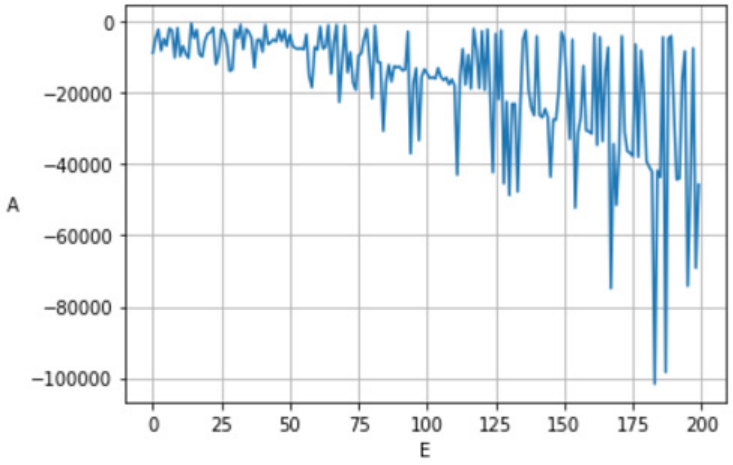

Fig. 3. Result of experiment 1

The best bot of the era is considered in the construction of graphs. As you can see, the reward for individuals is always negative and decreases with each epoch, which indicates that the genetic algorithm is not able to solve the problem of movement and conversion of values into the desired range at the same time. In further experiments, data conversion to the desired range will occur inside the code.

Experiment 2

Nothing changes in the experience except adding a manual translation to the desired range.

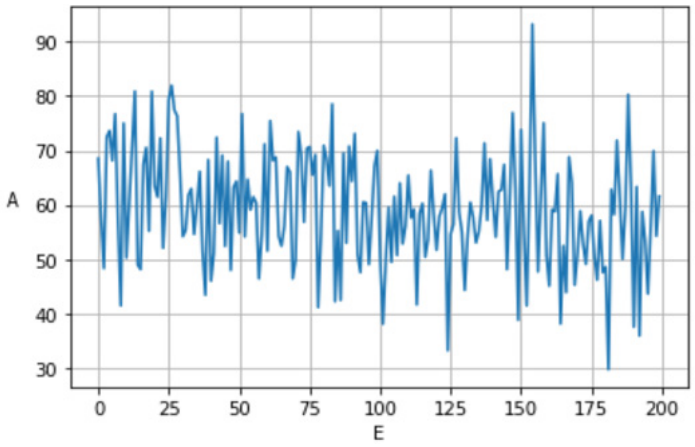

Fig. 4. Result of experiment 2

As can be seen in Fig. 4, manual conversion gives the best result, the value of the reward for each epoch has become positive, but this does not mean that the robot has run. When displaying a video of the robot's operation, it can be seen that it periodically turns over on its back (Fig. 5)

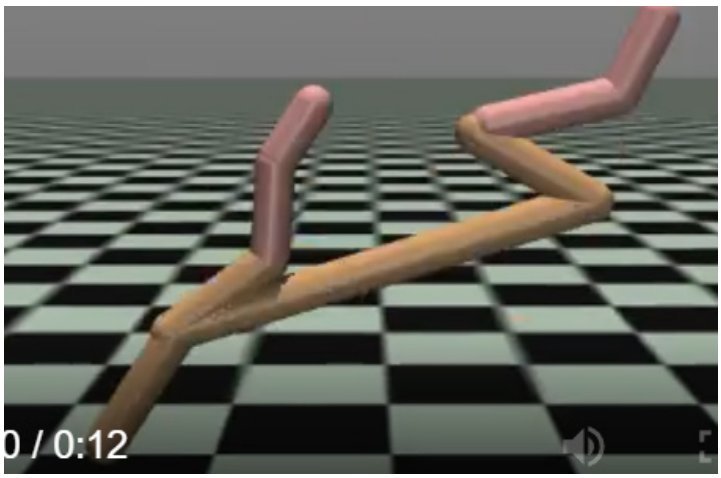

Fig. 5. Snapshot of the algorithm operation

An increase in the number of epochs (up to 2400) did not lead to an improvement in the result. This can be seen from the reward schedule in Fig. 6:

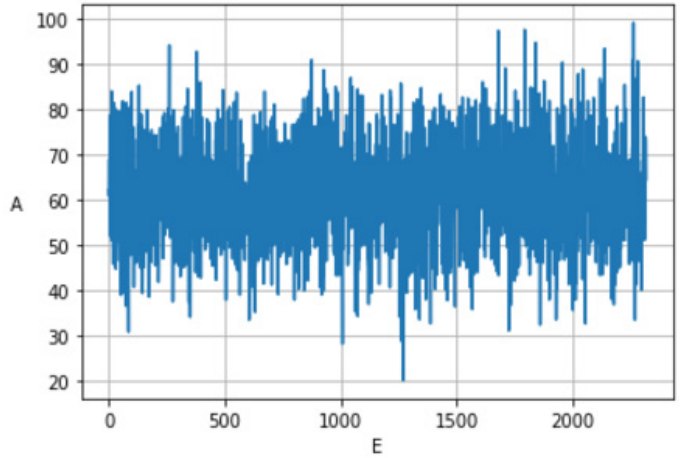

Fig. 6. A graph of the results of training the model for 2400 epochs

As you can see, the average value of the reward is kept around 60. There is no progress.

Experiment 3

It was decided to leave all the parameters of the model the same as in the previous experiment and launch the initial population for training again, but for 7 thousand epochs. The average reward value also remained around 60, however, the robot started running correctly.

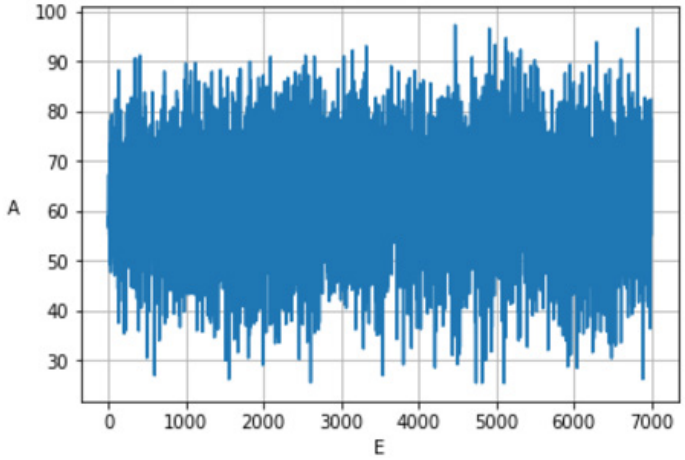

Fig. 7. The result of the work of experiment 3

Since the reward has not changed, but the work of the bot has become correct, it can be assumed that in the process of work the genetic algorithm has learned not to turn over on its back while running, but because of this it has reduced the speed, which led to the constancy of the value.

Experiment 4

In this experiment, the number of frames during which each bot performs a task has increased (120), as well as the number of bots in the population – 40 and the number of surviving bots – 20.

The model was trained on 15 thousand epochs and received the following results (Fig. 8).

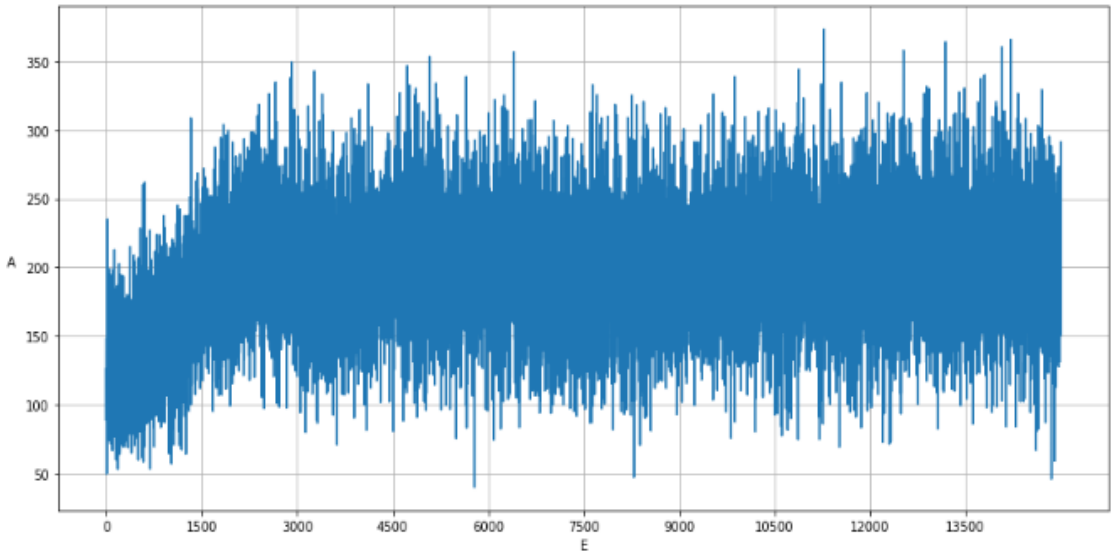

Fig. 9. Result of experiment 4

As you can see, this experience clearly shows an increase in rewards over the course of epochs at the beginning of training, and then an exit to the plateau, in which the bot refined the correctness of movements and corrected mistakes, without changing its speed. Also, it is worth noting that the model has an average reward value of about 200, which is also a positive difference from all previous models.

When displaying the result of the robot's work on the screen, there is also a noticeable difference in quality: the robot runs faster, does not turn over, and is also able to get out of difficult initial positions.

Conclusion

Genetic algorithms are one of the easiest ways to implement machine learning: they are able to give a good result in a small number of epochs, do not require preliminary sampling for training, and also have a fairly simple algorithm that allows you to use this technology without going too deep into machine learning.

The results of the experiments showed that the genetic algorithm is able to solve problems of movement and can be used in automated systems in order to automatically set the robot's movement. This technology allows engineers to automate the constant movements of robots performing secondary tasks (moving the robot in space, picking up parts and their layout) and to make a bias in programming complex processes that require high accuracy of robot movements. (welding, milling, assembly). In the future, the technology will be developed and optimized, which will lead to the possibility of learning to perform complex tasks without the help of programming.

References

1. Tom Husband, Yuval Davidor Genetic Algorithms and Robotics: A Heuristic Strategy for Optimization. – 1st ed. – Singapore: World Scientific Publishing Company, 1991. – 180 p.

2. Brunarsky Pavel Nikolaevich Teaching a mobile robot to move along a trajectory with complex constraints // Informatics, telecommunications and management. 2013. №1 (164).

3. MIREA // Artificial intelligence methods in robotics.

4. Mikhailenko Lyudmila Andreevna, Rusin Dmitry Sergeevich, Ustimenko Valeria Vladimirovna, Chubar Alexey Vladimirovich PARAMETRIC SYNTHESIS OF THE REGULATOR BY A ME-

TAHEURISTIC ALGORITHM IN THE ENVIRONMENT OF SimInTech // Spacecraft and technologies. 2020. №3 (33).

5. I. Ryadchikov, A. Gusev, S. Sechenev, E. Nikultsev A GENETIC ALGORITHM FOR FINDING PARAMETERS OF PID REGULATORS OF A WALKING ROBOT STABILIZATION SYSTEM // Proceedings of the R.E. Alekseev NSTU. 2019. No.1(124).

6. Half Cheetah // OpenAI gym URL: https://www.gymlibrary.dev/environments/mujoco/half_cheetah / (accessed 03.02.2023).

7. E. Badika, Y. Istomina, D. Zyryanov, V. Tsypilev GENETIC ALGORITHMS AND METHODS OF THEIR APPLICATION // II International scientific and practical conference "Issues of modern scientific research". 2023. № 6.

8. University of Artificial Intelligence // Tutorial Introduction to genetic algorithms.

TRACTION CONTROL SYSTEM

Barbera Antonino,
Miccichè Giulia
Computer Engineering and Networks Laboratory – Kore University of Enna – Italy
Email: antonino.barbera001@unikorestudent.it
giulia.micciche@unikorestudent.it

Abstract. *This project deals with the management of a traction control system for cars. Wheel slip is an event that can occur due to critical asphalt conditions caused by rain, snow, ice, mud or the presence of oil.*

The TCS system adjusts the power delivered by calculating the friction between the wheels and the asphalt.

Through sensors that detect the pressure applied to the accelerator pedal and the position of the steering wheel, we calculate the power, speed and number of wheel spins and these give us the value of friction. If the friction is high, the vehicle is in ideal conditions, if the friction is medium/low it means that there could be a slipping condition and consequently the power is adjusted to reduce this phenomenon.

INTRODUCTION

Traction Control (TCS) is a widely established device in modern cars, becoming one of the most important devices due to its impact on driving and its influence on driver and passenger safety.

TCS has a very important function: to prevent the drive wheels from slipping and causing loss of control of the vehicle, to avoid accidents. Regardless of the type of traction, traction control will intervene when grip on the ground is precarious, such as in the event of rain, wet or very smooth asphalt. In these cases, the TCS will reduce wheel spin and return full control of the car to the driver. The traction control works thanks to specific sensors which are used to detect wheel slip and manage the delivery of engine power which will eventually be cut or transmitted entirely to all the wheels with more grip.

This system also allows it to be activated or deactivated according to driver preferences or environmental circumstances. In fact, it may happen that in certain conditions such as mud, snow or ice it is not possible to transmit all the power to the wheels and consequently get stuck, for this reason, the TCS can often be inconvenient in situations of this type, and allow you to turn off the control can be very useful.

RELATED WORKS

Systems of this type such as the traction control system (TCS) are very popular nowadays and innovative technologies are continuously developed in this sector, because they allow not only to improve the quality of vehicles but also to increase safety, due to the increased performance of modern cars are growing. So it is very important to develop these systems to minimize response latency through new technologies, to create safer and more performing products.

Development should focus on creating more accurate sensors and improving data transmission to increase system quality. By improving the precision and speed of control we can obtain very reliable systems and reduce errors caused by the driver or by environmental situations. A research area could concern on artificial intelligence, to create an intelligent system to predict any vehicle behavior and react instantly to solve the problem and also choose the best action to take.

THE PROPOSED APPROACH

The entire system is controlled by a button which allows the user to activate or deactivate the traction control system. The button was managed through the use of an MBSD, through it you can decide if and when to activate the TCS. When the TCS is activated, the values recorded by the pressure sensor and the steering-wheel inclination sensor are sent to the controller and then to the regulator, returning the value of the controlled power. On the other hand, when the TCS is deactivated, only the power is calculated as a function of the pressure and steering-wheel inclination, recorded by the relative sensors, without being sent to the regulator.

The network architecture has been structured as follows:

Are used two wireless networks.

To the first wireless network are connected the pedal pressure sensor, the steering-wheel inclination sensor and the gateway. To the second network are connected the controller, the regulator and the gateway. The two wireless networks communicate with each other through the gateway that belongs to both networks.

In the network architecture there are the following elements:

- Two sensors, one which detects the pressure exerted on the pedal and the other which detects the inclination of the steering-wheel and they respectively represent node 1 and node 2 of network 1;
- The gateway, which represents node 3 of network 1 and node 2 of network 2, receives messages from the sensors present in network 1 and sends them to the controller, which is located in network 2.
- A controller, which represents node 1 of network 2. It calculates the generated power, the revolutions of the wheels and the speed, according to the values received from the sensors.
- A regulator that represents node 3 of network 2. It is responsible for estimating the value of the friction between the wheels and the asphalt and managing the delivery of power according to it.

The sensors, the gateway, the controller and the regulator are implemented using TrueTime Kernel blocks, each of them is connected to a battery. Two TrueTime Wireless Network blocks were used to implement both networks.

The blocks communicate as follows:

- The two sensors read the pedal pressure and steering-wheel inclination values as input, encapsulate the following values in messages and send them to the gateway.
- The gateway listens to network 1 and receives the messages sent by both sensors, which will respectively contain the pressure exerted and the inclination of the steering-wheel. Then it will send the following messages to network 2 and in particular to the controller.
- The controller will receive from the gateway the two values recorded by the sensors. The pressure on the pedal will be used to calculate the power to be delivered, the number of revolutions of the wheels and the speed; the steering-wheel inclination value will be sent, together with the values just calculated (i.e.: power, wheel revolutions and speed), to the regulator.
- The regulator will receive the power, the number of revolutions made by the wheels and the speed wirelessly from the controller, and it will use the Fuzzy Logic Controller to estimate the friction values according to the quantities received. After estimating the friction between the wheels and the asphalt, he will take care of managing the power delivery. If the TCS is off, the regulator will not receive any value and the power won't be managed.

The type of network used is 802.15.4 ZigBee.

SCENARIO

To simulate our scenario, we first set the traction control system on or off function.

Power on/off

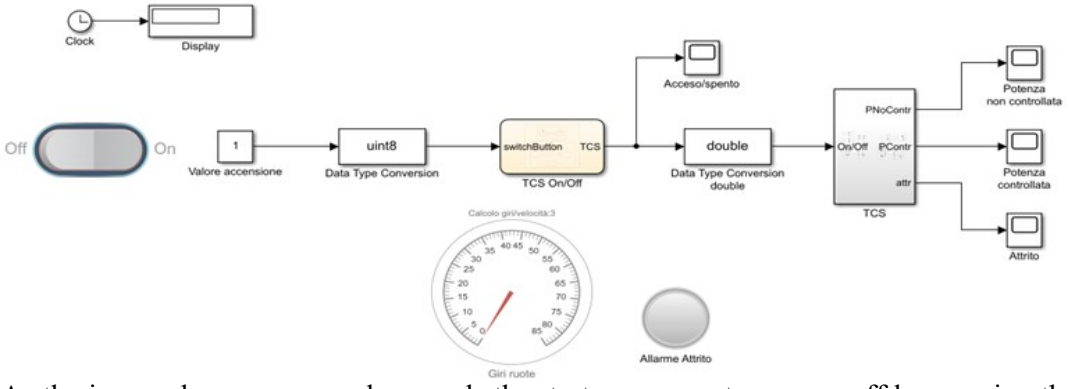

As the image shows, we can choose whether to turn our system on or off by pressing the on/off button. Power on and off is implemented using the debounced MBSD, in particular if the (On) button is pressed the constant block is set to one and we send the following value as input to the MBSD which carries out the check and switches to the on state. The output value is sent as input to the subsystem (TCS) and in particular to the regulator, where if turned on it will manage the power, otherwise it will not perform any power management. If instead the (Off) button is pressed, the constant block will be set to zero and consequently we will pass into state 1 (off).

Sensors

In our scenario there are two sensors belonging to the same network, respectively the sensor that detects the pressure of the pedal and the sensor that reads the inclination impressed on the steering-wheel, these two sensors are implemented with two TrueTime Kernel blocks connected to a battery.

In input to the first sensor there is a random number generator with values between [0 100] and sample time of one second to simulate pressure variations while driving, and the same is done for the second sensor with values between [0 90] and sample time of 0.5, where these values indicatively represent the degrees relating to the steering-wheel rotation. These sensors, once the input values have been read, send them to the gateway which belongs to both networks.

Controller

The controller receives the values recorded by the sensors from the gateway. After that, it sends the pressure as input to a MATLAB Function block, which calculates the power in Kw, the speed in m/s and the number of revolutions completed by the wheels considering the diameter of the latter; moreover, a random value is sent as input to this block which is used to simulate the static friction coefficient of the asphalt, that is to simulate any poorly adherent asphalt conditions, caused by various situations that may occur on the road.

Specifically, the number of revolutions of the wheels is added to the coefficient of the asphalt to simulate a possible increase in the number of revolutions compared to those generated by the power delivered.

A value of 43.18 cm was taken as the reference diameter of the wheel, and a constant k with a value of 0.4 was used to calculate the speed starting from the power.

Once the calculations have been made, the results are sent to the regulator, which will take care of reading these values and proceeding with the regulation.

The controller and its implementations are shown below:

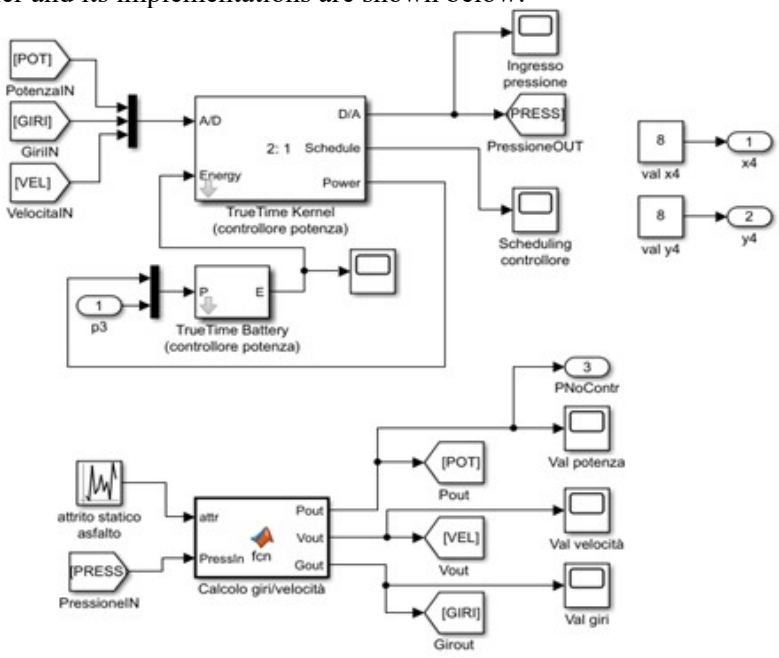

Regulator

The regulator receives from the controller the values of power, number of revolutions of the wheels, speed, degrees of the steering wheel and sends them in input to a Fuzzy Logic Controller to estimate what is the value of the friction between the wheels and the asphalt with a range between [0.1, 1].

Based on the input values, the Fuzzy Logic Controller estimates the following quantities:

- Low: if the friction is less than 0.3;
- Medium: if the friction is between 0.3 and 0.7;
- High: if the friction is higher than 0.7.

The estimated friction is sent as input, together with the power received from the controller to a MATLAB Function that manages the power delivery:

- if the friction is low, the power is set to a value equal to zero, that is no power is delivered;
- if the friction is medium, the power is decreased by 5 kW to recover grip;
- if the friction is high, the output power is equal to the input power, i.e. the effective power we are asking from the motor is delivered without making cuts.

Below is the image relating to the regulator and the fuzzy logic controller:

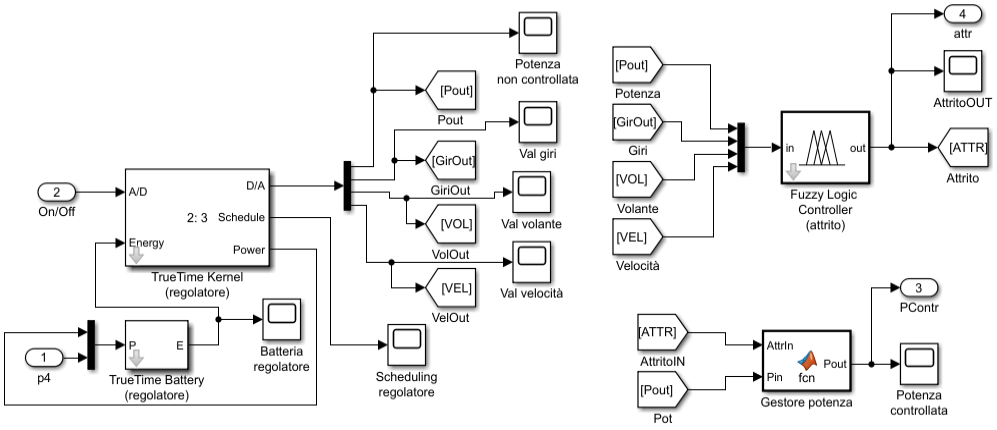

Led

Finally, we have implemented a LED with the use of an MBSD, to view the control action we are performing. The MBSD has three states, each represented by a color: green, yellow, red.

When the LED is red, we enter the first state and it means that the friction is less than 0.3 (low), and consequently we are cutting the power.

When the LED is yellow, we enter the second state, in an intermediate situation where the friction is medium and consequently, we decrease the power slightly.

When the LED is green, we enter the third state which represents an optimal situation where the friction is high and we are transferring all the required power.

The following MBSD with the LED is shown below:

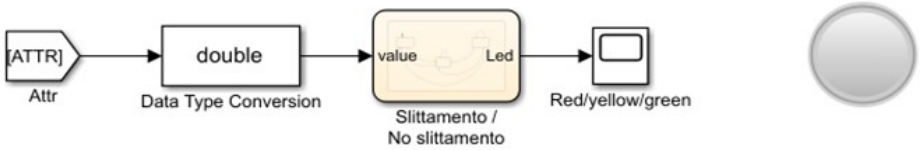

Final results

Below we show respectively the results of the check carried out, on the delivery of uncontrolled power, the value of controlled power and the value of friction.

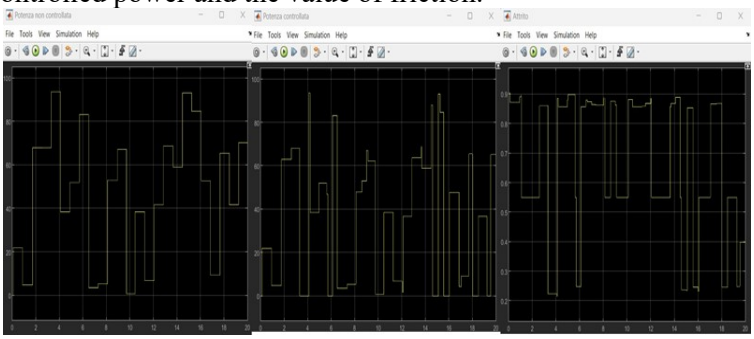

From the images you can see the power cuts in the respective points where the friction has a value of less than 0.3 and the uncontrolled power has high values, while doesn't make cuts where the required power is high and the friction is also high, otherwise decreases the power by 5 kW where the friction shows intermediate values.

PERFORMANCE EVALUATION

In systems of this type one of the most important aspects is the responsiveness and the number of checks that can be done. One of the main aspects is the speed of our system, in particular for the TCS it is important to have continuous feedback on the conditions in which we find ourselves, and to respond very quickly to critical situations. For this reason, the performances that we have analyzed are throughput, reaction time and response time, precisely because it is essential to understand how many measurements we are able to carry out and how long it takes to get feedback on these.

To make the measurements, we analyzed three 600-second simulations, making the measurements in three different instants of time, namely: [2-3], [300-301], [600-601] seconds.

First, we measured the number of packets sent by the sensors to the gateway and also those sent by the gateway, taking a one-second time sample and estimating an average of the values obtained. Our choice regarding the sample is due to the average frequency with which the driver varies the pressure of the pedal and acts on the steering wheel in normal driving situations and we have estimated that substantial variations are made in an interval of one second. We also made the measurements in three different temporal instants in particular in the intervals of [2-3] seconds, [300-301] seconds, [598-599] seconds. Below we show as an example a sample measured in the time interval [598-599], the results are as follows:

- We have estimated that an average of 20 packets are sent from the pressure sensor to the gateway in one second;
- We have estimated that an average of 21 packets are sent from the steering wheel sensor to the gateway in one second;
- For a total of 40 packets received in one second from the gateway by the sensors;
- While on average a total of 65 packets are sent in one second from the gateway to the controller.

As a second measure we analyzed the time it takes for the gateway from receiving the request to forwarding the packet to the controller, that is how much time passes from receiving the request to taking charge of it, and how long it takes for the system to receive the request at the beginning of the response. Also in this case we measured the performances by analyzing three samples in three different instants of time, for a total of 18 findings, below we show examples of some samples taken into consideration:

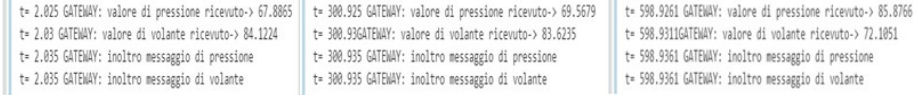

- We have seen that the average time it takes for a packet to actually be processed once it arrives at the gateway is 0.035 seconds.
- While the average time it takes for the system to send a packet from the gateway to the controller, that is the start of the system response, is 0.01 seconds.

Finally, as a last measurement we have considered the time that passes from sending the message to the gateway, to the response of the regulator, so, how long it takes our system from the moment the

request is made to the response of the system, to do this we used the same method applied before. Below we show an example of some samples:

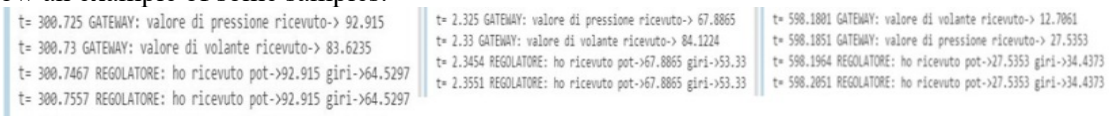

- We have obtained that the time it takes for the system to respond to the request made is 0.0324 seconds.

CONCLUSIONS

In conclusion, we can say that systems of this type are very important nowadays because they offer safety and allow the development of better performing cars by reducing tire and fuel consumption and offering a better and safer driving experience. However, systems of this type must be very precise and reactive because they must guarantee an immediate response and avoid inconveniences, and not return incorrect values.

Furthermore, in scenarios of this type it is very important not only to make precise calculations, but to have fast and precise communication and also to position the sensors and the entire network architecture in the correct way, to avoid disturbances and alterations of the transmitted messages.

REFERENCES

1. Matlab Simulink documentation MathWorks https://it.mathworks.com/help/matlab/
2. TRUETIME 2.0 – Reference Manual Anton Cervin Dan Henriksson Martin Ohlin Department of Automatic Control Lund University February 2016.

INDUSTRIAL DESIGN AS A METHOD OF POTENTIAL RISK AND SITUATION MANAGEMENT

Belova Maria
SaintPetersburg State University of Aerospace Instrumentation,
Saint Petersburg, Russia
E-mail: marebel13@mail.ru

Abstract. *Current trends dictate that current industries gain momentum in development and production capacity. Continuous improvements and the introduction of innovations allow enterprises to remain profitable in an environment of growing competition, which is caused by the opening of new fields of activity and the improvement of technologies. Each development, including a change in manufacturing technology, the introduction of new equipment, a change of suppliers, etc., contains certain risks that enterprises must calculate in order to avoid large losses [1].*

Table 1 shows examples of the main 7 types of losses that are common in production. Each loss brings its own losses, because of which many industries cannot reach a new level of development. Minimization of losses can be carried out with the help of Kobayashi's "20-key System", which consists of the introduction of a 100-point system that contributes to the creation of a systematic organization and the inclusion of these tools in the production process. The "20-key system" assumes that the "possession" of each of the keys will ensure the company's competitiveness in the market. The main task is to identify the leading types of activities and eliminate costly and non-profitable ones [2]. Thus, each enterprise must switch to lean technologies for successful development.

Table 1

Types of losses and their solutions

№	Types of losses	Example	Solution of losses created on the basis of the "20 key System" Kobayashi
1	Overproduction	Excess capacity of equipment	Rationalization of the management system (key 2) Accounting and distribution of working time (key 10) Production planning (key 16) General technology, production technology (key 20)
2	Excess stocks	Stocks of raw materials, semi-finished products, components	Ordering or bringing cleanliness and order (key 1) Reduction of inventory (key 4) Cost analysis of production operations (key 6)
3	Unnecessary transportation	Large distance between productions	Rationalization of the management system (key 2) Small group activities (key 3) Labor productivity management (key 17)
4	Unnecessary movements	Search for documents/tools	Ordering (key 1) Fast changeover technology (key 5) Related productions (Key 8) Production planning (Key 16) General technology, production technology (key 20)
5	Expectation	Waiting for approvals, inspections, decisions, permits	Maintenance of machinery and equipment (key 9) Accounting and distribution of working time (key 10)
6	Redundant processing	Redundant information flows	Reduction of inventory (key 4) Cost analysis of production operations (key 6) Energy saving and material saving (key 19)
7	Reject	Violation of technologies / additional costs for revision	Quality control system (key 11) Elimination of losses (key 13)

Problems in the organization from the point of view of lean technologies (lean manufacturing) are based on high costs and small profits from the products and services created. This concept divides technology processes into two categories: creating value and not adding value. Therefore, when implementing this technology, it is necessary to increase the number of the first and minimize the second.

Lean manufacturing includes 15 basic tools that need to be applied depending on the losses present in the enterprise (Fig. 1).

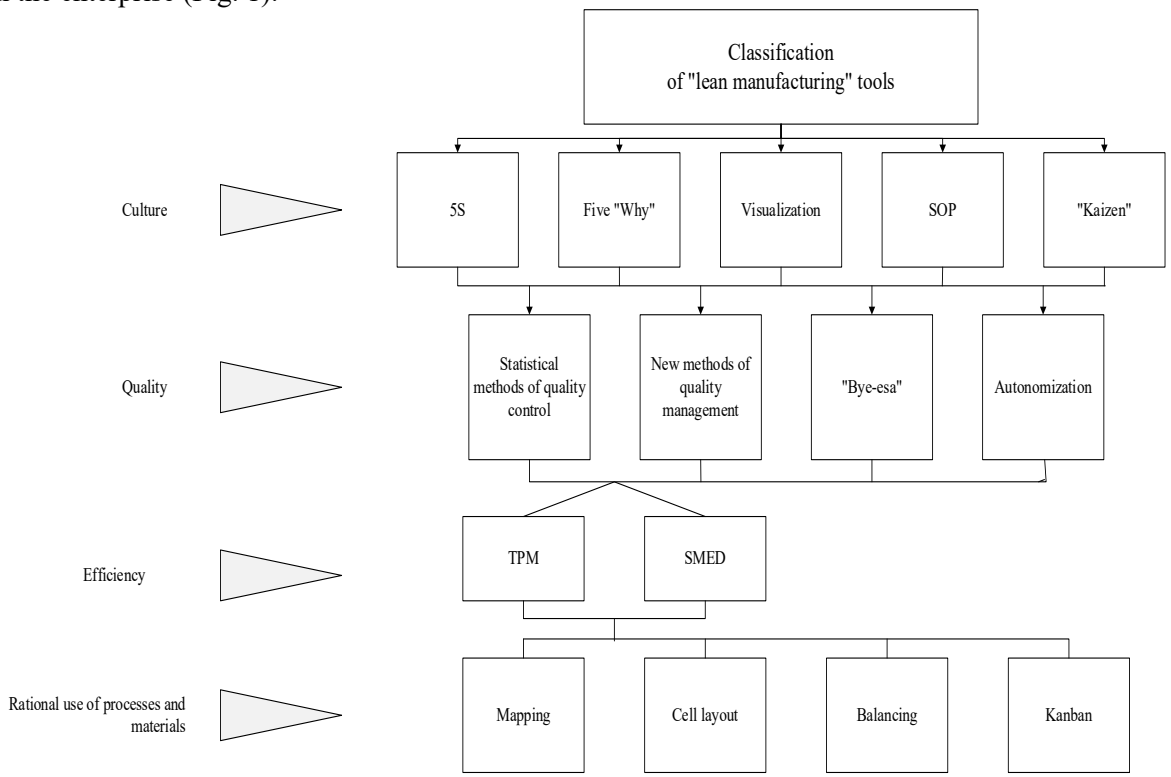

Fig. 1. Classification of "lean manufacturing" tools [3]

The inclusion of lean production tools in this process will not only reduce losses in the production chain, but also reduce costs, while increasing the capacity of the enterprise. As practice shows at the enterprises of the Russian Federation, 6 months after the introduction of this concept. the company is entering a new level of development, becoming competitive.

The tools are based on the main principles of operation [4]:

— Flexible approach (implementing tools into the system without breaking it);
— Creation of continuous updating of production of goods;
— Continuous improvement;
— Definition of the value stream.

Thus, production needs control, due to which it is possible to obtain data on the result of the introduction of lean production tools, evaluate them and determine all possible risks to minimize losses.

For competent process management, ensuring their continuous interaction, minimizing high-cost and similar actions, it is necessary to prepare production for the next level of development.

Since the production system should be dynamic in nature, be able to respond to a changing environment, while not contradicting its cost reduction strategy, then it is necessary to introduce such change and knowledge management that contributed to rapid development, met the requirements of trends, and also brought minimal losses.

Currently, a new paradigm of digital design and modeling is being actively developed and implemented (Fig. 2). Industrial design, originally designed to create the external design of mass-produced things, is becoming increasingly used and developed. Now industrial design is a system based on business models with certain technological conditions and a set of complex options for the development of customers' businesses. Industrial design as a traditional way of prototyping household appliances, production plants and their interfaces is fading into the background [5]. These technical capabilities allow us to apply the method of creating interfaces not only to the object, but to a system of objects, including a system of equipment that will be included in the technology of creating goods and services. Industrial design as part of the production control interface will display and control the running processes, preventing all risks and losses [6]. Thus, a simulation model will be created that includes not only graphical visualization of the process under study, but also has a contact parametric interface with the ability to monitor the process flow in real time and adjust its controlled parameters.

Digital twins for production systems are a separate type of organization of technical systems, which are based on the design base, management of production processes, control over them and ensuring joint functioning. Each production system contains a strategy aimed at reducing costs and production costs [3]. In the modern world, where development takes place daily and one system is being improved and replaced by another, in order for production to remain profitable and in demand, the production system must have a dynamic character – be able to respond to a changing environment and adapt to new concepts and technologies.

The personnel in the production at this time has a high qualification of training, but at the same time there are certain problems that consist in working within one template, which implies a large amount of time to change the type of activity, transition to another new task. Thus, the inflexibility of personnel and difficult-to-operate equipment are still key factors hindering the rapid transition to a new qualitative state of enterprise program concepts and, as a result, the introduction of new management systems.

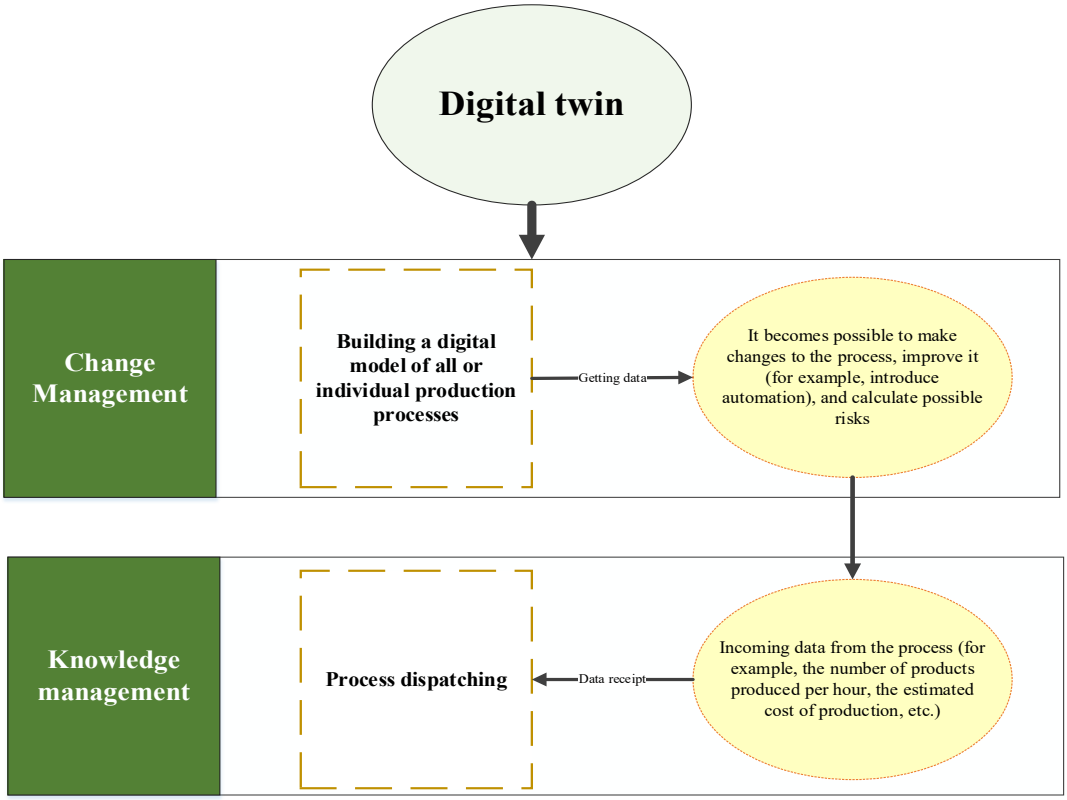

Fig. 2. Optimization of production processes by creating a mathematical model

The introduction of a digital twin will be effective at any stage of production:

1. At the initial stage of setting up the production process.

The digital twin is a simulation model supplemented not only with graphical visualization of the process under study, but also having a contact parametric interface with the ability to monitor the process flow in real time and adjust its controlled parameters. Digital doubles allow you to obtain valid data on the progress of the process, as well as to assess the risks when it changes.

2. At the stage of transition to a new process and its completion.

Digital dispatching allows you to control innovations, the course of unchanged processes, as well as the operation of the entire system. Digital control allows the company to quickly adapt to new conditions and trends, receive up-to-date data and use them effectively.

Thus, the use of digital design and modeling in practice will provide the greatest result for the integration of technological changes into the production processes of technological systems. It is the creation of digital equivalents that is a key component to the development of machine-building and instrument-making enterprises, therefore, the creation of machine-readable standards will be the first step towards the introduction of a digital ecosystem.

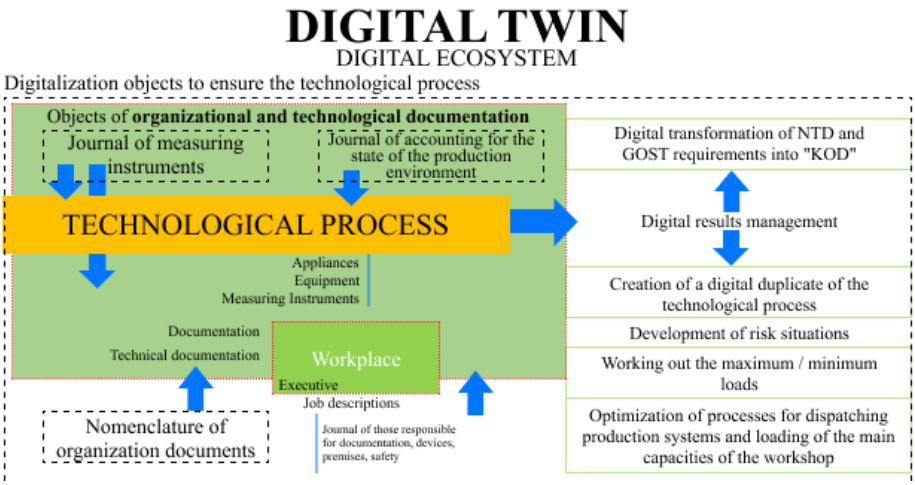

Fig. 3. Digital transformation of organizational and technological documentation

Fig. 3 shows a visualized process of transition from organizational and technological documentation on paper to a digital version, the transformation of which is achieved by transforming the NTD and GOST requirements into a "code" used in the future to create a digital duplicate of the technological process, working out risk situations and maximum/minimum loads, as well as optimizing the process.

Conclusion

The change of technological systems established by traditions in production processes occurs through great resistance caused by personnel performing monotonous and habitual activities based on outdated technical regulations, which is why changes should occur not with the introduction of a single management tool, but with a complete update of the approach to production development, which will occur with the least losses during preliminary creation a digitally adjustable model backed by a base of machine-readable standards available to both humans and machines. Thus, new approaches to development will provide a new level of output.

List of used literature

1. Frolov E.B., Klimov A. S. Digital twin of a production system based on MES software // Bulletin of the Bryansk State Technical University. 2018. No.12 (73). [Electronic resource] URL: https://cyberleninka.ru/article / (accessed: 02.04.2022).
2. Choosing priorities in the development of the production system. [Electronic resource] URL:https://www.cfin.ru/management / (accessed 04.04.2022).
3. Tarasov I. V. Industry 4.0: concept, concepts, development trends // Business strategies. 2018. №6 (50). [Electronic resource]URL: https://cyberleninka.ru/article/n/industriya-4-0-ponyatie-kontseptsii-tendentsii-razvitiya (accessed: 08.04.2022)
4. Tikhomirov S.G. Russian realities of using machine-readable format of normative documentation // Conference "Machine-readable standards: prospects of application in industry" 2021. [Electronic resource] URL: http://www.rgtr.ru/data/events/2021/маш_стандарты_25.02.2021 / (accessed: 11.04.2022).
5. GOST R ISO/IEC 15504-2-2009 Information technology. Evaluation of the process.Part 2 Evaluation. StandartInform.: M.-2009. – 18s.
6. Nazarevich S.A., Vinnichenko A.V., Kurlov V.V. Applicability of the reverse engineering model for unification tasks in the processes of system design of engineering enterprises. In the collection: A series of conferences JOP: Metrological support of innovative technologies. Krasnoyarsk Scientific and Technical City Hall of the Russian Union of Scientific and Engineering Associations. Krasnoyarsk, Russia, 2020. p. 52076.
7. V. P. Kupriyanovsky, O. N. Pokusaev, D. E. Namiot, A. A. Klimov, M. G. Zhabitsky Digital concrete: open BIM, machine-readable standards, Internet of Things, digital twins, logistics 4.0, lean construction and other industrial approaches using examples of transport infrastructures in the collection: International Journal of Open Information Technologies, 2021, pp. 133-173

RESEARCH OF THE CURRENT STATE OF IMPLEMENTATION OF SIMULATORS IN THE EDUCATIONAL AND CERTIFICATION FIELD OF ELECTRIC POWER INDUSTRY

Bobryshov Danil
Saint Petersburg State University of Aerospace Instrumentation,
Saint Petersburg, Russia
E-mail: danil.bobryshov@mail.ru

Abstract. *This article is devoted to the study of the current state of the problem of certification and training of employees of specialized organizations. It considers what a digital simulator is, its main tasks, functions and purpose. The main advantages of using such technology for educational purposes have been studied, it is worth noting the possibility of using this program not only for electric power companies, but also for training students of profile directions. The disadvantages of the considered technology are considered.*

The article presents the current recommendations, agreements and normative documents related to simulator training. At the same time, the requirements under consideration still applied to the personnel performing the training. The cases of distance learning implementation, in which simulators are the key instrument of training and certification, are considered.

The influence of correct decision probability of one group member on total group probability was considered. The influence of the probability of a wrong decision on the damage caused was assessed.

Purpose of electric power digital simulators

A digital simulator is a program or a system of programs that describes the functionality of a real object using mathematical dependencies on the basis of which the physical original works. The main task of such a digital analogue is to simulate the operation of a real object in order to study and understand the principle of operation and physical processes performed by the equipment and occurring in the simulated device. Basically, the direct purpose of digital simulators is for educational or certification purposes. For example, in the case of replacement or introduction of new equipment into the production process, using the twin program, it is possible to study the functionality and features of the production unit before its full implementation, and in the case of training, there is no need to occupy a working unit or allocate an additional one for personnel training.

The main advantage of mastering the equipment using the technology of digital simulators is a sufficient degree of safety of students. Using such systems, it is possible to simulate emergency and emergency situations, without the risk of harm to a person. Another advantage worth noting is the significantly lower cost of equipment and its maintenance in comparison with a digital copy. As a rule, a software product can contain several simulators of various industrial equipment, which is also a significant advantage and opens up the possibility of studying and mastering various systems. Another of the main advantages is the updating and maintenance of the program by the issuing company, updating the work and versions of the digital product. It is worth noting the possibility of working with the simulator from anywhere in the city and even the world, which is most relevant in the context of distance learning or the recent pandemic. There is no need to wait a long time for a physical sample to master it. The ability to run the program on several personal computers or other computing devices makes it possible to carry out training and testing simultaneously to a large group of people. There is no need to create a schedule and queue for the development of a new device. The relevance of the development of computer simulators lies in the propensity for the development of information technology. Constant complications of technological processes and the emergence of new control systems force high-quality training of all personnel. But developing information technologies open previously inaccessible horizons and opportunities. For example, the creation of new training and practice systems with equipment on a computer simulator that surpass their previous versions. Having the opportunity to try out absolutely any possible scenarios of working with equipment, regardless of the degree of their threat, allows you to conduct training more effectively than any other forms of training. The disadvantages include the accuracy of the parameters and the behavior of the system in complex production tasks, since the features of the location of the equipment under study, natural conditions, the condition of the elements, etc. may not be considered. An important fact is the likelihood of an emergency situation, breakage, disconnection of equipment elements or their incorrect functionality, most often such situations depend on the operating conditions of a real object.

The basis of training using a computer simulator is the formation of high–quality skills among employees, full orientation in goals and objectives. An employee with professional knowledge and skills that will allow him to quickly solve emerging problems in production should work with real equipment. The use of simulators to maintain the qualifications of personnel at the proper level contributes to the timely operational improvement of their professional level.

Regulatory requirements for personnel training using simulator technology

According to the national project "Digital Economy of the Russian Federation" As part of the implementation of Presidential Decrees No. 204 dated May 7, 2018 "On National goals and Strategic Objectives of the Development of the Russian Federation for the period up to 2024" and dated 07/21/2020. No. 474 "On the National Development Goals of the Russian Federation for the period up to 2030", including in order to solve the problem of ensuring the accelerated introduction of digital technologies in the economy and social sphere, the Government of the Russian Federation has formed the national program "Digital Economy of the Russian Federation" approved by the minutes of the meeting of the Presidium of the Council under the President of the Russian Federation for Strategic Development and national projects No. 7 dated June 4, 2019 [1]. The direction of the project called "Digital Technologies" is aimed at ensuring the technological independence of the state, the possibility of commercialization of domestic research and development, as well as accelerating the technological development of Russian companies and ensuring the competitiveness of their products and solutions in the market [2]. These draft laws are aimed at introducing new digital technologies into various spheres of human activity, and also form the directions for the development of technological independence of the state.

From the point of view of educational and certification activities, a scientific and practical conference "Using modern simulators to improve the level of education and practical skills of power system workers and students of energy specialties" was held in Minsk in 2017. It should be understood that the training of personnel using simulators should be regulated by the requirements. There are several documents developed by the working group of the CIS Electric Power Union describing the rules and agreements for the training of personnel in the electric power industry. It is immediately worth noting the agreement on cooperation of the CIS member states in the field of energy education, adopted by the Council of CIS Heads of Government Bishkek, Kyrgyz Republic, on June 7, 2016 [3]. Formed GOST 33066– 2014 "Organization of work with personnel in the electric power industry of the CIS member states", adopted by the Eurasian Council for Standardization, Metrology and Certification and registered No. 10147 on November 18, 2014 [4]. Draft recommendations for the introduction of distance learning for personnel of enterprises in the energy sector of the CIS member States, approved by the CIS Electric Power Council in accordance with Protocol No. 47 of May 26, 2015 [5]. Recommendations directly related to simulator training in the electric power industry of the CIS member States, approved by the CIS Electric Power Council in accordance with Protocol No. 51 of November 4, 2017 [6]. It is worth understanding the importance of personnel performing educational and certification functions of personnel using hardware and software tools. According to this, by the decision of the energy companies of the CIS member states, Protocol No. 51 of November 4, 2017, recommendations of the teaching staff were approved by the decision of the CIS Electric Power Council [7]. Methodological recommendations on the organization and conduct of Psychophysiological support of professional activity of personnel of electric power enterprises were also formed and approved. According to the decision of the CIS Electric Power Council, Protocol No. 50 of October 21, 2016 [8].

The latest approved recommendations confirm the request of specialized energy organizations in the development of digital simulators using virtual and augmented reality. This need was formed due to the detection of various kinds of phobias or inappropriate behavior among the staff in case of an emergency. For example, fear of heights or a lost state in the event of an emergency or non-standard situation, when the working staff is unable to perform decisive and correct actions. Such situations are quite difficult to simulate on real equipment, for training, due to the likelihood of a dangerous situation.

The organization of training should be organized not only by the formation of requirements and methodological recommendations for the organization or implementation of simulators, including digital ones. It should take into account the certification system, training requirements and similar rules to form a full-fledged system that organizes training and certification of personnel. Systems of voluntary certification in the field of training with the use of training equipment are already registered in Rosstandart.

For example, the rules for the functioning of the system of voluntary certification of software for training personnel in the electric power industry, the rules for voluntary certification of training instruc-

tors, the rules for voluntary certification of the system for diagnosing the quality of human capital of energy companies, etc.

This training is divided into primary, periodic, specialized, control-emergency and first aid. Since 2017, more than three thousand people have been trained in the distance format, using simulator training. The amount of training amounted to more than fifty thousand hours. It is worth noting that the introduction of distance learning has been carried out since 2006 [9].

Assessment of the feasibility of using simulator technologies in education and certification

From the above, it can be concluded that the introduction of digital simulators in the educational field will increase the degree of training and study of new equipment. Considering the degree of equipment development in this way of training, it is possible to assess the probability of making the right decision in an emergency situation and to determine the degree of damage to the enterprise.

$$P(A) = \sum_{i=1}^{n} P(H_i)P(A / H_i).$$

In this formula, P(A) is the probability of making a correct decision, P(Hi) is the weighting factor, P(A/Hi) is the probability of making a correct decision of a certain subject. Thus, the probability of making a correct decision by a group of 3 workers with separate probabilities of 0.8, 0.9 and 0.93, while the weighting coefficient of each subject will be 1/3, is 0.88. It is worth noting that the possibility of increasing the adoption of a correct decision is much higher with additional training of a worker with a lower probability of making a correct decision. Based on this, it is possible to assess the degree of damage caused in the event of an emergency.

The damage caused can be estimated using the following formula.

$$W_i = V_i(1 - P(A)).$$

In this formula, Wi is the damage from making a wrong decision, Vi is economic losses, P(A) is the probability of making a correct decision. Suppose the economic losses during the repair of a transformer substation of a residential building amounted to 20 million rubles. Let's assess the risks of two groups of electricians performing switching. Let's say the total probability of making a correct decision of the first group was 0.8, in which case the possible damage could amount to 4 million rubles. The probability of a correct decision of the second group is estimated at 0.92, in this case the damage will amount to 1.6 million rubles. By comparing the data of the probability of a correct decision with the damage received, you can get a graph.

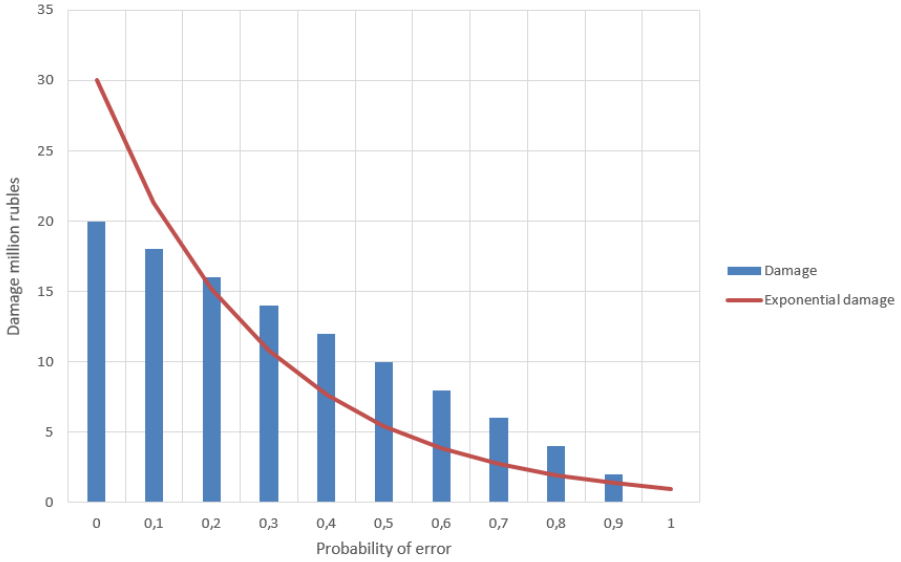

Fig. 1. Assessment of the damage of the enterprise depending on the degree of training of personnel

As can be seen from the graph, the degree of training of personnel directly affects the damage caused, while the graph also demonstrates the regularity of exponential reduction of damage from decision-making by personnel. Of course, in a real-life situation, there are significantly more factors determin-

ing the incorrectness of the decision or, in principle, the occurrence of an emergency situation, as mentioned above. But training is an important factor influencing the final result.

Conclusion

Summing up, it can be noted that the introduction and use of modern technologies for educational and certification purposes is an urgent and in-demand task. A striking example and impetus for the development of simulator technology is the development of new digital technologies and distance education. It is worth noting that at the moment there is a transformation of certification forms into a hybrid one, which includes both full-time and correspondence format. Another impetus to the development of such education and certification was not only the convenience and speed of learning, but also the global pandemic, during which all global companies and organizations had to use this method. At the same time, in the CIS countries, since 2006, the possibility of introducing additional education has been developed, and since 2015, agreements and regulatory documents have been adopted prescribing norms and actions on the topic of using the technology of simulators.

The theoretical evaluation showed a significant increase in the probability of correct results in the case of successful completion of training. To minimize the time spent and optimize the learning process, it is necessary to implement and use digital simulators that promote the development of new technologies. At the same time, it is possible to study various kinds of situations, including emergency ones, without threatening the life and health of the student. Reducing the probability of error reduces the financial damage that may occur in such a case.

References

1. The national program "Digital Economy of the Russian Federation". URL: https://digital.gov.ru/ru/activity/directions/858/?utm_referrer=https%3a%2f%2fyandex.ru%2f (Date of request: 20.02.22);

2. The project «The Digital Technologies». URL: https://digital.gov.ru/ru/activity/directions/878/ (Date of request: 22.02.22);

3. Agreement on cooperation of the member States of the Commonwealth of Independent States in the field of education in the field of electric power industry. URL: https://docs.cntd.ru/document/420390714 (Date of request: 24.02.22);

4. GOST ISO 33066-2014 Organization of work with personnel in the electric power industry of the CIS member states. URL: http://energo-cis.ru/wyswyg/file/RGK/Documents/ГОСТ33066-2014.pdf (Date of request: 27.02.22);

5. The project "Recommendations for the introduction of distance learning of personnel of enterprises in the field of electric power industry of the CIS member states". URL: https://online.zakon.kz/Document/?doc_id=37952342 (Date of request: 02.03.2023);

6. The project "Methodological recommendations on simulator training in the electric power industry of the CIS member states". URL: https://online.zakon.kz/Document/?doc_id=34736837 (Date of request: 03.03.2023);

7. The project "Recommendations for the qualification of teaching staff engaged in professional training of personnel of energy companies of the CIS member states using hardware and software". URL: https://continent-online.com/Document/?doc_id=33788094 (Date of request: 05.03.2023);

8. The project "Methodological recommendations on the organization and conduct of psychophysiological support of professional activity of personnel of electric power enterprises". URL: https://online.zakon.kz/Document/?doc_id=34764470 (Date of request: 09.03.2023);

9. Nikulicheva N.V., Dyakova O.I., Glukhovskaya O.S., Organization of distance learning at school, college, university. // Open education. No. 5. p. 4-17. (Date of request: 12.03.2023).

DATA PREPROCESSING IN MACHINE LEARNING

Bozhenko Viktoriya
Saint Petersburg State University of Aerospace Instrumentation,
Saint Petersburg, Russia
E-mail: vibozhenko@yandex.ru

Abstract. *The research describes the concept of data preprocessing, the main steps and features for effective analysis. The quality metrics of the models obtained from raw data and processed data are also compared. The research also presents the algorithm for cleaning and validation data before training machine learning models.*
Keywords: *data preprocessing, exploratory data analysis, machine learning.*

There are a lot of different data in many fields and their analysis and application of machine learning and artificial intelligence methods for predictions are relevant. However, preprocessing of data before direct training is one of the most important and labor-intensive steps, which is sometimes not performed properly. The majority of the real-world datasets for machine learning are quite dirty and corrupted with inconsistencies, noise, incomplete information and missing values. Data preprocessing is a method of data analysis, filtering, transformation and encodings to preparing the raw data and making it suitable for a machine learning model [1].

Fig.1 shows the steps that usually consist of preprocessing data [2]:

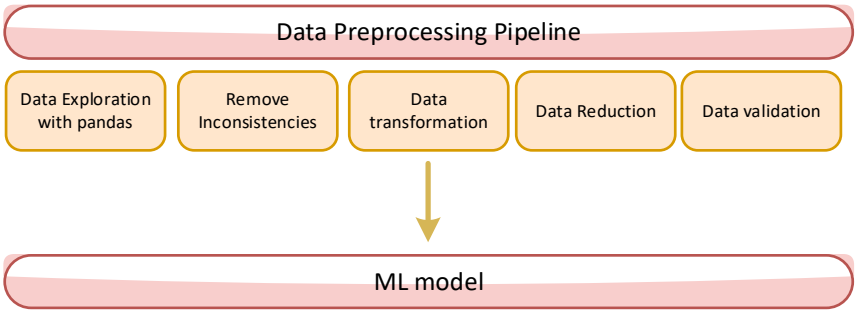

Fig. 1. Data preprocessing steps

1. Data evaluation or profiling:
- search for missing data,
- mismatching in data types,
- outliers in the dataset,
- abnormal data (incorrect spelling, incorrectly filled columns, duplicated data). Automatization the handling of such inconsistencies is one of the most difficult issues, and it is often necessary to resort to manual verification.

2. Data cleaning for fix the problems identified in the first step.
3. Data transformation – normalization, scaling.
4. Data reduction or compression – dimension reduction.
5. Data validation.

There are special libraries in programming languages such as Python that supports major functions for data analysis and make process easier, saving the user from manual data processing. For example, the pandas library is used to review data, handling missing values, duplicates. Standardization and normalization of data is performed using sklearn and the preprocessing functions [3].

However, without special knowledge, using of built-in functions will not bring the proper results, and at the moment the person who processes the data has a great responsibility for analysis output. Automation of this process is of interest, specifically, the development of a template that will become universal for different datasets and will help to perform part of the analysis without applying each function separately, but immediately perform a series of manipulations to clean up the data.

A program that allows to perform some preprocessing steps based on the uploaded dataset has been developed. The first step is to determine whether there are missing values in the dataset. Handling of missing values is an essential step of preprocessing. If there are no more than 10% of such values in the column, they are deleted. The data type is defined for each column. Empty values in quality columns are replaced with the value "unknown". For quantitative columns, empty values are replaced by mean, median or zero (an indicator that the value is missing). By default, the replacement is 0, but the user can call the function with a different argument, depending on the purpose of the analysis. There are more complex methods that require additional actions from the programmer such as replacement of missing values using interpolation or building a model to predict missing values [4].

Completely duplicated data is deleted in the program. The search for implicit duplicates is more difficult to automate, the developed function uses lemmatization [5] – a method of reducing words to normal form (lemma). Lemmatization allows to remove duplicates that differ only in word forms. This method is not perfect, but it helps to remove enough of implicit duplicates caused by errors or misprints in words.

Outliers can be detected and treated using box-plots [6]. An example of the graph is shown in Fig.2. Box-plots are used to identify the median, interquartile ranges and outliers. In the program box-plots are plotted for all quantitative columns, and outliers are removed from columns if the observation is 1.5 times the interquartile range exceeding the third quartile.

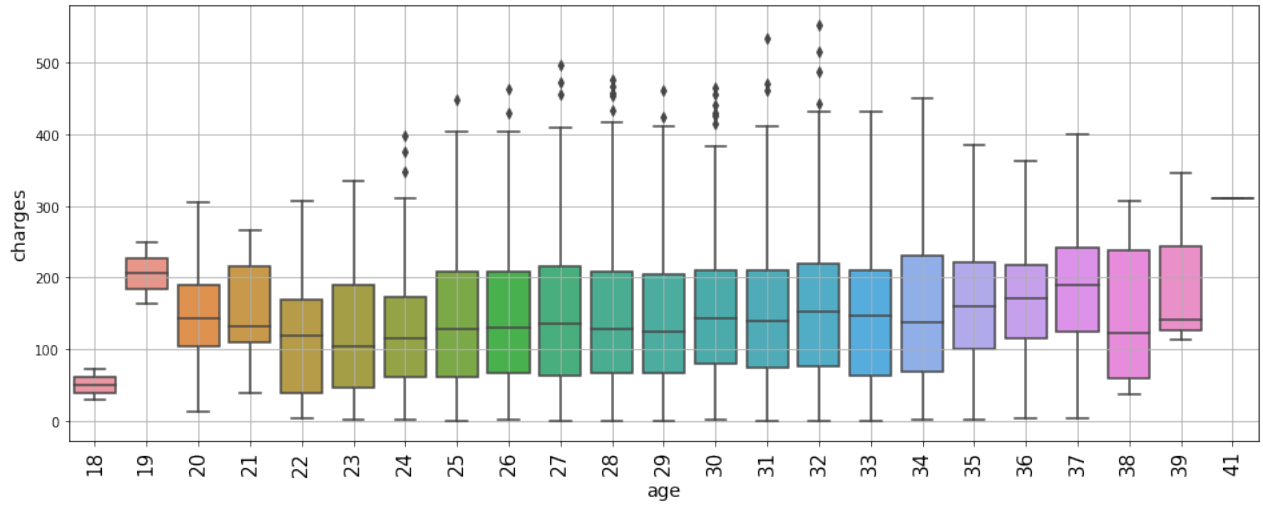

Fig. 2. Boxplot for distribution of age charges

Once data cleaning has been done, we need to use data transformation strategies. Two possibilities were implemented – the normalization using MinMaxScaler and standardization using StandardScaler from the sklearn library. Normalization helps to scale the data within a range to avoid building incorrect machine learning models in the future [7]. Scaling is especially important for distance-based models.

Sometimes, a column with string values, like names, will mean nothing to a model that depends only on numbers. So, to apply machine learning methods for qualitative data we need to process the data to help the model interpret it and we use One-hot-encoding. The categorical encoding method is applied to format string objects into numbers [8].

The next step of preprocessing is data reduction. This reduces the size of data by encoding mechanisms. Dimensionality reduction can be performed using techniques like Principal Component Analysis. Feature selection is the process of deciding which features are most essential to your analysis. It is also recommended to remove of multicollinear objects [7]. For example, if there are two variables that have a high correlation with each other, then it would be advisable to discard one of these features. At the same time, the attribute that has a lower correlation with the target attribute is discarded. This is necessary to remove of redundant information in the data in order to avoid bias of the model during training.

After preprocessing, the data is validated. Validation involves feeding the data into a machine-learning model to test its performance [2]. The main components of data quality include:

- completeness without missing attribute values,
- accuracy and reliability of information (absence of anomalies, such as negative age and others),
- matching data types,

- absence of redundancy.

In the research the classification problem was solved using the random forest method – determining the presence of a disease by various indicators, and Fig. 3 shows the quality metrics Accuracy, Recall and Precision [9] for two datasets: raw data without preprocessing and prepared data without missing values, duplicates were processed, after normalization. Obviously, all quality metrics are higher for preprocessed data.

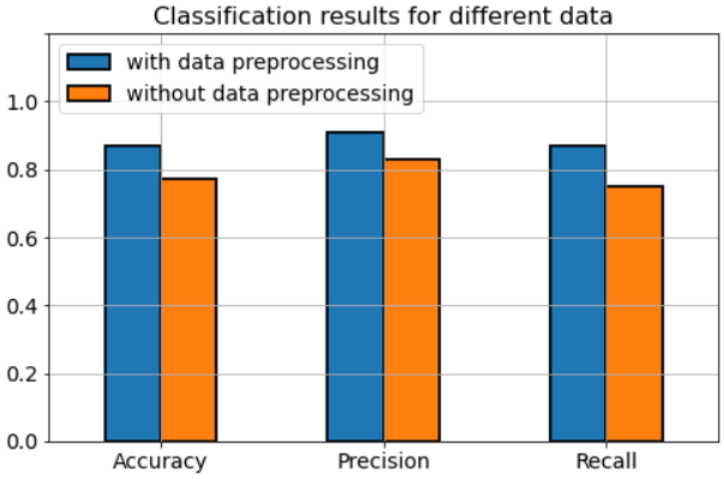

Fig. 3. The diagram of metrics for classification for different data

This indicates that the raw data before cleaning and preprocessing is usually not ready to obtain correct conclusions and qualitative results, using of models on raw data can lead to incorrect results, and sometimes raw data is completely unsuitable for analysis and using of machine learning methods is impossible. For example, if data contains errors, such as an incorrect name, a string type in a column with numbers, a large number of missing values, that data will not be able to be submitted to the model input for making a forecast.

In conclusion, good, preprocessed data can be as important as the most powerful algorithms and effective decision-making requires correct, prepared data. Machine learning is completely useless without the right data. Data preprocessing is essential tasks to making data suitable for a machine learning which also increases the accuracy and efficiency of training models.

References

1. David Mertz. Cleaning Data for Effective Data Science. Birmingham: Packt Publishing, 2021. 498 p.
2. Data Preprocessing in 2023, URL: https://research.aimultiple.com/data-preprocessing/
3. Data Preprocessing, URL: https://scikit-learn.ru/6-3-preprocessing-data/
4. Statistical Information Recovery from Multivariate Noise-Multiplied Data, a Computational Approach / Y.Lin, L.Mazur, R.Sarathy, K.Muralidhar // Ttansactions on Data Privacy, 2018.№11. P.23-45.
5. Stemming and Lemmatization in Python, URL: https://www.datacamp.com/tutorial/stemming-lemmatization-python
6. Understanding and interpreting box plots, URL: https://www.wellbeingatschool.org.nz/information-sheet/understanding-and-interpreting-box-plots
7. Mckinney Wes. Python for Data Analysis. M: DMK-Press, 2020. 540 p.
8. Data Preprocessing in Python, URL: https://medium.datadriveninvestor.com/data-preprocessing-3cd01eefd438
9. Bozhenko V.V., Klukanov V.K. Application of machine learning algorithms for classification and clustering // 2nd scientific conference «Information processing, transmission and protection in computer systems» (St.-Petersburg, April 11 – 15, 2022) / SPb.: Published by GUAP, 2022. P. 28-33.

DEVELOPMENT OF A DEVICE FOR AUTOMATING THE VERIFICATION OF MANUAL DIGITAL MEASURING INSTRUMENTS.

Casadio Daniele
Saint Petersburg State University of Aerospace Instrumentation,
Saint Petersburg, Russia
E-mail: kazdanila@gmail.com

To speed up the process and increase the efficiency of verification, a machine vision system was developed. This solution is optimally suited for calibration laboratories that use or implement verification automation in their work. It is important to note that the system does not perform mathematical or statistical processing of the recognized values – the recognized readings are transmitted according to the "here and now" principle. All operations for further processing of measured values are already performed by the user in some specialized software (Fig. 1).

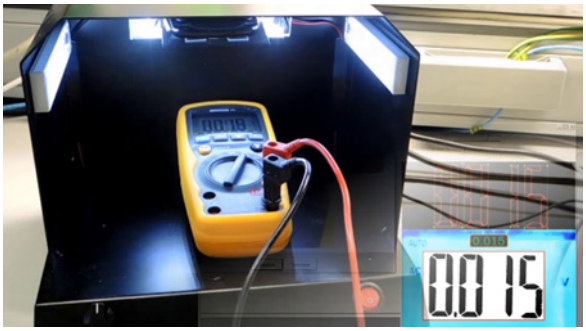

Fig. 1. Verification device

A multimeter is a multifunctional electrical measuring instrument. Its main purpose is to measure the characteristics of an electrical signal. Functionally, the multimeter combines the capabilities of an ammeter, voltmeter, ohmmeter and other electrical measuring instruments. This is a standard and common device used to solve various problems: diagnostics and repair of machines, installation and adjustment of electrical systems of buildings and equipment, production of electronic products, metrological control of measuring instruments, and others.

Digital multimeters are modern, reliable measuring devices characterized by high measurement accuracy and diverse functionality. Digital devices have replaced analog ones due to the possibility of wide application of semiconductor technologies. Currently, most of the manufactured multimeters are digital. Specialists working with electrical equipment, if necessary, can choose a model among digital multimeters that is focused on specific highly specialized tasks. Devices intended for professional use must be included in the State Register of Measuring Instruments and certified in an accredited laboratory within the established calibration interval. The advantages of digital multimeters are:

The highest possible measurement accuracy; Automatic polarity detection: if the probes are connected incorrectly, the correct values \u200b\u200bwith a minus sign will be displayed on the screen; Possibility of automatic and manual selection of measurement ranges; Multifunctionality; Does not require mandatory zero adjustment; The accuracy of the multimeter readings does not depend on the battery charge; Resistance to mechanical damage.

Machine vision is the application of computer vision to industry and manufacturing. While computer vision is a general set of techniques that allow computers to see, the field of interest of machine vision, as an engineering branch, is digital input / output devices and computer networks designed to control manufacturing equipment, such as robotic arms or machines for extracting defective products. Machine vision is a subsection of engineering related to computing, optics, mechanical engineering and industrial automation.

Measuring instrument – a technical instrument intended for measurements, having normalized metrological characteristics, reproducing and (or) storing a unit of physical quantity, the size of which is taken unchanged (within a specified error) for a known time interval.

A measuring instrument is a technical instrument used in measurements and having normalized metrological properties. Measuring instruments include measures and measuring instruments, converters,

installations and systems. The correct determination of the value of the measured quantity during the measurement process depends on the measuring instruments.

A measure is a measuring instrument designed to reproduce a physical quantity of a given size. For example, a weight is a measure of mass, a measuring resistor is a measure of electrical resistance, etc. Measures also include reference materials and reference substances.

If the measure must be used exclusively with values calculated according to the operating instructions, taking into account the amendments given in the accompanying documentation, then the measure is used not with a nominal, but with a real value.

An unambiguous measure reproduces a physical quantity of the same size. In fact, it reproduces either a unit of measurement or some specific numerical value of a given physical quantity. For example, a resistance measuring coil, a weight, a plane-parallel gauge block, a measuring bulb, a measuring resistor, a normal element, a capacitor of constant capacitance.

Sets of measures are assembled from unambiguous measures. A set of measures is a specially selected set of measures used not only individually, but also in various combinations in order to reproduce a number of similarly named quantities of various sizes, for example, a set of measuring capacitors, a set of plane-parallel end blocks of length, a set of weights.

A multi-valued measure reproduces a number of similar quantities of various sizes, for example, a variable capacitor, an inductance variometer, rulers with millimeter divisions.

Reference measuring instruments are designed to transfer the dimensions of units of physical quantities from standards or more accurate exemplary instruments to working instruments (Fig. 2).

Fig. 2. Reference for a multimeter

Reference measuring instruments are measures, measuring instruments and devices that have passed metrological certification and approved by state or departmental metrological service bodies as reference ones. According to the purpose, it is necessary to distinguish between the original and subordinate reference measuring instruments.

Reference measuring instruments are called initial, from which the size of the unit is transmitted with the highest accuracy in this subdivision of the metrological service.

Subordinates are called reference measuring instruments, to which the size of the unit is transmitted from the original reference measuring instrument directly or through other reference measuring instruments.

A simple analysis of the fleet of measuring instruments allows us to conclude that 50 – 70% of the total volume of instruments are hand-held digital measuring instruments. Verification of a multimeter, at first glance, the device, takes time comparable to verification of a desktop laboratory multimeter. If you only look at the number of modes in which such a hand-held multimeter can measure, analyze the number of measurement limits and the number of verified points, then the size of the verification protocol for such a device can be quite comparable in volume with the verification protocol for a desktop multimeter.

If we estimate the number of such devices in the park, we can see how big the load on the verification officers is.

Automation of verification of such devices becomes more complicated, since in most cases such measuring instruments do not have the ability to connect to a computer. This is also due to the price segment of this type of devices (Fig. 3).

Fig. 3. Analog multimeter verification

Solution for automatic recognition of readings of manual digital measuring instruments. The system supports any models of webcams provided that a set of drivers is available. Webcam operation modes (brightness, contrast) are controlled using the webcam driver. Possibility of training the program for different display of numbers (different display fonts) and saving them to the library – training can be carried out by the end user.

The optimal set of tools for adjusting the webcam image.

Conclusion

Automation helps to increase the number of verifications and their efficiency. This keeps manual operations to a minimum, allowing the same high speed to be maintained throughout the process. The overall performance is greatly improved. The big advantage is that repetitive and exhausting manual tasks can be left to the machine. Automation of such tasks provides an increase in the overall level of working conditions. The machines can run continuously at the same speed and settings, which improves the parameters of the production process in terms of the repeatability of the components under test and their compliance with quality specifications. Reducing the number of incorrectly performed verifications is one of the main advantages of this device.

List of used literature:

[1] Pavel Kosushkin Edition: Vector High Technologies No. 2 (23) 2016

[2] International Vocabulary of Metrology – Basic and General Concepts and Related Terms (VIM). 3rd edition (bilingual E/F).

EXPLORATION OPTICAL INTERFERENTION INFLUENCE ON LI-FI DATA TRANSMISSION

Davidovich Boris
Saint Petersburg State University of Aerospace Instrumentation
E-mail: davidovichborisvladimir@yandex.ru

Abstract. *This article presents the visible light range signal transmission technology study results. An experiment on data transmission via VLC was conducted. The results of the experiment were evaluated.*
Keywords: *optics, data transmission, noise immunity, sensor, processing, noise, illumination, filtering.*

Light fidelity (Li-Fi) is a wireless network technology based on the principle of visible optical range signal transmitting. The first device using this technology was created in 2016 by Lucibel and Pure Life. The Li-Fi technology allows to increase the number of connected devices and achieve connection rates above 10 Gbit/s [1].

Li-Fi networks can have both simplex and duplex communication channels using Visible Light Communication (VLC) technology. Blue phosphor-coated LEDs, gallium nitride microLEDs, RGB LED lamps should be installed in the transmitter, and a photodiode or photoresistor should be installed in the receiver to create VLC a simplex communication channel. In duplex communication systems, infrared LEDs are used as the second channel.

The Li-Fi network topology has a number of differences from the classical topologies such as point-to-point, ring and star (Fig. 1).

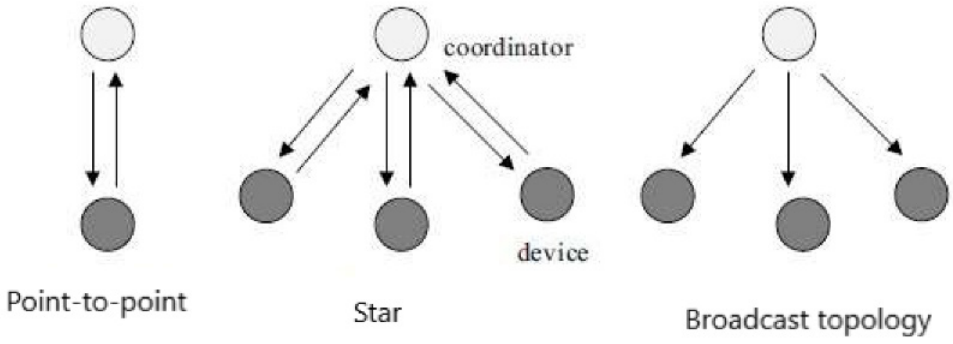

Fig. 1. Li-Fi network topologies

Каждое устройство, подключенное к сети Li-Fi, имеет уникальный 64-битный адрес, также по запросу во время коммутации устройству может присваиваться 16-битный адрес.

На рисунке 2 представлен стек протоколов, используемый в приемо-передающих устройствах работящих по технологии Li-Fi.

Each Li-Fi network device has a unique 64-bit address. A 16-bit address can also be assigned to the device during switching upon request.

Fig. 2 shows the protocol stack used in Li-Fi transceivers.

The protocol stack includes an optical transmission medium (Optical Medium); physical layer (PHY); a medium access control layer (MAC) and an intermediate service (SSCC) that provides its connection with the upper layers; logical link control layer (LLC); upper layers such as network and application. The optical medium represents one or more light sources. The physical layer includes transceivers, switches and commutators. In order to provide access for control signals physical addresses are assigned to devices at the MAC layer. Layered API (SAP) links these layers to the Device Management Entity (DME). The brightness is controlled by a power regulator (Dimmer) connected to the DME, which ensures its interaction with the PHY and MAC layers [2].

VLC (or LiFi) supports three types of physical layer configurations: PHY-I, PHY-II, PHY-III. Various configurations allow achieving different data transfer rates. LiFi networks can be used both indoors and outdoors.

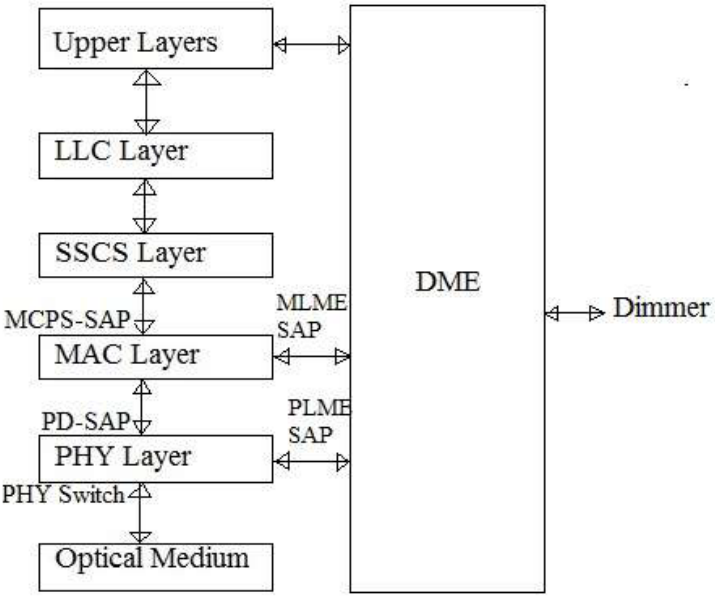

Fig. 2. Li-Fi protocol stack

These are various signal modulation schemes which are used depending on physical layer configuration:

- OOK – modulation "on-off key";
- VPPM – variable pulse position modulation;
- CSK – color switching.

Consider connecting two microcontrollers of the Atmel Atmega328PU family via simplex communication using VLC technology.

The diagram of the receiver and transmitter is shown in Fig. 3.

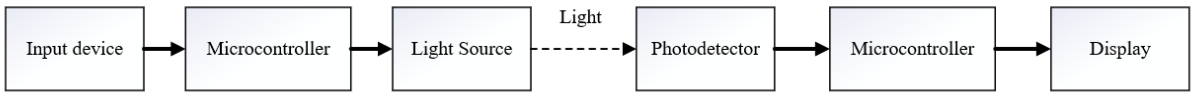

Fig. 3. Communication diagram of microcontrollers using VLC technology

Membrane keyboard 4×4 is the information input device.

The red LED BL-L102URC is the light source.

GL5516 photoresistor works as the photodetector. В качестве устройства отображения выбран ЖК-дисплей 2004.

The transmitter will operate using OOK modulation. A program written in the Arduino IDE executes the microcontrollers management. The layout scheme is shown in Fig. 4.

As a result, keyboard input was transferred between two devices using VLC technology (Fig. 5).

The experiment on signal transmission in the visible range between two microcontrollers can be considered successful.

Consider the mathematical apparatus necessary for Li-Fi data transmission. Orthogonal frequency division OFDM is a method of encoding digital data on multiple carrier frequencies, in which the input data stream is divided into parallel sub–streams with a lower data rate that modulate several subcarrier frequencies. The frequency-selective channel appears flat for each subcarrier as the transmission rate on parallel subcarriers decreases. Consequently, OFDM effectively converts a broadband frequency selective channel into a set of parallel narrowband channels with flat fading. OFDM has an advantage over frequency division multiplexing (FDM) in terms of spectral efficiency. The OFDM system consists of a fast Fourier Transform (FFT) and a parallel-serial converter on the transmitting side. A series-parallel converter and a fast reverse Fourier transform device are installed on the receiving side. The channel is optical, a light signal from an optical source propagates through it.

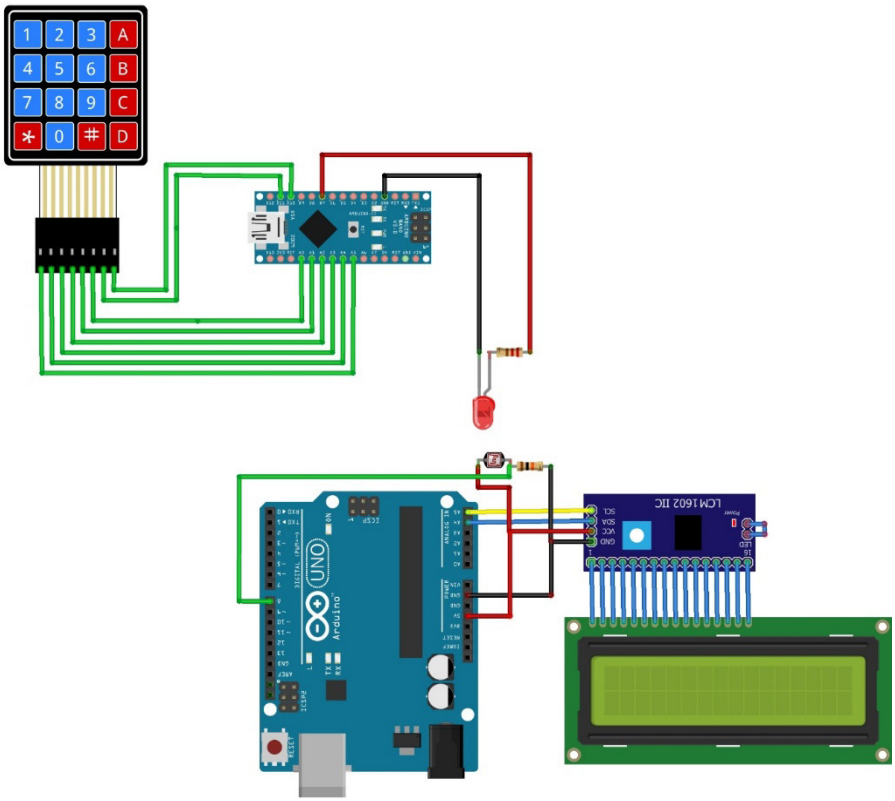

Fig. 4. The layout scheme

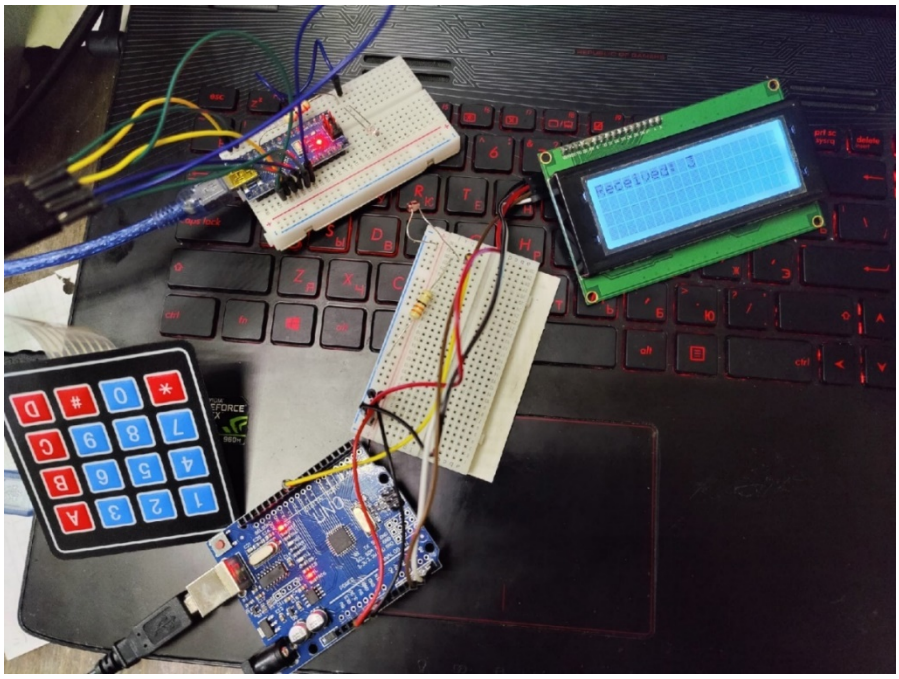

Fig. 5. Data transmission

The Hadamard transform (also known as the Walsh-Hadamard transform or Walsh transform) belongs to the class of Fourier transforms. It performs an orthogonal, symmetric, linear operation on 2^m real or complex numbers, (it must be noticed that the Hadamard matrices themselves are real). Hadamard Coded Modulation HCM, using a binary Hadamard matrix, is an alternative to OFDM. The HCM signal $x = [x_0, x_1, \ldots x_{N-1}]^T$ s generated from a data sequence u = $[u_0, u_1, \ldots u_{N-1}]^T$:

$$x = \left(H_N u + \bar{H}_N \bar{u}\right) \tag{1}$$

H_N – N order binary Hadamard matrix, $\bar{H}_N$ – matrix complementary to H_N, ($H_N - \bar{H}_N$) – Hadamard matrix. Hadamard matrices are square and bipolar matrices (that is, they contain only +1 or –1), the rows and columns of which are mutually orthogonal. It is assumed that the u components are M-ary pulse amplitude modulation (M-PAM) The computational complexity of HCM is equivalent to OFDM, since when calculating FWHT of size N, expressions of the order $N * \log_2 N$ are used. Binary Hadamard matrices are used to encode the input data stream. If N is a non-negative power of 2, the Hadamard matrix $N \times N$, denoted by H_N, is defined recursively as follows:

$$H_{2N} = \begin{bmatrix} H_N & H_N \\ H_N & -H_N \end{bmatrix} \tag{2}$$

The Hadamard matrix $N \times N$ has the following property

$$H_N H_N{}^T = N I_N, \tag{3}$$

I_N is a unit matrix of size N by N [4].

Consider a data transmission system using OFDM.

System parameters for OFDM: FFT size: 64, Number of tones used 52 (12 zero tones), Number of pilot signals 4 (data tones = 52-4 = 48 tones), Bandwidth: 20 MHz, Subcarrier spacing: Δf = 20 MHz / 64 = 312.5 kHz, OFDM symbol duration: TFFT = 1/Δf = 3.2 microseconds, Cyclic prefix duration: TGI= 0.8 microseconds, signal duration: TOFDM signal=TFFT + TGI (Fig. 6).

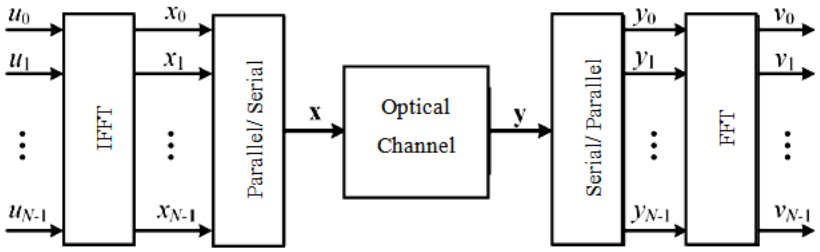

Fig. 6. General block diagram of the OFDM system

Consider a data transmission system using HCM.

FWHT size: 64, Number of tones used 52 (12 zero tones), Number of control signals 4 (data tones = 52-4 = 48 tones), Bandwidth: 20 MHz, Subcarrier spacing: Δf = 20 MHz / 64 = 312.5 kHz, Noise levels: -30 dBm, Cyclic prefix length: 4, the duration of the cyclic prefix: 0.8 microseconds (Fig. 7).

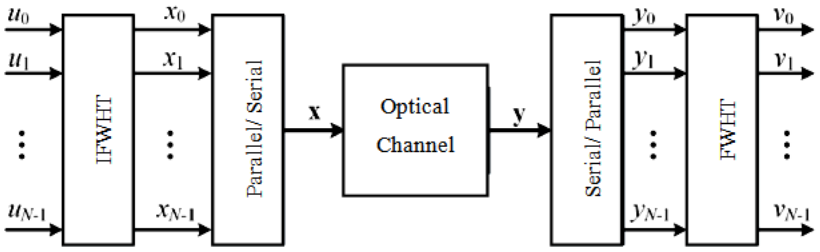

Fig. 7. General block diagram of the HCM system

The Hadamard code generator extracts individual orthogonal rows (a set of codes) from the matrix. Orthogonal codes can be used for propagation in communication systems in which the receiver is perfectly synchronized with the transmitter. The HCM transmitter performs coded Hadamard modulation of the input data [3]. As shown in Fig. 4.1, the u components are modulated using the expression (1).

Equation 1 can also be written as:

$$x = u\left(H_N + \bar{H}_N\right) + \frac{N}{2}[0,1,1\ldots\ldots1] \tag{4}$$

Let the first component of u be zero, then the M-PAM HTM calculation rate of is (N − 1)/N $\log_2 M$. Then, due to the fixed mutual correlation between these remaining N – 1 strings, the interference of Hadamard codewords with each other can be eliminated on the receiver side. Assuming that the noise due to the channel is additive white Gaussian noise (AWGN), BER M-PAM HCM is calculated:

$$BER_{HCM} = \frac{M-1}{M \log_2 M} Q\left(\sqrt{\frac{3}{M^2-1}} \frac{\sigma}{\sigma_2}\right) \quad (5)$$

The receiver for the HCM method is shown in Fig. 2. The decoded vector is obtained from the resulting vector as follows [5]:

$$v = \frac{1}{N}\left(yH_N{}^T - y\bar{H}_N{}^T\right) + \frac{1}{2}[1-N,1,1,\ldots 1] \quad (6)$$

bit error rate (BER) when using coded Hadamard modulation (HCM) for visible light communication is lower compared to orthogonal frequency division multiplexing (OFDM) for all power levels. The reason is that in the case of using coded Hadamard modulation, the ratio of the peak power of the signal to its average power (PAPR) is significantly lower. For an average optical power of 10 dB, the bit error rate is about $8 \cdot 10^{-2}$ for OFDM and $2 \cdot 10^{-2}$for HCM. That means HCM is better suited for communication using visible light [4]

Since the transmission is carried out using visible radiation, any external luminous flux can affect the quality of the signal. One of the sources of external illumination is sunlight. Li-Fi operates at high frequencies (more than 1 MHz), sunlight will be a constant component, so its influence can be eliminated by filtration. The study of the effect of shot noise on the quality of signal transmission [5] showed that the data transmission rate is reduced by 1.5% and 4.5%, provided that the detectors have dimensions of 0.19 mm^2 and 2 mm^2. Consequently, reducing the area of the detectors reduces the impact of shot noise. It is also necessary to take into account the influence of electrical appliances interference. They can be reduced by filters that suppress certain frequencies. For example, the refresh rate of a computer monitor does not exceed 140 Hz – significantly lower than the frequency of Li-Fi operation.

As a result of Li-Fi data transmission protocols analysis and the external interference study, it could be concluded that this is more noise-resistant than radio waves technologies.

References

1. Swarnkar, M., Bhadoria, R.S., Arya, K.V. (2018). Architectural Building Protocols for Li-Fi (Light Fidelity). In: Arya, K., Bhadoria, R., Chaudhari, N. (eds) Emerging Wireless Communication and Network Technologies. Springer, Singapore.

2. LiFi tutorial-LiFi network, protocol, PHY, MAC, bands, modulation URL:// https://www.rfwireless-world.com/Tutorials/LiFi-tutorial.html [Дата обращения 20.11.22]

3. Shrestha S. Hadamard Coded Modulation for Visible Light Communication // Journal of Nepal Physical Society. 2017. V. 4, №1, pp. 93-96. http://dx.doi.org/10.3126/jnphyssoc.v4i1.17342

4. . M.S. Islim, M. Safari, S. Videv, H. Haas A proof-of-concept of outdoor visible light communications in the presence of sunlight // LED Professional Symposium – Expo, 2016 (2016)

5. Z. Wang, D. Tsonev, S. Videv, H. Haas On the design of a solar-panel receiver for optical wireless communications with simultaneous energy harvesting // IEEE J. Sel. Areas Commun., 33 (8) (2015), pp. 1612-1623

APPLICATION OF QUASIORTHOGONAL CIRCULANTS FOR ENCODING IMAGES FROM PAYLOADS OF SMALL AIRCRAFTS

Devyatov Arkhip
Saint Petersburg State University of Aerospace Instrumentation,
Saint Petersburg, Russia
E-mail: xip2002@gmail.com

Abstract. *This article considers the general principles of encoding images from payloads of small aircrafts, using the example of the quadcopter DJI Mini 2. In this paper, special quasi-orthogonal circulants are used to encode images. Their advantages over the matrices of non-cyclic structure are considered. Images were masked and unmasked using matrices of different dimensions to determine whether the order of the matrix affected the formation of contours on the masked image.*
Keywords: *small aircrafts, encoding, quasi-orthogonal matrix, matrix masking.*

INTRODUCTION

An analysis of the scientific literature of recent [1-12] shows the active introduction of small aircrafts (SA) in such areas as land-surface mapping [4,6], data collection in restricted areas [1,5], environmental and agricultural monitoring [2-3,7-8], search and rescue operations [9,12], monitoring the state of smart cities [10-11], etc.

Frequently, information received from a payload is sent to a ground-based information and control center, where, depending on the situation, information is either promptly responded to or stored for post-processing.

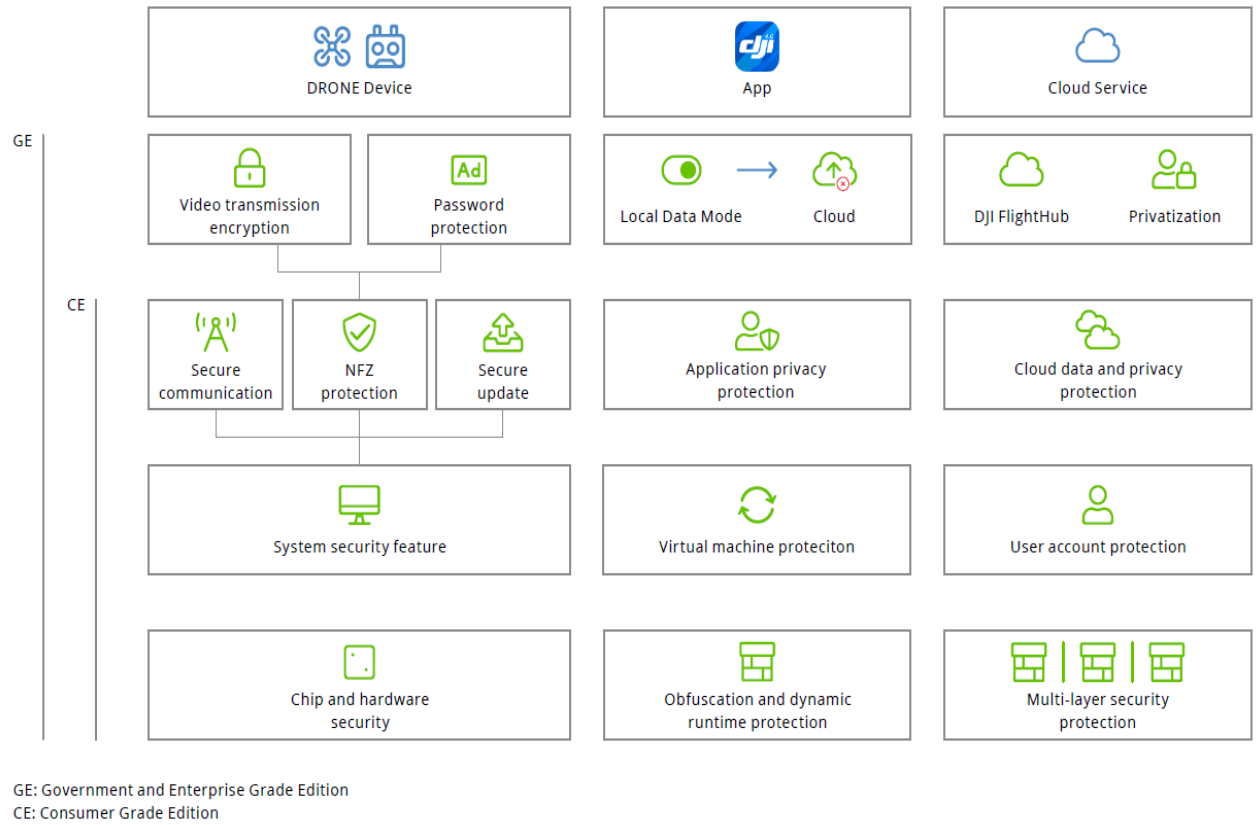

Fig. 1. DJI Quadcopters data privacy protection. Figure taken from [15]

Various sensors are used as payloads for SA monitoring systems, such as:

- television cameras;
- thermal imaging cameras;

- small-size on-board radar stations;
- multispectral cameras;
- gas analyzers;
- lidar;
- laser rangefinders,

as well as various options for their joint execution. At the same time, analysis of the SA payload market shows that in the consumer and commercial segment, optical sensors – photos and video cameras, multispectral cameras and thermal imagers [13] are most often used.

On the other hand, aerial photographs may contain confidential information that needs to be handled safely. It is essential to ensure the safe transmission and processing of SA optical sensor images, as these images may contain commercial secrets or may be obtained by third parties to the detriment of the mission operator.

Image and video encoding is the primary and effective means of securing and storing information from the SA`s payload [14]. Therefore, if the used data are not protected in a timely manner, the information obtained from the SA`s payload may be stolen, which may result in both reputational and financial losses and a risk to human safety.

Consider DJI's small aircraft as an example. Technical documentation analysis [15] shows that the SA`s communication channel – the control panel is encoded according to the AES standard for all quadcopters of the company, but the resulting video information is encoded only for the segment Enterprise and Government, as shown in Fig. 1. Therefore, it can be concluded that the most massive SA from the consumer segment (Mavic, Mini, Air and FPV series) are vulnerable to unauthorized access to video information.

Therefore, the confidentiality of photo and video information received from the consumer segment of the market by SA is a topical task, which is confirmed by scientific interest in this topic [16-19].

MATRIX MASKING, DEMASKING AND MATRIX SELECTION

To ensure the confidentiality of images, matrix masking and unmasking methods [20] are known in distributed systems, and their associated special orthogonal and quasi-orthogonal matrices [21]. Several definitions should be provided for certainty.

Definition 1. A quasi-orthogonal matrix is a square matrix A of order n, with unit maxima of the modules of each column satisfying the quadratic condition of the equation

$$\mathbf{A}^{\mathrm{T}}\mathbf{A} = \omega\mathbf{I},$$

where $\mathbf{I}$ – identity matrix; ω – degree of the matrix.

Definition 2. Matrix masking is the computational procedure of converting digital images using matrix operations, destroying it to a view perceived visually as noise.

Definition 3. Matrix unmasking is a computational inverse conversion using matrix operations to recover the original digital image from the masked one.

Since the masking quality of the image directly depends on the selection of the masking matrix, it is useful to search for such matrices. The work [22] discusses the merits of Adamar, Mersenne, Euler and Mersenne-Walsh matrices. These matrices for matrix masking are convenient in that no inverse matrix is required when performing an unmasking operation, because for orthogonal and quasi-orthogonal matrices $\mathbf{A}_n^{-1} = \mathbf{A}_n^{\mathrm{T}}$ is true. However, the matrices that are most convenient for practical implementation are those that also meet the following conditions:

- The matrix should be two-tiered if possible, as the increase in the number of levels inevitably entails memory costs for generating and storing information;
- The matrix should have the simplest possible design, ideally be a cyclic matrix, since then it is necessary to store only the first string (a circulant) for use.

These conditions are met by persimmetric quasi-orthogonal circulants based on Jacobi and Legendre symbols, as well as modified M-sequences considered in the works [23-25]. In this regard, it is advisable to consider their use to address the confidentiality of photos and video information from SA`s payload.

MASKING OF PAYLOAD INFORMATION BY PERSIMMETRIC QUASI-ORTHOGONAL CIRCULANTS

SA manufacturers often allow their communities to develop their own applications to add various software features to their products [26-28].

We will test the operation of double-sided matrix masking, in relation to the data obtained from the payload of the quadcopter of the consumer segment, namely DJI Mini 2, registration number 0462u74, which is shown in Fig. 2.

Fig. 2. DJI Mini 2

As an example, consider the process of masking the frames of the video stream obtained from the specified quadcopter. The flight mission was to fly around the perimeter of the gardening non-profit Wave, located at coordinates (59.215895, 31.448706).

Fig. 3 shows one of the video stream frames captured by the payload of the quadcopter, with Fig. 3a showing the original flow frame, Fig. 3b showing the masking result, and Fig. 3c showing the unmasking result. A masking matrix is a persimmetric quasi-orthogonal circulants based on a modified M sequence [24], size (7×7). As you can see, Fig. 3b does not show any clear contours that recognize the structure of the image shown in Fig. 3a.

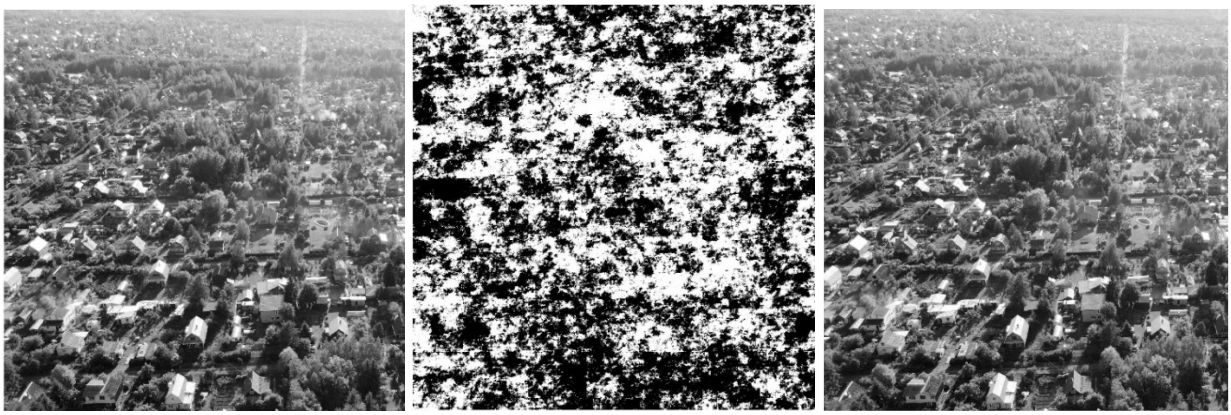

a) *b)* *c)*

Fig. 3. Original image (a), masking result (b), unmasking result (c)

Apply masking matrices of one structure – based on modified M-sequence, but of different orders – to test whether the order of the matrix affects the formation of contours on the masked image. The results are shown in Fig. 4.

a) Original image

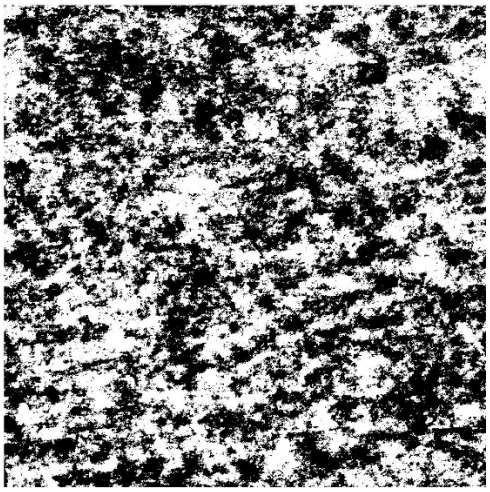

b) Matrix (255×255)

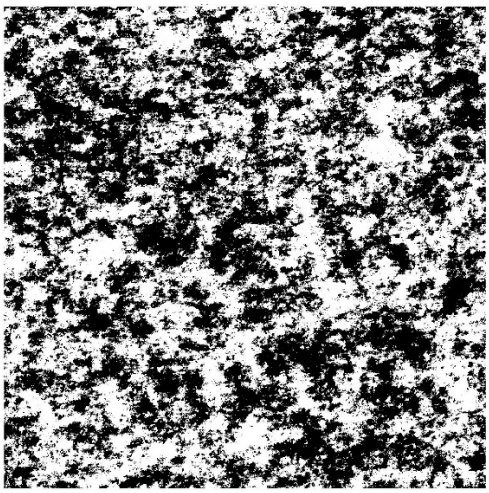

c) Matrix (63×63)

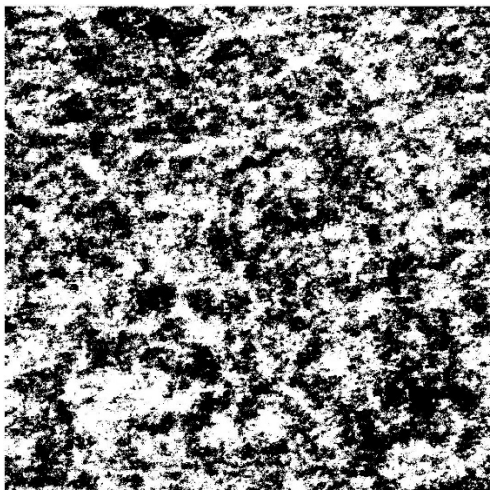

d) Matrix (511×511)

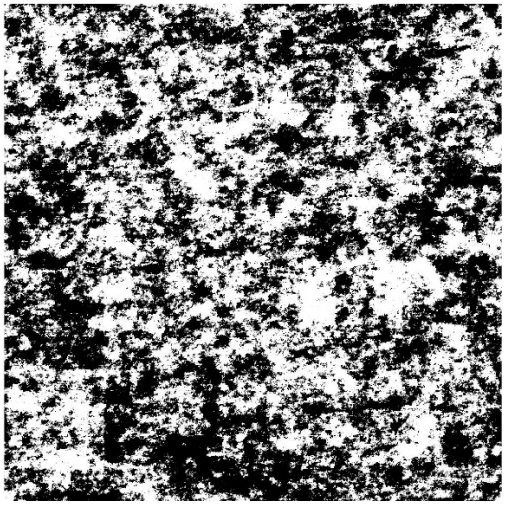

e) Matrix (15×15)

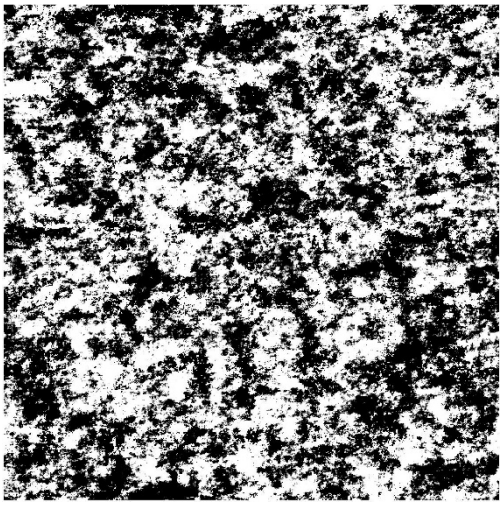

f) Matrix (127×127)

Fig. 4. Results of masking by different matrix orders

As you can see from the Figures, it is not possible to notice any structure masked (Fig. 4a – Fig. 4f).

CONCLUSION

The conducted research shows the relevance of the work on ensuring the confidentiality of information received by the payload of small aircraft of the consumer segment. In this area, an alternative to cryptographic methods may be matrix coding methods, such as masking, as it is a simple and efficient coding and decoding algorithm, whose complexity depends only on the complexity of the matrix multiplication algorithm, and is currently $O(n^{2.3728596})$.

Although the matrix masking operation and the choice of masking matrices have already been discussed in the scientific literature, the analysis of the work shows that the persimmetric quasi-orthogonal circulants have not yet been used for these purposes, but they are a good choice, because they meet the two-level criterion and are also cyclical [25]. Since no objective assessment of the quality of the original image to noise was found in the literature review, further work on developing such metrics would be useful.

ACKNOWLEDGMENT

The author expresses gratitude to the assistant lecturer of the Department of Computer Systems and Networks Grigoriev E.K. for scientific guidance in the preparation of this article.

REFERENCES

1. Shatalova, N. V. Potential of logistics development of the Arctic zone of the Russian Federation through the use of drones / N. V. Shatalova, O. M. Mikhov, O. V. Borodin // Marine intelligent technology. – 2021. – № 2-1(52). – С. 137-144. – DOI 10.37220/MIT.2021.52.2.020.

2. Matese, A.; Di Gennaro, S.F. Practical Applications of a Multisensor UAV Platform Based on Multispectral, Thermal and RGB High Resolution Images in Precision Viticulture. Agriculture 2018, 8, 116. https://doi.org/10.3390/agriculture8070116

3. M. Novák et al., "Multisensor UAV System for the Forest Monitoring," 2020 10th International Conference on Advanced Computer Information Technologies (ACIT), 2020, pp. 293-296, doi: 10.1109/ACIT49673.2020.9208993.

4. Lv, Z.; Qiu, X.; Cheng, Y.; Shangguan, S.; Li, F.; Ding, C. Multi-Rotor UAV-Borne PolInSAR Data Processing and Preliminary Analysis of Height Inversion in Urban Area. Remote Sens. 2022, 14, 2161. https://doi.org/10.3390/rs14092161

5. A. E. Ilyukhin, C. D. Bukharov, D. V. Dobrinin [et al.]. The use of a software and hardware complex on the basis of UAVs for solving the problems of operational monitoring of the SSVT. Works of P.G. Smidovich State Nature Reserve, Mordovia. – 2022. – № 30. – С. 216-228. – DOI 10.24412/cl-31646-2686-7117-2022-30-216-228.

6. Skondras, A.; Karachaliou, E.; Tavantzis, I.; Tokas, N.; Valari, E.; Skalidi, I.; Bouvet, G.A.; Stylianidis, E. UAV Mapping and 3D Modeling as a Tool for Promotion and Management of the Urban Space. Drones 2022, 6, 115. https://doi.org/10.3390/drones6050115

7. Ubina, N.A.; Cheng, S.-C. A Review of Unmanned System Technologies with Its Application to Aquaculture Farm Monitoring and Management. Drones 2022, 6, 12. https://doi.org/10.3390/drones6010012

8. Munawar, H.S.; Ullah, F.; Heravi, A.; Thaheem, M.J.; Maqsoom, A. Inspecting Buildings Using Drones and Computer Vision: A Machine Learning Approach to Detect Cracks and Damages. Drones 2022, 6, 5. https://doi.org/10.3390/drones6010005

9. Safarov, M. S. Application of modern remote sensing technologies for monitoring the selenium areas of mountain areas / M. S. Safarov, A. R. Fazylov // GeoRysk. – 2020. – Т. 14. – № 2. – С. 32-41. – DOI 10.25296/1997-8669-2020-14-2-32-41.

10. Ivashov, S. , Tataraidze, A. , Razevig, V. and Smirnova, E. Railway Transport Infrastructure Monitoring by UAVs and Satellites. Journal of Transportation Technologies 2019, 9, 342-353. doi: 10.4236/jtts.2019.93022.

11. Dimililer, K., Ever, Y.K., Al-Turjman, F. (2020). Machine Learning Applications for Internet of Flying Vehicles in Case of Critical and Environmental Cases. In: Al-Turjman, F. (eds) Unmanned Aerial Vehicles in Smart Cities. Unmanned System Technologies. Springer, Cham. https://doi.org/10.1007/978-3-030-38712-9_3

12. L. Qingqing et al., "Towards Active Vision with UAVs in Marine Search and Rescue: Analyzing Human Detection at Variable Altitudes," 2020 IEEE International Symposium on Safety, Security, and Rescue Robotics (SSRR), 2020, pp. 65-70, doi: 10.1109/SSRR50563.2020.9292596.

13. St. Petersburg [Electronic Resource] // Drone Usage Is Thriving in These Three U.S. States: https://www.businessinsider.com/drone-usage-is-thriving-in-these-three-us-states-2016-4 (date of access: 09.02.2023)

14. Allouch, A.; Cheikhrouhou, O.; Koubâa, A.; Toumi, K.; Khalgui, M.; Nguyen Gia, T. Utm-chain: Blockchain-based secure unmanned traffic management for internet of drones. Sensors 2021, 21, 3049.

15. St. Petersburg [Electronic Resource] // DJI – The World Leader in Camera Drones: https://security.dji.com/data/resources/ (date of access: 09.02.2023)

16. Alrayes, F.S.; Alotaibi, S.S.; Alissa, K.A.; Maashi, M.; Alhogail, A.; Alotaibi, N.; Mohsen, H.; Motwakel, A. Artificial Intelligence-Based Secure Communication and Classification for Drone-Enabled Emergency Monitoring Systems. Drones 2022, 6, 222. https://doi.org/10.3390/drones6090222

17. Bera, B.; Chattaraj, D.; Das, A.K. Designing secure blockchain-based access control scheme in IoT-enabled Internet of Drones deployment. Comput. Commun. 2020, 153, 229–249.

18. Alawida, M.; Teh, J.S.; Alshoura, W.H. A New Image Encryption Algorithm Based on DNA State Machine for UAV Data Encryption. Drones 2023, 7, 38. https://doi.org/10.3390/drones7010038

19. Dong, J.; Wu, G.; Yang, T.; Li, Y. The Improved Image Scrambling Algorithm for the Wireless Image Transmission Systems of UAVs. Sensors 2018, 18, 3430. https://doi.org/10.3390/s18103430

20. Vostrikov, A. A. Digital Visual Information Masking: Term and Basic Definitions / A. A. Vostrikov, M. B. Sergeev, M. Y. Litvinov // Information management systems. – 2015. – № 5(78). – C. 116-123. – DOI 10.15217/issn1684-8853.2015.5.116.

21. Balonin N.A., Sergeev M.B. Local Determinant Maximum Matrices // Information Management Systems. – 2014. – № 1. – C. 2–15.

22. On the choice of matrices for image masking and de-masking procedures / A. A. Vostrikov, O. V. Mishura, A. M. Sergeev, S. A. Chernyshev // Fundamental research. – 2015. – № 2-24. – C. 5335-5339.

23. Strategies for computation of persimmetric cyclic quasi-orthogonal matrices as bases of codes / B. A. Nenashev, E. K. Grigoriev, A. M. Sergeev, E. V. Samokhina // Telecommunication. – 2020. – № 10. – C. 58-61. – DOI 10.34832/ELSV.2020.11.10.008.

24. Search and modification of code sequences on the basis of persimmetric quasi-orthogonal circulants / E. K. Grigoriev, V. A. Nenashev, A. M. Sergeev, E. V. Samokhina // Telecommunications. – 2020. – № 10. – C. 27-33.

25. Evgeniy K. Grigoriev, Vadim A. Nenashev, Alexander M. Sergeev, and Sergey A. Nenashev "Research and analysis of methods for generating and processing new code structures for the problems of detection, synchronization and noise-resistant coding", Proc. SPIE 11533, Image and Signal Processing for Remote Sensing XXVI, 115331L (20 September 2020); https://doi.org/10.1117/12.2574238

26. St. Petersburg [Electronic Resource] // DJI Developer: UX SDK: https://developer.dji.com/ux-sdk/ (date of access: 13.02.2023)

27. St. Petersburg [Electronic Resource] // DJI Developer: Windows SDK: https://developer.dji.com/windows-sdk/ (date of access: 13.02.2023)

28. Detection and Speed Assessment of Moving Objects in Optic-Location Systems / A. P. Shepeta, V. A. Nenashev, E. K. Grigoriev, S. A. Nenashev // Scientific Session of GUAP: Compendium of Reports of the World Aviation and Space Day. In Parts 3, St. Petersburg, April 08-12, 2019 Saint Petersburg: Saint Petersburg State University of Aerospace Instrumentation, 2019. – C. 282-287.

MODELING OF A NORMAL ANISOTROPIC MARKOV FIELD

Dolgov Egor
Saint Petersburg State University of Aerospace Instrumentation,
Ivangorod Branch, Saint Petersburg, Russia,
E-mail: egorka.dolgov.2000@mail.ru

Abstract. *The work presents an algorithm for modeling an anisotropic normal Markov field used as a generating field for modeling non-Gaussian anisotropic Markov fields, in particular for modeling echo signals of underlying land and sea surfaces.*
Keywords: *modeling algorithm, anisotropic field, Markov process, non-Gaussian field, generating field, underlying surface.*

The work of on-board location systems that search for physical objects, environmental monitoring, mapping of agricultural fields, etc., is always accompanied by the presence of input signals caused by reflections of probing signals from the surface of the earth and from the surface of the sea. Throughout the entire life cycle of these systems, both in design and in research, mathematical modeling methods are used, most often – simulation modeling methods [1]. Because of that, researchers and designers need algorithms for modeling all the input signals of these complex on-board systems. Thus, the synthesis of machine-oriented algorithms for modeling echoes of the sea and the earth's surface, which can be both informational and interfering, is an important and urgent task, one of the possible approaches to its solution and is described in this work.

When viewing the underlying surface, the onboard equipment of the aircraft scans a certain area of the surface [2], on which there are "shiny" points, the echo signals of which form a location signal reflected from the surface, observed in the resolution elements of the onboard location complex [3]. The signals from these points are vector-summed within the resolution elements, forming the corresponding observed signals [4]. These signals are mathematically described by the amplitudes and phases of the radio pulses observed in each resolution element. When using incoherent processing, it is sufficient to simulate fluctuations in the envelope of these signals, which are amplitudes, or signal strengths proportional to the square of the amplitudes [5]. In this work, we will limit ourselves to modeling fluctuations in the power of echo signals observed in the resolution elements of the onboard complex.

Let the scanned section of the underlying surface, defined in the Cartesian coordinate system XOY, contain n elements of resolution at the X coordinate and m elements at the Y coordinate. Then, in the Cartesian coordinate system XOY, the location signal reflected from the underlying surface can be represented by some matrix $\mathbf{M}_{n,m}$, the elements of which are the capacities $p_{i,j}$, i=1,2,…n, j=1,2,…m, reflected from this surface of the location signal, that is

$$\mathbf{M}_{n,m} = \begin{Vmatrix} p_{1,1} & p_{1,2} & \cdots & p_{1,m} \\ p_{2,1} & p_{2,2} & \cdots & p_{2,m} \\ \vdots & \vdots & \ddots & \vdots \\ p_{n,1} & p_{n,2} & \cdots & p_{n,m} \end{Vmatrix}. \quad (1)$$

The columns of the matrix $\mathbf{M}_{n,m}$ represent the scan of the scanned zone by the X coordinate, and the rows by the Y coordinate. For modern on-board location systems, which are characterized by high resolution, the elements of the $\mathbf{M}_{n,m}$ matrix are correlated random variables.

The elements of the matrix $\mathbf{M}_{n,m}$ have a non-Gaussian distribution, therefore, to model the elements of the matrix, some matrix $\mathbf{U}_{n,m}$, is introduced, the elements of which are distributed according to the nm-dimensional normal law. This matrix is a Gaussian field, and the covariance matrix of its elements is formed in such a way as to provide the required correlation coefficients of the elements of the non-Gaussian field represented by the matrix $\mathbf{M}_{n,m}$ [6].

The objective of this work is to develop a machine-oriented algorithm for modeling the elements of the matrix $\mathbf{U}_{n,m}$ for a given nm-dimensional law of probability distribution of matrix elements $u_{i,j}$, i=1,2,…n, j=1,2,…m. Theoretically, this problem is solved as follows. The matrix $\mathbf{U}_{n,m}$ is transformed into a vector $\mathbf{V}_{n\cdot m}$

$$\mathbf{V}_{n\cdot m}=\left(v_1,v_2,\ldots v_n,v_{n+1},v_{n+2},\ldots v_{n+n},\ldots v_{n\cdot(m-1)+1},v_{n\cdot(m-1)+2},\ldots v_{n\cdot(m-1)+n}\right)^{\mathrm{T}}, \quad (2)$$

where $(.)^{\mathrm{T}}$ – is the transpose sign. The elements of the vector $\mathbf{V}_{n\cdot m}$ are the elements of the matrix $\mathbf{U}_{n,m}$, arranged line by line, that is, the element of the matrix $u_{i,j}$, i=1,2,…n, j=1,2,…m, passes into the element v_k the vector $\mathbf{V}_{n\cdot m}$ with the index $k=i+(k-1)\cdot n$.

The covariance matrix of the elements of vector $\mathbf{V}_{n\cdot m}$, which must be positive definite, and by the well-known method [5,6], using a standard sensor of normally distributed numbers, a sequence of random variables v_k , k=1,2,… $n\cdot m$ is formed. The generated vector $\mathbf{V}_{n\cdot m}$ is the generative vector. Next, a non-linear functional transformation of the elements of vector $\mathbf{V}_{n\cdot m}$, is used, which provides the required probability distribution law of the simulated vector and, accordingly, the elements of the matrix $\mathbf{M}_{n,m}$ [7,8].

For a positive-defined covariance matrix of a normally distributed vector $\mathbf{V}_{n\cdot m}$ the algorithm for forming its elements is known, but the square covariance matrix of vector $\mathbf{V}_{n\cdot m}$ has dimension $(n\cdot m)\times(n\cdot m)$. Considering that the values of n and m can reach hundreds and thousands, the dimension of the covariance matrix of the vector $\mathbf{V}_{n\cdot m}$, becomes too large to use these standard methods for effective simulation. Therefore, below, taking into account the physical features of reflections from the underlying surfaces of the earth and the sea [7,8], the algorithm for generating elements of the matrix $\mathbf{M}_{n,m}$, and, accordingly, the matrix $\mathbf{U}_{n,m}$ can be significantly simplified [9].

The peculiarity of the reflections of location signals from the underlying surfaces is that the echo signals observed from the same angle have almost identical correlation characteristics. In our case, this means that all columns of the matrix $\mathbf{M}_{n,m}$, considered as vectors of dimension n, have the same correlation matrices $\mathbf{K}_{n,n}$, and also all rows of the matrix $\mathbf{M}_{n,m}$, considered as vectors of dimension m, have the same correlation matrices $\mathbf{K}_{m,m}$. The same applies directly to the matrix $\mathbf{U}_{n,m}$. The dimensions of these correlation matrices are equal to $n\times n$ and $m\times m$ respectively, which is several orders of magnitude smaller than the dimension of the covariance matrix of the vector $\mathbf{V}_{n\cdot m}$.

This feature allows, using the method of multidimensional forming filters [6], to consider separately algorithms for the formation of random elements of columns of the matrix $\mathbf{U}_{n,m}$. Using a sensor of independent random numbers distributed according to the standard normal law with zero mean and unit variance, and algorithms for the formation of random elements of rows of the matrix $\mathbf{U}_{n,m}$. And using as a sensor formed on In the previous step, random vectors are columns of the matrix $\mathbf{U}_{n,m}$ [9].

When using algorithms for modeling random fields in practice, it is advisable to use another simplification, which further increases the speed of the algorithms. We are talking about the approximation of the correlation-spectral characteristics of the simulated numerical sequences. Since the exact characteristics of the correlation, functions are unknown, the modeling it is possible to limit ourselves only to reproducing the width of the spectrum of fluctuations or limited to the duration of the normalized correlation function at some level.

In this case, a function corresponding to the Markov process is used as an approximating correlation function, in particular, an exponential correlation function. We present an algorithm for modeling the elements of the matrix $\mathbf{U}_{n,m}$ precisely for this case, assuming that the neighboring elements of the columns of the matrix $\mathbf{U}_{n,m}$ have a correlation coefficient r_x along the X coordinate, and the correlation coefficient is equal to r_y along the Y coordinate. These coefficients determine the width of the spectrum of fluctuations in the power of echo signals and allow us to take into account the anisotropy of the simulated field determined by the matrix $\mathbf{M}_{n,m}$.

For the above restrictions imposed due to the physics of the simulated process, the algorithm for modeling the normal field in our particular case can be represented by the following sequence of steps.

Step 1. Fill the matrix $\mathbf{U}_{n,m}$ with normally distributed, independent in aggregate, numbers $\eta_{i,j}$ with zero mean and unit variances,

$$u_{i,j}=\eta_{i,j},\ i=1,2,\ldots n,\ j=1,2,\ldots m.$$

Step 2. Recalculate the columns of the matrix $\mathbf{U}_{n,m}$ according to the algorithm

$$\begin{cases} u_{1,j} = u_{1,j}, \\ u_{2,j} = r_x \cdot u_{1,j} + \sqrt{1-r_x^2}\,u_{2,j}, \\ \dots, \\ u_{i,j} = r_x \cdot u_{i-1,j} + \sqrt{1-r_x^2}\,u_{i,j}, \\ \dots, \\ u_{n,j} = r_x \cdot u_{n-1,j} + \sqrt{1-r_x^2}\,u_{n,j}\ , \end{cases} \tag{3}$$

j=1,2,…m, which ensures that the elements of the columns are correlated, but the columns themselves are uncorrelated.

Step 3. Recalculate the rows of the matrix $\mathbf{U}_{n,m}$ according to the algorithm

$$\begin{cases} u_{i,1} = u_{1,1}, \\ u_{i,2} = r_y \cdot u_{i,1} + \sqrt{1-r_y^2}\,u_{i,2}, \\ \dots, \\ u_{i,j} = r_y \cdot u_{i,j-1} + \sqrt{1-r_y^2}\,u_{i,j}, \\ \dots, \\ u_{i,m} = r_y \cdot u_{i,m-1} + \sqrt{1-r_y^2}\,u_{i,m}\ , \end{cases} \tag{4}$$

i=1,2,…n, which ensures the correlation of the elements of the rows of the matrix $\mathbf{U}_{n,m}$.

The matrix $\mathbf{U}_{n,m}$ formed by this algorithm is the desired generating matrix for the formation of a non-Gaussian anisotropic field represented by the matrix $\mathbf{M}_{n,m}$.

Bibliographic list

1. Izrantsev V.V., Shepeta D.A. Modeling of external signals of onboard instrument complexes of fifth-generation aircraft. Scientific instrumentation. 2000. Vol. 10. No. 2. pp. 14-19.
2. Shepeta A.P. Determination of the search area of a surface object according to preliminary target designation data // Information and control systems. 2012. No. 4 (59). pp. 98-99.
3. Blaunstein N.S., Sergeev M.B., Shepeta A.P. Applied aspects of electrodynamics. – St. Petersburg: Agraf+, 2016. – 272 p.
4. Isakov V.I., Shepeta D.A. Modeling of location signals reflected from the edge of the earth-sea // Information and control systems. 2017. No. 5 (90). pp. 89-94.
5. Shalygin A.S., Palagin Yu.I. Applied methods of statistical modeling- L.: Mechanical Engineering. Leningr. department, 1986. – 320 p.
6. Shepeta D.A. Development of mathematical models and synthesis of algorithms for modeling input signals of on-board information processing and control systems. Dissertation for the degree of Candidate of Technical Sciences / St. Petersburg, 2000.
7. Shepeta D.A., Bozhenko V.V., Dolgov E.N. Algorithm for modeling correlated numerical sequences distributed according to Weibull's law // In the book: Wave electronics and infocommunication systems. Collection of articles of the XXV International Scientific Conference. In 3 parts. St. Petersburg, 2022. pp. 130-134.
8. Dolgov E.N., Shepeta D.A., Yakovleva E.A. Modeling of logarithmic-normal processes by the method of forming filters / Young scientist. – 2022. – No. S47-1(442-1). – pp. 60-62. – EDN CXQGWX.
9. Shepeta A.P. Synthesis of nonlinear shaping filters for modeling input signals of location systems // Proceedings of the International Scientific and Technical Conference / Academy of Sciences of Ukraine; NPO Kvant. Kiev, – May, 1994, Issue 1. pp.81-85.
10. Shepeta A.P., Makhlin A.M.Decorrelation of echo signals of the sea surface during the restructuring of the carrier frequency of the onboard radar. Marine radio electronics. 2020. No.4 (74). pp. 36-38.

MODIFICATION OF THIN FULLERITE FILM BY ACCELERATED C_{60} ION BOMBARDMENT

Fedorenko Elizaveta
Peter the Great Saint Petersburg Polytechnic University,
29, Polytechnic str., Saint Petersburg, 195251, Russia
lizasever69@mail.ru

Abstract. *Formation of thin conductive corrosion resistant carbon-based nanostructured coating with possible use in polymer electrolyte membrane fuel cells is studied. Coating is formed under accelerated C_{60} ion bombardment of thin fullerite films created by fullerene molecules deposition at room temperature. Irradiation changes the structure of the fullerite film, increasing internal stress. The film peels off from the substrate in the case ion energy is not enough to reach substrate. Transition carbide layer is formed at the interface under irradiation with a mixed beam with energies of 7 and 14 keV. This layer significantly increases the adhesion of the coating. Diamond-like bond formation is not observed in carbon films at low ion doses. At high doses, the graphitization of the coating occurred. It was found that the longitudinal and transverse sizes of the grains of the carbon coating increase with the film thickness.*

Introduction

Polymer electrolyte membrane fuel cells (PEMFCs) have received intensive research from both alternative energy and environmental considerations owing to their attractive features of high-power density, low operating temperature and converting fuel to water as the only by-product [1,2]. The PEMFCs exhibit the most promising alternative source of energy for a variety of portable electronic devices, stationary and vehicle applications. Hence, the investigation of suitable materials for bipolar plates for applications in fuel cells has become a critical research issue. Currently, the most widely used material for bipolar plates is machined graphite, which provides excellent corrosion resistance and high electrical conductivity [3,4]. But bipolar plates made from it have insufficient mechanical strength. It is generally considered that the stainless steel is an optimal bipolar plate material for PEMFC as its high bulk electrical and heat conductivity, high strength, low gas permeability and ease of manufacture. The bare stainless steel suffers corrosion attack in the harsh acidic and humid environment. And the corrosion products could contaminate and poison other fuel cell stack components (notably catalyst and membrane). Moreover, the bare stainless steel forms passive layer under PEMFC operating conditions leading to high interfacial contact resistance. Both the corrosion products and the passive layer could result in decreasing in cell performance [5], [6], [7], [8]. The only exceptions are noble metals (gold, platinum, etc.) but its expensive [9]. Thus, surface modification by cost-effective, highly corrosion-resistant, and good conductive film is needed. This problem could be solved by coating the surface of metal bipolar plates with various carbon materials [10 – 12].

Graphite satisfies all the previously discussed requirements, with the exception of high mechanical strength and low manufacturing costs. Because of the similarities between carbon-coated materials and graphite, deposition of a carbon coating onto the surface of metallic bipolar plates is a logical choice. Nanocomposite obtained by accelerated C_{60} ion beam deposition is known as corrosion-resistant carbon coating [13]. It was shown in [14] that carbon nanocomposite (CNC) contains textured graphite nanocrystals separated by a layer of amorphous carbon. Graphene planes are normal to the coating surface which ensures high transverse electric conductivity of the coating. The described process of obtaining a nanocomposite coating requires heating of the substrate up to 400 C. On the other hand, it is of interest to increase amount of conducting graphite inclusions in a hard insulating diamond-like matrix. It is of interest to investigate the possibility to obtain low contact resistance nanocomposite at lower deposition temperature. In this work, we describe the formation and behavior of coatings obtained at room temperatures Ts on silicon substrate by accelerated C_{60} ion irradiation with use of neutral low-energy fullerene molecule co-deposition in different modes, i.e. irradiation of pre-deposited fullerite film, and fullerene layer deposition onto a C_{60} ion pre-irradiated surface and further irradiation of that sandwich structure.

Experimental

Deposition of the Coatings

To perform studies of deposition and sputtering during the interaction of accelerated C_{60} ions with the surface, a setup developed based on a VUP-5M vacuum station was used. The set-up used for film

fabrication is described in detail in [15]. An ion source with a saddle-shaped electric field was used. 99.5% purity C_{60} fullerene powder (NeoTechProduct, Saint Petersburg, Russia) was placed in two effusion cells and evaporated into ionization chamber of the ion source. The ion beam was primarily consisted of singly and doubly charged ions. The proportion of C^{++}_{60} ions was ~22%. The ion energy in the beam was 7 and 14 keV. The deposition was carried out onto Si substrate at room temperature. Heating of the substrates during processing did not exceed 10°C. Separate effusion cell was used to deposit fullerite film by C_{60} evaporation.

The deposition of carbon coatings took place in several stages, individual for each sample: for some, pure fullerene molecules were first deposited from effusion cells to get fullerite layer, then-irradiated with C_{60} ions. For others, the substrate surface was irradiated with C^{++}_{60}, then C_{60} was deposited, and again irradiated with ions. There are also films formed only by the deposition of fullerene molecules.

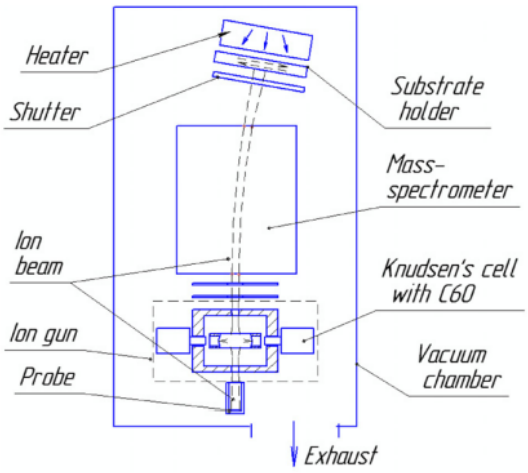

Fig. 1. Schematic diagram of set-up used for carbon film deposition.

Methods of Examination of the Coatings

The coatings were investigated using Raman spectroscopy, atomic force microscopy, and X – ray photoelectron spectroscopy (XPS). Raman measurements were performed by a Renishaw inVia Raman Microscope with laser excitation at a wavelength of 633 nm. The spectrum acquisition time was 120 sec. The surface topography was studied using a Nano-DST atomic force microscope (Pacific Nanotechnology). The AFM images were measured in semi-contact mode, which made it possible to minimize the effect of the probe on the sample surface with resolution of 1024 lines with 1024 pixels per line. A silicon tip NSG01 from TipsNano with a radius of 10 nm was used. The stiffness coefficient was 1.45–15.1 N/m. The Gwyddion software package was used for image processing. The bond structure was analyzed by X-ray photoelectron spectroscopy (Specs PHOIBOS 150 MCD-9) using Mg KαC radiation @1253.6 eV and electron flood gun SPECS FG20 at 10 eV and 5 μA.

Results and discussion

Structure of the Chemical Bonds

Fig. 2(a) shows the experimental C1s spectrum (black line). It consists of several lines as described below. Fig. 2(b) shows the O1s spectrum for the same sample. The structure of the C1s peak consists of three main components corresponding to bonds between carbon atoms and two types of bonds between carbon and oxygen atoms (C–O and C=O) [16]. In addition, a broad π-π* plasmonic oscillations peak, which is associated with the interaction of outgoing photoelectrons with π electrons, may occur. Taking into account possible bond structure of the coating, the following C1s peak components could occur: sp2 – bonds @ 284-284.5 eV, sp3 – bonds @ 285-285.5 eV. The distance between sp2 and sp3 peaks might be about 1 eV (±0.1 eV). Indeed, for a pure fullerite film, it makes sense to expect only a signal from sp2-bonded carbon atoms. For the C–O component, the binding energy is 286–287 eV, and for the C=O component, 289 eV. The width of each peak should be from 1.2 to 1.8 eV. The peak of plasmon oscillations should be in between 289 – 290 eV. The structure of the O1s peak in the studied material could consists of 2 main lines corresponding to the C–O (531.5 – 532 eV) and C=O (~533 eV) bonds.

Experimental curves were decomposed into Gaussian-like components as described above. The example of decomposition (green lines) together with the resulting curves (red line) are shown in Fig. 2 (a, b). The decomposition parameters obtained are summarized in Tables 1 and 2.

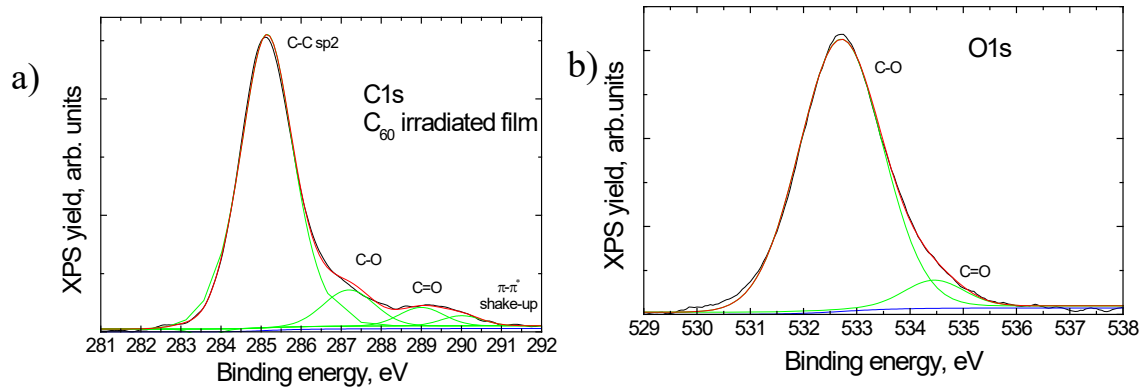

Fig. 2.XPS spectra from a fullerite film irradiated with C60 ions

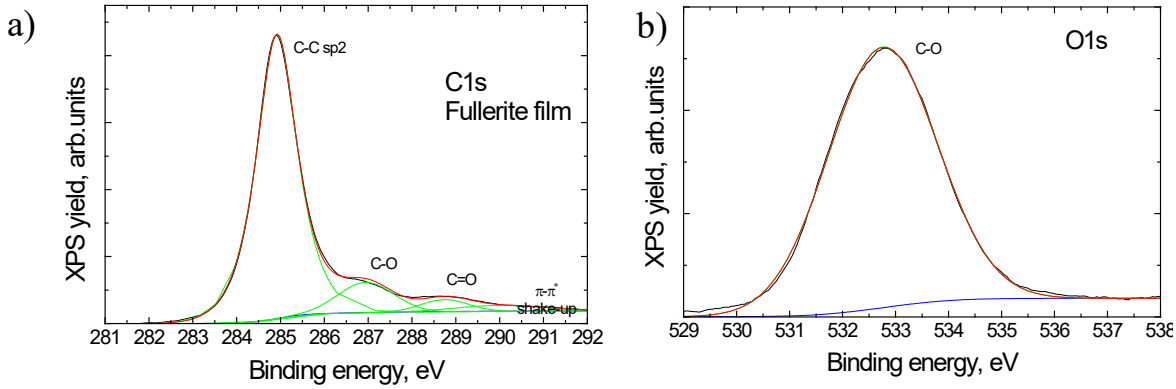

Fig. 3.XPS spectra from an unirradiated fullerite film

Table 1

C1s peak decomposition parameters. xc is the peak position, σ is the full width at half maximum, η – fraction of the line in the total peak area.

Bond type	Parameter	Fullerite film	C_{60} ion irradiated fullerite film
C-C	xc, eV	285.1	284.9
	σ, eV	1.1	1.55
	η, %	82	85
C-O	xc, eV	287.2	286.9
	σ, eV	1.5	1.5
	η, %	11	9
C=O	xc, eV	289.0	288.7
	σ, eV	1.3	1.3
	η, %	3.5	4
shake-up	xc, eV	290.0	290.1
	σ, eV	2.5	1.17
	η, %	3.5	2

Table 2

Decomposition parameters of O1s peak. xc is the peak position, σ is the full width at half maximum, η – fraction of the line in the total peak area.

Bond type	Parameter	Fullerite film	C_{60} ion irradiated fullerite film
C-O	xc, eV	532.8	532.7
	σ, eV	2.4	1.8
	η, %	100	94
C=O	xc, eV	-	534.5
	σ, eV	-	1.3
	η, %	-	6

It is seen that the fitting curves approximate well the experimental spectra. Huge amount of sp2 component indicates the graphite-like nature of the fullerite film structure. Indeed, for a fullerite film it makes sense to expect only a signal from sp2 – bonded carbon atoms. Interestingly, we do not observe any sp3 component even in the spectra acquired from samples after ion bombardment. This may be due to very small amount of diamond sp3-bonds are formed at low irradiation fluences used. Comparing Fig. 2 (b) and 3 (b), we see that in the case of a non-irradiated fullerite film, the C = O component is absent. This observation can be explained by assuming that the O atoms are "crosslinking" the carbon molecules. After ion bombardment there is a possibility of rearrangement of double bonds and binding of fullerene molecules via one oxygen atom.

Raman Scattering

The characteristics of the coatings were further analyzed by Raman spectroscopy. The Raman spectrum included a D band in the range of 1350 – 1370 cm^{-1} (corresponding to the "breathing" mode of six-fold rings) and a G band in the region of 1550 – 1590 cm^{-1} (corresponding to the in-plane bond-stretching motion of sp2 atom pairs), both of which are characteristic of amorphous carbon [18]. Also, in the spectrum should be present the peak of fullerene molacules. This peak corresponds to the vibrations of pentagons in C_{60} molecules (pinch-mode) [19].

Fig. 4(a) shows a typical spectrum obtained from a fullerite film. Two peaks located at 520 and 960 cm^{-1} are clearly seen. They arise due to scattering on the silicon substrate. Further, one can observe a broad peak with a maximum in the region of ~2300 cm^{-1} which is due to photoluminesce. A weak pinch-mode peak is also visible at 1459 cm^{-1}. In the spectrum obtained from irradiated film, in addition to abovementioned features, one can also see the features in the region 1100 – 1700 cm^{-1} that arise because of scattering by carbon structures, which are indicative of a DLC coating.

To analyze the features of the obtained spectra, the parameters of the photoluminescence peak were first derived. It was earlier established that the luminescence spectrum of a fullerite film consists of several lines [17], the shortest wavelengths of which are in the energy range from 1.5 to 1.8 eV. Considering the excitation wavelength (633 nm), the dependence of the light intensity was replotted as a function of the energy of radiation quanta. Next, we approximate the background with a straight line and decompose the PL curve into two Gaussian-like lines. Fig. 4 (b) shows an example of the resulting decomposition. The considered luminescence peak in all cases consists of two photoluminescence lines of different relative intensity, with maxima at energies of 1.64 and 1.7 eV.

Fig. 4(c) shows the Raman spectrum obtained after irradiation a fullerite film with mixed beam of C^{+}_{60} and C^{++}_{60} ions for 5 minutes with a current of 2 $\mu A/cm^{-1}$. the intensity of photoluminescence has not changed much (compare Figs. 4(a, c)). Pinch-peak is shifted towards lower energies. A slight shift from the normal position can be explained by the presence of bonds between the fullerite structure and oxygen atoms [19]. The PL signal was subtracted from the spectrum, which made it possible to consider the features in the range from approximately 1000 to 1800 cm^{-1}. In addition, after subtracting the photoluminescence background, a peak at 1459 cm^{-1} becomes clearly visible in the spectra (see Fig. 4(d)).

Based on the literature [20], we can say that the traditionally used characteristics, by which to evaluate the structure of DLC coatings, their physical and chemical properties, are the positions of the maxima of the G and D components of the decomposition, the ratio of their maximum heights Max(D)/Max(G) and the width at half height FWHM.

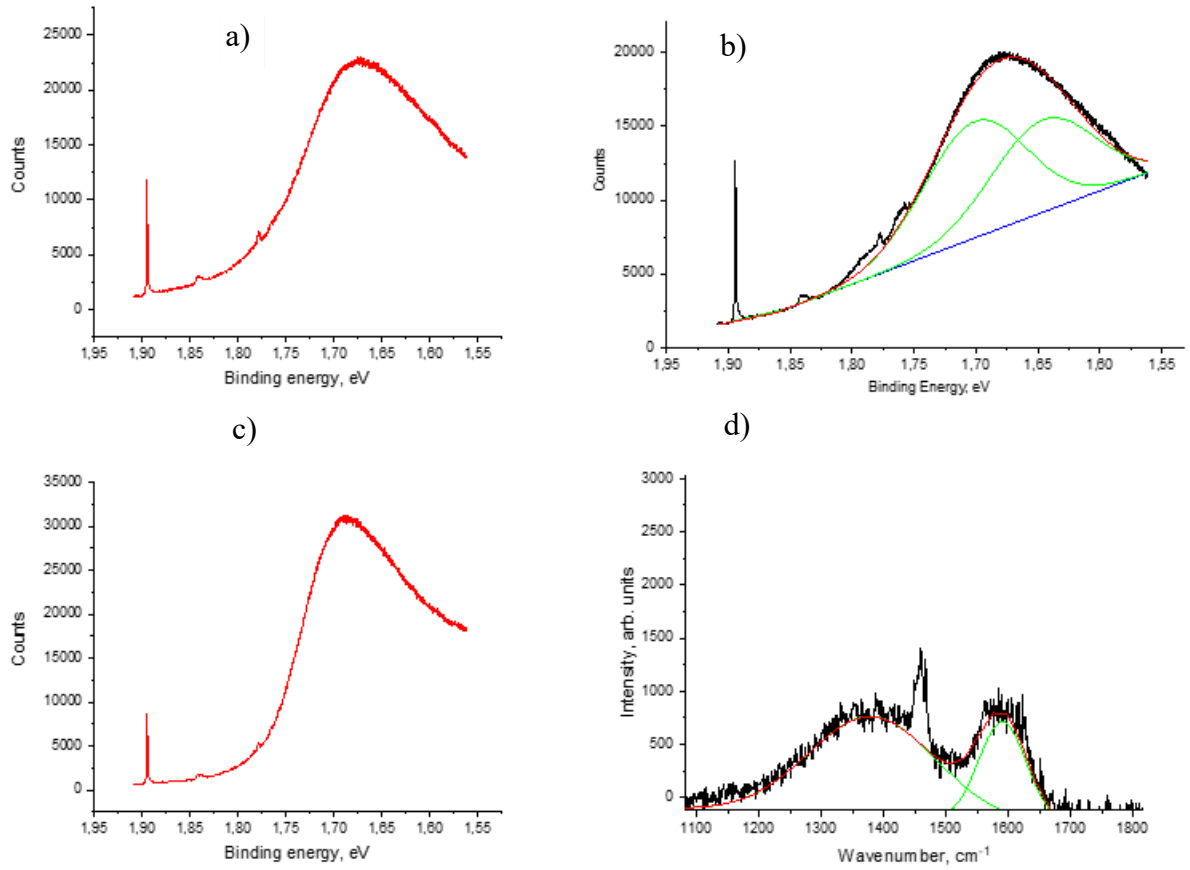

Fig. 4.Raman spectrum obtained from a fullerite film 70 nm thick on a silicon surface

It is also known that the G-component can shift to the region of large wavelengths with an increase in the concentration of sp^3 bonds and a decrease in sp^2, and, therefore, the value of the Max(D)/Max(G) ratio may decrease. From the data of Table 3, for the study samples, a decrease in the film thickness and an increase in the irradiation dose leads to a broadening of the G-peak from 83.81 to 170.80 cm^{-1}, and a slight change in the width of the D-peak from 194.1 to 235.14 cm^{-1}. This indicates an increase in the diamond-like and graphite-like phases in the coating due to an increase in the concentration of inclusions with sp^3- and sp^2 – hybridization. A high value of Max(D)/Max(G) makes it possible to judge the degree of graphitization and indicates a strong disorder of the structure [21].

Table 3

Raman Peak Decomposition Characteristics

Sample	Three-layer sample	Fullerite	Fullerite	
Peak D (Gaussian)	1350,56225	1371,79177	1370,82363	xc
	90021,80374	937851,61165	160244,56113	A
	235,14745	232,73491	194,10503	w
Peak G (Gaussian)	1550,74816	1591,25649	1590,66875	xc
	97982,41058	439828,27439	76704,57019	A
	170,80645	96,02961	83,81496	w
Max(D)/Max(G)	0,91875	2,13231	2,08912	

Surface Examination (AFM)

Images of the surface topography of the samples were obtained using atomic force microscopy. Typical surface relief is shown in the Fig. 5. Modification of the coatings was traced with a change in the

thickness of the films and the accelerating energy of fullerene ions. AFM scans were processed using the Gwyddion software package.

Fig. 5 shows the scans of the surface of the original fullerite films. The films represent a cluster densely packed periodic structure. Image a) illustrate the surface of a fullerite film on a silicon substrate before ion bombardment. The thickening of the coating and the absence of the ion bombardment stage leads to an increase in the size of the longitudinal diameter of the nanoparticles from about 35 to 64 nm. The homogeneity and density of their packing increases.

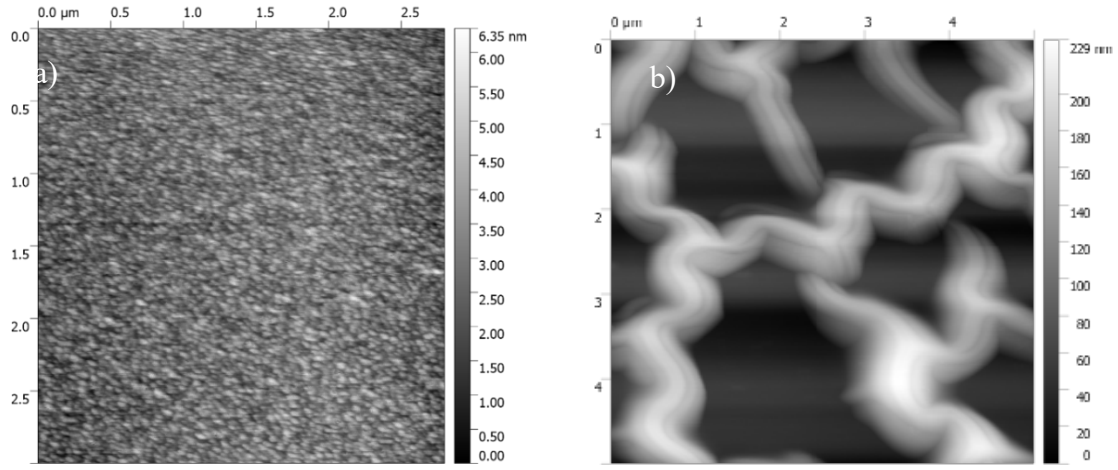

Fig. 5.The morphology of the sample surface obtained by AFM

Comparing images 4 (a) and 4 (c), we can say that irradiation did not change the film structure much. Therefore, the nature of the photoluminescent peak remains unchanged, since fullerene molecules in large quantities remained intact.

From Fig. 4 (b) we see that high protrusions have formed on the film. Apparently, the film in these places is torn off from the substrate surface due to the appearance of internal mechanical stresses during ion bombardment. The reason for this may be that singly charged ions do not have enough energy to penetrate the fullerite film through, so that interaction occurs not only with it, but also with the substrate. The adhesion of the fullerite film is insufficient to ensure complete retention of the DLC coating formed during ion bombardment. But the film is flexible enough and it does not break into small pieces, which can happen with brittle coatings. As a result, wrinkles are formed on the coating.

In the case of irradiation with a mixed ion beam, no wrinkles form on the film, and its roughness turns out to be significantly less than that of the initial fullerite film. This can be explained by the fact that the energy of the C^{++}_{60} ions (14 keV) is sufficient to reach the substrate surface. In this case, interaction occurs simultaneously throughout the entire volume of the fullerite coating, including ionic mixing of carbon and silicon at the interface between the fullerite and the Si substrate. As a result, a transition layer of silicon carbide is formed, and the adhesion of the coating is significantly improved.

Conclusions

Summarizing the results of AFM, Raman spectroscopy and XPS data, we can conclude that the irradiation with small doses does not lead to the destruction of the fullerite film. As the dose increases, the film is destroyed, and a carbon coating is formed. It has a soft graphite structure. Therefore, there is a rapid decrease in the intensity of the PL peak and the disappearance of the pinch-peak of the fullerene. The roughness of the surface relief also decreases. When the energy of the bombarding ions is insufficient, the resulting coating exfoliates from the substrate due to poor adhesion. The use of single and doubly charged ions in the beam removes this problem.

At room temperature of the substrate, the formation of a diamond matrix with graphite inserts is not observed. As a modification of the coating growth method, one can propose simultaneous irradiation of the substrate surface with C60 ions and deposition of fullerene molecules.

References

1. B. C. H. Steele and A. Heinzel, Nature, 2001, 414, 345.

2. H. C. Kuan, C. C. M. Ma, K. H. Chen and S. M. Chen, J. Power Sources, 2004, 134, 7.

3. CreNeC multilayer film on 316L stainless steel as bipolar plates for proton exchange membrane fuel cells using closed field unbalanced magnetron sputter ion plating. Yi P, Peng L, Zhou T, Huang J, Lai X. J Power Sources 2013;236:47-53.

4. Electrodeposition of ruthenium oxide on ferritic stainless steel bipolar plate for polymer electrolyte membrane fuel cells. Kim KM, Kim JH, Lee YY, Kim KY. Int J Hydrogen Energy 2012;37:1653-60.

5. N. de las Heras, E.P.L. Roberts, R. Langton, D.R. Hodgson Energy Environ. Sci., 2 (2009), pp. 206-214

6. A.A. Renato, L.O. Mara Cristina, E. Gerhard, E. Volkmar Int. J. Hydrogen Energy, 35 (2010), p. 3632-3647

7. C.H.S. Brian, H. Angelika Nature, 414 (2001), pp. 345-352

8. D.P. Davies, P.L. Adcock, M. Turpin, S.J. Rowen J. Appl. Electrochem., 30 (2000), pp. 101-105

9. Standardized testing framework for quality control of fuel cell bipolar plates / Shaigan N., Yuan X.Z., Girard F., Fatih K., Robertson M. Journal of Power Sources, Vol. 482, 2021. P. 228972.

10. Nanocomposite-carbon coated at low-temperature: A new coating material for metallic bipolar plates of polymer electrolyte membrane fuel cells / Lee S.H., Pukha V.E., Vinogradov V.E., Kakati N., Jee S.H., Cho S.B., Yoon Y.S. International Journal of Hydrogen Energy, Vol. 38, No. 33, 2013. pp. 14284-14294.

11. Carbon composite coatings on Ti for corrosion protection as bipolar plates of proton exchange membrane fuel cells / Gao P., Xie Z., Ouyng C., Wu X., Lei T., Liu C., Huang Q. Micro & Nano Letters, Vol. 13, No. 7, 2018. pp. 931-935.

12. Corrosion protection of amorphous carbon coating for the bipolar plates of PEMFCs / Gang C., Tao T., Ping-Ping G., Zhi-Yong X., Xiao-Bo W. Surface Review and Letters, Vol. 26, No. 9, 2019. P. 1950059.

13. Evaluating the effect of metal bipolar plate coating on the performance of proton exchange membrane fuel cells / Ijaodola O., Ogungbemi E., Khatib F.N., Wilberforce T., Ramadan M., El Hassan Z., Thompson J., Olabi A.G.Energies, Vol. 11, No. 11, 2018. P. 3203.

14. S. H. Liao, C. Y. Yen, C. H. Hung, C. C. Weng, M. C. Tsai, Y. F. Lin, C. C. M. Ma, C. Pan and A. Su, J. Mater. Chem., 2008, 18, 3993.

15. Ultra-thin carbon-based nanocomposite coatings for superior wear resistance under lubrication with nano-diamond additive / M. Khadem, O. V. Penkov, V. E. Pukha, M. V. Maleyev, D. E. Kim. RSC Advances., 6 (2016), 56918.

16. Nano scale investigation of particulate contribution to diamond like carbon film by pulsed laser deposition / Madhusmita Panda, G. Mangamma, R. Krishnan, Kishore K. Madapu, D. Nanda Gopala Krishna, S. Dash and A. K. Tyagi. The Royal Society of Chemistry/ 2016, 6. – 6016 – 6028 с.

17. Temperature dependence of the photoluminescence in polymeric solid C60./ U. D. Venkateswaran, D. Sanzi, A. M. Rao,P. C. Eklund, L. Marques, J.-L. Hodeau, M. Nunez-Regueiro. PHYSICAL REVIEW B 57, 6, 1 1998-II

18. Спектроскопия аморфного углерода на стеклянной подложке и на тонком слое меди. / М. Ю. Барабаш, А. А. Колесниченко, Д. С. Леонов. Nanosistemi, Nanomateriali, Nanotehnologii/ 2017, т. 15, № 4, 757 – 769 с.

19. Evaluation of Raman spectroscopy to detect fullerenes in geological materials / J. Jehlicka, O.Frank, J. Pokorny, J.-N. Rouzaud. Spectrochimica Acta, 2005., – 2364 – 2367 с.

20. Interpretation of Raman spectra of disordered and amorphous carbon /. A. C. Ferrari and J. Robertson. PHYSICALREVIEWBVOLUME61, 20 2000-II

21. Светопоглощающие покрытия на основе алмазоподобного углерода. / Н.М. Чекан, И.П. Акула, Н.В. Логуновская. Электронный научно – технический журнал «Контенант», 2014. № 1, 24-35 с.

THE PACEMAKER (PCMK)

Giuseppe Pera, Marco Fiandaca
Computer Engineering and Networks Laboratory – Kore University of Enna – Italy
Email: *giuseppemichele.pera@unikorestudent.it*
marcovincenzo.fiandaca@unikorestudent.it

Abstract. *The proposed system (PCMK) has been designated to monitor the heartbeat of patients with or at high risk of bradycardia (conditions where the heart beats very slowly). The operating perimeter focuses entirely on the patient, as the device contains a sensor that can detect the heart-rate and act through appropriate logic. The data forwarded by the sensor is received by a controller that checks the patient's condition and instructs the Actuator system to send electrical impulses that have the function of restoring the heartbeat. Through a lighting indicator light located inside a wireless device, the patient in question can periodically check his or her condition.*

INTRODUCTION

The "PCMK" project is used for the resolution of several problems, the one on which we are going to focus our study is **Brachycardia** (which we explain below):

Bradycardia or **brachycardia** is a condition defined as a reduction in heart rate below 60. It can manifest itself physiologically in athletes (a condition also called 'athlete heart') and sometimes in the elderly.

Severe and rapid bradycardia may require emergency drug treatment (particularly with **sympathomimetics**); in chronic forms (or pathological conditions at risk of severe bradycardia) the implantation of a pacemaker may be indicated.

A **pacemaker** is a small battery-powered electronic device, consisting of a computerized pulse generator and one or more electrocatheters that, when connected to a heart with a rhythm that is too slow, too fast or irregular, it normalizes its contractions. So the installation of a pacemaker requires surgery lasting a few hours during which the patient usually remains conscious.

Depending on the structure and operation, we can recognize different types of pacemakers:

A. A pacemaker can be a **continuous stimulator** of the heart or a **stimulator on demand**, it all depends on the type of arrhythmia present: if the arrhythmia permanently alters the heart rhythm the pacemaker will have to carry out a continuous activity (**continuous stimulator**); if the arrhythmia is sporadic, the pacemaker will intervene only when necessary (**stimulate on request**).

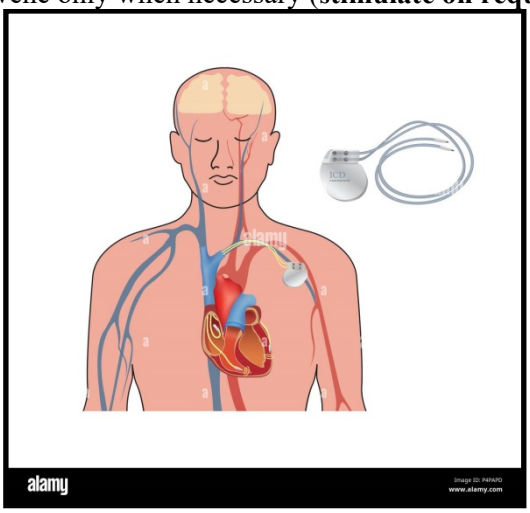

B. A pacemaker based on the number of electrocatheters can be: **single-cameral**, **bicameral** or **biventricular**.

The proposed computer project realizes a **single-camera PCMK on demand** because it focuses on the main aspect of the problem: '*Adjust the heartbeat by sending electrical impulses on demand*'.

The 'PCMK' system consists of sensors, controllers and actuators. The sensor will send the data at a set time range to the controller, the controller (through appropriate logic) will communicate the outcome of the processing to the actuator. The controller determines the appropriate value based on research

by the OSM (ORGANIZZAZIONE MONDIALE DELLA SANITA') on the values that make a person suffering from bradycardia in danger . The actuator determines the actions to be taken based on the communication received from the controller, i.e. to send an electrical impulse (of different intensity) based on the patient's state of health.

At the structure level, the component blocks of the PCMK are Wireless and are located inside, while outside, there will be a shock signal that will be installed in a device that can connect via Wireless network.

THE PROPOSED APPROACH

The PCMK system is made using the MATLAB application using truetime blocks, more precisely: truetime Kernel and a truetime wireless network.

In more detail, we saw the PCMK system as a network consisting of 4 nodes: sensor, controller, actuator and shock signal that take advantage of the energy-efficient wireless communication protocol 802.15.4 (ZigBee) (which includes a PAN network). Below is the topology of the network:

Where:

- **Nodo wireless Sensore (Network 1 – Node 1**
- **Nodo wireless Controllore (Network 1 – Node 2)**
- **Nodo wireless Attuatore (Network 1 – Node 3)**
- **Nodo wireless segnalatore scossa (Network 1 – Node 4)**

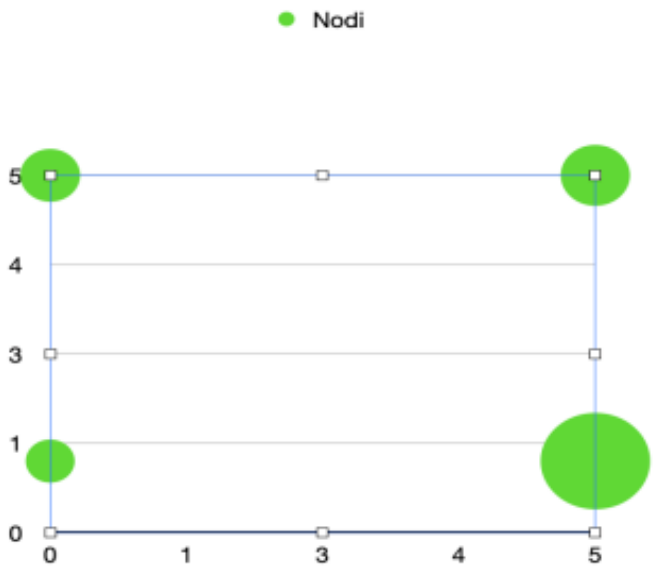

Fig. 1: Spatial position of the nodes

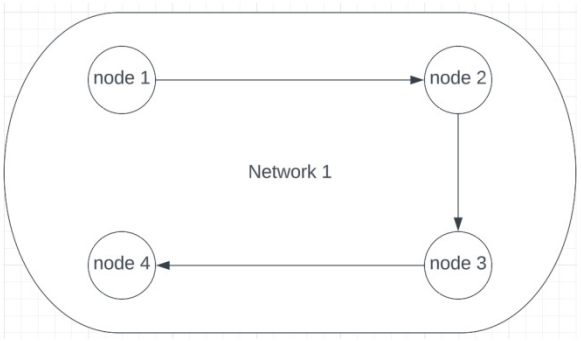

Fig. 2: Network topology

Task Sensor – Battito cardiaco

The sensor task consists of two files, the first of initialization and the second of function. The initialization file (named '*Pacemaker_sen_battito_init*') provides the following instructions:

• Initialization of kernel using fnctn **ttInitKernel()** -> used to configure task scheduling priority as '*fixed-priority scheduling*';

• Configuring the power consumption of the truetime kernel (the sensor) through the fnctn **ttSetKernelParameter()** which sets the '*energyconsumption*' parameter to 0.010 i.e 10mW.

• The creation of three mailboxes that are: *heartbeat, health_state and shock_value* through the fnctn **ttCreateMailbox()**

• The creation of the sensor task (that is periodic) using the fnctn **ttCreatePeriodicTask()** by specifying the following parameters: *function name*, *task name*, *starttime*, *period* and *data* .

The function of the sensor (implemented in the file: '*Pacemaker_sen_battito_fnctn*') is to read the heartbeat and send the data to node 2 (controller). In more detail:

• Takes the value (i.e. the heartbeat) generated by the UNIFORM RANDOM NUMBER block through the **ttAnalogIn(1)** command;

• Assign an identifier to the package, i.e. it is numbered in order to detect any loss rate related to network performance;

• Calculate the timestamp (simulation execution instant) using the **ttCurrentTime** command;

• Indicates the type of message (type = heartbeat);

• Sends the packet to node 2 (controller) using the **ttSendMsg()** command by specifying: *the target*, *message*, *and message size.*

Task controller

The task controller also has two files, the first of initialization and the second of function.

The initialization file (named: '*Pacemaker_controller_init*') includes:

• The same instructions used in the sensor init file (which are: **ttInitKernel()**, **ttSetKernelParameter()** which also sets the "*energyconsumption*" parameter to 0.010 i.e. 10mW and **ttCreateMailbox()**); the difference that the controller task is aperiodic (i.e. it is generated only when you receive a response from the sensor) so we using the fnctn **ttCreateTask()**, which receives the following parameters: *function name*, *task name* and its *deadline*;

• Creating and configuring the network interface (i.e. listening to node 2 on the network) using the fntcn **ttCreateHandler()** that receives as parameters: *handler name* (unique), *function name* and *task priority*, and fntcn **ttAttachNetworkHandler()**. The handler (in this case) is listening to data from the sensor's wireless network interface.

The controller function (implemented in the file: '*Pacemaker_controller_fnctn*') is regulated by two operational portions:

1. In the first portion, the message is taken from the '*heartbeat*' mailbox (previously defined) by calling **ttTryFetch()** and verifies that the content is not empty, calculates the *end-to-end delay* (shown in output by sending the value to a scope) and the received packets/possibly lost packets. Finally, by calling **ttAnalogOut(1, date.beat)** forwards the data to the *Fuzzy Logic Controller* which will determine the patient's health status.
2. In the second portion, the value of the patient's health status (returned by the fuzzy controller) is taken from the call **ttAnalogIn(1)** and entered into a structure together with the type ('*health_status*'), the package identifier and the timestamp. Finally, forward the structure to node 3 (actuator) by calling **ttSendMsg()** by specifying: *the target*, *message(structure)*, and *message size*.

Task actuator

The actuator task also has two files, the first of initialization and the second of function.

The initialization file (named: '*Pacemaker_att_init*') contains:

• The same instructions used in the sensor and controller init file (which are: **ttInitKernel()**, **ttSetKernelParameter()** which sets here the parameter "*energyconsumption*" to 0.020 i.e 20mW and **ttCreateMailbox()**); since the actuator task is also aperiodic (i.e. it is generated only when receives a response from the controller) the creation of the task is done by the fnctn **ttCreateTask()**, which receives the following parameters: *function name*, *task name* and its *deadline*;

• Creating and configuring the network interface (i.e. you listen to node 3 on the network) using the fntcn **ttCreateHandler()** which receives as parameters: *handler name* (unique), *function name* and *task priority*, and fntcn **ttAttachNetworkHandler()**. Please note that the handler (in this case) is listening to data from the wireless network interface controller.

The actuator function (implemented in the file: '*Pacemaker_attuator_fnctn*') is regulated by two operating portions:

1. In the first, the data is taken from the previously defined '*shock_value*' mailbox and verifies that the content is not empty, calculates the end-to-end delay (shown in output by sending the value to a scope) and the received packets/possibly lost packets and sends by the **ttAnalogOut(1, data.output)** call the value to a Matlab function that generate the value of the shock (based on appropriate checks carried out on the state of health of the patient received by the controller)
2. In the second, the value of the shock is taken using the call **ttAnalogIn(1)** and entered into a structure along with the type ('*shock_value*'), the package identifier, and the timestamp. Finally, forward the structure to node 4 (shock_signal) using the **ttSendMsg()** call, specifying: the *target, message(structure)*, and *message size*.

Task shock_value

The shock_value task also includes two files, the first of initialization and the second of function.
The initialization file (named: '*Pacemaker_lampadaScossa_init*') includes:

- The same instructions used in the init file of the sensor, controller and actuator (which are: **ttInitKernel()**, **ttSetKernelParameter()** which also sets the parameter "*energyconsumption*" to 0.010 i.e. 10mW and **ttCreateMailbox()**); being also a non-periodic task (that is generated only only when receive a response from the actuator) the creation of the task is done using the fnctn **ttCreateTask()**, which receives the following parameters: *function name*, *task name* and related *deadline*;
- Creating and configuring the network interface (i.e. you put the listening node 4 on the network) using the fntcn **ttCreateHandler()** that receives as parameters: *handler name* (unique), *function name* and *task priority*, and the fntcn **ttAttachNetworkHandler()**. The handler (in this case) is listening to data from the actuator wireless network interface.

The shock_signal function (implemented in the file: '*Pacemaker_lampadaScossa_fnctn*') is regulated by two operating portions:

3. In the first, the value is taken from the '*shock_value*' mailbox, if it is not empty, it saves that value in a variable called *data.valScossa*, and (as for the other nodes) the end-to-end delay (shown in output by sending the value to an scope) and the received packets/possibly lost packets is calculated.
4. In the second using the **ttAnalotOut(1, data.valScossa)**, the value is sent to an MBDS system that will turn on an LED (different color based of the received value from actuator) that will notify the patient of the presence of an abnormal condition

Handler

As for the handler, let's define a file ("*Pacemaker_netHand_fnctn*") that defines its function:

- Receives the message and according to the type field (specified in the structure of each message) writes it to the appropriate mailbox through the **ttTryPost()** call. Finally (always depending on the type of the message) it goes to create (start) the appropriate task by calling **ttCreateJob()**.

Matlab Function *Gestione salute*

The Matlab Function in our project is used with the aim of generating the right shock value to the patient. This receives in input the value of the patient's health status, based on the presenting values the right electrical impulse is generated that will allow the body to return to optimal conditions. Through then a DBMS system, the severity of the patient's health status will then be reported by LED.

SCENARIO

The PCMK system in simulated environment was developed by a personal engineering approach (not discriminating from a potential realization) One of the most significant factors in the Matlab environment simulation of the PCMK system is the simulation time that we have set (to find enough data to verify the behavior of the system) at 1050 seconds. We can divide the system into four levels:

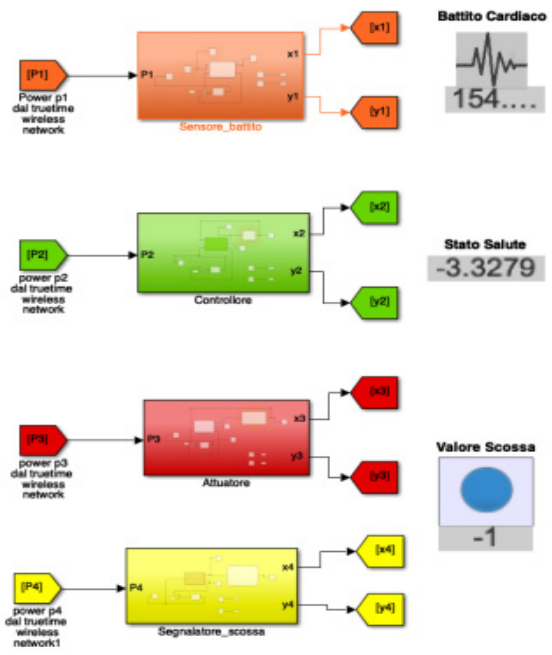

(1) The **first level** of development is the *sensor*, which has the task of defining heartbeat behaviors (making the data close to a suitable operational reality). It is figured by the SubSystem Block **"*Sensor_beat*"** containing within it a TrueTime kernel that receives incoming random values (generated by a component "*Uniform Random Number*") that indicate our patient's heartbeat.

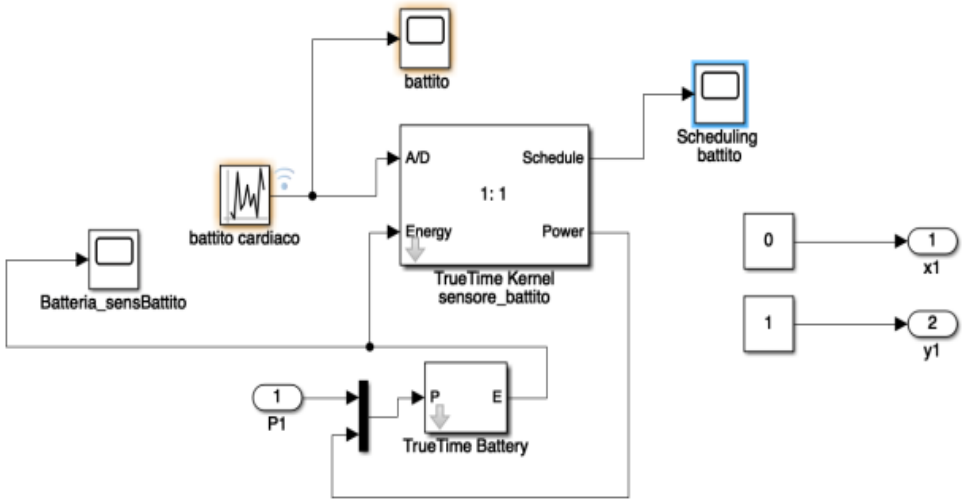

Fig. 3. Internal representation node 1 (sensor)

The heartbeat range is from 10 to 220 (Debugging input and output values is made possible by scope blocks). The sensor is powered through a battery that has a capacity of 15W (on average a battery of a pacemaker can last up to 8 years). Virtual links between the various components are made possible through from and *goto* blocks in order to make the project more visually understandable.

The wireless network, to which the sensor belongs, is defined by the TrueTime Wireless Network block that requires at the entrance the spatial positions of each node belonging to the network, conventionally we have decreed that the sensor – controller – actuator systems are placed at a very close distance between them because at the hardware level a pacemaker has a size in order to 3-4 centimeters

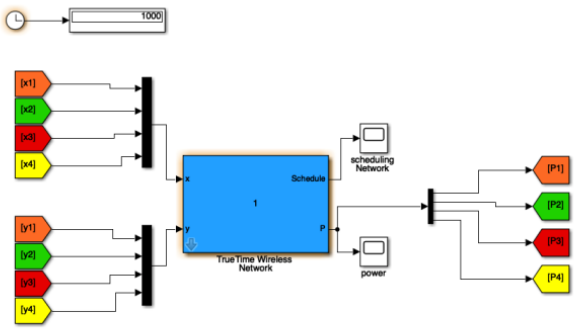

(2) The **second level** of development is that of the *controller*, which has the task of determining the patient's health status based on the detected heartbeat.

It is figured by the SubSystem Block '***Controller***' containing within it a TrueTime Kernel (powered by a battery with a capacity of 15W) that receives data from the TrueTime Kernel **Sensor_beat**.

The data received (*Heart rate*) are the input to a fuzzy logic controller. The fuzzy component (defined as '*health*') is used in order to digitally map what the health index is (in a range from [-5,10]).

The classifications of the heart rate ranges are as follows: *Critical* [10,30], *Bradycardia* [30,60], *Normal* [60,110], *Tachycardia* [110,200]; each range and its label, similarly represents the classification of beats in our discretion. Based on the ranges described above the operational health ranges are defined, which are as follows: *Tachycardia* [-5:0], *Critical_Health* [0:3], *Low_Health* [3:6] and *Better_Health* [6:10].

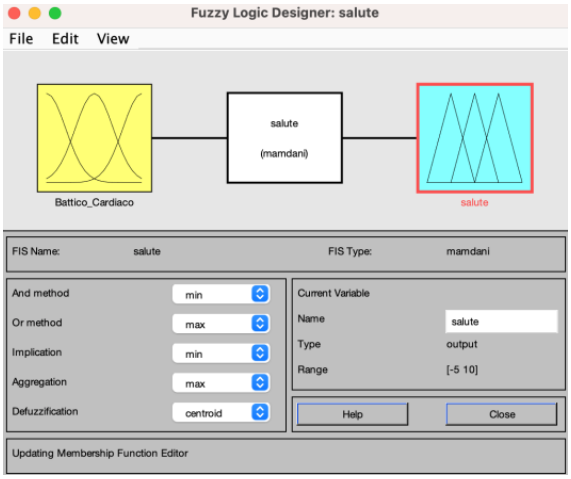

The parameters output from the fuzzy logic controller will be input of the actuator where the matlab function resides. The fuzzy logic components implemented, follows the *Mamdani* language model based on fuzzy inference rules between antecedent and consequent. The *centroid* was chosen as the method of defuzzification.

(3) The **third level** concerns the actuator that has the task of generating an electrical impulse to restore the patient's state of health.

It is figured by the SubSystem Block '***Actuator***' containing within it a TrueTime Kernel (powered by a battery with a capacity of 25W) that receives in input the value of the health that has been send to it by the *controller*. Based on the value shown, the state of health (which we remember to be between [-5,10]) corresponds to an integer ranging from [-1,2] that shows the electrical impulse that the patient receives. This process is regulated by a properly defined *Matlab Function*.

Only in cases where the state of health is excellent or tachycardia, the patient will not receive electrical impulses.

Obviously at the design level, each pulse value corresponds to a voltage ranging from 0.5V to 7.5V, unfortunately, for reasons of timing, this could not be implemented.

(4) The **fourth level** of development is that of the shock indicator that has the task of notifying the patient's condition by means of an LED lamp (obviously each condition corresponds to an LED lamp of different color)

It is figured by the '***Shock_Reporter***' SubSystem containing a TrueTime Kernel (powered by a battery with a capacity of 10W) that receives the shock value from the actuator and places it in the State-flow simulink input to determine which LED should be activated.

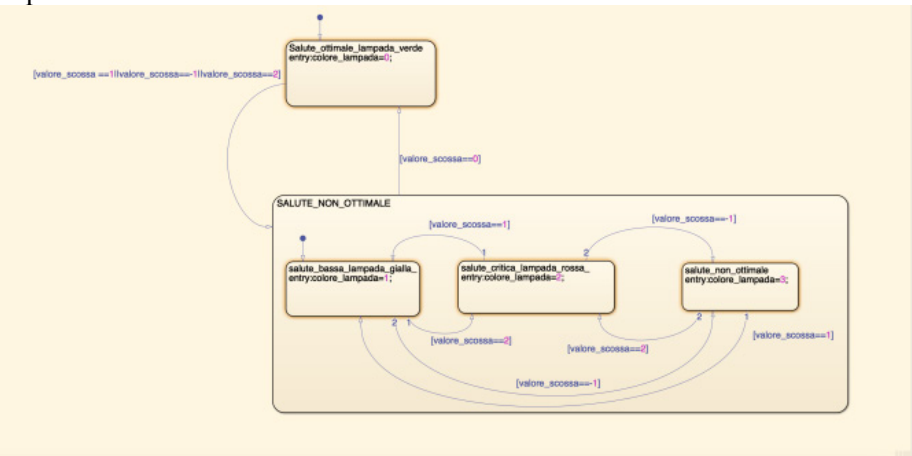

Fig. 4: DBMS

The Stateflow component is a logical control tool used to model reactive systems using state machines and flowcharts within a Simulink model. Within the Stateflow Simulink the shock value can correspond to 4 types of LEDs indicating the patient's condition. These LEDs are represented by a light that can have the following colors: red, yellow, green, blue . These are activated based on the output received:

- Value -1 -> Blue Led > Tachycardia Range
- Value 0 -> Green Led -> Normal Health Range
- Value 1 -> Yellow Led -> Bradycardia Range (Small Shock)
- Value 2 -> Red Led -> Critical Range (Strong Shock)

Battito Cardiaco	Stato salute	Scossa	Luce Led
Critica [10-30]	[0:3]	2	Rossa
Bradicardia [30-60]	[3:6]	1	Gialla
Normale [60-110]	[6:10]	0	Verde
Tachicardia [110-200]	[-5:0]	-1	Blu

Fig. 5: table that showing the logical structure of the PCMK system

PERFORMANCE EVALUATION

The performance metrics we measured are:

- The **responce time** in each node as the time interval between the generation of the heartbeat and the response of the system (namely the function that each node performs).
- The **end-to-end delay** between communicating nodes: in our project the nodes communicate in pairs, that means *beat_sensor* sends date to the *controller*, the *controller* to the *actuator* and this to the *shock_reporter*
- The p**acket loss** that show us the loss rate of packets

It's important underline the difference between **response time** and **end-to-end delay**: the ***response time*** *refers to the time it takes to get a response from a system, while the* ***end-to-end delay*** *refers to the time it takes for a data packet to travel from the source to the final destination across a network.*

Response time

We measured the response time graphically using the *Logic Analyzer* (Matlab toolbox that allows you to view graphically the result of the various signals produced in our pacemaker in relation to time).

Having set an *exectime* = 0.05 for each segment, we ran two simulation on three different samples. Below we show the measurements:

1°sample: Heartbeat 70 taken at the Execution Time 300 s

Actuator	Controller	Led
50.68ms	0.35ms	151 ms
50.68ms	0.34ms	151 ms

2°sample: Heartbeat 18 taken at the Execution Time 500s

Actuator	Controller	Led
90.7ms	40,34ms	191.02ms
90.68ms	40.34ms	191.02ms

3°sample: Heartbeat 39 taken at the Execution Time 820s

Actuator	Controller	Led
130.7ms	80.1ms	231ms
130.7ms	80.34ms	231.1ms

According to the result obtained, it emerges that there's a degradation of the network: by network degradation we mean the decrease in the performance of a network due to problems such as traffic congestion, packet errors, interference and hardware or software problems.Network degradation can manifest itself in several ways , including a decrease in transmission speeds, an increase in latency, a loss of packets or a decrease in network availability: *In our case we have increase in latency.*

By averaging the values obtained, we have an average response time for each block of:

- Actuator : 90,7ms
- Controller: 40,30ms
- Shock_value: 191,02ms

To try to reduce time that elapses between the generation of the signal by the sensor and the generation of the corresponding response by each component node we are going to reduce the executive in each segment of the TrueTime kernel functions, (that means we set *exectime* = 0.001 -> 10ms, leaving the sensor parameters unchanged).

With this new setting we get the following values:

1°sample: Heartbeat 70 taken at Execution Time 300 s

Actuator	Controller	Led
10.68ms	0.34ms	31.02 ms
10.67ms	0.33ms	31.01 ms

2°sample Heartbeat 18 taken at Execution Time 500 s

Actuator	Controller	Led
50.7ms	40.3ms	71.0ms
50.58ms	40.3ms	70.97ms

3°sample: Heartbeat 39 taken at Execution Time 820 s

Actuator	Controller	Led
89.7ms	79.3ms	110ms
90.7ms	80.3ms	110ms

The results obtained show a significant improvement in the response time, averaging the values int the table, resulting in an average response time for each block of:

- Actuator: 50.5 ms
- Controller: 40.24 ms
- Shock_value: 70.66 ms

We consider acceptable this values compared to the previous.

Delay end-to-end

In addition to the response time, we measured the end-to-end delay between the *source_node* and the *destination_node*.

- Sensor-controller
- Controller-actuator
- Actuator-Shock_reporter

And it is equal to 0.00034s or ***0.34ms***

Packet loss

For the packet loss, we have implemented an algorithm that bases his operation on the *sequence number* that each sent_packet has as an identifier.

We use the following three variables (initialized to 0 in each node's init file):

1. *Data.segnalegenerato_packet* -> used as identifier for the packets that each node sends
2. *Data.packet* -> used to check the packets received from the node.
3. *Data.lost_packet* -> check if a packet is loss during the transmission

Our model is entirely wireless, so the packet loss check is done for each communication between *source_node -> destination_node*

(Except for the shock_reporter which does not perform any sending function for the other nodes)

More in detail:

A check is performed which consists in seeing if the received packet has the sequence number (figured by the variable data.generated_packet_signal) that the node expects to receive. There are two possible scenarios:

1. The sequence number matches: we have been no losses and data.packet variable is increment
2. The sequence number doesn't match: then the variable of the data loss is incremented (**data.lost_packet)**

The values of the *data.packet* and *data.lost_packet* variables are printed with the "**disp**" function for each packer sent, so that packets can be tracked while the simulation is running,

CONCLUSIONS

The proposed PCMK Project as introduced integrates perfectly with the pacemakers that are already in place on the international market.

Thanks to the remarkable technological advances of recent years, patients with pacemakers can lead an absolutely normal life, without particular limitations.

The system could be the subject of future developments, in fact we are thinking about a first prototype of a pacemaker that recharges with the energy of the heart. The device has been presented in recent weeks at the congress of the European Society of Cardiology in Barcelona (Spain), the most important event in the world dedicated to cardiology.

The principle of operation is reminiscent of that of rechargeable wristwatches. The prototype in question collects the energy, stores it and, if necessary, uses it to generate the electrical impulse.

Tests were conducted on pigs, because the hearts of pigs are similar in size to ours and this device is structured so as to wrap the heart. The pacemaker has corrected the arrhythmia of the pig and the energy it collects is enough to stabilize even the beats of a human heart.

Although the mechanism works, it is difficult to install, as it requires an open heart operation, Highly dangerous; you are trying to switch to biological pacemakers that do not need batteries from To recharge.

REFERENCES

1. Essential MATLAB for Engineers and Scientists Brian D. Hahn, Daniel T Valentine ISBN 13: 9780081029978
2. Numerical Analysis Using MATLAB and Excel Steven T. Karris ISBN 13: 9781934404041
3. Matlab Simulink documentation MathWorks https://it.mathworks.com/help/matlab/
4. TRUETIME 2.0 – Reference Manual Anton Cervin Dan Henriksson Martin Ohlin Department of Automatic Control Lund University February 2016
5. https://www.my-personaltrainer.it/salute-benessere/pacemaker.html
6. https://www.fondazioneveronesi.it/magazine/articoli/cardiologia/il-pacemaker-senza-batteria
7. https://www.focus.it/tecnologia/innovazione/il-pacemaker-che-si-ricarica-coi-battiti-cardiaci
8. https://www.issalute.it/index.php/la-salute-dalla-a-alla-z-menu/t/tachicardia
9. https://healthy.thewom.it/esami-e-analisi/frequenza-cardiaca/

INTELLIGENT IRRIGATION SYSTEM

Giovanni Fanara
Computer Engineering and Networks Laboratory – Kore University of Enna – Italy
Email: giovanni.fanara@unikorestudent.it

Abstract. *The proposed irrigation system is based on minimising water waste and regulating the flow of water into cultivated land. A series of sensors are installed, which collect data, which are then used to extract a certain power value of the water flow necessary for the soil to reach, or maintain, a pre-set humidity range. A regulator is responsible for notifying the amount of water to be dispensed and the new value of soil moisture. The outgoing water is supplied by a tank, where an actuator dynamically checks the remaining capacity. In case the tank is empty, an alarm is triggered.*

INTRODUCTION

One of the biggest problems of today's civilization is reducing waste. Unfortunately, infrastructure resources are not always being used efficiently. For this reason there is a need to contain and reduce, where possible, waste. Of these there are all kinds, we will linger in the waste of water.

69% of water consumption is absorbed by agriculture. It is therefore in the fields that we should modernize irrigation systems to reduce water waste, and to follow in vegetable gardens, urban and domestic. Technology has made great strides to reduce the waste of water in agricultural crops, which also affect the final price to the consumer of a product, and among these, for example, drip irrigation is a very effective technique. We can also use it in our gardens, on the balconies, in the garden and in the pots that house the plants. [1]

The proposed irrigation system has been called "intelligent" because it uses mechanisms to limit, as little as possible, water waste. Surely it will not be able to solve every kind of problem, but if it will be used, it will help to defeat this great paradigm.

Agrotechnology is the field in which technology applied to agriculture is studied, providing a physical and logical infrastructure that helps farmers improve their processes. How? Getting a return on investment (ROI) in the short to medium term thanks to a strategic line of innovation that allows them to be one step ahead of their competitors. [2]

These technologies allow greater efficiency in cultivation, so as to adapt to the external conditions of the surrounding environment. We also point out the fact, that often certain parameters such as soil moisture, dew point, presence of parasites in plants, are not always monitored in many agricultural plants. The proposed project, on the other hand, takes into account some of the parameters mentioned in such a way as to allow not only a lower water consumption, but also a high efficiency in cultivation.

In the next sections we will cover the following topics:

- Section II: presentation of a project already present in the literature that deals with the same themes as the one proposed
- Section III: illustration of the techniques used and detailed description of the approach used
- Section IV: presentation of the simulated network scenario
- Section V: evaluation of system performance
- Section VI: conclusion and illustration of possible uses of the plant presented

RELATED WORKS

Nowadays, many companies have moved in the field of agriculture, managing, through the use of new technologies, to create very sophisticated irrigation systems. Their strong point is the accuracy and the amount of data that are collected. They also offer state-of-the-art services and allow not only efficient agriculture, but also environmentally sustainable agriculture.

One of the most important projects was realized by the company "Netsense", leader for years in the agro-meteorology sector. The project in question has been called " WiSense 2.0" and is a complete system of monitoring and automation of irrigation sectors suitable for all major crops (open field, trees, greenhouses, pottery, etc.) and compatible with all major types of irrigation system.

The system allows a significant reduction in irrigation volumes and higher product quality. This is possible thanks to sensors, which will allow you to maintain an optimal level of soil moisture, and manage irrigation times with a uniform yield, reducing living costs such as water, diesel and plant wear.

Irrigation shifts can be programmed via web, from the cloud portal LiveData, and can be connected to the level of ground, rain or evapotranspiration sensors (also wireless with Netsens IoT technology), to automatically adapt to field conditions. [4] In addition, this facility enables different activities:

- You can set irrigation programs, sector by sector, without going into the field
- The programming basis can be daily or weekly
- Irrigation shifts can be automatically changed based on field sensor measurements
- Alarms can be received on system problems based on the readings of the liter counters or pressure switches
- Up to 4 fertigation channels can be managed

As can be seen, the system described is both innovative and effective. Compared to several years ago, it offers very smart and sophisticated functions, but it has a very high cost. This product is suitable for large land and for leading companies in the agricultural sector. So let's say that the costs of this irrigation system are affordable for those with special needs.

PROPOSED APPROACH

We will consider a predominantly clay soil, which has well-defined characteristics. One of these is the humidity of the soil; it is characterized by some constants that depend on the composition of the soil, and are:

- maximum water capacity (M.W.C.): the point of water saturation of the soil, usually it is reached when an irrigation or abundant rain occurs
- field capacity (F.C.): represents the ideal situation for the water supply of plants that draw on water without much effort
- withering or wilting point (W.P.): the point where the plants grown in that soil are no longer able to draw on water from it. The water present in the soil at the point of withering cannot be used by plants.

The moisture content at each potential value is extremely variable depending on the nature of the soil. In other words: at the same potential two different soils can make available to the plants different quantities of available water. For example, a clay soil may contain more water than a sandy soil. This property is reflected in the irrigation technique because, with the same amount of water to be administered, in the first soil it is possible to intervene with larger irrigation volumes at larger intervals (shifts); in the second soil, on the other hand, to avoid water losses due to percolation, it is necessary to reduce volumes and adopt shorter shifts. [3]

The soil considered in the proposed irrigation system, will be characterized by the following values:

$$M.W.C. = 45\%$$

$$F.C. = 30\%$$

$$W.P. = 10\%$$

The aim of the project is to maintain a soil moisture oscillating in an interval ranging from 18% to 25%.

The system consists of 3 different networks including a wired CSMA/CD Ethernet and two wireless 802.15.4 (ZigBee).

The first network is wireless and is used by sensors to communicate with the gateway.

3 sensors are used in this irrigation system. In particular, reference was made to the datasheets of some sensors on the market:

- Aranet Soil Moisture Sensor (Wireless Soil Moisture Sensor) [5]
- Aranet T/RH IP67 sensor (Wireless Temperature and Humidity Sensor) [6]
- Bitline RP-1 (Wireless Detector of Rain) [7]

The sensors have the task of transmitting the detected data to a gateway, which will then forward them to a controller.

The first sensor is used to detect the value of soil moisture.

A second sensor will detect the humidity and temperature of the area where the soil is present. They are other 2 parameters to be kept under observation and will be considered as "ideal" those values ranging respectively, from 50% to 70% and from 20° to 30°.

Finally, there is a last sensor that detects the intensity of precipitation, so that it will signal the system to stop the water flow.

According to datasheets, all sensors are fitted with 2800 mAh AA batteries, except for the rain detector (1a), which requires direct current. For the latter, a 12 V battery pack with a capacity of 4000 mAh

was used, to which is attached a transducer that converts the current received into the one desired by the sensor. This same battery is also used to power the gateway.

The gateway, since it belongs to all networks, is responsible for sorting messages that arrive to it.

The second network is wired and includes the gateway, controller and regulator.

The controller receives from the gateway the data coming from the sensors, processes them and thus will get a certain power value of the water flow to be delivered. This, along with other information, will be forwarded to the regulator.

The regulator is used to adjust, through the received data, some parameters and sends the updated values of soil moisture and the amount of water to be dispensed to the gateway, which in turn will deliver them to the soil moisture sensor and actuator respectively.

The third network is wireless and allows communication between gateway and actuator or conversely.

The actuator receives information, which comes from the regulator, processes it to determine the values of tank capacity and alarm, which will then be forwarded to the gateway to be received by the regulator.

SCENARIO

The design proposal was simulated using Matlab, specifically Simulink with the use of the TrueTime toolbox.

We can see the scenario as if it were divided into 4 parts: Sensors and Gateway, Controller, Regulator and Actuator.

SENSORS AND GATEWAY

The scenario begins with sensors that detect data. To do this, let's look at the image (1a): we can see that the input to the kernel of the soil moisture sensor, coincides with its own output. This is because the soil moisture is updated by the regulator, which will forward the new value to the sensor. For the other sensors, instead, there are signal builder blocks in which are loaded the values of temperature, humidity and intensity of rain recorded over a whole day, measured at a rate of one minute. Why with such a cadence? In the datasheets of the sensors used [5] [6] [7], the periods that can be supported by these sensors are precisely specified and, among many, a period of 1 minute is chosen. Therefore 1 real minute will coincide with 1 second in the simulation. In addition, the sensors are not exactly accurate, as for the temperature and humidity sensor, there is a margin of error of ± 0,3° and ± 2% respectively.

All sensors forward an initial timestamp to the gateway to determine some performance metrics. In particular, the timestamp generated by the soil moisture sensor passes between the various nodes of the system.

The gateway (1c) has 9 outputs, but has no input. All these outputs are used to show the user the performance related to reaction time, packet loss and packet trends coming to the gateway.

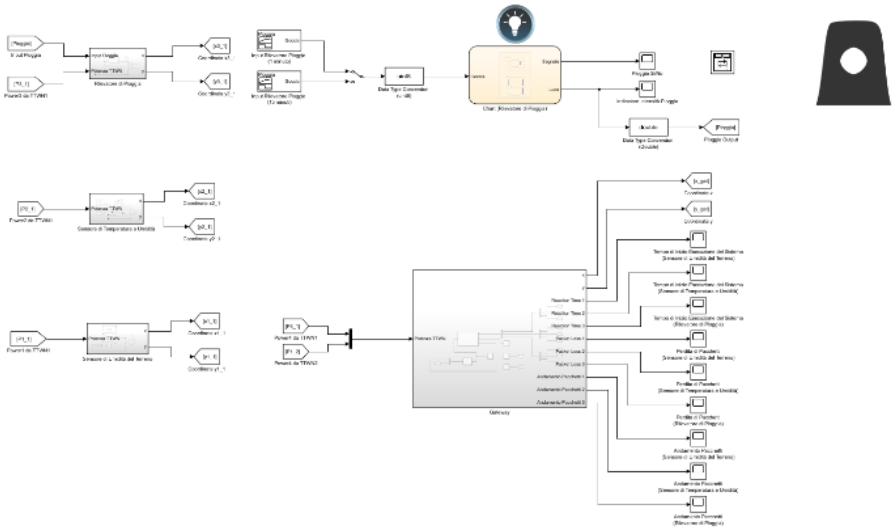

Image 1: (a) on the left two sensors are shown, (b) on the top the rain detector and (c) on the right the gateway

The rain detector has a characteristic that distinguishes it from the others: it has a plate sensitive to water drops and, since it may happen that a few drops of water from various events outside the rain arrive, for example condensation or excessive humidity, there has been implanted a heating mechanism of this plate to prevent the accumulation of water and incorrectly detect rain. In the simulated scenario, the MBSD technique (2) was used to detect the intensity of rain and prevent false revelations. For the latter, an anti-rebound control has been implemented.

The input of the Chart (1c), corresponds to a block signal builder in which the values related to the rain are recorded. At the exit of the Chart there will be two values, one tells us in general if it rains or not, turning on the lamp in the positive case, the other signals the intensity of the rain and, in addition to being sent in input to the rain detector, will cause the alarm to color a certain way according to how strong it is raining. The colors will be: Green (=0), Yellow (=1), Orange (=2), Red (=3).

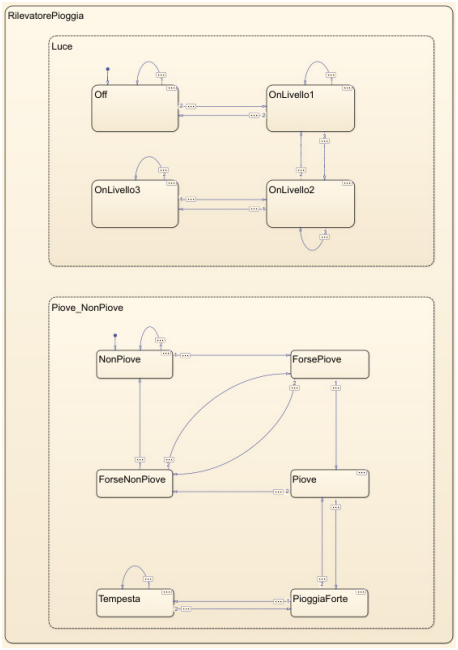

Image 2: The entire Chart is shown with the Light status at the top and the Rain_NotRain status at the bottom.

CONTROLLER

The controller (3a) determines the power value and calculates the system start response time for each message sent by the sensors. It is part of the wired 2 network and receives messages through the gateway.

It receives the values from the sensors and immediately outputs them to controllers that adopt fuzzy logic. The first fuzzy controller takes the input temperature and humidity and determines the weather that takes values from 1 to 10. If the value is low, the weather will be cold and dry, while if it is high, the weather will be hot and humid. If the Weather variable takes a value between 5 and 7, it will be considered ideal.

In the second fuzzy controller, soil moisture and weather enter the input. Between the two will have a greater weight the soil moisture, because if the soil is too dry or wet, it risks to die the vegetation.

The power, that exits from the second fuzzy controller, enters, along with the value of the Rain, in a matlab function. Rain can affect the power of the water flow to be dispensed, for this reason the matlab function has been introduced whose output will correspond to the new power value. The latter, will then be the input of the controller that will send it to the regulator.

REGULATOR

The regulator (3b) belongs to the wired network 2 and takes care of the regulation of water flow and soil moisture. It receives messages from the controller and the actuator, which will contain data that will be output in order to pass through a matlab function. From the latter, the new soil moisture and the amount of water that must be removed or not from the tank are determined. Once these two values are

received in input, the regulator forwards them, through the gateway, respectively to the sensor and the actuator.

ACTUATOR

The actuator (3c), because it consists of a detector of the water capacity contained in the tank, receives the energy needed to operate from a battery. It is also located in network 3 where only he and the gateway are present. It is activated when it receives a message from the regulator and its purpose is to dispense water from the tank to irrigate the ground and notify, by means of an alarm, whether the tank is empty or not. It is located near the gateway, at 30 meters, in order to receive data quickly and limit the end-to-end delay, which will be determined by it. We can see the presence of a test tube and a siren, which indicate respectively the capacity of the tank and the value of the alarm. When the alarm has a value of 1, it will make the siren red (=1), otherwise it will remain black (=0).

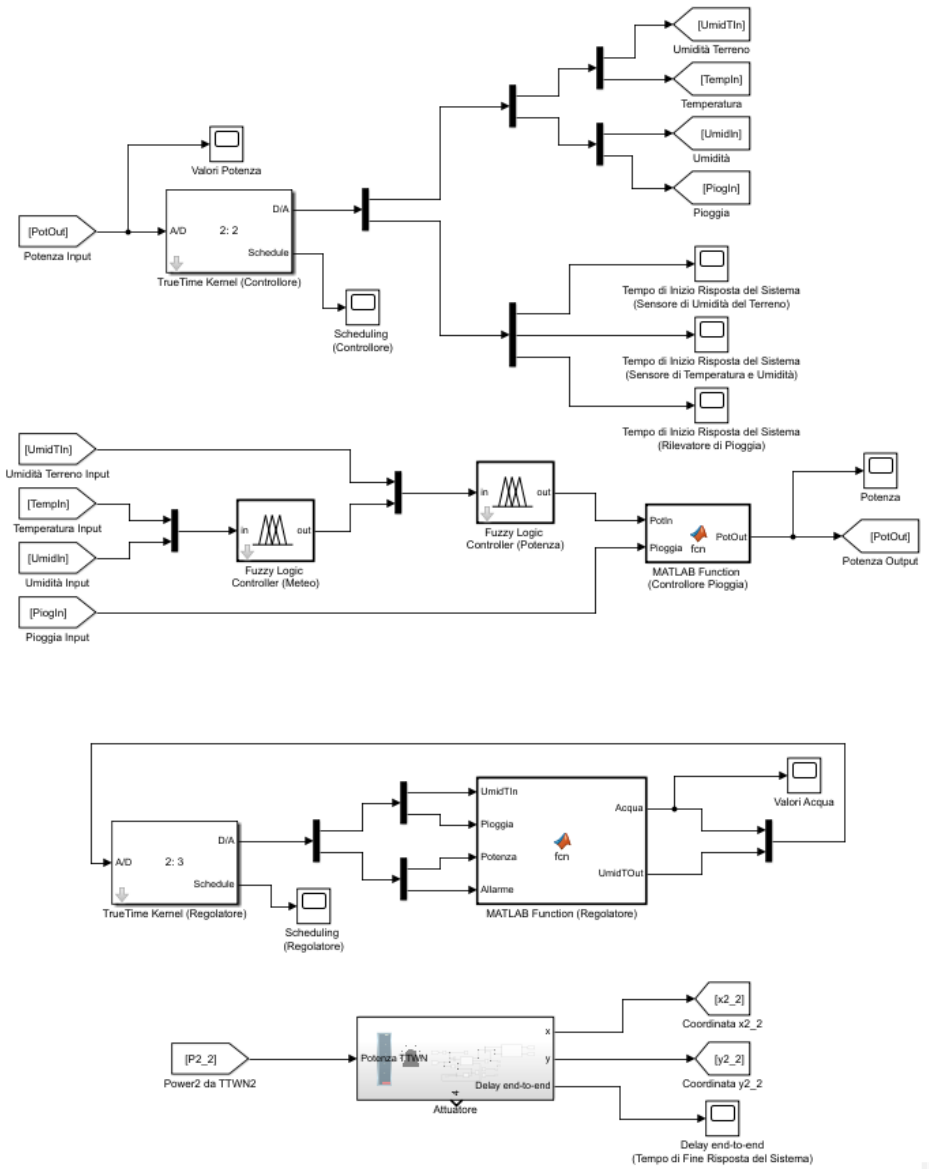

Image 3: From top to bottom are shown: (a) the controller, (b) the controller and (c) the actuator.

PERFORMANCE EVALUATION

In the proposed system some performances have been calculated. They are used to evaluate the quality of the irrigation system in terms of speed, safety and efficiency. The performance metrics calculated are:

- Reaction time
- Initial Response time
- Final response time

- Packet loss

We will analyze only those related to the soil moisture sensor, because they will be almost the same for all the others. All plots consider a 60% probability of packet loss.

The reaction time corresponds to the time interval between the forwarding of a request to the system and the start of its execution. It varies continuously, because more messages arrive at the gateway, more it creates a slight delay caused by the queue.

The initial response time corresponds to the time interval between the forwarding of a request to the system and the start of its response. We can see how the initial response times of the system, worsen from time to time and then suddenly improve, and continue in this way cyclically.

The final response time, or also called end-to-end delay, corresponds to the time interval that subsist between the forwarding of the request to the system and the end of its response. We immediately notice that the delay end-to-end turns out to be decidedly elevated in some moments. Because this happens? It is due to the high probability of packet loss, caused by the different obstacles that the signal encounters to reach the destination, such as logs, leaves, plants, greenhouses, and as a result it will take longer to arrive, provided it is not lost.

The packet loss corresponds to the number of packets lost during transmission. It is calculated in wireless transmissions because the signals, propagating in the ether, are subject to phenomena of refraction, reflection and reflation, noise and other phenomena that cause their loss.

CONCLUSIONS

The system produced, proposes some technologies already implemented in many devices used today, but at the same time is innovative under two factors:

- The first is the alarm that triggers as soon as the tank is empty
- The second consists of the heated plate present in the rain detector that makes sure to avoid wrong readings

In the literature there will certainly be more performing systems, such as the one shown in section II, with additional features. However, it is difficult to find on the market a system that offers the two characteristics shown above and that makes it interesting from every point of view. Surely it can be improved both in terms of performance and efficiency. On the other hand, this would require additional and not insignificant costs. The purpose of the proposed system is precisely to offer good quality at a sustainable price by all.

BIBLIOGRAPHY

[1] https://www.nonsprecare.it/spreco-acqua-pubblica-italia-reti-idriche-colabrodo?refresh_cens

[2] https://jgambin.com/it/cose-lagricoltura-intelligente-ecco-come-la-tecnologia-sta-influenzando-il-suo-sviluppo

[3] https://www.unirc.it/documentazione/materiale_didattico/1462_2016_412_27418.pdf

[4] https://www.netsens.it/prodotti/risparmio-idrico-4

[5] https://cdn.bfldr.com/FS48XT6B/at/c6qvt88pw3f5nz8zjhvf495r/Aranet_Soil_Moisture_sensor_datasheet_v12_WEB.pdf

[6] https://cdn.bfldr.com/FS48XT6B/at/fp2wmwsz5k4j85t9pxnrhx87/Aranet_TRH_IP67_sensor_datasheet_v22_WEB.pdf

[7] https://www.bitline.it/rp1.pdf

[8] https://docs.rs-online.com/4fc1/0900766b8167401b.pdf

[9] Anton Cervin, Dan Henriksson, Martin Ohlin: "TrueTime 2.0 – Reference Manual". Department of Automatic Control, Lund University, Sweden, April 2016.

IOT FOR INDUSTRY A FACTORY 4.0 STUDY

Ferlante Salvatore, Palermo Alessio Maria
Computer Engineering and Networks Laboratory – Kore University of Enna – Italy
Email: salvatore.ferlante@unikorestudent.it
alessiomaria.palermo@unikorestudent.it

Abstract. *The case study is based on the need to optimize resources in order to produce a number of pens. In this simulation the goal is to produce 1000 pens in 24h. The structure of the project is hierarchical where a control center is responsible for managing the levels of demand that, passed to the production management centers (islands), cause the switching on/ off of production chains.*

INTRODUCTION

The following project simulates an industrial scenario, which, through embedded systems and automated assembly lines, manages the demand for the production of pens.

The management of materials warehouses (plastic, metal, cartridges, etc.) is entrusted to a decision controller that, through a fuzzy logic complete with information mapping, ensures the continuous availability of materials as efficiently as possible.

In order to automate the production process, a hierarchical management of requests has been implemented. Through a controller that, by processing the information (consumption, available quantities, required quantities, etc.), communicating with the islands, manages the requests necessary to finalize the objective.

For appreciation, the project has been coded through colored sections:

- The production section has been highlighted in green. You can notice four distinct regions such as (top to bottom):
  1) Island that manages production of caps
  2) Island that manages production of tips
  3) Island that manages production of cases
  4) Island that manages pen assembly
- The control section has been highlighted in blue. You can notice two distinct regions such as:
  - In red the logistics center with the decision controller.
  - In gray the control center with controller.
- In orange was highlighted the storage section with warehouses related to:
  - Plastic
  - Metal
  - Cartridges
  - Caps
  - Cases
  - Tips
  - Pens
- The analytical section has been highlighted in purple. You can see two embedded systems aimed at analyzing network statistics such as:
  - Reaction Time
  - Response Time
  - Packet Loss

RELATED WORKS

Nowadays, automation is one of the most active areas of research. In the literature, you can appreciate a wide choice of standards and definitions that help us to characterize the project.

In order to be able to compare the project, we first need the characterization in order to compare the results with the production standards of the more general field.

From the article 'How to Define Industry 4.0: The Main Pillars Of Industry 4.0' it emerges that the most modern industrial trend focuses on the adoption of certain technologies defined enabling.

The enabling technologies proposed are:

- Advanced production solution.

- Additive manufacturing.
- Augmented reality.
- Simulations.
- Industrial Internet of Things.
- Cloud.
- Sicurezza Informatica.
- Big Data Analytics.

By comparing the requirements, it is possible to say that the project already presents flexible, adaptive and interconnected systems for the optimization of both the use of materials and productive infrastructures.

In addition, through various simulations, it was possible to further optimize the individual processes that give life to the overall industrial project.

We can also talk about the industrial internet of things because the production chain is based only on intelligent machines capable of communicating to external controllers through network protocols.

The project is predisposed to the distribution of information and cloud computing by replacing the embedded controller with a centralizer able to communicate with cloud systems for the service host and implementation of a demilitarized subnet(dmz) (between centralizer and machinery) and a network equipped with security systems able to guarantee the confidentiality of the information transmitted.

Finally, in order to optimize production according to plausible demand (set at 1000 for simulative simplicity), a market analysis should be introduced.

Comparing now a factory 3.0 (most common case in Italy) we can see the disparities between the two.

Features	Industry 3.0	Industry 3.5	Industry 4.0
Core Concept	Highly automated system	Decision making ability with the improvement of existing environments	Smart factory with CPS and IoT
Production Strategy	Mass Production	Flexible Manufacturing (diverse products with small lot size)	Mass Customization
Quality Control	Statistical Process Control	Advanced Process Control	Self-aware; Self-predict
Resources Management	Materials Management; Human Resource Management; etc.	Total resource Management	Self-configure; Self-optimize
Development Priorities	Investment of hardware	Integration of ability of data analysis and experience of management	Construction of CPS and IoT

As can be seen from the above table, the main differences are based on the adaptability of the production process. Moving from a totally static production strategy and arbitrary values to a flexible one, there were marked improvements in production, drastically reducing production redundancies in the short term. Instead, in order to optimize production in the long term, we need a preventive and periodic market study.

To optimize the resources needed for production, using a generic study is not enough to minimize waste or to always guarantee the necessary quantity that could vary due to any waste due to errors. In order to optimize production as much as possible and, consequently, revenue, it is necessary to develop an adaptive system in order to implement customized material requests. A dedicated infrastructure is not enough, as it is burdened by the amount of data to be processed. Therefore, it is necessary to "listen" to the instantaneous demands of the machinery in order to be able to optimize, based on the available quantity and on the times of obtaining the resource, the quantity, distributed in a time span t, optimal for completion of the production forecast.

In conclusion, more intelligent and interconnected systems allow us to estimate with a fair precision, the future trend of production with less computational load due to a smaller amount of data processed in real time. Without a doubt, a self-adapting process will be much more optimized than a periodic optimization process.

THE PROPOSED APPROACH

The system is divided into sections, in which we find regions, which communicate by interconnecting five cable networks and one gateway.

1. **Management section, Network 1**

In this section, fixed a quantity of pens to be produced, the controller calculates the amount of material needed, net of the amount already produced, and, through the network, send the islands a percentage value of the requests for each item to be produced necessary for the construction of the pen.

2. **Production section, production area of caps, tips, cases (Network 2, Network 3, Network 4)**

In this section, data from the network for the production of components arrives and based on the required percentage, the actuator processes the optimal number of machines to be turned on.

3. **Statistics section, Network 5**

In this section, the sensors, observing the statistics coming from each single network, analyze the network in order to be able to find any leaks and bottlenecks inside.

SCENARIO

This scenario was simulated using Matlab with the help of the Simulink plugin and the "TrueTime" library, the networks are connected to each other via CSMA/CD (Ethernet) and the relative exchange of data happens through gateway that distributes the information based on the type forwarding them to the network of competence. The proposed simulation was performed by simulating an entire working day (86400 sec).

1. **Management section, Network 1**

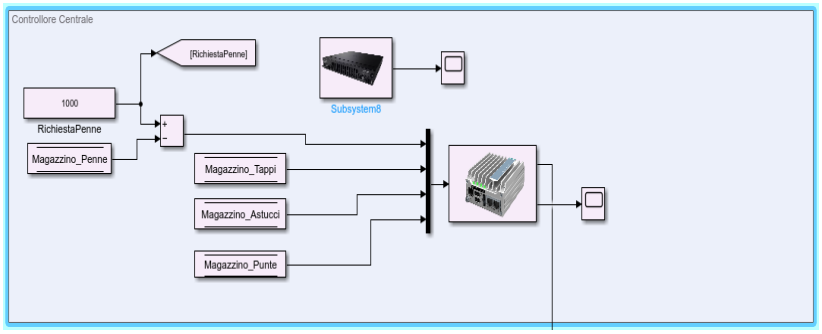

The controller receives the input number of pens to be produced, which is also sent to the logistics center via the block "Go To", which is subtracted from the number of pens already produced in the pens warehouse and also reads the number of material available for each warehouse. Calculate the percentage for each component and send it to the gateway.

2. **Production section, production area of caps, tips, cases (Network 2, Network 3, Network 4)**

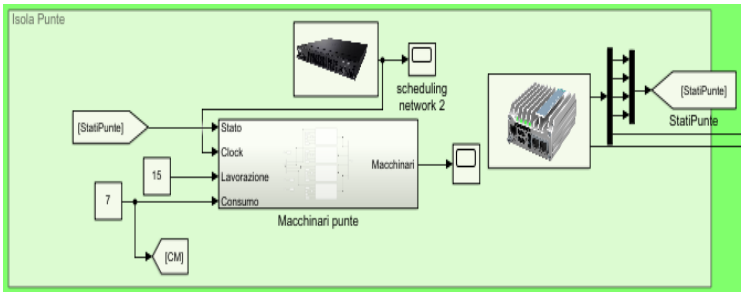

The actuator receives the percentage of caps to be produced and processes the number of machines to be turned on. Once the number is processed, it sends the states (0 turned off and 1 on) to the machines, designed by "MBSD", through a communication bus (symbolized by a FROM and a GO TO).

The machine system receives the input status of the drill bits from the actuator, the clock, the processing time and the material consumption.

At this point, the machines that receive state equal to 1, are activated and, through a direct control on the presence or not of material, begin the processing.

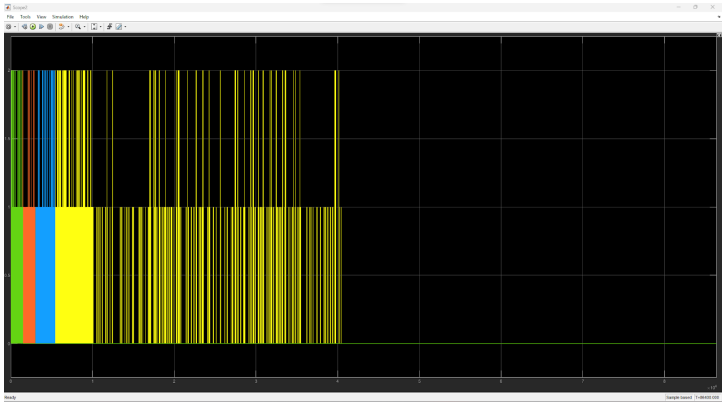

The machine, to monitor its state of operation, emits a signal that takes the values:

- Off
- 1)Processing
- 2)Error in production
- 3)absence of material

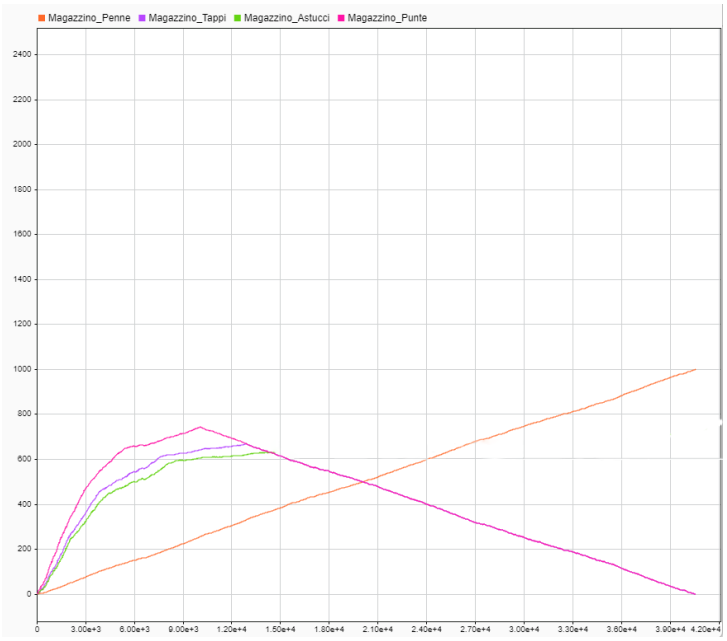

After processing, the machines increase the quantity of the product available in stock.

3. Statistics section, Network 5

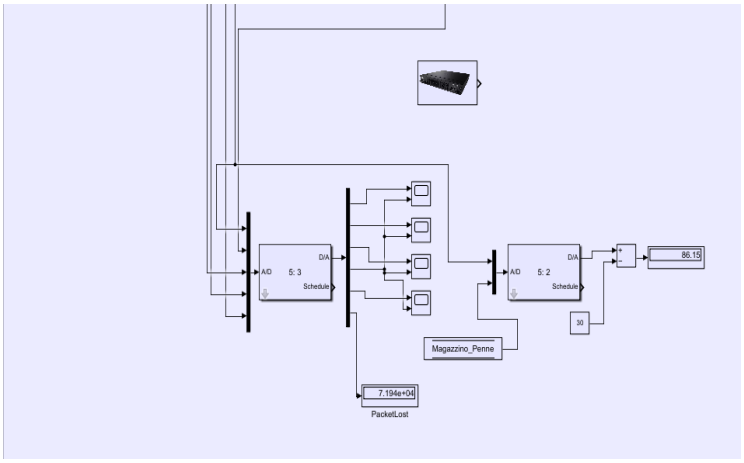

The sensors receive incoming data from the network, in particular the "Current Time" of the emission/ reception of the package and processes them in order to obtain: "Response Time", "Reaction Time" and "Packet Loss".

4. Gateway

It is responsible for sorting information from the controller. Depending on the destination of the message, contained in the "type" tag, the gateway forwards the said to the right network of competence.

5. Pen assembler

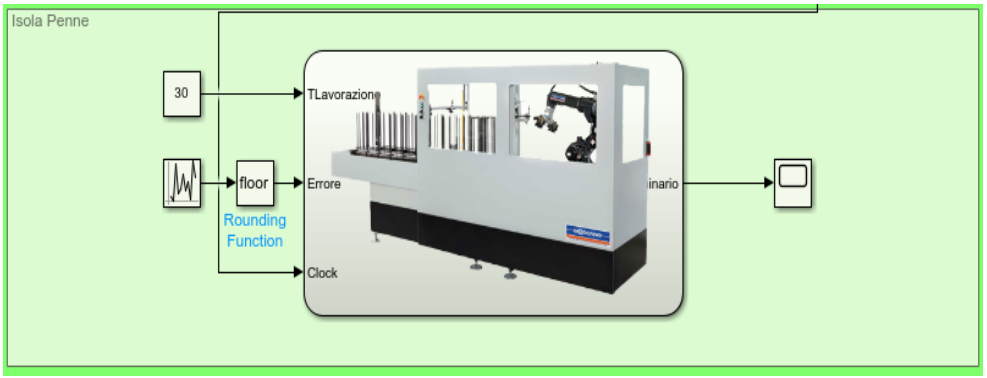

It receives analog input processing time, a random number for error and a clock.

As soon as the components needed for assembly are available, a pen is output and loaded into the storage.

6. Logistic center

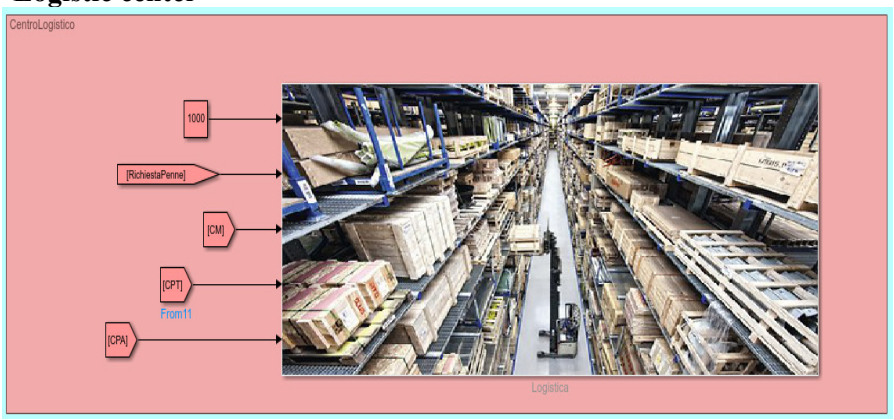

The Logistics Centre receives:

- The size of the maximum transport of material.
- The request for pens
- The specific consumption of machinery

This information, together with the quantities already present in the warehouses, are pre-mapped and then fed to the fuzzy who, through the rules, are reworked in the amount necessary to order that being remapped turns into order of real load.

PERFORMANCE EVALUATION

The following performances were obtained following a simulation of 24h or (86400 sec).

1. Reaction Time

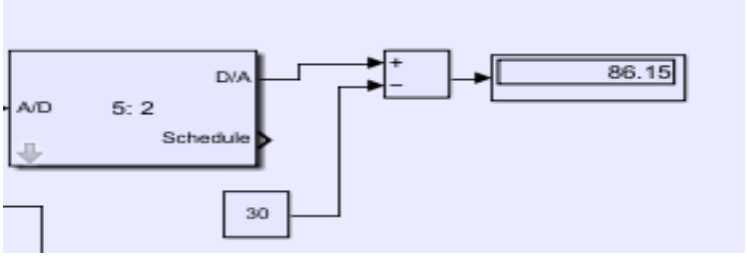

The display shows the average reaction time value.

It is calculated through the summation of the reaction times of the single requests in turn calculated as the difference between the timestamp of the pen realization and the timestamp of the request for pen production.

2. Response Time

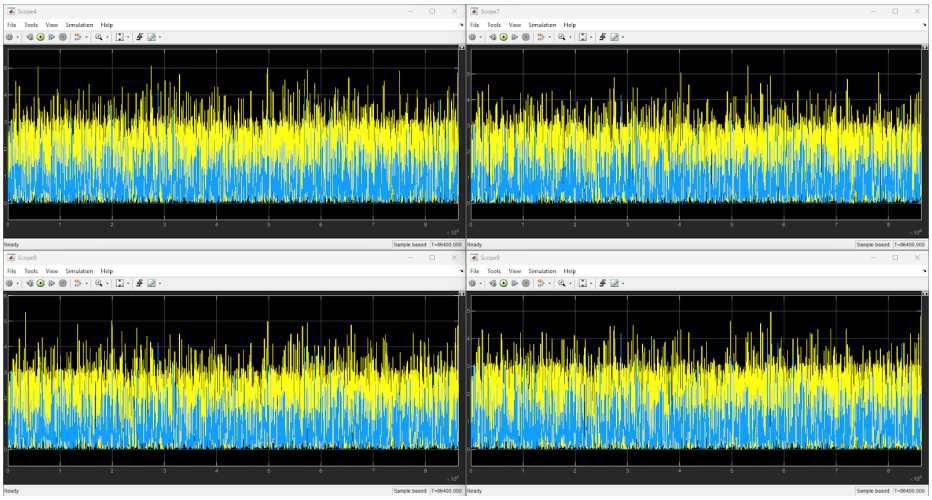

In blue is represented the response time between the controller and the gateway, while in yellow the response time between the controller and the actuator. Consequently, the subtended value between the yellow curve and the blue curve represents the response time between the gateway and the actuator. In general, we calculate the response time as the difference between the timestamp of the message reception and the timestamp of the message sending.

3. Packet Loss

Above is the lost packet counter, which corresponds to about 2.4% of total packets

CONCLUSIONS

In conclusion, having managed to get the result in just 12h we can consider the system sufficiently efficient. Analyzing the data from the network we can observe that:

- The packet loss corresponding to 2.4% of the total packets is consistent with the statistics of the reference devices.
- The reaction time is adequate to the sum of the medium response time of the single machinery and the gateway.
- The mode of response time is very close to their median.

We can consequently say that the network has been quite solid for the purposes of simulation. Also, we could probably increase the number of pens to be produced in 24h.

REFERENCES

1. *Aiman, M. et al. 2016. Industry 4.0: A review on industrial automation and robotic. Jurnal Teknologi (Sciences & Engineering)*
2. *A Conceptual Framework for "Industry 3.5" to Empower Intelligent Manufacturing and Case Studies*
3. Klaus Schwab, The Fourth Industrial Revolution, World Economic Forum, 2015, trad. La quarta rivoluzione industriale, Franco Angeli, 2016
4. https://www.fpmgroup.it/ita/Presse-stampaggio-a-caldo-metalli-non-ferrosi/ROVETTA-FO-350.html

5. http://it.top-aluminumlife.com/aluminium-extrusion-machine/2000t-aluminum-profile-extrusion-press.html
6. https://powerjetmachine.cn/plastic-machine/pet-preform-injection-molding-machine/#video
7. https://www.cisco.com/c/en/us/products/collateral/routers/4000-series-integrated-services-routers-isr/data_sheet-c78-732542.html
8. https://support.industry.siemens.com/cs/attachments/31255333/GS_BoxPC627B_enu_en-US.pdf
9. https://en.wikipedia.org/wiki/Advanced_manufacturing
10. https://it.wikipedia.org/wiki/Produzione_additiva
11. https://it.wikipedia.org/wiki/Realt%C3%A0_aumentata
12. https://it.wikipedia.org/wiki/Simulazione
13. https://en.wikipedia.org/wiki/Industrial_internet_of_things
14. https://it.wikipedia.org/wiki/Cloud_computing
15. https://it.wikipedia.org/wiki/Sicurezza_informatica
16. https://it.wikipedia.org/wiki/Big_data_analytics
17. https://www.cisco.com/c/en/us/products/collateral/switches/catalyst-9400-series-switches/nb-06-cat9400-ser-data-sheet-cte-en.html

ABOUT TYPICAL NONLINEARITIES IN AUTOMATIC CONTROL SYSTEMS

Goncharova Victoria
Saint Petersburg State University of Aerospace Instrumentation
Saint Petersburg, Russia
goncarovav344@yandex.ru

Abstract. *The paper considers typical characteristics of nonlinear automatic control systems (ACS). The elements of the systems that correspond to the characteristics under consideration are listed.*
Keywords: *nonlinear characteristics, automatic control systems, dead zone, backlash, hysteresis effect.*

Any ACS is essentially nonlinear. This is due to the fact that if, for example, we assume that the system is linear in the first approximation, then the amplifier-force element (USE) of the regulator will always be nonlinear, due to the large gain and limited power of the control element.

As an example, let's take (US), the characteristics of which in general have the form in Fig. 1, where the input value of the USE is postponed along the abscissa axis, the output value along the ordinate axis. In the marked area a, the system has a linear appearance. In regulators that operate with a large gain (with low static), the specified value a can vary in the range less than 0.005 – 0.01. Often in an adjustable system, the deviation x1 is much larger, so the regulated system almost always behaves as a nonlinear one [1].

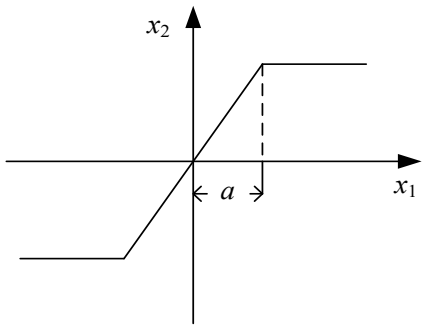

Fig. 1 – General view of the characteristics of the amplifier-power element of the regulator

The USE elements include

— micro-telephone amplifying element of the handset membrane;
— an electro-vacuum amplifying element, which is a well-known vacuum electron lamp;
— a semiconductor amplifier element, which is a semiconductor triode (transistor);
— a superconducting amplifying element, otherwise called a cryotron;
— a magnetic amplifier element, more briefly called a magnetic amplifier;
— dielectric amplifier element (dielectric amplifier).

We will also consider common examples of elements with an insensitivity zone. The general view of the characteristic of which has the form in Fig. 2.

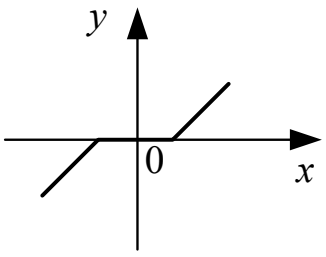

Fig. 2 – General view of the "dead zone" characteristic

This characteristic is possessed by most executive mechanisms. For example, the electric motor of the actuator will be at rest until the torque exceeds the moment of resistance on the motor shaft. The nonlinear function will have the form

$$y = \begin{cases} k(x-b), \text{ при } x \geq b; \\ 0, \qquad \text{при } |x| < b; \\ k(x+b), \text{ при } x \leq -b, \end{cases}$$

where k is the proportionality coefficient (k = tg α) [3].

The next well-known characteristic of nonlinearity is backlash or dry friction. This characteristic is usually inherent in mechanical transmissions and is due to the gap (backlash) in the joints of the elements. An example of the characteristic is shown in Fig. 3 and the circuit model in Fig. 4.

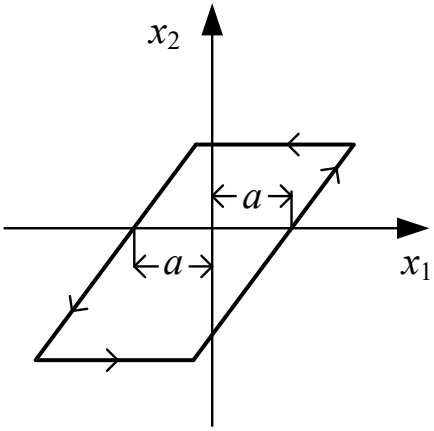

Fig. 3 – Characteristics of the scheme of a nonlinear element of the backlash type

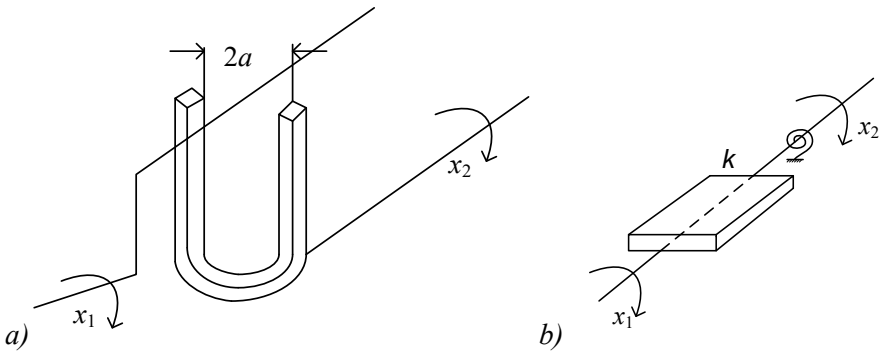

Fig. 4 – A model of a nonlinear element circuit with a backlash type characteristic

The analytical description of it is practically not used, because it is very complex and impractical. It is usually replaced by a verbal one.

If the value increases, then the dependence corresponds to a straight line shifted to the right from zero by an amount. If the value decreases, then the dependence corresponds to a straight line shifted to the left of zero by an amount. When the sign of the velocity of the magnitude x changes, idling will be observed at first, that is, the output value will not change during the time until x changes by a value greater than 2.

Next, consider the nonlinearity, the model of which is shown in Fig. 5 and its characteristic (Fig. 6) with the presence of a hysteresis effect.

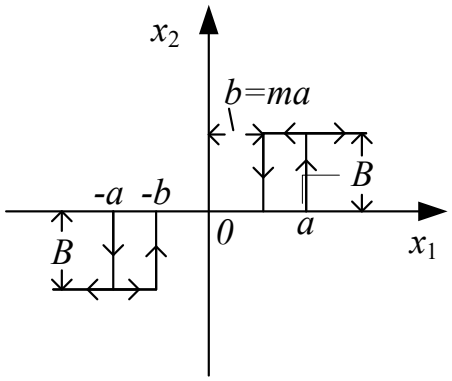

Fig. 5 – Characteristic of the scheme of a nonlinear element with the presence of a hysteresis effect

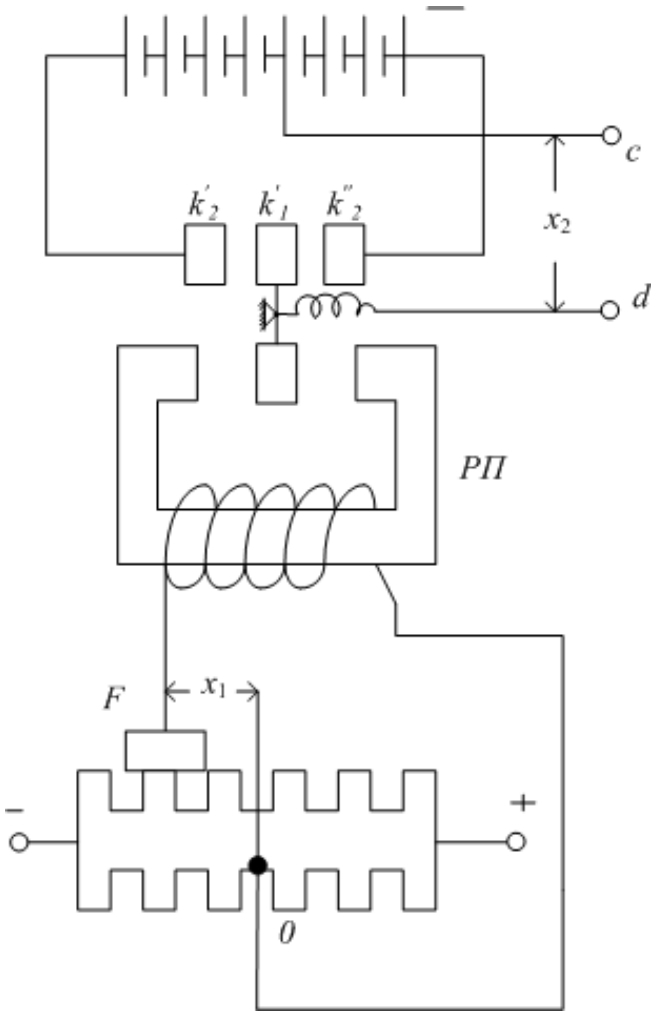

Fig. 6 – A model of a polarized relay circuit of a nonlinear characteristic element with the presence of a hysteresis effect

When changing x_1 in the range from 0 to a, x_2 remains equal to 0. When changing $x_1 > a$, x_2 is constant and equal to B. When x_1 is reduced to the value $b=ma$, x_2 remains constant and equal to B. When $x_1=ma$ x_2 changes abruptly to 0. The value of x_2 is an odd function of x_1. The polarized relay (Fig. 6) has a movable contact k_1, which, depending on the magnitude and direction of the current in the relay winding, is connected to a fixed contact k_1' or k_1'', or is in the middle position between them. [1-4]

Thus, some types of nonlinear elements, their characteristics and possible physical correspondences are considered. It should be noted that the system may include not only one type of nonlinear ele-

ment, but two or more at once, connected in parallel or in series, which imposes a number of restrictions on the operation of the system. Such limitations should be taken into account when operating the system.

References

1. L. S. Goldfarb, On some nonlinearities in control systems, Automaton. and Telemech., 1947, volume 8, issue 5, 349-383

2. G.S. Tsykin, Amplifiers of electrical signals, ed.. 2nd, pererabot., M., "Energy", 1969, 384 p.

3. Edited by V.V. Solodovnikov, Fundamentals of automatic regulation, Mashgiz, 1954, 1117 p.

4. G.V. Zeveke, Standard instruction on automatic regulation of excitation, Moscow, Gosenergo-izdat, 1944

ABOUT AUTOMATION OF RECOGNITION AND COUNTING OF REINDEER LIVESTOCK IN AERIAL PHOTOGRAPHS

Gordeev Mikhail
Saint Petersburg State University of Aerospace Instrumentation,
Saint Petersburg, Russia
E-mail: gordeevm2019@internet.ru

Abstract. *The work considers the solution of an urgent problem in the field of research of the North – monitoring the state of biological resources, which include wild reindeer. Using the example of the task of recognizing and counting the number of deer on aerial photographs as objects with variability, the issue of automation and options for its implementation are considered. The use of a convolutional neural network with training on reference images of animals in the MS COCO dataset and subsequent additional training on images of wild reindeer is considered.*
Keywords*: recognition, automatic counting of animals, wild reindeer, neural network training, training.*

Introduction

The problem of recognition in the image of various objects has been known for more than 70 years [1]. Today there is a task of automatic recognition of objects with their classification and counting of the number. In this form, the problem has not been completely solved, but examples of efficient algorithms for some particular problems are known [2, 3].

These objects include (Fig. 1):

natural objects – people in clusters, animals and birds in the natural environment, plant groups, medical objects (leukocytes, etc.) during calculations, etc.;

technical objects – cars in a stream, precious stones in sorting, parts on a conveyor, etc.

Fig. 1. Examples of images of objects for recognition and counting their number

Methodological approaches to solving this problem for the given objects are similar, but each of them has its own specifics. An individual approach is required when recognizing animals, since they have variability in photographs and can overlap each other in the image.

The aim of the work is to analyze the existing methods for automated counting of objects with variability and formulate recommendations for their application on the example of the problem of counting the number of wild reindeer.

Recognition and counting of wild reindeer

One of the urgent tasks in the field of research of the North is the task of monitoring the state of its bioresources. In particular, for many years there has been an active monitoring of wild reindeer, their migration and abundance [4].

The counting of adults and young animals is carried out on the basis of processing of photographs, performed, as a rule, from aircraft. A herd of deer is recorded in the natural environment, which complicates the task of their automatic recognition and counting. Recognition of deer in photographs is affected by: their relative position in the herd; difference in size; location in a lighted area or in the shade; the presence of objects similar in features to deer (stones, bushes), etc.

The above factors appear to be variable.

The currently used methods for counting the number of wild reindeer in Taimyr, Chukotka, and Yakutia are based on the fact that in hot weather they gather in crowds of many thousands in a limited area [5]. The-

se clusters are photographed from an aircraft. At the same time, there can be 1000 or more deer in a photograph. The number of animals not included in the aggregations is estimated by approximation [6].

Processing photographs and counting the number of reindeer by biologists in manual mode can take months, and the results are needed within one or two weeks after the aerial survey [7].

Approaches to solving the recognition problem

Methodically, the problem of deer recognition is solved using various approaches.

The first approach is feature recognition, which gives a well-structured software solution. The second approach is pattern recognition, in which the image of a deer is compared with its reference image to select the most "similar" pattern.

Deer recognition computer systems are built using these two approaches. In pattern recognition systems, convolutional neural networks (CNN) are widely used [8, 9]. In such systems, they are trained on a set of images in which deer are pre-labeled as references. Articles [10,11,12] present systems for recognizing animals (elephants, fur seals, etc.) that are completely different in size, areola, and habitat in the wild from photographs using CNNs. These projects are significant, developed jointly by universities and large companies, including using not only aerial photography, but also the results of satellite imagery.

Recognizing deer in aerial photographs

The general principles of building pattern recognition systems are described in the work [13] and consist of 4 stages.

Image processing. An increase in the distinguishability of deer is achieved by cleaning the image from interference and noise with averaging filters [14]. Additionally, the contrast and sharpness of the image is increased by switching to a monochrome view [15]. This simplifies the subsequent binarization process [16]. With well-distinguishable boundaries, Roberts, Kirsch, Prewitt, Laplace filters [17] are used to highlight the boundaries.

On fig. 2 shows a fragment of a color aerial photograph and its monochrome version. As you can see, the deer in the monochrome image are more distinguishable.

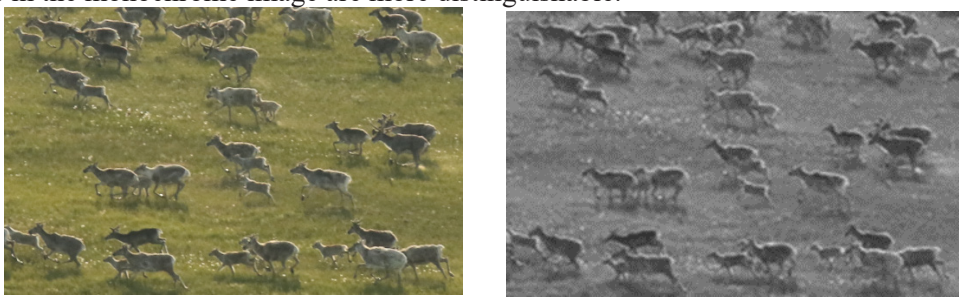

Fig. 2. An example of a color and monochrome picture representation of deers for further processing

On fig. 3 shows a fragment of a real aerial photograph, in which the deer are visually distinguishable, and background details are removed.

Fig. 3. Real aerial photograph of a herd of wild reindeer

Binarization – finding pixels related to images of deer. If the pixel can be attributed to the image of a deer, then it is assigned a value of 1, otherwise – 0. The main difficulties at this stage are associated with the high variability of images of deer (size, position relative to the shooting point).

To solve this time-consuming task, a program was developed at the St. Petersburg State University of Aerospace Instrumentation [18]. It allows the operator to display the image, scale it, put marks on the image, count the selected deer by category, and save the results (tag coordinates and number) in a text file. Fig. 4 shows the interface of this program.

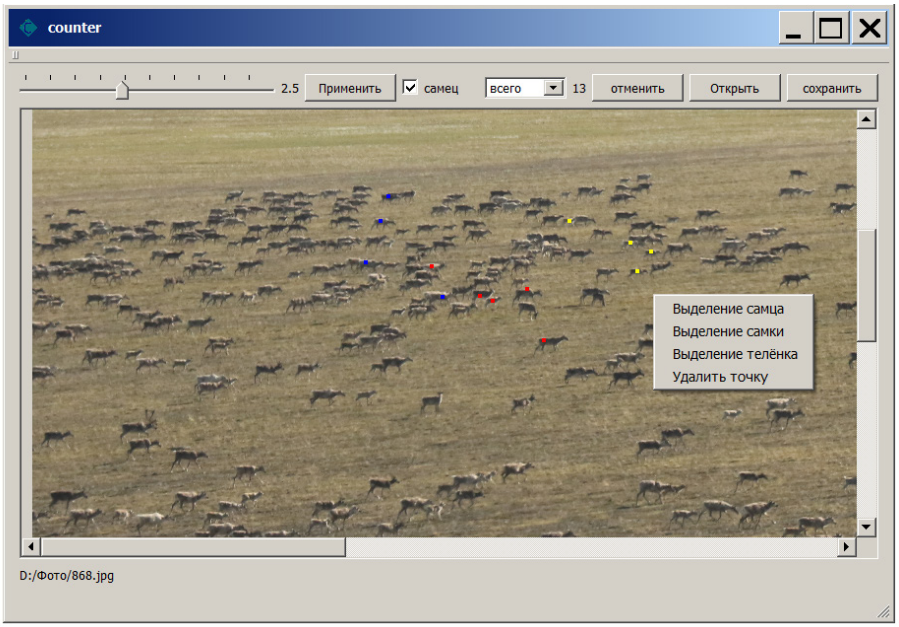

Fig. 4. Interface of the program for manual image processing

The error in counting the number of deer by the operator when using this program was no more than 2%. However, when working with large images with about 1000 deer, the error increases significantly, which is due to the high variability of the deer in the photograph, the conditions and location of the shooting, and the presence of other objects perceived by the operator as a deer.

Segmentation – selection of related groups of pixels related to a single deer. Binary image segmentation algorithms are well known [14] and quite reliable. As a result of their work, each connected set of pixels receives its serial number and can be separated into a separate image for subsequent counting.

Determination of the number of deer. The main problem with counting deer is that they can merge into one set of segmented pixels. To solve it, the distribution of segments over the area must be analyzed, which makes it possible to estimate the number of deer in a fused segment. If the area of the segment is significantly less than the average area of the representation of a deer in the image, then it is not taken into account in the calculation.

Automate the counting process using the scanning window algorithm. The image is sequentially scanned by the search window and a classifier is applied to each of its positions. The algorithm works quickly due to the fact that the system of learning and selecting the most important features is fully automated and does not require human intervention.

Deer recognition using CNN (convolutional neural networks)

For deer recognition, CNN are increasingly being used, training them from reference images of deer [19]. The main training array for CNN was the MS COCO dataset (Microsoft Common Objects in Context) [20], which contains more than 328,000 images. These images are used for machine learning models to solve detection and segmentation problems. However, deer images are not included in the MS COCO dataset and CNN by default is not able to distinguish them from other animals – cows, horses, etc.

On fig. 5 shows the results of deer recognition in an fragment of aerial photograph using a CNN trained on MS COCO dataset. In the picture, correctly recognized images of deer are marked in green, there are only 6 of them. Objects mistaken for deer are marked in red.

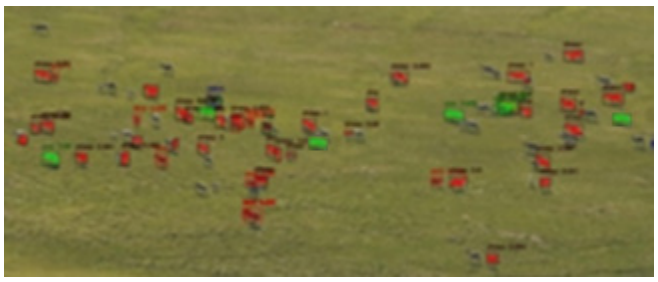

Fig.5. The result of deer recognition using CNN trained on MS COCO dataset

So, network training must be carried out taking into account:

– features of the image of wild reindeer on aerial photographs;

– their differences from stones, bumps and other objects characteristic of northern landscapes.

The task of recognizing reindeer from aerial photographs is not trivial. Therefore, to solve it, a two-stage CNN training procedure is used [7]:

– initial training on images of other animals included in the MS COCO dataset, so that the network learns to recognize animals as a class of objects;

– retraining of the network on the array of labeled aerial photographs of reindeer herds.

On fig. 6 shows the result of deer recognition by the additionally trained system based on aerial photographs of reindeer herds. Its recognition accuracy was 75%. At the same time, she never mistook for a deer an object that is not a deer. On average, the model correctly recognized 82% of deer on the entire training test dataset [7].

Fig.6. The result of deer recognition using a retrained network

Conclusion

The development of a reindeer recognition and counting system can be based on two main approaches.

The presence of ready-made CNN architectures trained for recognition on images of various animals makes it possible, through additional training, to create applications focused on the recognition of wild reindeer.

Prospects for the development of automation of deer counting on aerial photographs suggest a decrease in recognition errors by increasing the size of the training sample.

The described approach during the initial training of the CNN on the MS COCO dataset array and subsequent additional training without changing its architecture and interface can be used to recognize and count other inhabitants of the north, including rare ones.

Gratitude

The author thanks A. M. Sergeev for guidance in the preparation of this work and N. V. Soloviov for valuable consultations on the topic of the work.

References

1. Duda, R., Hart, P. Pattern classification and scene analysis. New York, Wiley. 1973. – 512 p.
2. Gonzalez R., Woods R. DIgital Image Processing. Prentice Hall. 2002. – 779 p.
3. Forsyht D., Ponce J. Computer Vision: A Modern Approach (2nd Edition). Pearson India. 2011. – 792 p.

4. Mikhailov V.V., Kharin Y.V. On the Developing of an Animal Recognition and counting system for aerial Photographs 1. Analysis of Recognition Methods // Informatsionno-upravliaiushchie sistemy [Information and Control Systems]. 2011. № 2. P. 22-28.

5. Zyryanov V. A., Pavlov B. M., Yakushkin G. D. Ecological bases of accounting for the number of commercial animals in the tundra zone of Taimyr. Problems of the hunting economy of the Krasnoyarsk Territory. Krasnoyarsk. 1971. P. 70-72.

6. Chelintsev N. G. Mathematical foundations of animal accounting. M., 2000. – 431 p.

7. Mikhailov V. V., Kolpaschikov L. A., Sobolevskii B. A., Soloviev N. V., Yakushev G. K. Methodological approaches and algorithms for recognizing and counting animals in aerial photographs // Informatsionno-upravliaiushchie sistemy [Information and Control Systems]. 2021. № 5. P. 20–32 (In Russian). doi:10.31799/1684-8853-2021-5-20-32

8. Simon J. D. Prince Computer Vision: Models, Learning, and Inference. Cambridge, Cambridge University Press, 2012. – 598 p

9. Ayyadevara K., Reddy Y. Modern Computer Vision with PyTorch: Explore deep learning concepts and implement over 50 real-world image applications. Birmingham, Packt Publishing, 2020. – 824 p.

10. Norouzzadeh M. S., Nguyen A., Kosmala M., Swanson A., Palmer M., Packer C., Clune J. Automated Animal Identification Using Deep Learning Techniques // Proc. of the Nat. Acad. of Sciences of the USA. 2018. №115. P. 5716-5725. doi.org/10.1073/pnas.1719 367115. 5

11. Duporse J., Isupova O., Reece S., Macdonald D., Way T. Using very high-resolution satellite imagery and deep learning to detect and count African elephants in heterogeneous landscapes. bioRxiv the preprint server for biology. doi: httpps://doi.org/10.1101/2020.09.09.289231. 6

12. Kaggle: how our nets counted sea lions on the Aleutian Islands. https://habr.com/ru/company/ods/blog/337548/ (accessed18.08.2022).

13. Tou J., Gonzalez R. Pattern recognition principles. Addison-Wesley Publishing Company. 1977. – 377 p.

14. Vostrikov A. A., Sergeev A.M., Soloviev N. V., Solovieva T. N. Introduction to segmentation of raster images: a textbook. St. Petersburg: GUAP, 2017. – 34 p.

15. Sergeev M. B., Soloviev N. V., Stadnik A. I. Methods of increasing the contrast of raster images for digital video processing systems // Informatsionno-upravliaiushchie sistemy [Information and Control Systems]. 2007. № 1 (26). P. 2-7.

16. Sergeev, A.M., Soloviev N. V. Recognition of multiple objects of the same type with high variability in the image. Scientific session of the GUAP: Sat. dokl.: at 3 h. Ch. II: Technical Sciences. St. Petersburg: GUAP, 2019. P. 427 – 430.

17. Erosh I. L., Sergeev M. B., Soloviev N. V. Image processing and recognition in preventive security systems: a textbook. St. Petersburg:GUAP, 2005. – 152 p.

18. Sergeev, A.M., Soloviev N.V., Yakushev G.K. Program for counting the same type of objects in a compressed image. Certificate of state registration of the computer program No. 2019666902, date of registration 17.12.2019.

19. LeCun Y. Haffner P., Bottou L., Bengio Y. Object Recognition with Gradient-Based Learning // Shape, Contour and Grouping in Computer Vision. 1999. P. 319 – 345.

20. Solawetz J. An Introduction to the COCO Dataset. Roboflow, 2020. https://blog.roboflow.com/coco-dataset/ (accessed 17.08.2022).

POWER SUPPLY SYSTEM FOR STUDENT NANO-SATELLITE

Kalinichev Mikhail
Saint Petersburg State University of Aerospace Instrumentation,
Saint Petersburg, Russia
E-mail: mihail.kalinichev@gmail.com

Abstract. *This article discusses the general principles of developing a power supply system for a CubeSat student nanosatellite in the cheapest and easiest to develop version. Simulations of the orbital movement of the satellite and the operation of the power supply system were carried out to assess the influence of the most popular type of orbits.*
Keywords: *student nanosatellites, CubeSat format, power supply system*

Introduction

The satellite power supply system (PSS) is one of the most important systems of the spacecraft, since the parameters of the power supply system largely determine the parameters and features of the designed satellite, in particular, the payload using energy. However, the construction of a power supply system is largely limited by the characteristics of the orbit, as well as the design features of the satellite, such as: the dimensions of the apparatus, the permissible mass of the apparatus, the surface area, which in turn depend on the chosen form factor of the developed apparatus. The general scheme of the PSS is shown in Fig. 1 [1].

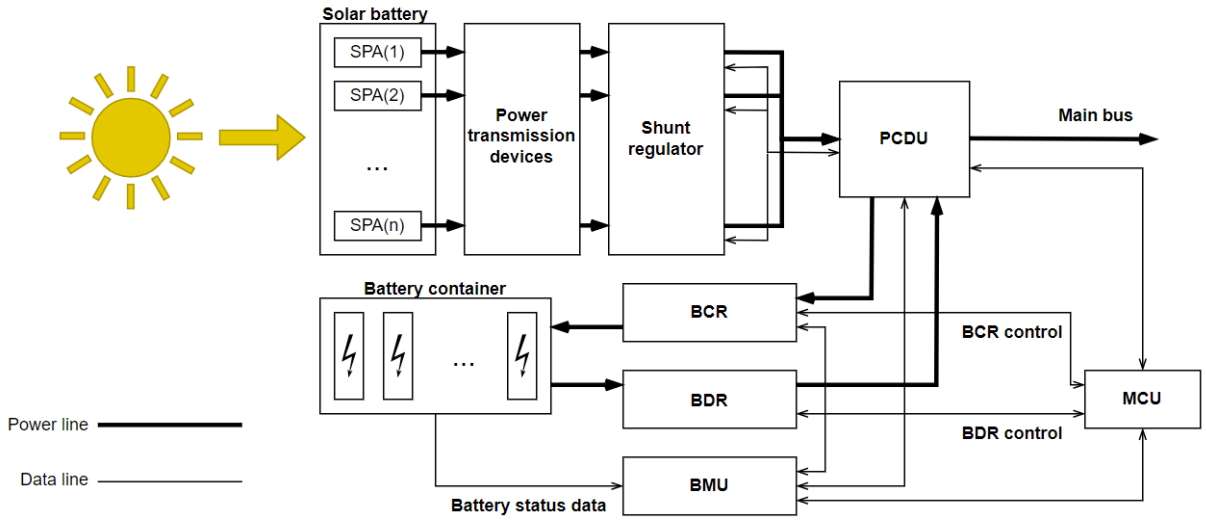

Fig. 1. General scheme of the PSS

The energy received from the sun by the solar panels installed in the solar energy node modules (SPA) goes to the power control and distribution unit (PCDU), which is responsible for power distribution and monitoring the condition of the power busbars. It also regulates the power of the solar battery using a shunt regulator. The main directions of energy movement are the charge / discharge of batteries and the output of energy to the main bus. The charging and discharging of the batteries is controlled respectively by the battery charge regulator (BCR) and the battery discharge regulator (BDR). The main function of the BCR is to provide a constant charge of the battery in the sun, and the function of the BDR is to supply constant power to the bus while operating in the shade. The battery management unit (BMU) is used to control battery cell parameters [1].

The power consumed by the vehicle can be divided by the average power in the illuminated part of the orbit P_{sun} and in the Earth's shadow $P_{eclipse}$. Power P_{sun} is less than the power received from solar panel P_{array}, since a significant part of its P_{charge} goes to charge the battery, which is necessary to ensure operation in the shade. The scheme of energy movement in the system is shown in Fig. 2.

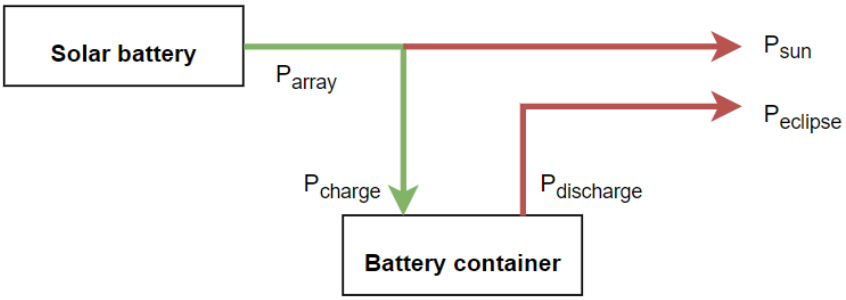

Fig. 2. Scheme of energy movement in the system

Thus:

$$P_{array} = P_{sun} + P_{charge} \tag{1}$$

Turning to energy, we get:

$$P_{array} \cdot \tau_{sun} = P_{sun} \cdot \tau_{sun} + P_{charge} \cdot \tau_{sun} \tag{2}$$

Considering that part of the energy is lost during charge/discharge:

$$P_{charge} \cdot \tau_{sun} = \frac{1}{\eta} P_{eclipse} \cdot \tau_{eclipse} \tag{3}$$

where $\eta = \eta_{BRD} \cdot \eta_{BCR} \cdot \eta_{AR}$, the product of the efficiency ratings of the power conversion modules.

$$P_{array} \cdot \tau_{sun} = P_{sun} \cdot \tau_{sun} + \frac{1}{\eta} P_{eclipse} \cdot \tau_{eclipse} \tag{4}$$

If the power consumption in the shade and in the light is the same:

$$P_{array} = P \cdot \left(1 + \frac{1}{\eta} \frac{\tau_{eclipse}}{\tau_{sun}} \right) \tag{5}$$

So the available power is:

$$P = \frac{P_{array}}{1 + \frac{1}{\eta} \frac{\tau_{eclipse}}{\tau_{sun}}} \tag{6}$$

Form factor selection

The CubeSat format has become widespread in the field of small and ultra-small spacecraft, which is explained by the low cost and simplicity of both the development and launch of such devices due to the unification of their bodies and parameters, as well as the possibility of convenient cluster launch of a large number of devices using one launch vehicle. The basis of the format is a cell with dimensions of 10x10x10 cm called 1U (1 Unit). Other standard CubeSat format cases consist of several 1U cells and are named respectively: 1.5U, 2U, 3U, 6U and 12U. Run statistics are shown in Fig. 3.

Considering the statistics of launches, one can pay attention to the fact that 3U nanosatellites are more popular than 1U, which can be explained in comparison with the large volume available for the payload, and also, due to the elongated shape of the device, the ability to accommodate equipment that has an elongated shape, for example, optical systems of small telescopes, jet engine nozzles or extended mechanical devices.

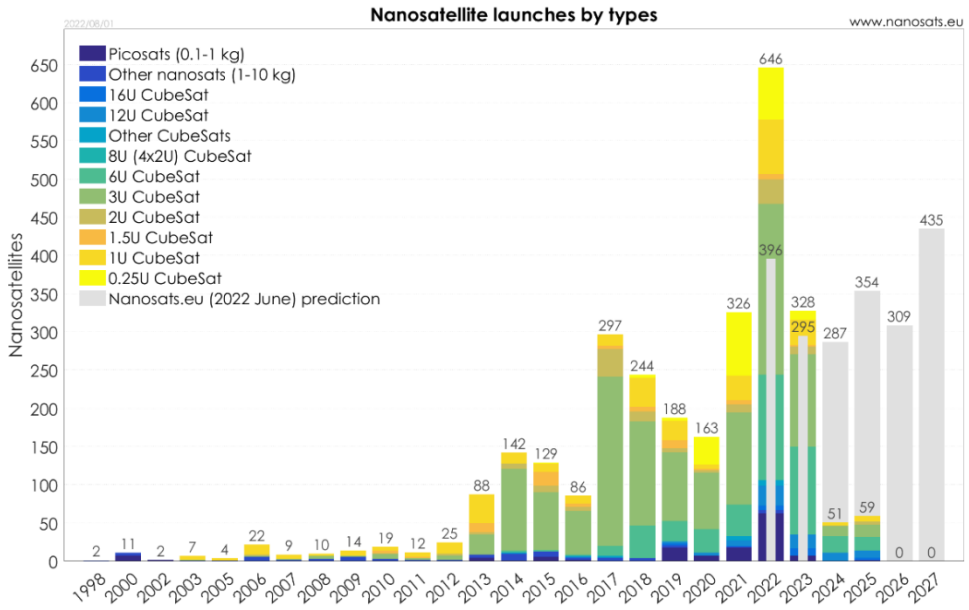

Fig. 3. Statistics of launches of nanosatellites of various form factors [2]

Also, 3U have a large allowable weight, which reaches 6 kg. The 6U format also has a certain popularity. However, the 1U format remains the preferred format for small, low-budget educational or research projects conducted by educational institutions due to the low cost, since the cost of launch is directly proportional to the size of the satellite. The use of formats smaller than 1U is not advisable due to the small amount of payload.

Solar panels

The requirements of minimum cost and ease of development on the part of educational institutions in relation to the device also impose restrictions on the use of active moving parts and mechanisms, in particular limit the use of actively oriented solar panels. It also affects other systems of the apparatus that indirectly affect the power supply system, for example, orientation systems are not used.

Summarizing the above, the requirements imposed on the mass and size characteristics of a nanosatellite due to the development of a satellite by students of educational institutions limit all possible design options for the device to the CubeSat 1U format with dimensions of 10 × 10 × 10 cm and a maximum mass of 2 kg, and rigidly fixed solar panels. Due to the lack of an orientation system to maximize power generation, the panels are placed over the entire area of the apparatus, as was done on the Ecuador UTE-SWSU apparatus, which is shown in Fig. 4 [3].

Fig. 4. Placement of solar panels of the satellite «Ecuador UTE-SWGU» [3]

Thus, the primary source of electricity is 6 solar panels with sides of approximately 8.3×8.3 cm and therefore an area of approximately 69 cm^2. It must be taken into account that out of 6 panels, no more than 3 can be simultaneously oriented to the sun, and their power directly depends on the orientation of the panels relative to the direction of the sun's rays.

The output power of P_{array} solar panels can be determined by the formula (7).

$$P_{arrya} = s\eta F_{SB} S_{SB} \cos(\alpha) \tag{7}$$

where s is the flux density of solar radiation energy, 1000–1500 W/m^2; η – efficiency, for gallium arsenide elements can reach 24-32%; F_{SB} is the degradation coefficient of solar batteries, taking into account changes in the emission of photocells of the battery due to the influence of space factors; S_{SB} is the area of the solar battery; α is the angle of orientation of the solar panels relative to the Sun, defined as the angle between the direction to the Sun and the normal to the surface of the solar battery [4].

Since in formula (7) only cos(α) depends on the orientation in space, and the remaining values are constant, the calculation of the average generation of a solar panel randomly oriented in space is reduced to the calculation of the average value of cos(α). This can be done by considering the orientation of the panel as a point on a sphere with unit radius in spherical coordinates, where the point is the projection of the normal vector to the plane of the panel. The Z axis of the coordinate system has a direction to the Sun. The zenith angle θ is measured from the Z axis to the radius vector of the point and has the meaning of the angle α in formula (7) – the angle between the direction to the Sun and the normal to the surface of the solar battery. Angle φ is the azimuth angle. The average value of cos(α) over the area of the sphere is calculated as the double integral of cos(θ) over dθ and dφ divided by 4π – the area of the unit sphere:

$$\overline{\cos(\alpha)} = \frac{\int_0^{2\pi}\int_0^{\frac{\pi}{2}} \cos(\theta)\cdot\sin(\theta)\,d\theta\,d\varphi}{4\pi} \tag{8}$$

When integrating, the angle φ changes from 0 to 2π, thus making a full circle. The angle θ changes from 0 to π/2, passing only a quarter of the circle instead of half for a full sphere. This is done because cos(α) in the range from 0 to π/2 changes from 1 to 0, and at a larger angle becomes negative, while the generation of the solar panel at angles greater than π/2 remains equal to 0. Sin(θ) in this expression is the Jacobian $r^2 \cdot \sin(\theta)$ for spherical coordinates, where for a sphere with unit radius r = 1.

The average power generated by all 6 solar panels of such an apparatus when in the sun can be calculated by formula (9) by substituting (8) into formula (7). The resulting formula must also be multiplied by 6 – the number of solar panels of the apparatus. When calculating, it is considered that the device has a random orientation in space since it does not have an orientation system and all possible positions in space are equally probable.

$$P_{array} = s\eta F_{SB} S_{SB} \frac{\int_0^{2\pi}\int_0^{\frac{\pi}{2}} \cos(\theta)\cdot\sin(\theta)\,d\theta\,d\varphi}{4\pi} \cdot 6 \tag{9}$$

Taking the average values s = 1300 W/m^2, η = 0.28, and S_{SB} = 0.0069 we get:

$$P_{array} = 1300 \cdot 0.28 \cdot 1 \cdot 0.0069 \cdot \frac{\int_0^{2\pi}\int_0^{\frac{\pi}{2}} \cos(\theta)\cdot\sin(\theta)\,d\theta\,d\varphi}{4\pi} \cdot 6 = 3.767 \tag{10}$$

Thus, a system of 6 solar panels of a non-orientable vehicle can generate an average of up to 3.767 W while in a constantly lit state in the absence of degradation of the panels due to their damage. Since the power directly depends on the current position in space, jumps from 2.5 W are possible if the device is oriented perpendicular to the direction of the sun and up to 4.4 W when the device is oriented diagonally along the direction to the sun.

Orbit influence

An important aspect in the design of the PSS is the orbit on which the satellite will be placed, since the duration and nature of the periods of the apparatus being in the illuminated part of the orbit and being in the shadow of the Earth, where the apparatus will not be able to use solar panels, depend on its parameters.

The vast majority of nanosatellites were launched into various sun-synchronous orbits (SSO) [2], which are polar orbits with a small eccentricity, altitudes from 460 to 1200 km, and an inclination of about 98°. The main property of this orbit is that the apparatus passes over any point on the Earth's surface at the same local solar time, which is used in remote sensing of the Earth. However, a more important feature is that a satellite in such an orbit never falls into the Earth's shadow and its solar panels can operate continuously, which is due to the precession of the line of nodes of the orbit.

A significant number of small satellites are launched into orbits close to the ISS orbit: about 400 km high, 51.6° inclination. The advantage of launching in this orbit is the ease of launching directly from the ISS or as a side load when delivering cargo, however, the illumination of this orbit is lower than that of the SSO.

The periods of being in the shadow $\tau_{eclipse}$ and in the illuminated part of the orbit τ_{sun} can be found by simulating the motion of the spacecraft along the orbit.

Modeling code snippet in MATLAB:

```
[x, y, z] = Orbit(1:T*cnt, tp, a, e, i, w, Omg);
[Tsun, Teclipse] = sun(x,y,z,T)
hold on

function [v] = v(t,tp,a,e)
    M = (sqrt(3.98718108e+14)/(a^(3/2)))*(t-tp);
    E = M;
    for t = 1:10
        E = M + e*sin(E);
    end
    v = 2*atan(sqrt((1+e)/(1-e))*tan(E/2));
end

function [x,y,z] = Orbit(t,tp,a,e,i,w,Omg)
    M = 5.9742*10^24;
    G = 6.674*10^(-11);
    m = 1;
    mu = m*M*G;
    vt = v(t,tp,a,e).*57.2958;
    r = (a*(1-e^2))./(1+e.*cosd(vt));
    u = w + vt;
    er = [cosd(u)*cosd(Omg)-
cosd(i)*sind(u)*sind(Omg);cosd(u)*sind(Omg)+cosd(i)*sind(u)*cosd(Omg);sind(i)
*sind(u)];
    x = r.*er(1,t);
    y = r.*er(2,t);
    z = r.*er(3,t);
end

function [Tsun, Teclipse] = sun(x,y,z,T)
    t_max = length(x);
    Tsun = 0;
    Teclipse = 0;
    Re = 6378000;
    plot3(x,y,z,'b.','LineWidth',1)
    hold on

    for i =1:t_max
       if (sqrt(z(i)^2+y(i)^2)<Re) && (x(i)<0)
           Teclipse = Teclipse + 1;
            z(i) = 0;
            x(i) = 0;
            y(i) = 0;
```

```
        else
            Tsun = Tsun+1;
        end
    end
    plot3(x,y,z,'r.','LineWidth',1)
    hold on
    annotation('textbox',[0 0.7 0.3 0.3],'String',{['Teclipse =
',num2str(Teclipse)],['Tsun = ',num2str(Tsun)],['T =
',num2str(T)]},'FitBoxToText','on');
    hold on
end
```

The result of the simulation is shown in Fig. 5. Blue shows the part of the orbit passing in the shadow of the Earth. The orbit was calculated based on the current parameters of the ISS orbit [5].

The duration of the $\tau_{eclipse}$ period is 2080 seconds or about 34 minutes out of 92 minutes of the orbital period, τ_{sun} is respectively 3493 seconds or about 58 minutes. Thus, the device will be in the shade almost 37.3% of the time. Considering that the efficiency of BCR and BDR modules is about 90%, then substituting into (6) we get that the average power available to the systems of the device is:

$$P=\frac{3.767}{1+\frac{1}{0.81}\frac{2080}{3493}}=2.171 \quad (11)$$

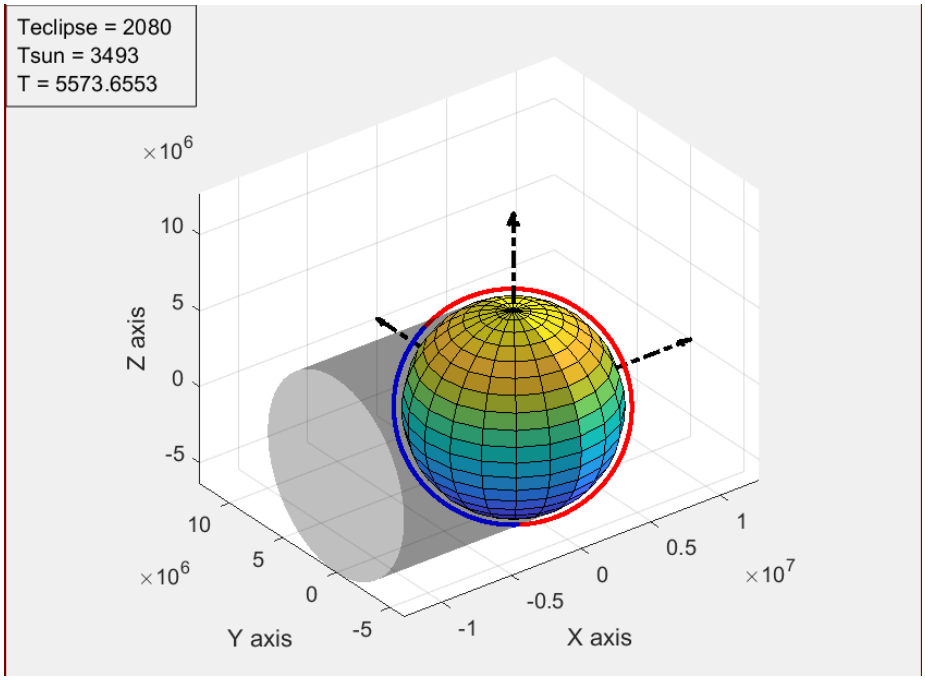

Fig. 5. Simulation result

МОДЕЛИРОВАНИЕ РАБОТЫ СИСТЕМЫ

Assuming the power of the solar panels P_{array} = 3.767 W, and the average power consumption P = 2.171 W, it is possible to simulate the operation of the power system over several orbits close to the ISS orbit.

Modeling code snippet in MATLAB:

```
figure();
subplot(1,2,1);
P_array = SolarPanel(x,y,z);
plot(P_array,'k-','LineWidth',1);
title('Generation');
xlabel('Time [sec]')
ylabel('Power [W]')
hold on
xline((1:cnt).*T);
```

```
hold on
yline(mean(P_array),'--',['Average = ',num2str(mean(P_array))]);
area(1:T*cnt, max(P_array, 0), 0, 'EdgeColor', 'none', 'FaceColor', [0.6 1
0.7])


subplot(1,2,2);
[P_sun, P_discharge] = comsuption(x,y,z, 2.171, 0.81);
plot(P_sun,'k-','LineWidth',1);
hold on
plot(P_discharge,'LineWidth',1);
COM = P_sun+P_discharge;
title('Energy consumption in the sun and in the shade')
xlabel('Time [sec]')
ylabel('Power [W]')
hold on
xline((1:cnt).*T);
hold on
yline(mean(COM),'--',['Average = ',num2str(mean(COM))]);
area(1:T*cnt, max(P_sun, 0), 0, 'EdgeColor', 'none', 'FaceColor', [1 0.7
0.7])
area(1:T*cnt, max(P_discharge, 0), 0, 'EdgeColor', 'none', 'FaceColor', [1
0.5 0.5])

figure();
subplot(1,2,1);
P_charge = P_array-P_sun-P_discharge;
plot(P_charge,'k-','LineWidth',1);
title('Charge and discharge of battery')
xlabel('Time [sec]')
ylabel('Power [W]')
hold on
xline((1:cnt).*T);
hold on
area(1:T*cnt, min(P_charge, 0), 0, 'EdgeColor', 'none', 'FaceColor', [1 0.5
0.5])
hold on
area(1:T*cnt, max(P_charge, 0), 0, 'EdgeColor', 'none', 'FaceColor', [0.6 1
0.7])
hold on
yline(mean(P_charge),'--',['Average = ',num2str(mean(P_charge))]);

subplot(1,2,2);
Battery = cumsum(P_charge);
plot(Battery,'r');
xlabel('Time [sec]')
ylabel('Energy [J]')
title('Storage of energy in the battery')
hold on
plot(polyval(polyfit([1:T*cnt],Battery,1),[1:T*cnt]),'--');
hold on
xline((1:cnt).*T);

function [Generation] = SolarPanel(x,y,z)
    t_max = length(x);
    Re = 6378000;
    Generation = 0;
    for i =1:t_max
       if (sqrt(z(i)^2+y(i)^2)<Re) && (x(i)<0)
            Generation(i)=0;
       else
           Generation(i)=3.767;
       end
    end
```

```
end

function [Sun, Discharge] = comsuption(x,y,z,P,ECE)
    t_max = length(x);
    Re = 6378000;
    for i =1:t_max
        if (sqrt(z(i)^2+y(i)^2)<Re) && (x(i)<0)
            Sun(i) = 0;
            Discharge(i) = P*(1/ECE);
        else
            Sun(i) = P;
            Discharge(i) = 0;
        end
    end
end
```

Graphs of power generation and energy consumption are shown in Fig. 6. It is important to note that the indicated average value of generation and consumption are the same, which indicates that all energy is consumed. Dark red shows consumption in the shade, taking into account energy losses during charge-discharge.

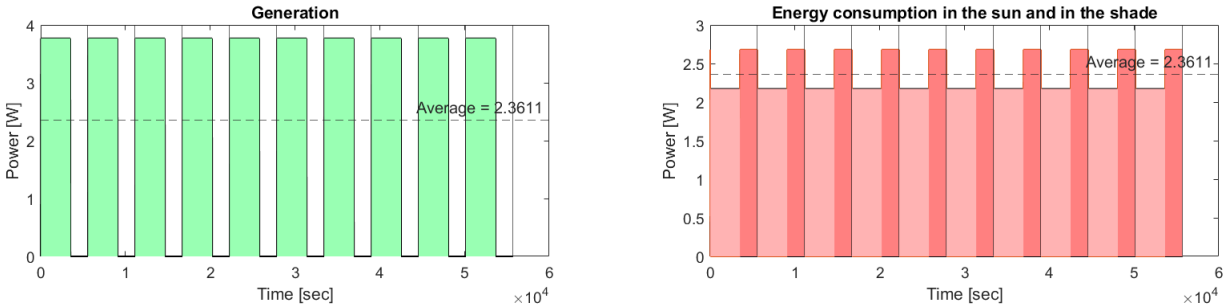

Fig. 6. Graphs of generation power – on the left and energy consumption – on the right

The charge-discharge graph of the battery and the graph of energy accumulation in it are shown in Fig. 7. The average value of the charge-discharge power tends to zero, which also indicates the equality of energy generation and consumption, which indicates that the system is balanced – there is no obvious power imbalance. However, a slight imbalance towards generation is still more preferable than towards consumption. Since excess energy in the system can always be simply eliminated. It can even be useful as a backup in case of unforeseen circumstances. In turn, the imbalance towards consumption can lead to premature battery discharge and emergency shutdown of the load.

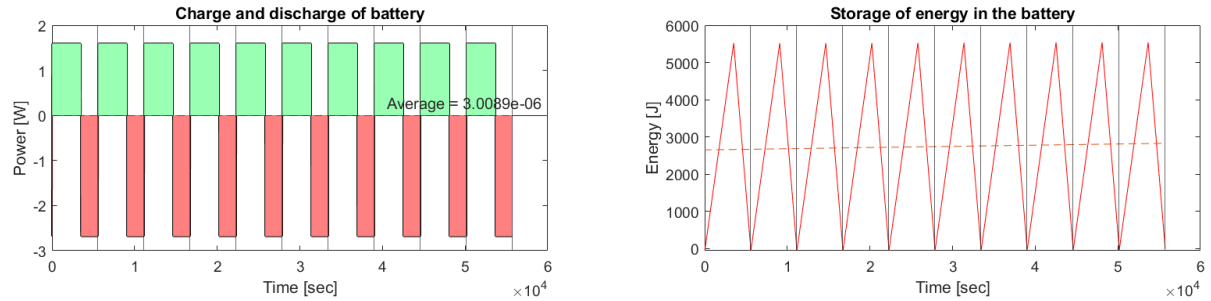

Fig. 7. Battery charge-discharge graph – on the left and energy accumulation graph – on the right

The graph of energy accumulation in the battery of the device was obtained by integrating the charge-discharge power graph. The dotted line shows the trend line. According to the schedule, you can evaluate the required battery capacity and the nature of its work. In this case, the minimum capacity is 5500 J, which is equivalent to approximately 420 mA·h for Li-ion batteries. However, the capacity should be higher due to the need to store a reserve of energy for an emergency and because of the instability of generation and consumption, as well as because of the harm of deep discharge of batteries.

Simulation of work on SSO with an average power consumption close to the generation power shows the absence of energy accumulation, because it is all consumed directly, but the need for a battery does not disappear for the above reasons.

Conclusion

Modeling is a powerful tool in the development of spacecraft, the accuracy of which directly depends on the complexity of the model being implemented and the number of factors taken into account. So, for example, when developing a low-budget student nanosatellite, relatively simple modeling already makes it possible to estimate the influence of orbit parameters on the main characteristics of the device, to estimate the possible payload power and the required battery capacity. Further complication of the model will make it possible to study in more detail the features of the device under development and draw more accurate conclusions during its development.

References

1. Development of spacecraft systems / Ed. P. Fortescue, G. Swinerd, D. Stark; Per. from English. – M.: Alpina Publisher, 2016. – 764 p. [Разработка систем космических аппаратов / Под ред. П. Фортескью, Г. Суайнерда, Д. Старка; Пер. с англ. – М.: Альпина Паблишер, 2016. – 764 с]
2. World's largest database of nanosatellites. URL: https://www.nanosats.eu/
3. Small spacecraft "Ecuador UTE-SWGU". URL:https://swsu.ru/space/ekvador-ute-yuzgu-rs3s/
4. Ablameyko, S.V. Small spacecraft: a manual for students of the faculties of radiophysics and computers. Technologies. Minsk: BSU, 2012. – 159 p. [Абламейко, С. В. Малые космические аппараты : пособие для студентов факультетов радиофизики и компьют. Технологий. Минск : БГУ, 2012. – 159 с.]
5. ISS – Orbit. URL: https://heavens-above.com/orbit.aspx?satid=25544&lat=59.9408&lng=30.2962&loc=Unnamed&alt=0&tz=RFTm3

MODERN TRENDS IN THE DEVELOPMENT OF THE ELEMENT BASE AND PROGRAMMING CAPABILITIES OF ELECTRONIC EQUIPMENT

Kleshnin Boris
Saint Petersburg State University of Aerospace Instrumentation,
Saint Petersburg, Russia
E-mail: boria456@gmail.com

Abstract: *the article discusses the possibilities of modern lithography in the creation of microprocessors, a thesis analysis of ways to improve and optimize microcontrollers is carried out.*
Keywords: *Moore's law, lithography, microprocessors, microcontrollers*

In the world of electronics, there is Moore's law, which states that, in simple words, every two years the number of transistors placed on a chip doubles. This happened by reducing the size of the microprocessor elements. The distance between the transistors reached values of 45nm, after which classical ultraviolet lithography could not provide the process of creating more advanced processors at a wavelength of 193nm. Today, we can say that this law is no longer relevant. However, every year technologies strive to make the processor layout such that the maximum number of transistors can be accommodated on the minimum area. The smaller the transistor size, the faster the signal transmission and less power consumption, and it also becomes possible to increase the number of elements on one chip. This is done, first of all, to increase productivity. However, an increase in the crystal itself is undesirable due to the increased risk of manufacturing errors. Today, the EUV lithography method is widely used, a laser is used, thanks to which it was possible to create 14 and 10 nanometer chips, mass-produced by Intel, UMC, TSMC, Samsung, Micron, SK Hynix, Toshiba Memory, GlobalFoundries, and there are also 7 nanometer chips produced only by TSMC and Samsung. With regard to the production of systems for creating microchips, it was decided to provide this task to only one company – ASML.

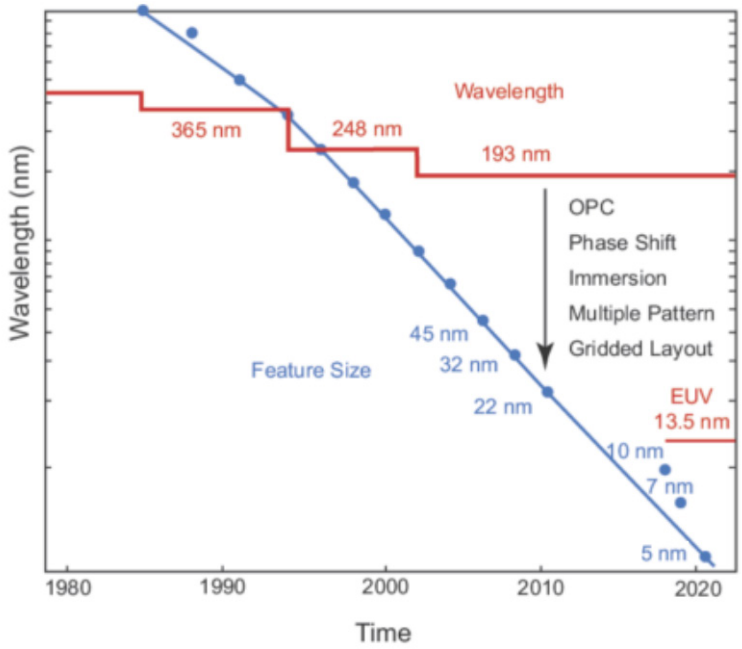

Fig. 1 – Is a graph showing the dependence of the laser wavelength (left), the time of implementation of the technological process (bottom)

Computing systems are microprocessor and microcontroller. The main difference is that the microcontroller has a processor, RAM and a storage device, and all these elements include a single crystal. In microprocessor systems, all elements are arranged discretely. The microcontroller consumes a fairly small amount of energy and is used in a fairly simple technique that does not work with a large amount of data. Microcontrollers have tasks, in connection with the specifics of which, various models are created.

Software optimization can be designated as a bottleneck. The microprocessor system, in turn, has a large size and power, and the capabilities of this system greatly exceed the capabilities of the microcontroller.

In the period from 2006 – 2010 to the present day, chip manufacturers use innovations such as multicore and multithreading (Hyper-Threading). Several cores are made on one chip, each of which functions independently of the others, and, in addition to this, each core was divided into several threads, which made it possible to simultaneously perform even more tasks.

Today, microprocessors are no longer the bottleneck of machines based on the von Neumann architecture, and transistors are now used in RAM, portable and fast storage devices. As for storage devices, recently technologies have moved away from hard drives to a faster SSD, which is solid-state memory on transistors. The disadvantages of such a transition include the high cost of production and a limited number of rewrites. To bypass the bottleneck on the von Neumann architecture, Directstorage technology is used, which allows the processor to directly access the memory device, and AMD's Smart Access Memory technology allows the video card to communicate directly with the disk or processor, which is limited to accessing video memory directly.

Suppose you need to add an element to a certain position located in a set of numbers. This set can be represented as an array or as a registry. If you represent it as an array, then in order to insert an element into the middle, you need to shift all the elements starting from the middle by one, which will take some time. To insert an item in the middle of the registry, you need to go to the middle of the registry. The difficulties are the same. However, the array is much more efficient. This is due to the fact that the array elements are sequentially located in memory, and the registry elements are chaotic. For example, a series of 1000 elements is given. If this is an array, it will be necessary to spend from 1 to 4 cycles per element, and in the worst case it is possible to sort through all the elements in 4000 cycles, while the registry will be sorted using 200 cycles per element, which will be 200,000, that is, 50 times longer. This is due to the fact that the data in the case of the registry is taken from RAM, and in the case of the array – from the cache of the first level[1].

Despite the technological solutions to the problems, the algorithm created by the developer plays an important role. The solution to the problem with code optimization is solved by using the processor cache, which allows reducing the number of accesses to RAM. There is a certain hierarchy of memory. Processor registers store frequently used data, and the processor cache serves as a buffer zone storing a fragment of data from relatively slow RAM. RAM serves as a buffer for slow hard drives. A good algorithm is not always faster than a bad one.

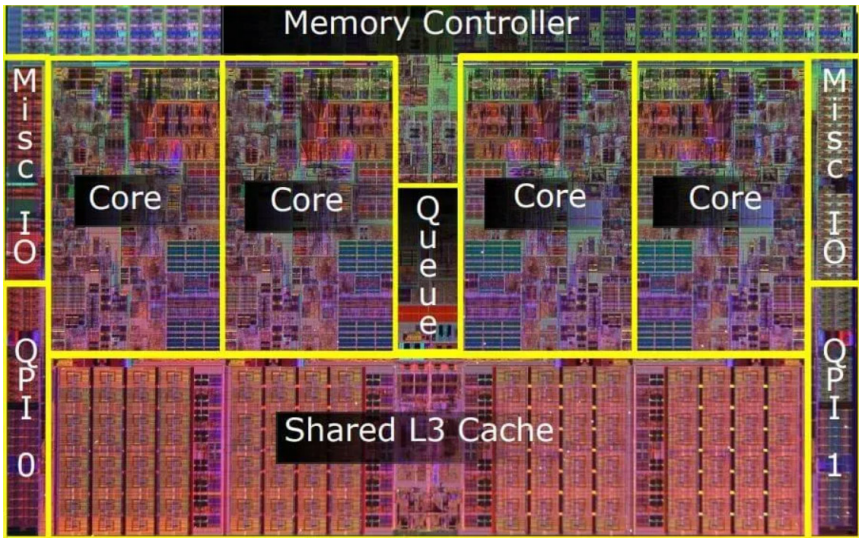

Fig. 2 – Intel Core i7 processor crystal consisting of 4 cores

In the processor, the data goes through a kind of pipeline. The compiler optimizes the code itself to use it on the processor pipeline, but changes only the "safe" sections. Several obstacles stand in the way of the compiler, which have a global impact on the result of the code: pointers, branching, data dependency and function calls. Summing up, we can say that for the best optimization of the executable code of the application, the compiler requires:

1) using more efficient algorithms;

2) using the memory hierarchy, getting rid of unnecessary memory accesses;

3) reducing branching and replacing conditional control transfer with conditional data transfer to improve the result of instruction prefetching by the processor during execution;

4) reducing the number of transitions in the code: for example, the use of embedding functions or unwinding the loop allows in many cases to speed up the execution of the program at the cost of increasing the size of the code;

5) transferring large computations to an internal loop;

6) using dissociation to reduce dependencies;

7) placing code and data close to each other, access to which is needed in the near future;

8) using parallelization of operations[2];

Even despite the optimization given in the paragraphs above, there are still problems that will have to be optimized manually. To do this, profilers are used that track resources, the time of calling and operation of functions, and their result.

References

1. E. M. Anodina-Andrievskaya, B. D. Kleshnin, Modern trends in microprocessor technology // Economic strategies and new opportunities in modern conditions. Proceedings of the International Scientific and Practical Conference on December 6, 2022. – St. Petersburg: Scythia-print Publishing House, 2023. – pp. 6-9.

2. E. N. Dolgov R. A. Kovalenko – Characteristics of the development of the elementary base and software capabilities. Optimization methods // The Seventy-fifth International Student Scientific Conference of GUAP (April 18-22, 2022): Sat. dokl.: at 4 h. h. 2: Technical Sciences. – St. Petersburg: GUAP, 2022. – pp.288 – 292.

AUTOMATION OF THE SYSTEM OF SEARCH OPTIMIZATION OF A WEB RESOURCE

Komarov Timofey
Student
Saint Petersburg State University of Aerospace Instrumentation,
Saint Petersburg, Russia
tim1kom@yandex.ru

Introduction

Information technology shortens the path of the buyer from finding the necessary thing to acquiring it through the provision of high-speed service. Only an optimized web resource that has all consumer properties can take on such functions.

Thus, it is required to find, study and implement such an automated method of promoting a web resource that would give the most opportunities, while acting automatically and being a profitable investment in quality.

In the presented work, an improved method for optimizing a web resource has been developed.

Analysis of stakeholder requirements in the field of information technology

The field of information technology affects not only specialists in this field, but also companies interested in increasing sales through promotion.

To study the requests and expectations of stakeholders, a survey was conducted using the SERVQUAL method, as a result of which it turned out (Fig. 1) that the most significant requirement is the "output" of a web resource to the leading position of a search resource for a specific request.

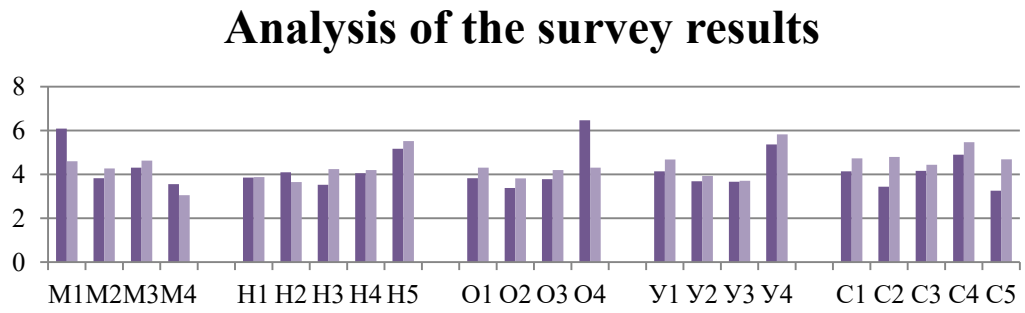

Fig. 1. Requirements of stakeholders, where the first column is an assessment of the level of expectations of respondents, and the second is the level of perception

Thus, equipping an IT company with modern technology, improving the ergonomics and interface of web resources, round-the-clock technical support, prompt response are the criteria that stakeholders single out in the first place. However, the survey showed that companies do not meet the level of expectations and need to be improved in these areas.

Features of the development of the information technology market

At the moment, a trend is being built in the design of ergonomics and the control interface of the technical system, but without changing the technical component of the system itself.

Using the example of the well-known Tinkoff Bank, we will consider how the trend affects the promotion of bank services. At the beginning of 2020, Tinkoff carried out a significant update of its application, introducing many new features and services. [1]

Among them were:

1) Adding a dark theme
2) Ability to book hotels and restaurants directly from the application
3) The possibility of extending the CMTPL policy and quick registration of an insured event

Thus, the bank did not add a single new function, but only changed the way of interaction, which allowed the company to bring the company to record levels of net profit. Thus, the company's profit for 2020 amounted to 195.8 billion rubles, which is 22% higher than in the previous year. [2]

Study of the efficiency of search engine optimization of web resources

Before developing a new web resource, it is necessary to refer to the chronology of the development of indicators among analogues in order to form a general trend and choose the right direction. The following web resources were chosen as analogues: Guild of Masters (2010), V-events (2011), Anteprise (2012), Adventure Academy (2013), "Trand event" (2014), "Main Division" (2015), "Over" (2016), "Rent Event" (2017), "April 4" (2018) and " Division" (2021). The characteristic values are given in Table 10. [3]

Table 1 shows that the characteristics have very disparate values, sometimes exceeding two or even three times. Comparison of samples by indicators is shown in Fig. 2.

Table 1

Retrospective analysis

№	Characteristic	2010	2011	2012	2013	2014	2015	2016	2017	2018	2022
1	Number of website visitors per week	98	127	132	112	168	202	251	247	199	309
2	Number of orders from the site per week	9	13	12	18	19	15	16	15	14	16
3	Web page loading speed, sec	3,29	3,2	2,28	1,5	0,9	0,6	0,2	0,32	0,25	0,22

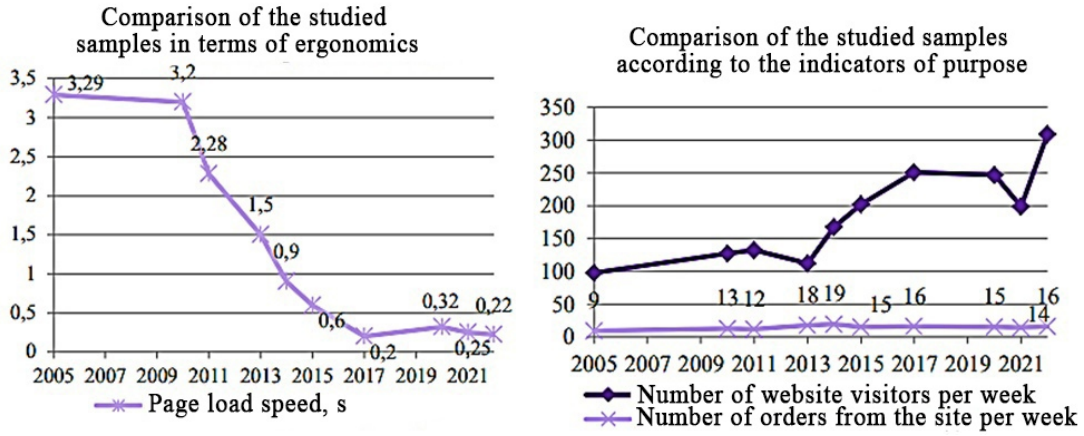

Fig. 2 (a,b). Comparison of the studied samples by indicators

If you look at Fig. 2 (a), you can conclude that every year the web page load time is decreasing, and the number of orders and visitors is growing (Fig. 2, b). So, you can keep up with the trends.

The study of possible models for the implementation of search engine optimization of a web resource

To improve the quality of search engine optimization of a web resource, you need to choose a method for its development.

Valid alternatives are: Website powered by Wordpress (A_1), Website powered by Joomla (A_2), Website powered by Tilda (A_3), Website powered by Wix (A_4).

The following criteria were chosen for evaluation: cost of implementation (K_1), time spent on creation (K_2), functionality of the final web resource (K_3), time spent on maintaining the web resource (K_4), search engine optimization (K_5).

Let us determine the criteria weights using formulas (1) and (2).

The sum of marks is calculated by the formula (1):

$$C_{ni} = \sum K_n , \quad (1)$$

Table 2

Collapse alternatives by criteria

Alternatives	Criteria					Weighted scores alternatives
	K_1	K_2	K_3	K_4	K_5	
	0,20	0,25	0,16	0,11	0,27	
A_1	0,31	0,09	0,50	0,10	0,45	=0,31***0,20**+0,09***0,25**+0,50***0,16**+0,10***0,11**+0,45***0,27** = ***0,30***
A_2	0,32	0,17	0,14	0,16	0,29	=0,32***0,20**+0,17***0,25**+0,14***0,16**+0,16***0,11**+0,29***0,27** = ***0,22***
A_3	0,28	0,43	0,28	0,44	0,17	=0,28***0,20**+0,43***0,25**+0,28***0,16**+0,44***0,11**+0,17***0,27** = ***0,29***
A_4	0,09	0,31	0,08	0,29	0,10	=0,09***0,20**+0,31***0,25**+0,08***0,16**+0,29***0,11**+0,10***0,27** = ***0,17***
					∑	1

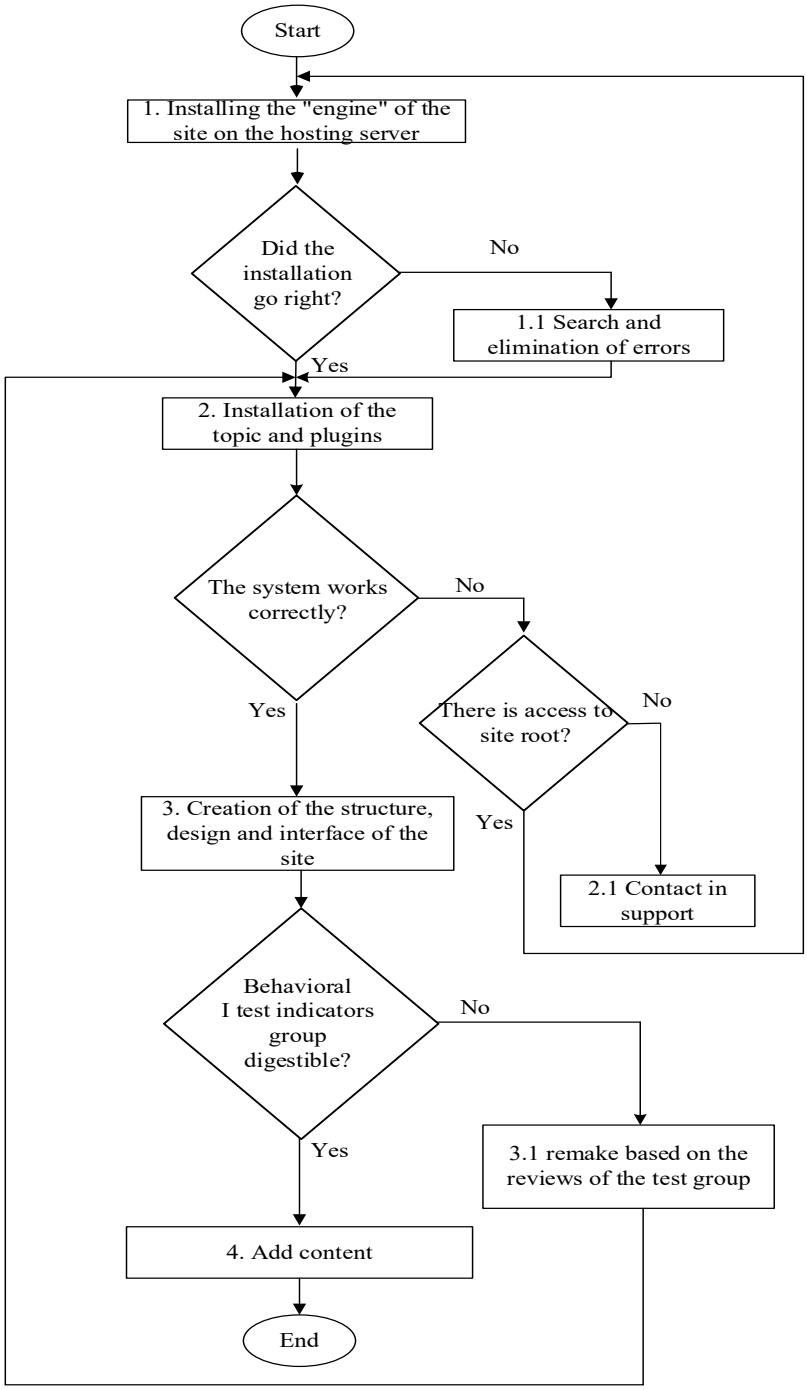

Fig. 3. Web resource optimization algorithm

where C_{ni} – the sum of the evaluation of each criterion; Kn – the value of the assessment of the n-th criterion (in our case, from 1 to 5).

The weight of goals is calculated by the formula (2):

$$V_n = \frac{C_{ni}}{\sum C_{ni}}, \quad (2)$$

where V_n – goal weight of the n-th criterion; C_{ni} – the sum of the scores of the n-th criterion (in our case, from 1 to 5).

Point scale for evaluating criteria: 1 – equal importance, 2 – moderate superiority, 3 – significant superiority, 4 – strong superiority, 5 – very strong superiority

A convolution of the weighted sum scores of alternatives is presented in Table 2. Thus, the best alternative is A_1 (Website powered by Wordpress), which has a maximum weighted score of 0.30; the least preferred option is a Website powered by Wix (A_4) with a weighted score = 0.17.

Development of a quality assurance model for the process of search engine optimization of web resources

The web resource optimization algorithm is shown in Fig. 3.

Thus, the optimization process consists of 5 main operations with a total duration of 100 minutes.

CONCLUSION

At the moment, the area of competitive promotion of commercial web resources of interested parties, which are both consumers and suppliers, has received great development. Equipping an IT company with modern technology, improving the ergonomics and interface of web resources, round-the-clock technical support, prompt response – these are the criteria that stakeholders single out in the first place.

To improve the quality of search engine optimization of a web resource, a method was chosen for its development – a site on the Wordpress engine.

The web resource optimization algorithm consists of 5 main operations with a total duration of 100 minutes.

References

[1] Тинькофф: «Тёмная тема», e-Sim и многое другое [Электронный ресурс]. – Режим доступа: URL: https://www.tinkoff.ru/about/news/27102020-tinkoff-updated-and-added-new-services-to-the-superapp/ (21.10.2022).

[2] Тинькофф: Рекордная прибыль [Электронный ресурс]. – Режим доступа: URL: https://www.tinkoff.ru/about/news/11032021-tcs-group-holding-plc-fin-results-fy-2020/ (21.12.2022).

[3] Яндекс Метрика. [Электронный ресурс]. – Режим доступа: URL: https://metrika.yandex.ru (15.01.2023)

[4] Варжапетян А.Г., Семенова Е.Г. Квалиметрия. – СПб: РИЦ ГУАП, 2019. – С. 196.

APPLICATION OF ADAPTIVE LED LIGHTING TECHNOLOGY IN EDUCATIONAL INSTITUTIONS

Kuzmenko Yuri
Saint Petersburg State University of Aerospace Instrumentation,
Saint Petersburg, Russia
E-mail: spider22boy@mail.ru

Abstract. *The subject of this article is the design of the lighting system of educational institutions, with automatically regulating the control system of lighting devices. The influence of waves and spectra of light radiation of LED artificial lighting on the human body is considered. An analysis of lighting control technology, using universal asynchronous UART transceiver technology is carried out.*
The aim of the presented research is to assess the feasibility of using a controller for intelligent control of artificial lighting in educational institutions, based on a digital driver XDPL8221.

Introduction

In educational establishments, lighting is a quite important factor, as much of the effectiveness of learning depends on the light within the classroom. Today, due to the move to LED lighting sources, it has become possible to control lighting devices through automatic and user-controlled adjustment systems of luminaires. Thanks to the ability to design such systems, it has become possible to take into account the biological characteristics of people of all ages in the room. These requirements must be taken into account not only in interior lighting, but also in the screens and displays of modern electronic devices. Ergonomic design with lighting requirements is described in GOST R ISO 24502-2012 Russian Federation national standard "Requirements for the brightness and contrast of colored light sources for people of different age groups. This standard prescribes rules for taking into account the visual capabilities of older people in the design of signs and displays [1]. Requirements for the state of lighting are described in the national standards of the Russian Federation "Lighting of workplaces inside buildings" GOST R 55710-2013 and "Lighting devices with LED light sources" GOST R 55705-2013.

In terms of regulatory framework, artificial lighting in educational institutions is regulated by two regulations – SanPiN 2.4.2.2821-10, 2.2.1/2.1.1.1278-03 code of practice SP 52.13330.2016. The first standard describes the types of lighting fixtures that must be used, the rules for installing lighting fixtures and the minimum illumination of the student workplace in the classroom 300 lux and in the gym 200 lux [2]. The second document addresses similar issues, but gives an allowable value of the ripple factor of not more than 10% [3].

Consideration of customer requirements for lighting systems increases the cost of these systems, additional costs are due to the need for more complex components, for example, to control a large number of parameters or with separate control zones of the premises.

Influence of diode lighting on the student

Research on the effect of diode lighting on the human eye has long been the subject of debate, often quite controversial

For example, according to a study [4] LED lighting, unlike gas-discharge or incandescent bulbs has no negative effect on vision and attention.

When testing conducted at the Research Institute of Scientific and Research Center for Health of RAMS, a result was obtained indicating that the use of LED lighting with low correlated color temperature, the preconditions for the negative impact of this type of lighting on the retina, with increasing correlated color temperature reduces the impact on the vision, but in any case, excessive blue light led to an accelerated degeneration processes, which in future may create risks for visual impairment, compared with eu

According to the dissertation study, we can say that today, due to the development of LED lighting systems, there is a significant decrease in the spectral range of artificial light, compared to the previous environment in which human cells developed.

Examining modern lighting systems, we can conclude that there is a downward trend in the use of infrared and near-infrared light sources from artificial lighting systems. This phenomenon was provoked

not only by the use of energy-saving lamps, but also by NIR windows which do not allow near-infrared waves.

Research indicates that the lighting industry is focusing on visible light, around 390 nm to 740 nm. This range can cause damage to human vision. Medical and biological studies show that exposure to high-intensity blue light at night affects sleep disturbance, which causes effects on the human nervous system.

Visible light, with predominant blue radiation, can suppress the production of melatonin, which affects the day and night cycles of the human body. This phenomenon contributes to myopia, as evidenced by the rapid growth of this phenomenon in Asian countries, mainly using LED lighting.

It is worth noting that, despite its negative impact, short-lived emissions of the blue spectrum contribute to increased productivity and concentration. This is the reason why artificial lighting systems with a safe portion of the blue spectrum are used in offices for natural daylight hours [6].

Lighting system based on the XDPL8221 controller will solve these problems due to more complete information about the work of the luminaire and therefore can independently adjust both the color temperature and brightness levels, which will combat the problem of ripple and reduce the impact of the UV light share on the retina.

UART as a key element of "smart lighting"

The Universal Asynchronous Receiver-Transmitter (UART) serial communication interface offers new control and analysis capabilities. With UART, you can control the power conversion in an AC to DC converter like a typical mixed-signal controller, with the advantage of being able to update, exchange, and store data about the converter's status and operating conditions. System problems and faults, such as high or low output voltages, can be instantly monitored using the UART monitoring functions. This allows faults to be pinpointed accurately, maintenance personnel will be directed to the right place with the necessary spare parts to repair the faulty device. This significantly reduces costs, since maintenance personnel do not need to search for faulty devices and spare parts for repair.

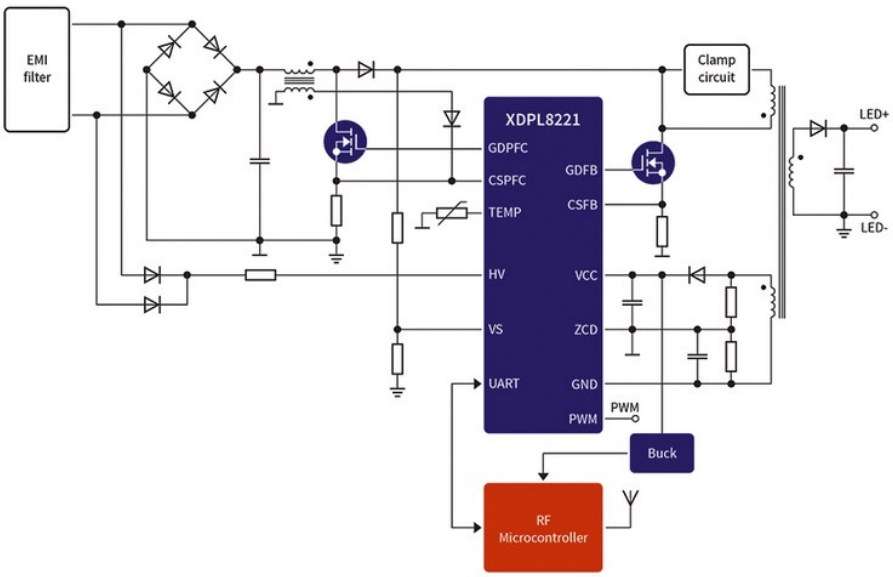

Fig. 1. Driver application diagram and enabling UART for management and analysis

In addition, real-time measurement data are available via UART. Operating data such as output voltage and output current can be read at any time. The constant availability of these values allows, for example, the actual output power to be determined and therefore gives a detailed view of the power consumption of the device and allows it to be controlled. Furthermore, regular monitoring of the current and voltage readings of the LEDs allows the wear and tear of the device to be judged. This enables the maintenance personnel to analyze the performance of the device and therefore allows maintenance planning. With this preventive maintenance, only necessary costs are incurred and downtime is minimized. Given the large areas of educational facilities that are illuminated by LEDs, having UART in each of these luminaires allows real-time data access to each LED matrix.

Security features

A comprehensive set of security features makes the new driver resistant to crashes and unsafe conditions. Two of them are output undervoltage and overvoltage protection, which usually occurs when the pin is shorted or disconnected from the LED.

Thanks to the features of the controller, it is possible to organize flexibleprotectiony against high and low input voltage. This makes it possible, to adjust the lighting so that it is suitable for use in networks where major repairs have not been made and, therefore, voltage drawdowns are possible below the permissible limit.

Another important feature is the protection against overheating, as the service life of the diodes themselves and the LED driver often depends on their operating temperature and their susceptibility to overheatingy. An internal or external temperature sensor can be used to detect and activate the protection. The internal sensor protects the light source and any external components that have sufficient thermal coupling to the device. An external sensor can be placed to protect external components such as a transformer, field-effect transistors, or on the light element of a diode.

The internal temperature protection initiates a shutdown if the temperature exceeds a critical level. External temperature protection is triggered if the critical resistance of the negative temperature coefficient (OTC) exceeds the threshold value. This method of protection allows you to implement temperature protection with smooth automatic adjustment. This tripping protection reduces the output current until the temperature drops below the appropriate threshold to protect the load or driver from overheating. The operation of the protection is as follows: as long as the OTC resistance is below the temperature threshold, the driver reduces the current. As soon as the OTC resistance exceeds the temperature threshold, the device again incrementally increases the output current. Thus, the controller blocks reaching the critical temperature, extending the service life of the driver. If lowering the current to the minimum permissible value does not reduce the temperature, then the overheat protection is triggered and a complete shutdown occurs. For all cases of overheating protection, the controller will only restart when the temperature drops below the configurable threshold. Overheating protection is important to ensure the safety of users, preventing serious accidents and preventing material losses. In fact, high temperatures are usually associated with faster device aging and performance degradation. In addition, the GET UART command allows you to read the temperature. This дает enables maintenance personnel to regularly monitor the driver's temperature [7].

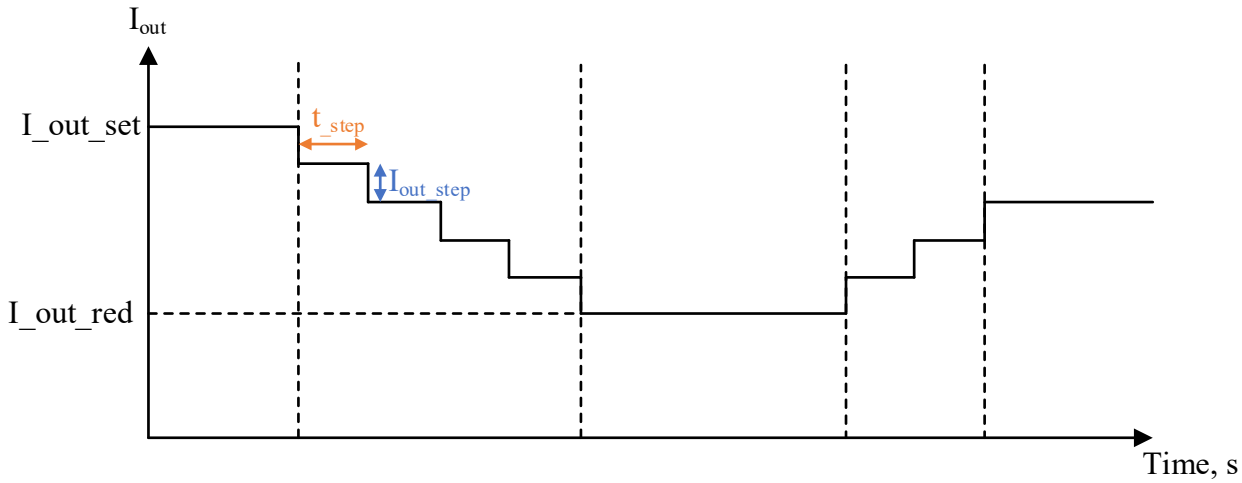

Fig. 2. Diagram of external temperature protection operation

Conclusion

To increase the energy efficiency of LED lighting systems in general, it is necessary to optimize the operation of both individual lighting devices and the lighting system as a whole, as well as use control algorithms that consider the characteristics of this type of product and the environment. Thanks to the use of UART technology based on the designated controller, these tasks will be performed, which will definitely allow you to meet the requirements of existing regulatory documentation at a different quality level.

It is necessary to ensure an adequate level of safety of luminaires, which will be based on reducing the proportion of blue light, it is necessary to conduct further research and develop a regulatory

framework for determining the requirements for biological safety, considering changes in natural cycles, days, seasons and other conditions characteristic of a particular area.

The use of such lighting control technology will allow the operation of lighting installations with greater efficiency and greater flexibility, which is necessary for use in schools and other educational institutions. Alsoe б, thanks to the UART interface, a much more flexible and adaptive configuration of the lighting system is possible.

To solve the tasks described above, the greatest effectiveness can be obtained after using the controller indicated above, since it provides the proper level of control and observability for the operation of LED lighting equipment.

References

1. GOST R ISO 24502-2012 National standard of the Russian Federation ergonomic design "Requirements for brightness and contrast of colored light sources for people of different age categories" URL: https://docs.cntd.ru/document/1200098798 (Accessed 15.02.23);

2. SanPiN 2.4.2.2821-10 "Sanitary and epidemiological requirements for the conditions and organization of training in general education institutions";

3. Code of Rules of SP 52.13330.2016 "Natural and artificial lighting" Updated version of SNiP 23-05-95;

4. Influence of LED lighting of school recreation areas on visual acuity and psych emotional state of first-graders in the dynamics of the school year URL: https://cyberleninka.ru/article/n/vliyanie-svetodiodnogo-osvescheniya-shkolnyh-rekreatsiy-na-ostrotu-zreniya-i-psihoemotsionalnoe-sostoyanie-pervoklassnikov-v (Accessed: 20.0.02.2.23);

5. Kuzmenko V..P.. models and methods of quality assurance of LED lighting devices: dis. PhD M., 2021. https://fs.guap.ru/dissov;

6. Models and methods of quality assurance of LED lighting devices URL: https://cyberleninka.ru/article/n/obrazovatelnaya-svetovaya-sreda-professionalnogo-uchebnogo-zavedeniya (Accessed on 20.02.23);

7. New LED power supply technology – a new level of «smart lighting» URL: http://lightingmedia.ru/wp-content/uploads/2020/11/32.pdf (Accessed on 20.02.23);

USAGE OF TREE-SPLI TTING ALGORITHMS FOR COLLISION RESOLUTION AT THE STAGE OF CONNECTING DEVICES TO THE BASE STATION

Mikhailov Valentin
Saint Petersburg State University of Aerospace Instrumentation,
Saint Petersburg, Russia
E-mail: valyamih1@gmail.com

Abstract. *Due to rise in popularity of Internet of Things and machine-type communications, massive number of devices can connect to the base station at the same time. Therefore, algorithms for such connections have to be more advanced. In this paper, we focus on tree-splitting algorithms. We will provide brief history of tree-splitting collision resolution algorithms, and their role and usage in modern cellular networks.*
Keywords*: cellular networks, tree algorithm, random access procedure, collision resolution.*

INTRODUCTION

In modern cellular networks, random access (RA) procedures are used to connect a device to a base station. In recent years, due to the development of the "Internet of Things" technology, RA procedures have been studied more intensively. After all, the "Internet of Things" implies a huge number of devices that can transmit their data simultaneously.

When multiple devices try to access the network at the same time, conflicts arise in the communication channel, and the more devices, the more difficult it is to resolve these conflicts. There are several approaches to reduce the impact of this problem. For example, conflict resolution algorithms. One of them, more efficient than those currently used, is a tree-like algorithm.

B. Tsybakov and V. Mikhailov in 1978 [1] and D. Kapetanakis in 1979 [2] first proposed the tree-splitting conflict resolution algorithm. Already in these papers, it is shown that in comparison with the generally accepted ALOHA conflict resolution algorithm, the tree-splitting algorithm allows you to get a lower delay.

Next, we will consider the concept of a tree-splitting algorithm, describe the history of theoretical research in this area, and then show how a tree-splitting algorithm can be used in modern cellular networks.

Concept of tree-splitting algorithm

In this algorithm, all devices monitor the output of the system and, if a conflict occurs, build a so-called conflict resolution tree, according to which a decision is made about the action in this time slot. Let us describe the algorithm in more detail.

All devices listen to the output of the RA channel. Three events can occur in the channel: – "Success" – when only one device is transmitting in the slot, "conflict" – when two or more devices are transmitting in the slot, and "empty" – when no one is transmitting in the slot. Devices that came to the system later wait for the end of the tree, and after that, they transmit their messages. At the moment of the initial conflict, a root of the tree is created, and each of those devices that transmitted a message in a slot with a root conflict is equally likely to choose whether to transmit in the next slot or not. If the device chooses to transmit, it moves to the left branch of the tree, if not, then to the right (it is determined later). If the conflict occurs again, the devices continue to build the tree according to the same rules. If the left branch turned out to be the end – that is, there was no conflict in it, then the right branch is built in the next slot. In [1], two variants of the algorithm were presented. An example of how the algorithm works according to the first variant described earlier is shown in Fig. 1. In this example, a conflict between the three devices is resolved. The number of devices transmitting in this slot is written inside the top of the tree. This option was called "conflict resolution by stages". In another option, which was called "conflict resolution by zugs", both branches of the current level of the tree are first transmitted, and only after that, if there is a conflict, further branching occurs. An example of the operation of such a variant of the algorithm is shown in Fig. 2.

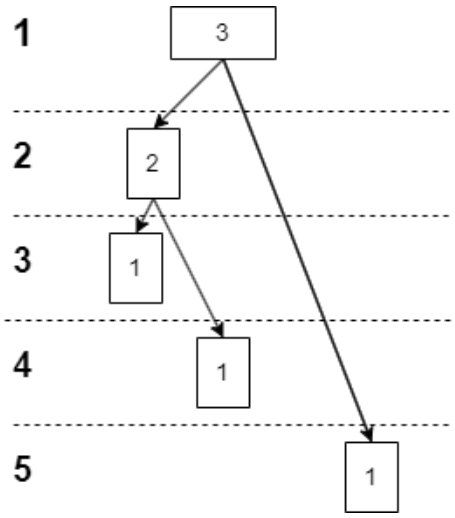

Fig. 1. Conflict resolution by stages

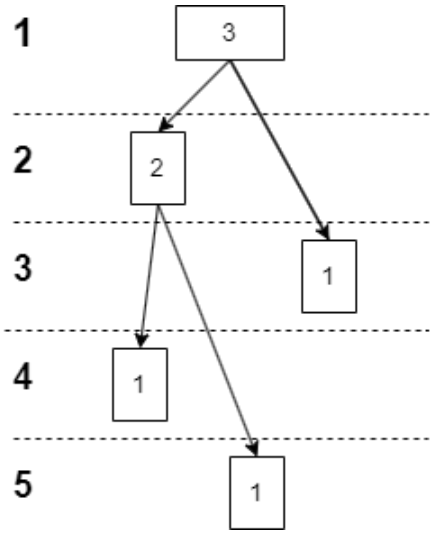

Fig. 2. Conflict resolution by zugs

The average time for conflict resolution in the variant by stages and “by zugs” is the same, and from the point of view of implementation, it is easier to resolve the conflict by stages. Mainly in further works, the algorithm of conflict resolution by stages is considered. In [3], a variation of this algorithm was presented – the contention stack algorithm. The main difference is that the device does not need to wait until the tree is fully built, it can transmit its message in any free slot.

Further improvements in algorithms

Tree-based conflict resolution algorithms are still being researched and improved. The key point in these studies was a paper published in 2007, in which it is proposed to use the method of successive interference cancellation together with such algorithms [4]. This method suggests not discarding the data from the conflict but saving it. Therefore, later when subtracting already known signals from the general data, the remaining signals can also be decrypted. Thus, this method significantly reduces the latency in the system by using the computing power of base stations. This approach has been developing for a long time, through the efforts of many scientists. In an extensive analysis [5] the main implementations of this approach were presented. Further improvement is considered in [6].

The random access channel of modern cellular networks uses an ALOHA based algorithm. Currently, it is proposed to use tree-like algorithms to improve the efficiency of work. One of the possible options is introduced in the article [7]. It suggested using the approach described in [1] "conflict resolution by zugs" and the non-binary conflict resolution tree. An example of this algorithm is shown in Fig. 3.

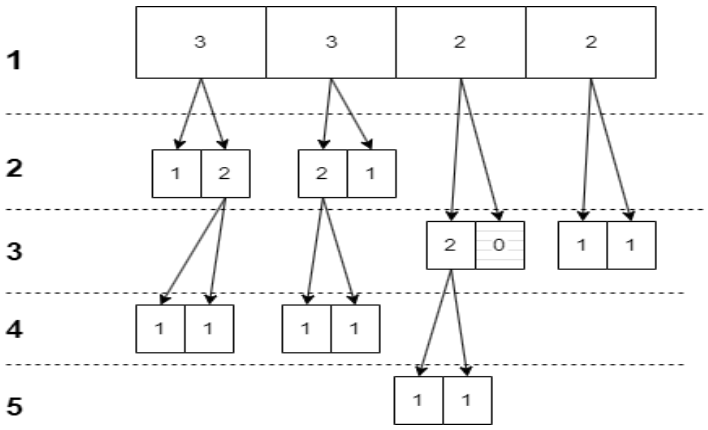

Fig. 3. Tree-splitting from [7] paper

Considering random access channel characteristics and utilizing its implementation, authors claims that proposed scheme can resolve up to 30000 devices, which arrived simultaneously. This approach greatly outperformed existing LTE RA procedure: it could resolve up to 5000 devices at max, but even in 1000 devices, the outage probability (percentage of devices not completing the RA procedure before the maximum number of transmissions is reached) is over 50%. While in [7] approach even at 30000 devices outage probability is no more than 1 percent. Authors tries different number of branches, and compare performance. Due to RA channel configuration, which provides 54 preambles at every level of tree, number of branches such as 6, 9 and 18 are considered. For 18 branches minimum of mean transmissions per device can be achieved. However, minimum average delay, experienced by resolved device, achieved with 6 branches.

Thus, in real life use of this technique, tradeoff between acceptable delay and power usage of device will take place.

To eliminate this drawback, Dynamic Tree-splitting Algorithm was proposed [8]. Major difference from the previous one is that the number of branches is determined dynamically at each step, depending on the intensity of conflicts. The authors of this algorithm claim that they managed to increase the throughput in the random access channel by 12.5% compared to the branching algorithm for a given number of branches, and by 98% compared to the standard ALOHA algorithm. This approach shown in Fig. 4.

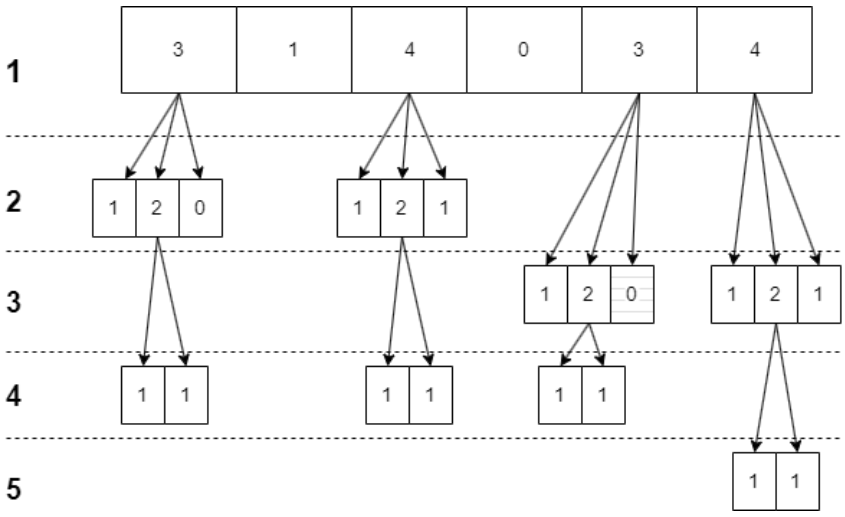

Fig. 4. Dynamic Tree-splitting from [8] paper

CONCLUSION

The paper briefly describes the history of research on tree-like algorithms for conflict resolution from 1978 [1] to the present [6]. The papers [7-8] shows an example of usage tree-splitting algorithms in the random multiple access channel of modern cellular networks. It should be noted that the approaches

from [7-8] and similar works do not fully implement results of researches in the field of tree-splitting algorithms. Such implementation is necessary for better performing collision resolution at the stage of connecting real-life devices to the base station.

REFERENCES

1. Tsybakov, B. S.; Mikhaĭlov, V. A. Free synchronous packet access in a broadcast channel with feedback. Problems Inform. Transmission 14 (1978), no. 4, 32-59

2. J. Capetanakis, "Tree algorithms for packet broadcast channels" // IEEE Transactions on Information Theory, vol. 25, no. 5, pp. 505-515, September 1979, doi: 10.1109/TIT.1979.1056093.

3. Tsybakov, B.S. and Vvedenskaya, N.D., 1980. Random multiple-access stack algorithm. Problemy Peredachi Informatsii, 16(3), pp.80-94.

4. Yu, Y. and Giannakis, G.B., High-throughput random access using successive interference cancellation in a tree algorithm.// IEEE Transactions on Information Theory, 53 no.12 (2007), pp.4628-4639.

5. Stefanović, Čedomir & Deshpande, Yash & Gürsu, Murat & Kellerer, Wolfgang. Tree-Algorithms with Multi-Packet Reception and Successive Interference Cancellation. // preprint arXiv:2108.00906, August 2021.

6. Vogel, Q., Deshpande, Y., Stefanović, C., & Kellerer, W. (2023). Analysis of d-ary Tree Algorithms with Successive Interference Cancellation. arXiv preprint arXiv:2302.08145.

7. G. C. Madueño, Č. Stefanović and P. Popovski, "Efficient LTE access with collision resolution for massive M2M communications," 2014 IEEE Globecom Workshops (GC Wkshps), Austin, TX, USA, 2014, pp. 1433-1438, doi: 10.1109/GLOCOMW.2014.7063635.

8. H. Althumali, M. Othman, N. K. Noordin and Z. M. Hanapi, "Dynamic Tree-Splitting Algorithm for Massive Random Access of M2M Communications in IoT Networks" // IEEE Systems Journal, doi: 10.1109/JSYST.2021.3097715.

ALGORITHM FOR AUTOMATIC RECOGNITION OF NOTES IN THE AUDIO SIGNAL

Miroshnichenko Nikita
Saint Petersburg State University of Aerospace Instrumentation,
Saint Petersburg, Russia
E-mail: Nikitos_mir.1997@mail.ru

Abstract. *This article discusses and compares manual and automatic algorithms for recognizing musical notes of audio signals in the MATLAB software environment. The sound source can be a single note, or a gamma, which will be processed by the mathematical apparatus underlying the analysis of frequency properties. In the manual algorithm, harmonics are arranged using the frequency spectrum and the frequency value is found according to the note correspondence table. In the automatic algorithm, the letter sequence of musical notation will be determined using the note frequency formula.*
Keywords: *frequency, musical note, signal spectrum, algorithm, identification*

Introduction

Nowadays, music in its various manifestations has become not just a way of satisfying aesthetic needs, it can also be considered as an instrument of informational, psychological and social impact on a person [1].

Many amateur musicians are faced with the task of converting their vocal and musical material into notes. Automated recognition of sounding notes with the help of special software would speed up and improve the convenience and quality of recording notes. There are countless solutions for transferring a reproduced melody to a musical notation, however, most of them are designed to work with musical instruments and are not capable of qualitatively processing melodies sung only by voice. Solutions that allow you to work only with the voice also exist, but they are aimed at identifying melodies, and not for obtaining musical notation [2].

Description of musical notes

A musical note is a kind of instrument that reproduces a sound wave with a specific frequency, which is in the range from 16.35 Hz – 31.608 kHz. If you form a series of such waves into one consecutive track, then you can compose a melody. Each note has its own name and frequency (Table 1).

Table 1

Matching notes to frequencies

Notes	Sub-konto-octave	Counter-octave	Big	Small	1-st	2-nd	3-rd	4-th
C	13,35	32,7	65,41	130,82	261,63	523,26	1046,52	2093,04
C#	17,32	34,65	69,3	138,59	277,18	554,36	1108,72	2217,44
D	18,35	36,71	73,42	146,83	293,66	587,32	1174,64	2349,28
D#	19,45	38,89	77,48	155,57	311,13	622,26	1244,52	2489,04
E	20,6	41,2	82,41	164,82	329,63	659,26	1318,52	2637,04
F	21,83	43,65	87,31	174,62	349,23	698,46	1396,92	2793,84
F#	23,12	46,25	92,5	185	369,99	739,98	1479,96	2959,92
G	24,5	49	98	196	392	784	1568	3136
G#	25,96	51,91	103,83	207,65	415,3	830,6	1661,2	3322,4
A	27,5	55	110	220	440	880	1760	3520
A#	29,14	58,27	116,54	233,08	466,16	932,32	1864,64	3729,28
B	30,87	61,74	123,47	246,94	493,88	987,76	1975,52	3951,04

The frequency determines the pitch of the sound, and the pitch determines which note is played.

Table 1 also shows the octaves, which represent the established segments of the sound range. Each musical octave consists of seven white notes with the following names: "Do" (C), "Re" (D), "Mi" (E), "Fa" (F), "Sol" (G), "La" (A), "Si" (B) and of five black notes with the following names: "C-sharp" (C#), "D-sharp" (D#), "F-sharp" (F#), "G-sharp" (G#) and "B-flat" (A#).

Implementation of a manual algorithm for identifying musical notes in audio signals

Using the mathematical apparatus underlying the analysis of the frequency properties of the audio signal, we identify the notes of the audio signal in manual mode.

To test the method for determining musical notes, we use a sound signal with three notes. The MATLAB software environment will be used to implement the task.

To begin with, we will demonstrate the entire sound signal on the graph (Fig. 1).

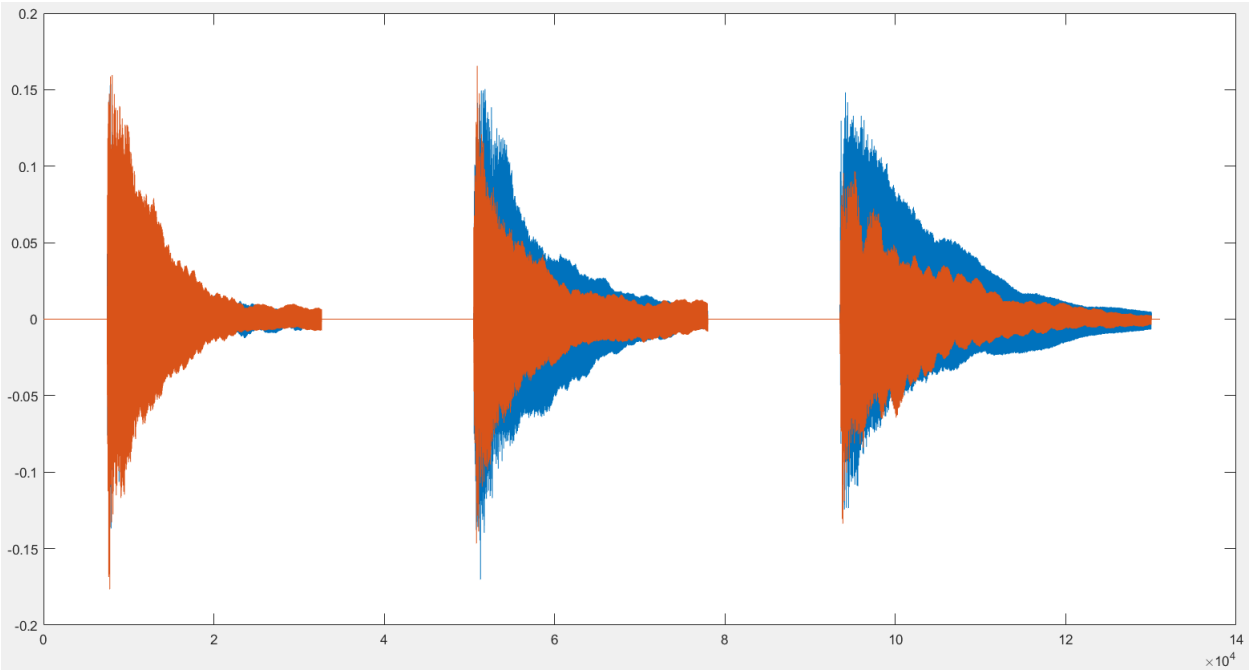

Fig. 1. Test audio signal graph

According to this graph, you can see how three musical notes are demonstrated, but it is impossible to determine which note is depicted. This requires an algorithmic implementation based on the fast Fourier transform, in which spectral analysis on a sliding window will be demonstrated.

Let's make an algorithmic implementation for each note and demonstrate the signal spectrum (Fig. 2).

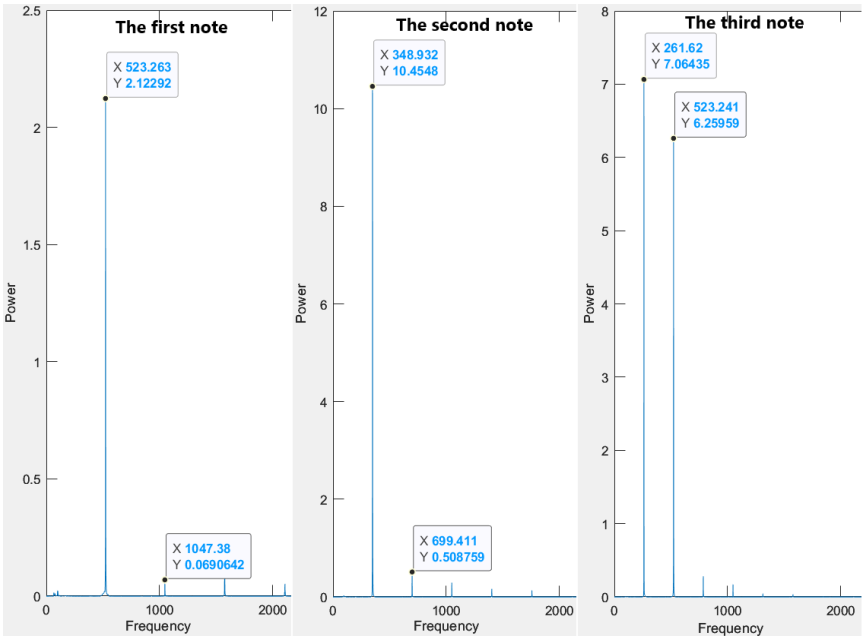

Fig. 2. Spectral analysis of notes in a text audio signal

According to the spectral analysis of musical notes, which is shown in Fig. 3, it is possible to see harmonics with frequencies of 523.26 Hz, 348.93 Hz and 261.62 Hz. These frequency values were compared with the table of correspondence of notes to frequencies (Table 1) and revealed musical notes: "To" (C) of the second octave with a frequency of 523.26 Hz, "Fa" (F) of the first octave with a frequency of 349.23 Hz and "To" (C) of the first octave with a frequency of 261.63 Hz. There is no data on the second harmonic, if everything is correctly implemented, it should be twice as high in frequency of the first harmonic and be in the table of musical notes for the same note, but an octave higher. When comparing the second harmonics, the notes were obtained: "To" (C) of the third octave, "Fa" (F) of the second octave and "To" (C) of the second octave. It can be concluded that this method determines whether the notes are found correctly.

Implementation of an automatic algorithm for identifying musical notes in audio signals

The main idea of this article is the implementation of an automatic algorithm for recognizing notes in audio signals. This method, as well as the method described in the last paragraph, is applied using the mathematical apparatus underlying the analysis of the frequency properties of the audio signal.

To find the frequency of a note, it is necessary to determine the maximum amplitude of the first harmonic (max(A)) using the "max" function. Also output the sampling rate (Fs) of the entire audio signal, as practice shows, the standard sampling rate is 44100 Hz. The next step is to find the largest dimension of the array (N) using the "lenght" function. Next, we find the frequency using the following formula (1):

$$F = \frac{\max(A) \cdot Fs}{N} \tag{1}$$

An important part of the job is to identify the note correctly. Table 1 demonstrates the correspondence of notes to frequencies, but in real life notes do not sound exactly according to the values in the table, there is always a range of minimum and maximum frequencies from the reference. This range in the program was found using the arithmetic mean formula (2):

$$\overline{X} = \frac{\sum_{i=1}^{n} x_i}{n}, \tag{2}$$

where $\overline{X}$ – is the arithmetic mean simple, x_i – is the value of the varying feature of the i-th element, n – is the number of features.

For example, the note “To” (C) of the first octave has a frequency of 261.63 Hz, to find its minimum range value, it is necessary to apply formula 2 with the note “Si” (B) of a small octave with a reference frequency of 246.94 Hz. As a result, after solving this example, we get a frequency equal to 254.29 Hz. By analogy, the maximum value of the range of the note “To” (C) of the first octave is found, only instead of the note “Si” (B) of the small octave, the frequency of the note “C-sharp” (C#) of the first octave will be used. This procedure is applied to the twelve notes of the first octave. To correctly find the remaining notes in the program, a condition was implemented that takes into account the minimum and maximum values of the range of twelve notes, which are equal to 254.29 Hz and 508.57 Hz. This condition is implemented in such a way that if the found frequency of the audio signal is less than the minimum frequency of the range, then it will be multiplied by 2 until it is in the desired range, and if the frequency is greater than the maximum frequency of the range, then, on the contrary, it will be divided by 2 until it is in the desired range. The octaves change so that if the tone is lower, it drops by 1 (for example, from the first octave to a small one), and if higher, it is added by 1 (for example, from the first octave to the second).

We will demonstrate the result of applying this algorithm on a test audio signal with three notes (Fig. 3).

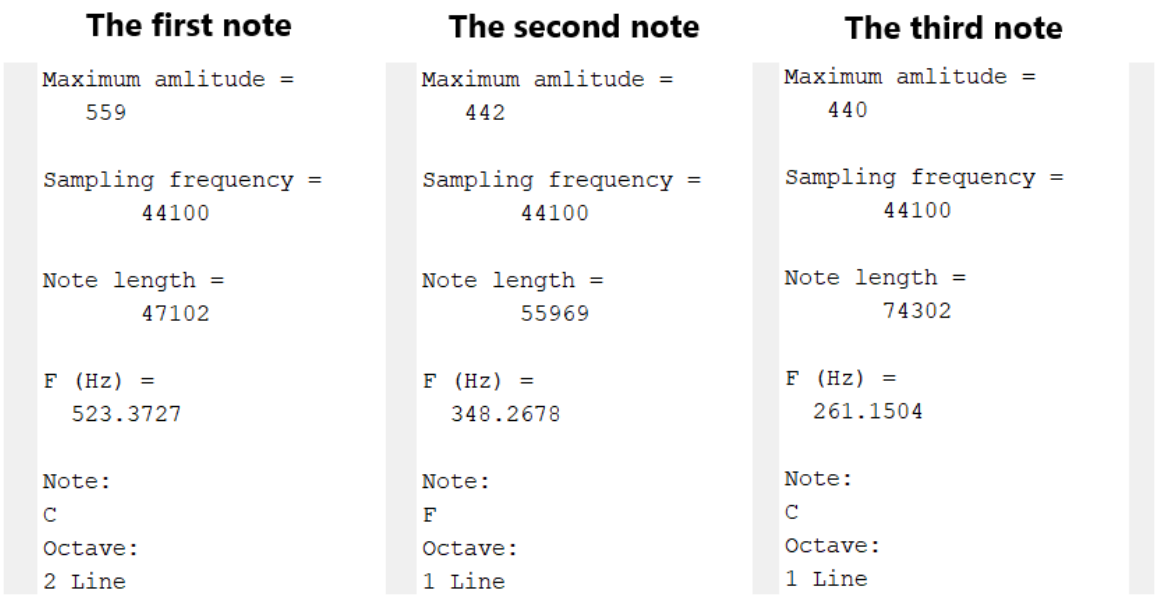

Fig. 3. The result of an automatic algorithm for finding notes in a text audio signal

It can be noticed that the result of the manual algorithm and the automatic one are similar in finding the notes of the test signal, which in turn confirms the correctness of the program.

Conclusion

In the article, using the mathematical apparatus underlying the analysis of frequency properties, manual and automatic methods for identifying musical notes of a test signal with a successful solution result were demonstrated.

An automatic algorithm identifies the notes of melodies of any instruments, including the voice.

Also, the methods presented in this article can be used for technical diagnostics and tuning of musical instruments.

References

1. Kokowska, M. Pesronality, music preference and mood regulation by music tendencies in healthy people and with depression / M. Kokowska, M. Dymnikowa // Norwegian Journal of Development of the International Science. – 2021. – No 55-2. – P. 56-65. – DOI 10.24412/3453-9875-2021-55-2-56-65. – EDN WXIWAM.

2. Automatic recognition of musical notes / A. A. Konev, A. A. Onishchenko, E. Yu. Kostyuchenko, A. Yu. Yakimuk // Scientific Bulletin of the Novosibirsk State Technical University. – 2015. – No. 3(60). – S. 32-47. – DOI 10.17212/1814-1196-2015-3-32-47. – EDN UNEYMB.

COMPRESSED SIGNAL SIDELOBES SUPPRESSION

Nenashev Sergey,
Ryzhov Konstantin
Saint Petersburg State University of Aerospace Instrumentation,
Saint Petersburg, Russia
E-mail: nenashev_sergey178@mail.ru konstantin.r02.27@gmail.com

Abstract. *Coding of radar signals can be performed using sequences for phase coding, such as Barker codes and corresponding nested codes. The purpose of this work was to obtain results in the area of broadband signal processing in terms of sidelobes suppression. In obtaining the results, simulation modelling gear was used, as well as experimental investigation of Barker codes and nested code sequences. The results are the autocorrelation functions of Barker code constructs with suppressed sidelobes. These results are the basis for greater noise immunity of such broadband signals and prove the feasibility of their application to various detection systems for civilian applications..*
Keywords: *Barker codes, sidelobes suppression, autocorrelation function.*

Introduction

Pulse compression is a method of processing broadband signals, which allows to obtain a high resolution of the "range" coordinate using coded signals [1-8]. At the same time, such a compressed signal has sidelobes, for which it is required to implement a suppression process.

Sidelobe suppression process

The sidelobes of the autocorrelation function (ACF) for the Barker code are equal to one. Some sidelobes of the ACF of the Barker code can be brought to zero if the corresponding matched filter is followed by a linear sidelobe suppression filter with the impulse response given by the formula:

$$h(t) = \sum_{k=-N}^{N} \beta_k \delta(t - 2k\tau_0), \tag{1}$$

where N is the filter order, the coefficients β_k $(\beta_k = \beta_{-k})$ must be determined by

$\delta()$ by the delta function and τ_0 by the pulse width of the Barker subcode. A filter h(t) of order N produces (Fig. 1) N zero sidelobes on the sides of the main ACF lobe. The amplitude and width of the mainlobe do not change.

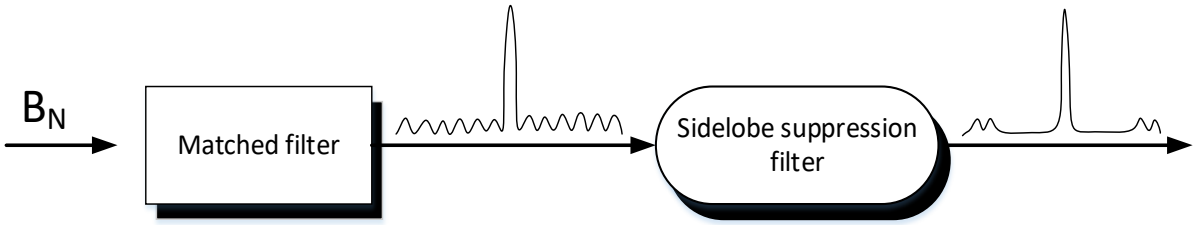

Fig. 1 − Linear sidelobe suppression filter order N can be used to obtain N zero sidelobes lobes in autocorrelation function (N=4)

To illustrate this approach, we consider the case where the input data to the corresponding filter B_{11} and assume $N=4$. The ACF values for B_{11}

$$R_{11} = \left\{ \begin{matrix} -1,0,-1,0,-1,0,-1,0,-1,0,-11,0,-1,0,-1,0, \\ -1,0,-1,0,-1 \end{matrix} \right\} \tag{2}$$

The output of the transversal filter is a discrete convolution between its impulse response and the sequence R_{11}. At this stage we need to calculate the coefficients β_k which will provide the desired output signal from the filter (i.e., an unchanged main lobe and four zero levels of sidelobes).

Performing discrete convolution as defined in formula (2) and collecting equal terms $(\beta_k = \beta_{-k})$ gives the following set of five linearly independent equations:

$$\begin{bmatrix} 11 & -2 & -2 & -2 & -2 \\ -1 & 10 & -2 & -2 & -2 \\ -1 & -2 & 10 & -2 & -1 \\ -1 & -2 & -1 & 11 & -1 \\ -1 & -1 & -1 & -1 & 11 \end{bmatrix} \begin{bmatrix} B_0 \\ B_1 \\ B_2 \\ B_3 \\ B_4 \end{bmatrix} = \begin{matrix} 11 \\ 0 \\ 0 \\ 0 \\ 0 \end{matrix}. \quad (3)$$

The solution of the system of linear equations (3) gives

$$\begin{bmatrix} B_0 \\ B_1 \\ B_2 \\ B_3 \\ B_4 \end{bmatrix} = \begin{matrix} 1.1342 \\ 0.2046 \\ 0.2046. \\ 0.1731 \\ 0.1560 \end{matrix} \quad (4)$$

Note that the value of the first equation is 11, and the one of all other equations is 0, and then the solution for β_k is the result of the fact that the main peak will remain unchanged, and that the next four sidelobes will be 0. So far, it has been assumed that the encoded pulses are rectangular in shape. Using pulses of other shapes, such as Gaussian, it is possible to reduce the sidelobes and increase the compression ratio of the codomodulated signal.

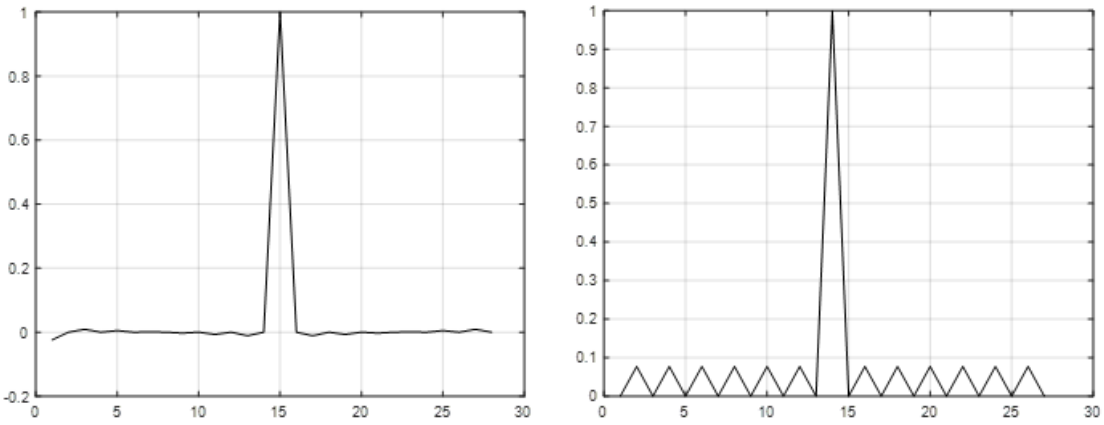

Fig. 2 − ACF of the Barker code at N=13 before (a) and after (b) sidelobe suppression

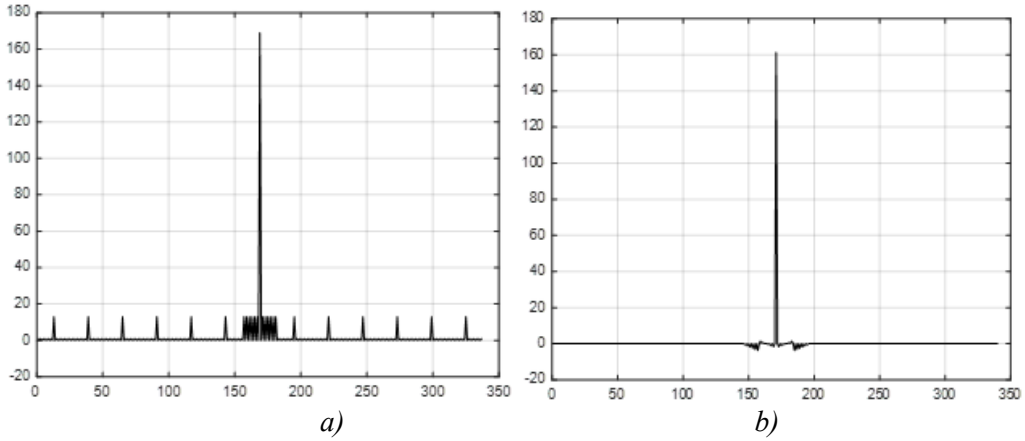

Fig. 3 − ACF of the nested Barker design at N= 13×13 before (a) and after (b) sidelobe suppression

The result of compression with simultaneous suppression of sidelobes are shown in Fig. 2 and 3.

Conclusions

In this paper we considered the suppression of sidelobes of the compressed signal modulated by Barker code and a similar process for nested code constructions. The significance of the results is provided by the perspective of the research, affecting the formation and development of methods for the extraction, detection and processing of useful information. The results of the work have a long-term effect, because with the emergence of original new codes and code structures there is a need for their research, modification, generalization and expansion of the field of application.

Gratitude

The authors express his sincere gratitude to his supervisor, Associate Professor V.A. Nenashev for his help and valuable advice in the preparation of this article.

Reference

1. Varakin L. E. Communication systems with noise-like signals: Radio and Communications, 1985, 384 p.

2. A. Radiolocation systems: textbook for universities. Moscow: Radiotekhnika, 2004. 320 p.

3. Trukhachev A. Radiolocation signals and their applications. Voenizdat. 205, P. 320.

4. A.S. Verba, B.G. Tatarsky. Radar Systems of Aerospace Monitoring of Earth Surface and Airspace. Monograph. b.m.: Radiotekhnika, 2014 P. 576.

5. Nenashev V.A., Sinitsyn V.A., Strakhov S.A. Investigation of the effect of industrial interference on the characteristics of the compression of phase-manipulated signals in the primary radars // Innovative technologies and technical means of special purpose: Proceedings of IX All-Russian Scientific and Practical Conference. In 2 volumes, St. Petersburg, November 16-18, 2016 / Ministry of Education and Science of the Russian Federation; Baltic State Technical University "Voenmeh" named after D.F. Ustinov. – St. Petersburg: Baltic State Technical University "Voenmeh", 2017. – P. 351-355.

6. R., Mahafza B. Radar Systems Analysis and Design using MATLAB. Chapman & Hall. 2000, p. 532.

7. Shepeta A. P., Nenashev V. A. FM pulse compression system in the tasks of high-precision mapping. Chronicles of the united fund of electronic resources. Science and education. 2014, P. 14.

8. Kristal V.S. Optimal processing of radar signals. Moscow: Novoe Vremya, 2014. – 208 p.

IMPLEMENTATION OF DIGITAL AUDIO PROCESSING ALGORITHMS IN PYTHON.

Nesterenko Alexander
Saint Petersburg State University of Aerospace Instrumentation,
Saint Petersburg, Russia
E-mail: vinmitya@gmail.com

Abstract. *The paper considers the main audio sound effects, with implementation in Python.*
Keywords: *digital signal processing, modulation, sound effects, Python.*

Currently, several ready-made software products allow you to implement certain sound processing algorithms. However, these programs clearly distinguish between the developer and the user, thereby not allowing to reveal of the mathematical essence of the algorithms underlying the signal conversion. Therefore, the main goal of this work was to create a ready-made software solution that allows both processing sound and directly interacting with sound processing algorithms.

A fairly large number of audio signal processing algorithms are associated with the concept of "modulation".

Amplitude, frequency, and phase modulation are the basis of many sound effects, in particular, the modulation effect is used to model the characteristic sound of individual musical instruments. The use of amplitude modulation results in a "tremolo" effect.

In audio engineering, when creating sound effects, a broadband periodic sound signal acts as a carrier frequency and is modulated by a low-frequency periodic sound waveform with a frequency usually below the audio range. So, to implement amplitude modulation, the following algorithm is used:

$$y(n) = x(n) + m \cdot m(n)\, x(n)$$

Where: (n)-input signal, (n)-modulating signal, (n)-output signal, m-modulation depth.

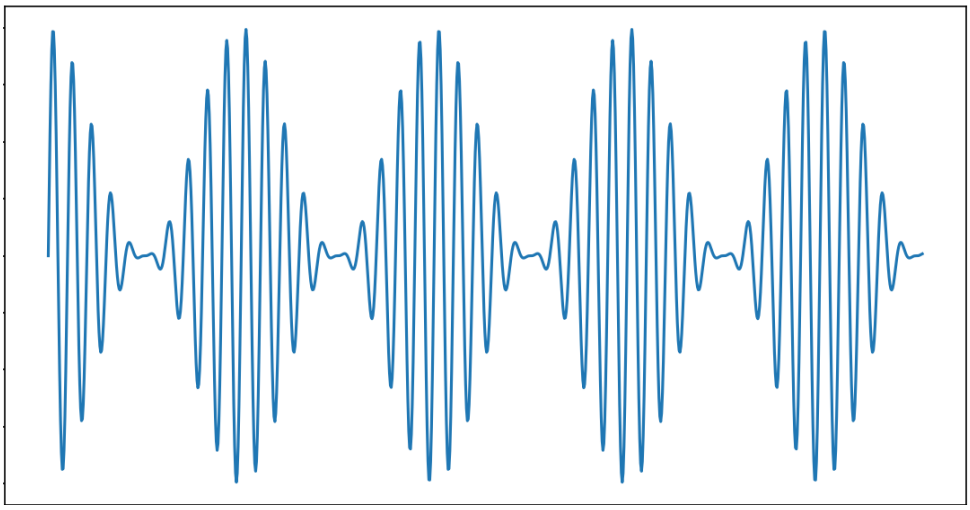

Fig.1. Graphical result of the tremolo effect

A block diagram illustrating the simulation of the effect is shown in fig. 2.

Phase and frequency modulation is also quite often used to implement various sound effects. In particular, to create the effect of "vibrato". Since there are no fundamental differences between them with harmonic frequency and phase modulation, although their implementations differ sufficiently to implement the “vibrato” effect, it is permissible to use both types of modulation in this work, frequency modulation was implemented.

In the discrete-time domain, the modulated oscillation is the expression:

$$y(n) = A_m \cdot \sin\left(2 \cdot \pi \cdot F \cdot n + I \cdot \sin\left(2 \cdot \pi \cdot F_{md} \cdot n\right)\right)$$

where A_m – modulation amplitude, F_{md} – modulation frequency, I – the frequency modulation index, (n) – output signal.

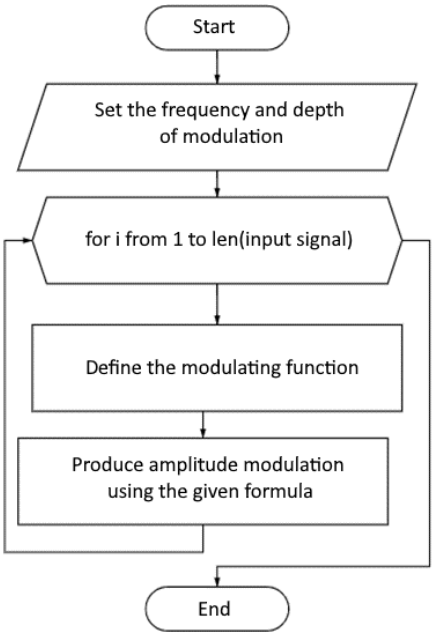

Fig. 2. Block diagram of the program for implementing the "tremolo" effect

```
# Tremolo
def tremolo(signal_in,sr):
    #Modulation frequency
    fq=100
    #Modulation depth
    Amp=np.amax(signal_in)*0.3
    for i in range (len(signal_in)):
        #Modulation function
        signal_add[i]=m.cos((2*fq*i*m.pi)/(sr))
        #Amplitude modulation
        signal_out[i]=signal_in[i]*Amp*signal_add[i]+ signal_in[i]
    return(signal_out)
```

Fig. 3. Modeling the tremolo effect in Python

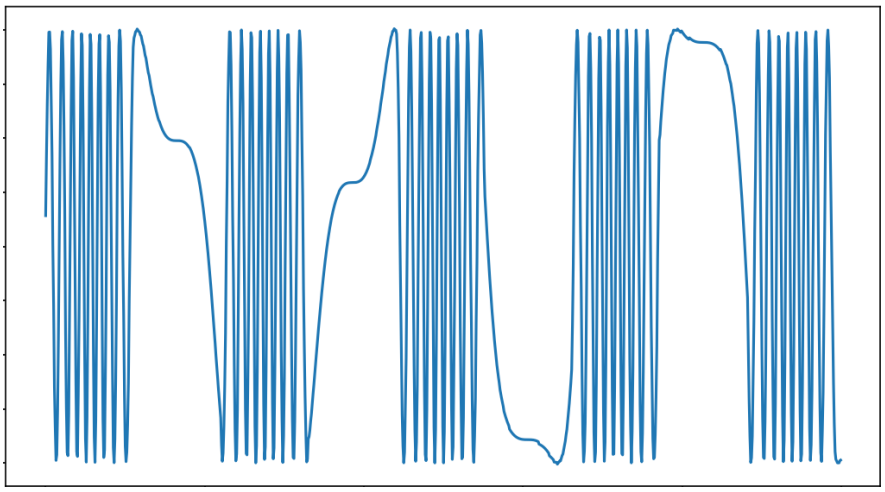

Fig. 4. Graphical result of the "vibrato" effect

But the use of this algorithm is not entirely appropriate, since the program usually receives not it, but several unknown harmonics, which greatly complicates the application of this expression.

Instead, to implement frequency modulation, we manipulate not the frequency, but the playback speed of the sample following the modulating signal, thereby achieving a similar effect.

Below is a flowchart and program illustrating the simulation of the effect.

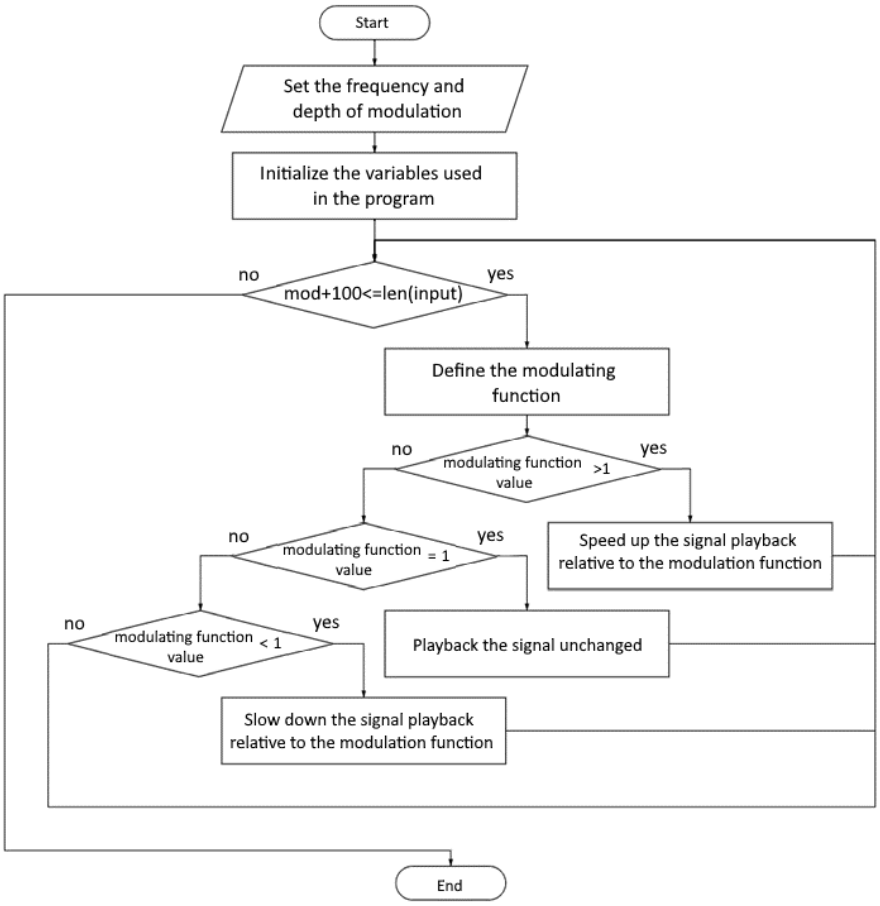

Fig. 5. Block diagram of the program for implementing the "vibrato" effect

```
#Vibrato
def vibrato(signal_in,sr):
    sl=len(signal_in)
    #Modulation frequency
    fq=5
    #Depth
    Amp=0.2
    #Auxiliary variables
    i=0
    mod=0.0
    signal_add=[]
    signal_out=[]
    while mod+100<=sl:
        #Modulating function
        signal_add=np.append(signal_add,1+Amp*m.sin((2*fq*i*m.pi)/(sr)))
        #Frequency modulation
        if signal_add[i] > 1:
            mod+=signal_add[i]
            signal_out=np.append(signal_out,signal_in[round(mod)])
        elif signal_add[i] == 1:
            mod+=1
            signal_out=np.append(signal_out,signal_in[round(mod)])
        elif signal_add[i] < 1:
            mod+=signal_add[i]
            var=mod-round(mod)
            inter=signal_in[round(mod)]*(1-var)+var*signal_in[round(mod)+1]
            signal_out=np.append(signal_out,inter)
        i+=1
    print(mod)
    return(signal_out)
```

Fig. 6. Modeling the "vibrato" effect in Python

In addition to the above simple effects, an effect such as the “echo” effect is often used to give soundtracks a natural effect. To implement this effect, delay lines are usually used. Using one or more delay lines in conjunction with feedback allows you to mix the original signal with its attenuated and time-shifted copy, creating the illusion of an echo. Feedback creates an infinite number of repetitions of the sound, following at intervals equal to the delay time. However, in reality, due to the sound-damping effect, the number of repetitions perceived by the ear is usually small. Therefore, for illustration, we can limit ourselves to three repetitions when simulating the operation of such a device.

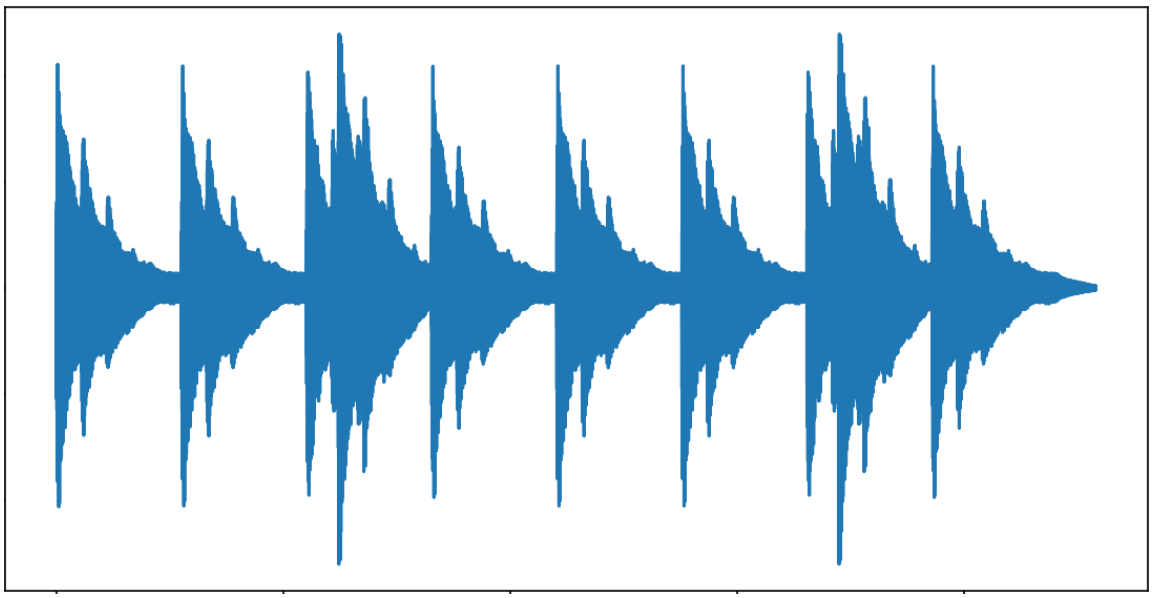

Fig. 7. Graphical result of the "echo" effect

On fig. 8 shows the software implementation of the "echo" effect in Python.

```
#Echo
def echo(signal_in,sr):
    #Dalay
    dalay=round(sr/4)
    for i in range (s_len):
        signal_out[i]=signal_in[i]
        #Echo overlay
        if i<dalay*2 and i>=dalay:
            signal_out[i]+=signal_out[i-dalay]*0.4
        elif i<=dalay*3 and i>=dalay*2:
            signal_out[i]+=signal_out[i-dalay]*0.4+signal_out[i-dalay*2]*0.2
        elif i>=dalay*3:
            signal_out[i]+=signal_out[i-dalay]*0.4+signal_out[i-dalay*2]*0.2+signal_out[i-dalay*3]*0.05
    return(signal_out)
```

Fig. 8. Modeling the "echo" effect in Python

Also, one of the important types of effects is various signal distortions, such as the “distortion” effect. The name itself does not carry any limitation, and in the vast majority of cases, distortion refers to the distortion of the sound waveform. Therefore, there are many types of implementation of this effect. In this paper, an algorithm of the effect is presented, the essence of which is to cut off any signals above a certain amplitude. And in place of this signal, the noise of the amplitude close to the amplitude of the cut is modeled

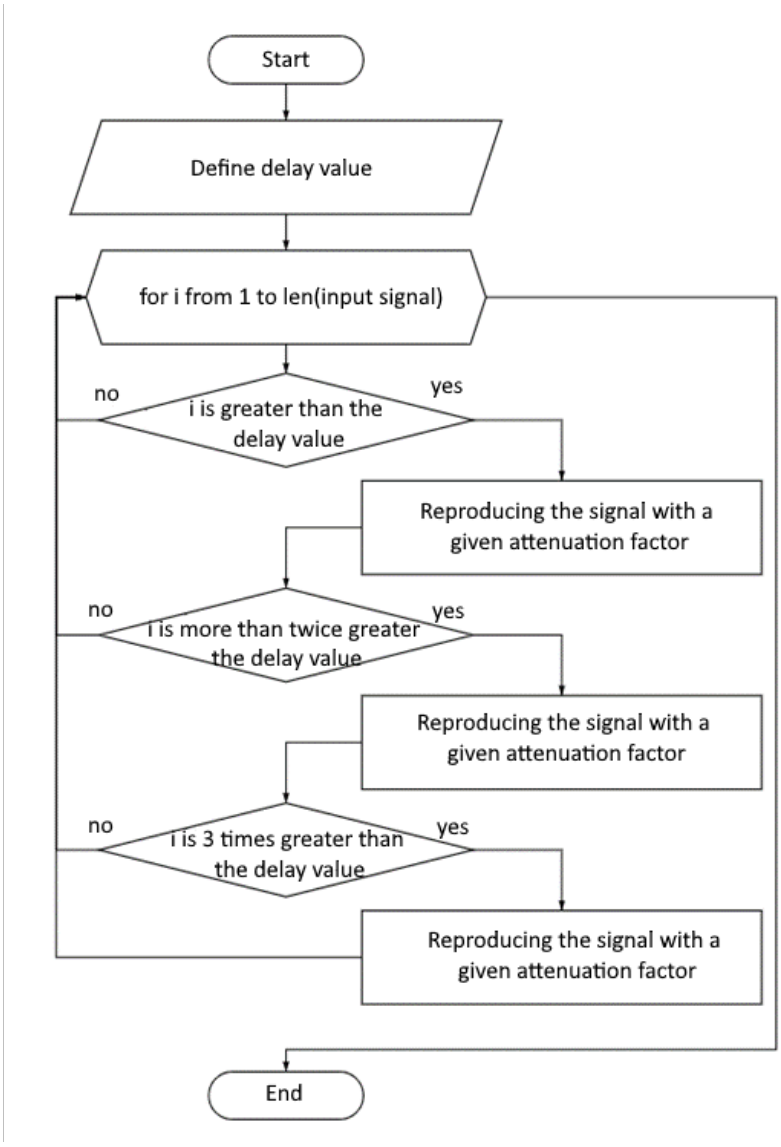

Fig. 9. Block diagram of the program for implementing the "echo" effect

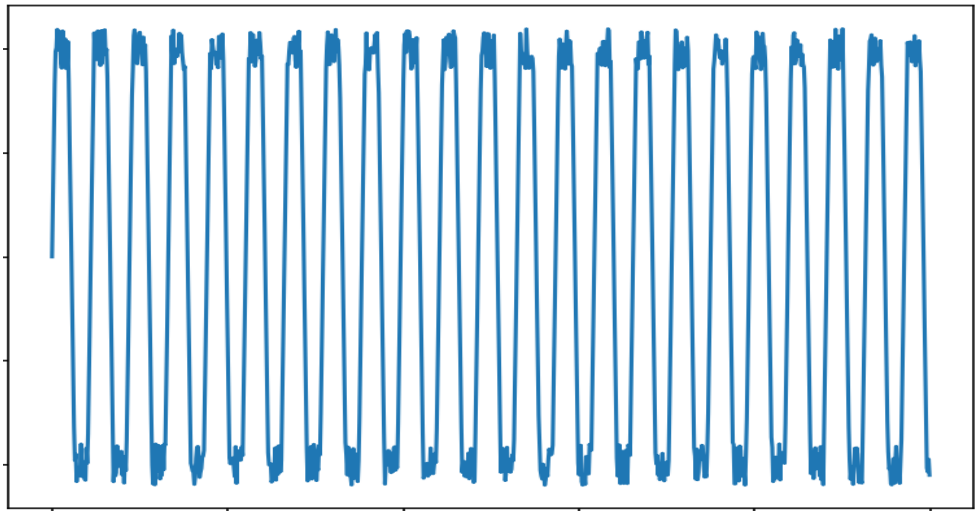

Fig. 10. Graphical result of the "distortion" effect

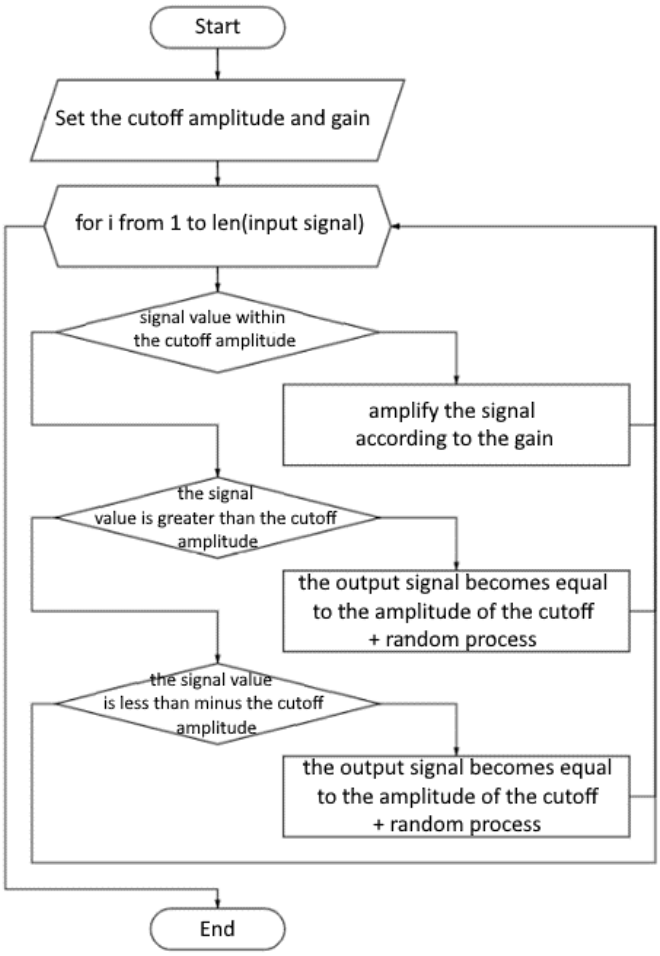

Fig. 11. Block diagram of the program for implementing the effect of "distortion"

```
#Distortion
def distortion(signal_in):
    Amp=0.5
    up=1/amp
    for i in range (s_len):
        if signal_in[i]<=Amp and signal_in[i]>=-Amp:
            signal_out[i] = signal_in[i]*up
        elif signal_in[i]>Amp:
            signal_out[i] = Amp*up
        elif signal_in[i]<-Amp:
            signal_out[i] = -Amp*up
    return(signal_out)
```

Fig. 12. Modeling the effect of "distortion" in Python

Conclusions

Implementing these algorithms in a language like Python has several advantages. First, because of the breadth of a given programming language, there are always ways for a given implementation to improve and personalize. Secondly, Python is an easily implemented language, with the help of which these algorithms can not only be implemented and analyzed but also translated to other devices. What makes algorithms universal? And thirdly, the popularity of the Python language makes the perception of both algorithms and implementation accessible to a wide range of people.

References

1. Vologdin E.I. Methods and algorithms for processing audio signals. St. Petersburg: KORONA, 2012. 96 p.

2. Lutz M. Python Programming, Volume I, 4th Edition. – Per. from English. – St. Petersburg: Symbol-Plus, 2011. – 992 p., ill.

AUTOMATION OF THE QUALITY CONTROL SYSTEM IN THE PRODUCTION OF PAINT AND VARNISH PRODUCTS

Puzyreva Victoria
student

Saint Petersburg State University of Aerospace Instrumentation,
Saint Petersburg, Russia
vikap1999@mail.ru

Abstract. *The article discusses potential directions for improving and automating the method for analyzing the size distribution of particles of fine grinding. The process algorithm is being developed. Opportunities for improvement are offered.*
Keywords: *laser diffraction, improvement of the method, paint and varnish products, fine particles*

The chemical industry, and in particular the paint and varnish industry, is rapidly developing both throughout the world and in Russia and in St. Petersburg in particular. Most of the paint and varnish products are made on the basis of finely ground powders, which are subject to ever higher quality requirements every year. [1]

GOST 2093-82 prescribes the use of sieve analysis to study the particle size distribution. However, the laser diffraction method has the largest measurement range, which, based on the intensity of the projected beams, is able to infer the size of the particles.

Hypothesis 1. An in-depth analysis of particle size and shape distribution is meaningless

The analysis of particle size and shape is important for quality control, which allows you to maintain and document the characteristics of the particles. An abnormal size or shape can, in the worst case, mean that the final product is unusable and the subsequent manufacturing process may fail (Fig. 1).

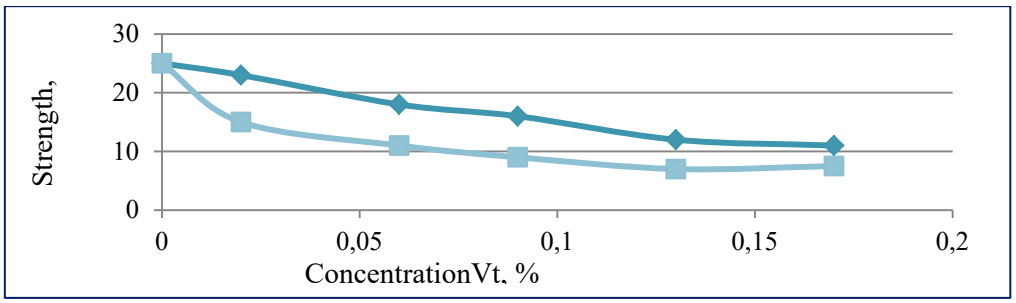

Fig. 1. Dependence of the strength of composites on the content of particles at different sizes, where the upper graph corresponds to particle sizes of 40–60 μm, and the lower graph corresponds to 100–160 μm [2;4]

Thus, detailed information about the shape and size of the particles is necessary, so hypothesis 1 is rejected.

Hypothesis 2. There is no technology that can measure both relatively small and relatively large particles

Of course, all analysis methods have limitations, including the analyzed range (Fig. 2). The laser diffraction method has the largest range.

RBS LLC conducted its own study of particle size distribution. The powder pigment was ground using proprietary technology at Netzsch Premier Technologie's (Exton, USA) to an ideal consistency. The size distribution is shown in Table 1.

Thus, the smallest average size was 1.16 μm, and the largest was 95.6 μm. Most industrial powder paints have a particle size of 10 to 100 microns. For the electrostatic powder spraying method, powder particles with sizes from 15 to 75 μm are acceptable, and ideal particles are from 25 to 45 μm. Thus, the laser diffraction method has great potential, and hypothesis No. 2 is refuted.

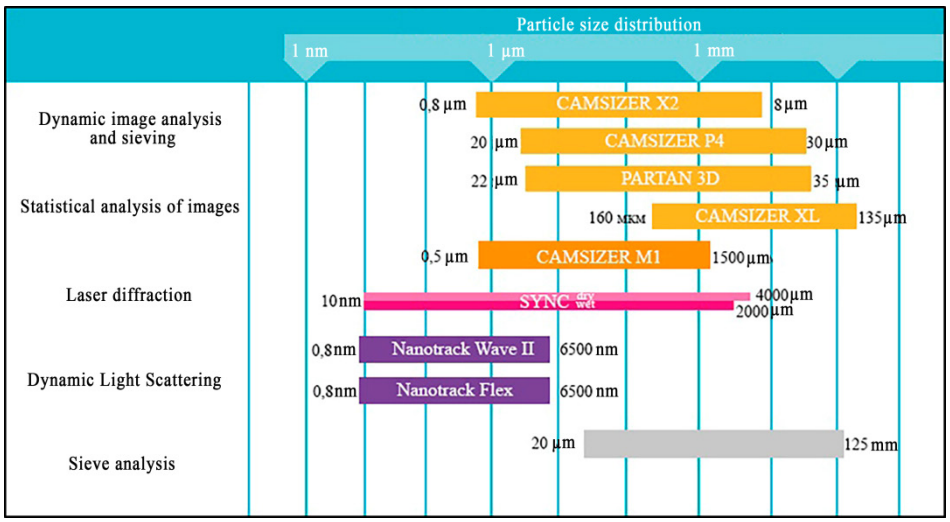

Fig. 2. Methods for analyzing the distribution of particle sizes and shapes

Table 1

Pigment results on LA-960 at various grinding times [2]

Grinding time, min	Geometric mean, µm	Average size, microns	Average size in comparison with the average value, %
0 (start)	30,9	95,6	10
30	1,01	1,48	85
60	0,895	1,23	92,5
90	0,812	1,16	99,5

Hypothesis 3. Existing methods cannot be combined

By enumeration, the most compatible pair of methods was determined: microscopic and laser diffraction. It was proved that the measurement of parameters by the microscopic method (Fig. 3 b) and the laser diffraction method (Fig. 3 a) coincide by 60%. At the same time, the microscopic method gives an idea of the shape of the particles.

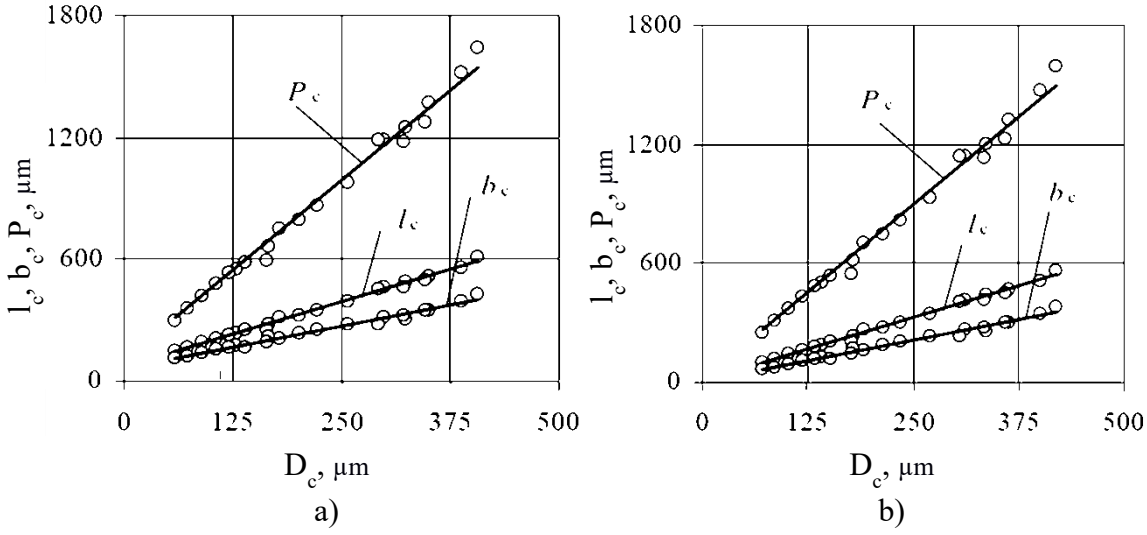

Fig. 3. Dependence between the average geometrical parameters of the grains of the fractions by the laser diffraction method (a) and the microscopic method (b) [3]

Thus, hypothesis No. 3 is rejected: the methods can be combined, but only if it is really expedient.

Developing a way to automate a method

The algorithm of the new automated analysis of the size distribution of fine particles is shown in Fig. 4.

Consider step 3, which involves reading and analyzing particles for size and shape. It is proposed to improve the existing installation by supplementing the measuring cell with an ultra-high-speed digital camera.

A schematic representation of the installation is shown in Fig. 5-6.

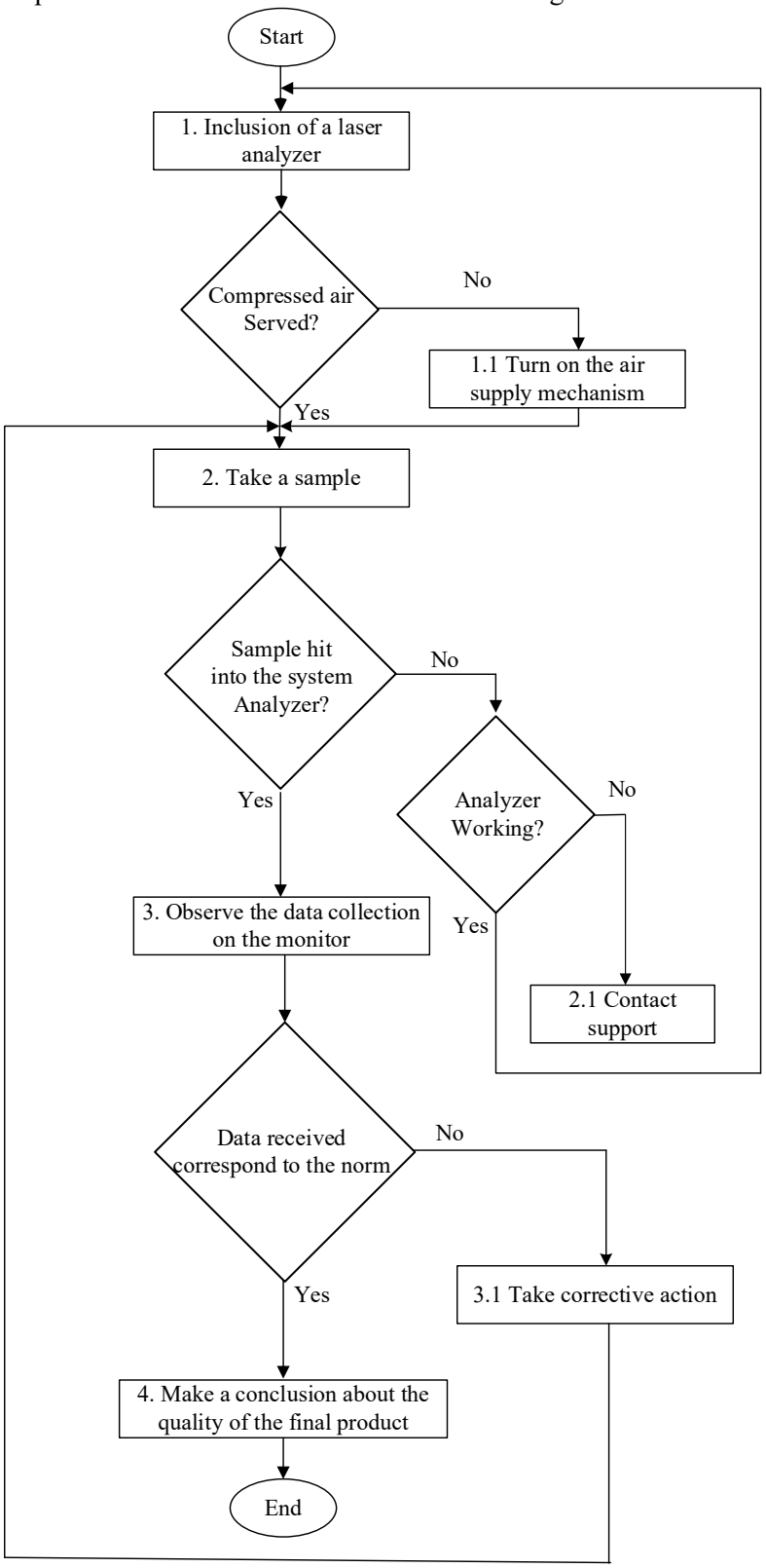

Fig. 4. Algorithm of the analysis process

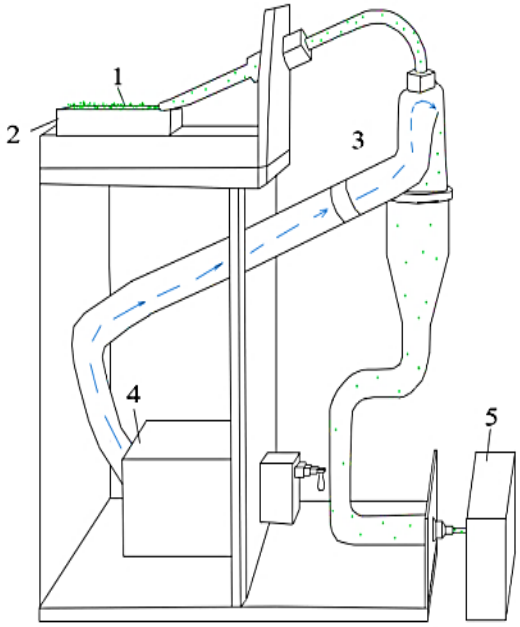

Fig. 5. Schematic representation of the developed laser analyzer

Sample 1 to be tested is placed on tray 2 and sucked into the analyzer system. The sample delivery system 3 directs compressed air 4 through the built-in nozzles, providing "braking" of the material particles before being fed into the measuring cell 5.

The internal schematic representation of the measuring cell is shown in Fig. 6.

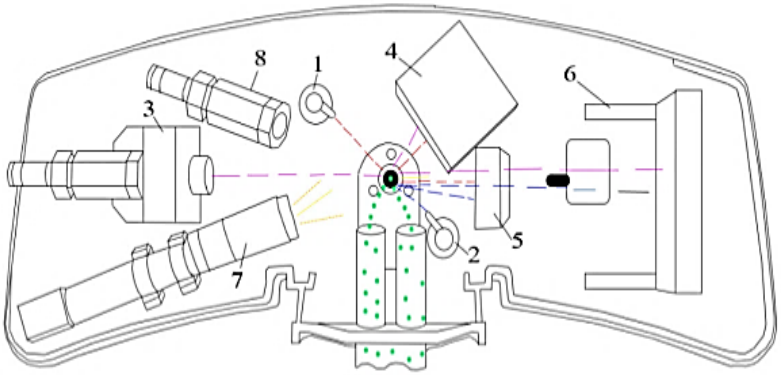

Fig. 6. Schematic representation of the optical system of the developed laser analyzer

Laser diodes and image analysis systems are used for measurement. The optical system consists of three diode lasers 1,2,3, three always-on detectors 4,5,6 located at fixed points. Laser detectors pick up light scattered at an angle of 165o. At the same time, a separate LED light source 7 illuminates the sample cuvette, while a high-speed digital camera 8 captures the image of the particles. The data are analyzed using special software using a functional empirical model (1):

$$\hat{y} = 100,28 - 6,87X_1 - 4,89X_3 - 7,48X_1X_2 - 7,29X_1X_3 - 7,03X_2X_3, \quad (1)$$

where X_1,X_2,X_3 – these are the factors affecting the particle. [6]

Thus, the consumer receives accurate data on the characteristics and parameters of the particles. The system analyzes not only the size, but also provides an image of the studied particles.

CONCLUSION

In order to solve the problem of having a particle shape analyzer, it was decided to develop a system that would “slow down” the particles during the analysis process so that their shape could be captured on the camera.

Thus, the system manages to analyze these particles in a short time and capture the shape, while the consumer receives accurate information about the characteristics and parameters of the particles without direct human participation. Such a detailed analysis improves the quality of paint and varnish products, reducing the human factor, which significantly increases their competitiveness in the market.

References

[1] Пузырева В.С. Анализ лакокрасочной промышленности в мире, России, регионе. Пенза: 2021. №7. С. 13-16.

[2] Салви, П. Измельчение и диспергирование. [Электронный ресурс]. – 2021. – URL: https://www.netzsch-grinding.com/ru (12.09.2022)

[3] Пузырева В.С. Анализ рискованности проекта. Пенза: 2022. №9. С. 10-12.

[4] Пузырева В.С. Построение функциональной эмпирической модели распределения по размерам частиц тонкого помола. Пенза: 2022. №9. С. 10-14.

IMPROVING THE EFFICIE NCY OF RANDOM MULTIPLE ACCESS ALGORITHMS USING PREAMBLE-BASED EXPLORATION

Rachugin Roman
Saint Petersburg State University of Aerospace Instrumentation,
Saint Petersburg, Russia
E-mail: rro1699@gmail.com

Abstract. *We present a description of the multichannel ALOHA algorithm using orthogonal preambles. We focus on theoretical throughput analysis. We also present the results of simulation modeling of the dependence of throughput on the input arrival rate, the dependence of the number of lost messages on the total number per frame, and the dependence of throughput on the number of channels.*
Keywords*: multichannel ALOHA, maximum throughput, random multiple access, Internet of Things.*

INTRODUCTION

Currently, there is an active development of wireless communication technologies, caused by a large increase in the requirements for the number of operating devices and the amount of transmitted data. A prime example is the Internet of Things (IoT) technology. IoT devices are devices with infrequent activity, therefore, random access is considered for their interaction. As a rule, varieties of algorithms such as ALOHA [1] and its modifications are considered. he existing algorithms have restrictions on the limiting output arrival rate (throughput). There are various approaches to increase the throughput of algorithms. Thus, approaches based on the use of non-orthogonal multiple access (NOMA) [2] [3], sequential interference cancellation (SIC) [4] and orthogonal preambles are proposed. However, NOMA and SIC methods are computationally intensive. Therefore, in this article we will consider an approach using orthogonal preambles. The work [5] considers a system with independent channels and a multichannel ALOHA algorithm that uses orthogonal preambles to implement work with two phases. The exploration phase (EP) is the phase of evaluating possible collisions using preambles. Users then transmit messages in the Data Transmission Phase (DTP) based on the results of the EP. In this paper, we will take as a basis the model of such a system.

Description of the algorithm.

Let us introduce a system of assumptions for the system under consideration:

Assumption 1. The entire time of the channel operation is divided into frames of the same length. A frame consists of two phases: an exploration phase (EP) and a data transmission phase (DTP). Each phase is followed by a response from the base station (BS). Users know exactly the boundaries of the division into frames and phases and can transmit data only at the beginning of the corresponding phase at the beginning of a new frame.

Assumption 2. There is a set of K independent channels. All users have unique preambles. A preamble is a sequence of bits of a certain length, which is much less than the length of the message. The preamble transmission rate is the same. The BS can reliably determine the number of preambles on each channel.

Assumption 3. In each channel, during each phase of the frame, one of the following events can occur:

- Event “Success”. If the data was transmitted by one user.
- Event “Empty”. None of the users transmitted data.
- Event “Conflict”. Simultaneously, 2 or more users were transmitting data. If a conflict occurs during the EP, then the BS will successfully determine the number of preambles. If a conflict occurs during the DTP, then the users’ messages overlap and cannot be processed on the receiving side.

At the end of each phase, all users will reliably know what event happened in the channel.

Assumption 4. The system has M users. The system receives a Poisson input flow of intensity λ. The intensity of all users in the system is the same and is equal to λ/M. Each user has an unlimited buffer, in which new messages of the user are added

Assumption 5. The time of the data transmission phase will be taken as a unit of time, and the time of the exploration phase will be taken as 0.

According to *Assumption 1*, each frame consists of 2 phases: EP and DTP. In EP, users randomly select one of the K channels and send a preamble over it. The BS then estimates the number of preambles in each channel and broadcasts this information to all users. After that, users are divided into two groups. The first group (G_S) includes users in whose channels one preamble was transmitted. All other users fall into the second group (G_C). Channels selected by users in G_S are assigned to them, and all other channels belong to the second group.

Then comes DTP phase. G_S users transmit data with a probability of one. Users of the G_C decide whether to transmit data to them with a probability equal to $p_{dtp} = \min\left\{1, \frac{K - |G_S|}{|G_C|}\right\}$. Users of the G_C group who decide to transmit data randomly select one of the channels of the second group and transmit their data. The base station then informs all users about the events that have occurred in each channel via the feedback channel.

Theoretical analysis of throughput

Denote by U the number users who decide to transmit data from second group. Then the average number of messages without collisions for second group is calculated as:

$$\bar{N}_{dtp}(U, K - |G_S|) = U\left(1 - \frac{1}{K - |G_S|}\right)^{U-1}.$$

The average number of messages without collisions for system is calculated as:

$$\begin{aligned} &\bar{N}\left(U, K - |G_S|, |G_S|\right) = \bar{N}_{ep} + \bar{N}_{dtp} = \\ &= |G_S| + U\left(1 - \frac{1}{K - |G_S|}\right)^{U-1}. \end{aligned} \tag{1}$$

The values U and $|G_S|$ depends by K and M, then:

$$\begin{aligned} &\bar{N}\left(M, K\right) = \bar{N}_{ep}\left(M\right) + \\ &+ \bar{N}_{dtp}\left(U \mid M, K - |G_S|\right). \end{aligned} \tag{2}$$

For large values of M and K, the values of $K - |G_S|$ and $|G_C|$ will also be large, then:

(3)

Upper bound $\bar{N}_{dtp}$ is calculated as:

$$\bar{N}_{dtp}\left(K - |G_S|\right) = \left(K - |G_S|\right)e^{-1}. \tag{4}$$

Since $|G_S|$ depends by $\bar{N}_{ep}\left(M\right)$ then from (4) following:

$$\bar{N}_{dtp}\left(K - |G_S|\right) = \left(K - \bar{N}_{ep}\left(M\right)\right)e^{-1}. \tag{5}$$

Further, substituting (3) and (5) into (2), we obtain the maximum throughput:

$$\begin{aligned} &\bar{N}\left(K\right) = \bar{N}_{ep}\left(M\right) + \left(K - \bar{N}_{ep}\left(M\right)\right)e^{-1} = \\ &= Ke^{-1} + \bar{N}_{ep}\left(M\right)\left(1 - e^{-1}\right). \end{aligned}$$

For large values of M, $\bar{N}_{ep}\left(M\right) \approx Ke^{-1}$. Then the maximum throughput of the multi-channel ALOHA algorithm using orthogonal preambles and the exploration phase is:

$$\bar{N}(K) = Ke^{-1} + Ke^{-1}\left(1 - e^{-1}\right) = Ke^{-1}\left(2 - e^{-1}\right).$$

Also, we can calculate exact value throughput of the multi-channel ALOHA algorithm using orthogonal preambles and the exploration phase for 1 channel as:

$$\bar{N}(1) = \lambda e^{-1} + \sum_{i=2}^{\infty}\left(1 - \frac{1}{i}\right)^{i-1}\frac{\lambda^i}{i!}e^{-\lambda}. \quad (6)$$

Results of simulation and theoretical analysis

As a result of modeling, the throughput per channel for the multi-channel ALOHA algorithm using orthogonal preambles is similar to the calculated values obtained by formula (6). The throughput per channel for the multi-channel ALOHA algorithm coincides with the calculated values obtained by $\lambda e^{-\lambda}$ (Fig. 1).

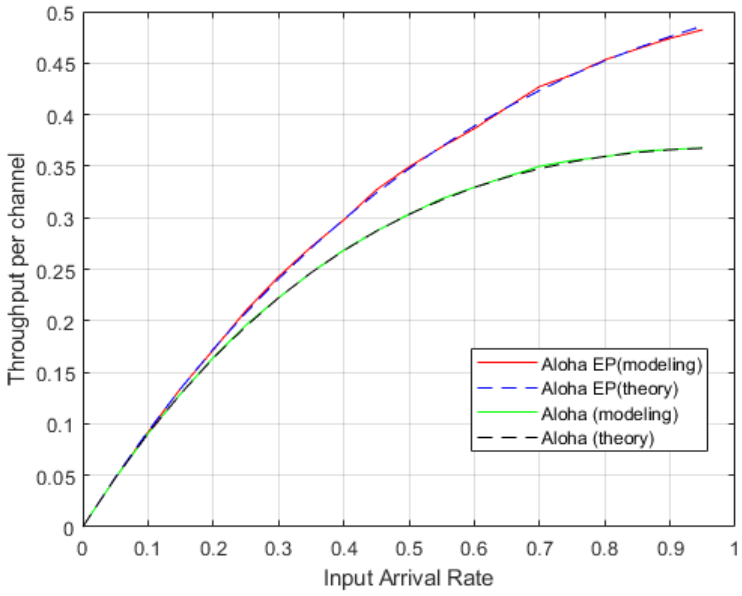

Fig.1. The dependence of throughput on the input arrival rate.

In addition, the results of the ratio of the number of lost messages to the total number of incoming messages in the frame (Fig. 2).

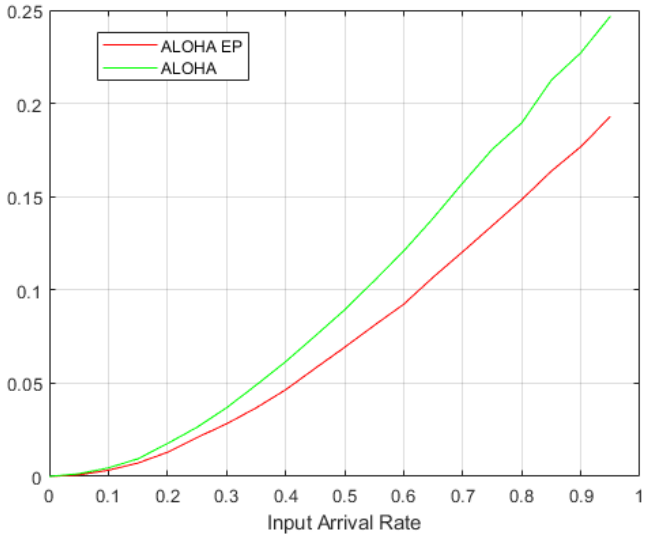

Fig.2. The dependence number of lost messages to the total number of incoming messages.

With the help of simulation modeling, it is proved that with an increase in the number of channels, the throughput per channel for the multi-channel ALOHA algorithm using orthogonal preambles reaches a value of 0.6 (Fig. 3).

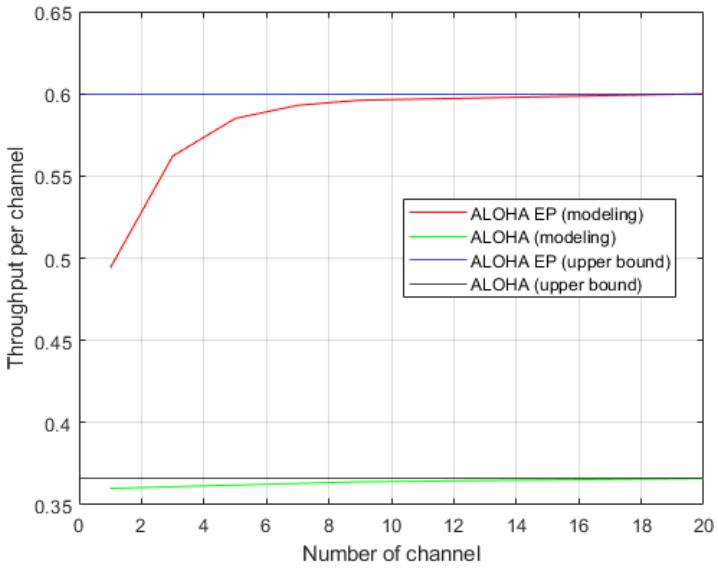

Fig. 3. The dependence of throughput on the number of channels.

CONCLUSION

The paper describes the multi-channel ALOHA algorithm using orthogonal preambles. The principle of operation of this algorithm is presented. A theoretical analysis of the throughput for the presented algorithm has been made. The results of simulation modeling and theoretical calculation of throughput, the number of lost messages and the dependence of throughput on the number of channels are presented.

REFERENCES

[1] N. Abramson, “THE ALOHA SYSTEM: Another alternative for computer communications,” Fall Joint Computer Conference, pp. 281–285, ACM, 1970.

[2] J. Choi, “NOMA-based random access with multichannel ALOHA,” IEEE J. Selected Areas in Communications, vol. 35, pp. 2736–2743, Dec 2017.

[3] Benjebbour A., Saito K., Li A, “Non-orthogonal multiple access (NOMA): Concept, performance evaluation and experimental trials,” 2015 International Conference on Wireless Networks and Mobile Communications (WINCOM), pp. 1– 6, January 14, 2015.

[4] E. Paolini, C. Stefanovic, G. Liva, and P. Popovski, “Coded random access: applying codes on graphs to design random access protocols,” IEEE Communications Magazine, vol. 53, pp. 144–150, June 2015.

[5] J. Choi, “On improving throughput of multichannel ALOHA using preamble-based exploration,” Journal of Communications and Networks, Volume: 22, Issue: 5, pp. 380-389, Oct. 2020.

ANALYSIS OF WAYS AND MEANS OF IMPLEMENTING THE SMART GRID SYSTEM IN COTTAGE AETTLEMENTS

Romanenko Vitaly
Saint Petersburg State University of Aerospace Instrumentation,
Saint Petersburg, Russia
E-mail: ***SBVitaly@yandex.ru***

Abstract. *The energy system of the world needs big changes. Today, with the growth of the population, there are problems such as lack of resources and climate change of the planet due to human activity. Also, technological progress does not stand still, and the informatization of cities is growing, capturing almost every sphere of human life. These aspects require constant uninterrupted power supply, the main spheres of human life, such as: global networks (Internet), electric transport, housing and communal services, etc.*

Most of Russia's power grids were built back in the 20th century, during the technological revolution of the 80s. Since then, no major improvements have been made to the operation of the systems, and as a result, the existing electrical equipment began to become obsolete, and the load on the network and the need for electricity continued to increase constantly.

Today our life directly depends on electrical energy. Such spheres as the banking system, communication networks, food industry, medicine and many others that have become necessary for the normal life of society depend on the continuity of electricity supply. In order for the power grid to be able to provide energy consumers at the proper level, new approaches are required for the generation and distribution of electricity between them.

The most relevant and real method is the construction of networks based on the concept of Smart Grid (Smart Grid). The idea of smart grids appeared in the 20th century and implied the decentralization of the network, the accumulation of energy and the use of alternative energy sources. But the effective application of this technology was not possible, because the construction of networks based on Smart Grid concepts implies the management, accounting and analysis of electric energy at all stages of distribution and consumption of electricity. Today, with the development of the Internet of Things (IoT), which forms the basis of Smart Grid energy systems, it becomes possible to organize constant monitoring of the transmission of energy from source to consumer. Accordingly, to implement such a network, powerful computing centers are needed that will process data on the quality of electricity, on consumption modes, on environmental climatic conditions, on emergency situations and on the technical condition of electrical installations.

The use of smart grid technologies makes it possible to create a discrete energy system that allows you to analyze energy leaks and identify defaulters, create a remote monitoring system that will increase the service life of equipment, reduce modernization costs and prevent system failures.

Since the technology of smart grids is only developing now, its implementation in large cities involves large labor costs and investments. Therefore, the most reasonable option for the development of this technology are small settlements, for example cottage settlements, in which testing of the Smart Grid network will give a large amount of data, which will eventually allow us to develop a certain strategy for the implementation of this technology in the entire energy system of the country.

Smart Grid Network Structure

The creation of a Smart Grid system is based on the construction of an electricity supply network with its own information system, which provides an uninterrupted information flow along with the energy flow. This synergy is achieved through the application of fundamental methods of building a smart network, such as: the use of smart sensors and sensors and the introduction of a SCADA system. A not unimportant part of the smart grid is the presence of small generation and a decentralized energy transmission system.

Structure of the data processing information system

For a smart network on a city scale, the data transmission system must have a distributed information processing structure due to the number of consumers and the complexity of the network. Such a

structure implies the interaction of governing bodies in the same network, but physically located in different places (Fig. 1). Such a system increases the stability of the entire network. But the system of cottage settlements is a small part of the country's power grid. According to the analysis "Suburban real estate market in 2007: analysis, trends, prospects", the average number of houses in a cottage village is 69 pcs. Adhering to this figure, it can be concluded that for greater efficiency and reasonableness in terms of resource use, it is most rational to use 1 computing center without creating a complex distributed data processing structure. The computing center of the cottage settlement will be part of the information system of the country's electricity supply network and must be connected to it.

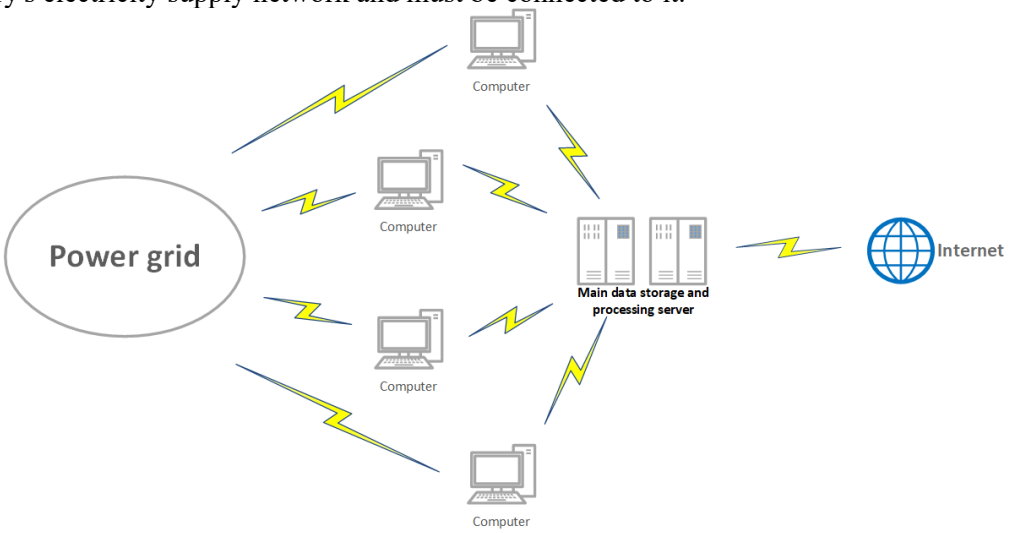

Fig. 1. Distributed data processing system of the SmartGrid urban system

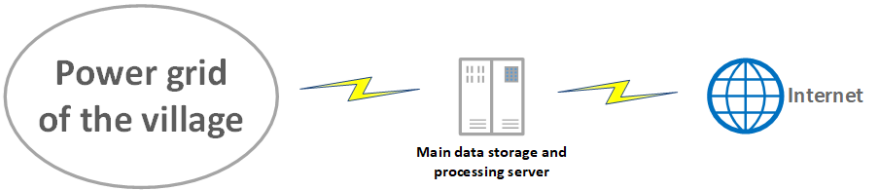

Fig. 2. Cottage settlement data processing system

The data transmission network for smart power supply networks should have the following key features:

- the traffic flow must have a periodic character;
- communication model: two-way, limited peer-to-peer network;
- protocol stack: proprietary, heterogeneous, IPv6;
- switches must have a communication interface no worse than IEEE 802.3 in terms of the 100BASE-FX 802.3 interface in terms of the 100BASE-FX interface, and communication interfaces that meet the requirements of no worse than IEEE 802.3 in terms of the 1000BASE-LX interface;
- The guaranteed time of message/stream delivery, including reception and transmission, between network switches should not exceed 0.025 ms (with a maximum message/stream length of 1536 bytes).

Methods, methods and means of building an information system of the power supply network are presented in the standard of the organization "Standard technical requirements for the organization and performance of technological LAN in the automated control system of the PS ENES" [2].

Software

The smart grid is managed through special programs that provide various opportunities to employees of energy companies. Many companies such as Schneider Electric, Nvidia, Intel, ENERGORESURS JSC, RTSoft, etc. are engaged in the development of such software today. The SCADA control system is used for monitoring, analysis and management of the system. The software is based on the use of the principles of Big Data, digital twins, remote control of equipment.

Intelligent information and control systems that ensure an increase in the economic efficiency of energy supply through coordinated management of distributed energy resources. Due to the software, a wide range of optimization tasks are solved in automatic and/or automated control mode, including:

- reduction of the cost of purchased electricity;
- ensuring the reliability of power supply;
- capacity management of overloaded power transmission lines and power centers;
- optimization of the use of distributed energy resources in autonomous power systems.

Information security of the network

The energy network is a strategic object of the country. Therefore, the Smart Grid system must have a high level of information security to prevent unauthorized interference in the processes occurring inside the system. As a result of cyberattacks, violators can obtain personal data of customers, affect the process of energy transmission and undermine the uninterrupted supply of important facilities. Some of the measures necessary to improve the security of the information system are listed below [3].

Protection in the field of management:

1. Non-disclosure agreements, employment contracts, contracts with clients must contain clauses that clearly indicate personal security responsibilities. Each user should familiarize himself with the requirements imposed on him and sign in the appropriate journal that he is familiar with them

2. All Smart Grid employees (managers, SCADA administrators, Smart Grid administrators) must undergo mandatory trainings and be regularly notified of all changes in security policies and procedures related to their duties.

Application and database protection:

1. Use input data filtering in the customer information system/SCADA system/payment system

2. Use the firewall of web applications for the website of the customer information system.

Network protection:

1. Use encryption when generating and transmitting packets

2. Use a firewall for the servers of the customer information system/SCADA system

Protection of employees' mobile devices:

1. Use the Google Apps Device Information Security Policy

2. Develop a corporate policy for the write-off of mobile devices

More detailed models of information threats are compiled on the basis of federal laws on information protection [3,4,5,6].

Sensors and sensors

Sensors and sensors are the "sense organs" of the smart grid system. Due to the development of metrological equipment to the digital level, it became possible to make the power supply network controlled. Measuring devices in the energy sector are divided into:

- electricity metering devices;
- smart measuring devices of network parameters;
- relay protection and automation (RZA);

1) Electricity metering devices

An electric power meter (smart meter) is an electric meter that measures the consumed active and reactive power and transmits information through a specified communication channel to a data processing server. Has two-way communication, server-client and/or client-server. These devices have the ability to transmit data via various communication channels such as bluetoth, 4G LTE, GPRS, radio communication. This device allows you to more accurately record electricity consumption, which will allow you to create differentiated tariffs and, consequently, more favorable price incentives for home consumers (intelligent market). Thanks to the use of smart meters in the system, daily load schedules will be built up to the minute, which will make energy consumption more profitable without overloading the network.

2) Smart electrical appliances

Smart electrical appliances are divided into two types:

- measuring devices installed at distribution points (RU) and transformer substations (TP) for monitoring network parameters;
- relay protection and automation for remote control of devices at distribution points (RU) and transformer substations (TP)

Digital measuring instruments are no longer new, in the IEC 61850 standard "Networks and communication systems at substations" there is a separate protocol for transmitting the measured current and voltage, IEC 61850-9-2 SV (Sampled Values). According to this protocol , the following electrical devices interact with each other:

- devices for converting analog quantities into SV streams. These include current transformers (TT), voltage transformers (TN), PASS for KIV and PASS in the CRU input cell for differential transformer protection or low voltage bushing;
- devices for processing the received values of SV flows and calculating the effective values of currents, voltage, power, frequency, etc. These include relay protection and automation terminals (RPA), measuring converters of instantaneous values into effective values, electric energy meters, etc.

The management of the substation's REA is implemented using digital terminals that perform the following functions:

– conversion of signals from sensors, control of relay protection and automation;
– interaction with the main server of the system in order to exchange information;
– execution of commands coming from control rooms.

The block diagram of the Smart Grid system is shown in Fig. 3.

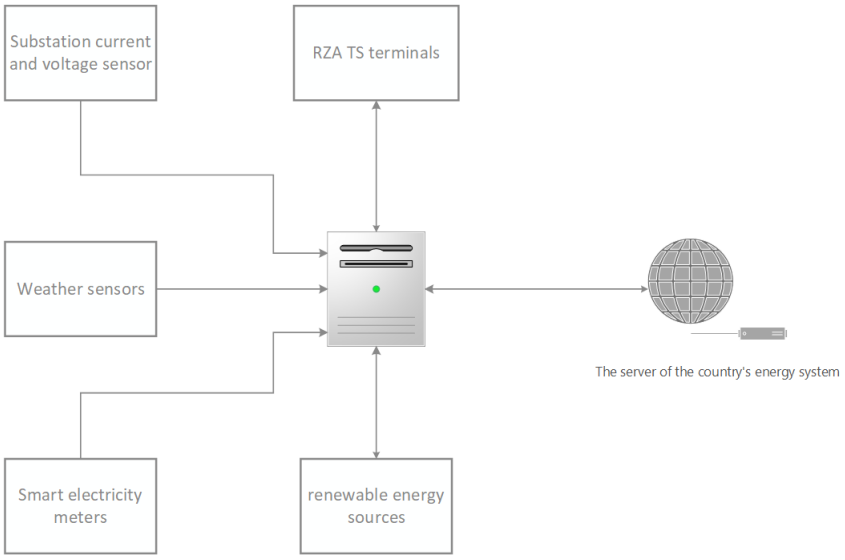

Fig. 3. Block diagram of the Smart Grid system

Microgeneration

Since Smart Grid technologies are designed to increase the efficiency of the energy system, microgeneration plays an important role.

Microgeneration based on renewable energy sources (RES) is the generation of electricity from alternative energy sources. The introduction of RES into the "smart grid" will reduce the load on the country's energy system, which will increase its overall stability, reduce the number of emergencies and reduce the need to build new traditional energy sources that differ from RES at a higher cost.

The use of the type of renewable energy strongly depends on the geographical location and weather conditions. The efficiency of renewable energy sources in each region is calculated separately on the basis of reports on the meteorological situation of the region, on the basis of which a conclusion is made in the profitability of the construction of stations with alternative energy sources.

Efficiency of implementation of Smart Grid technology

Based on the collected data on the results of tests of Smart Grid systems both in Russia and in other countries, it is concluded that the combined effect of technological effects on balance conditions leads to their mutual strengthening (synergy). As a result of changes in the demand for electricity and installed capacity of power plants are more than calculated as a simple sum of effects. Estimates made for the initial balance conditions of the basic option Reduction of the required installed capacity, GW 0 10 20 30 40 2020 2025 2030 Reduction of the maximum load of consumers in demand management Reduction of the reserve in generation, taking into account the increase in reliability by means of the AAS power

plant and reduction of the maximum load 34 24 7 Reduction of electricity demand, billion kWh 0 50 100 150 2020 2025 2030 Reduction of final electricity consumption in demand management Reduction of losses in networks, taking into account new technologies, loss management and reduction of final electricity consumption 93 140 23 32 of the General Layout of electric power facilities, show that the implementation by 2030 The main measures to create intelligent energy in Russia will reduce the need for installed capacity by more than 10% (by 34 GW) and electricity consumption by almost 9% (140 billion kWh). At the same time, the relative level of losses in networks will consistently decrease by 30% – from 12 to 10% in 2020 and up to 8% in 2030 [8].

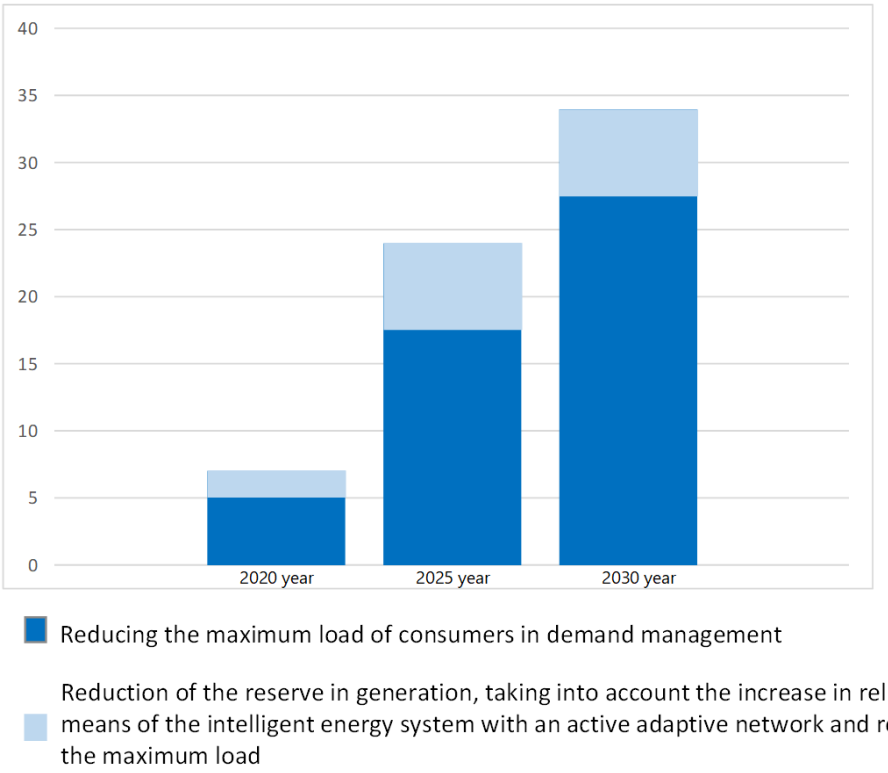

Fig. 4. Diagram of reduction of the required installed capacity, GW

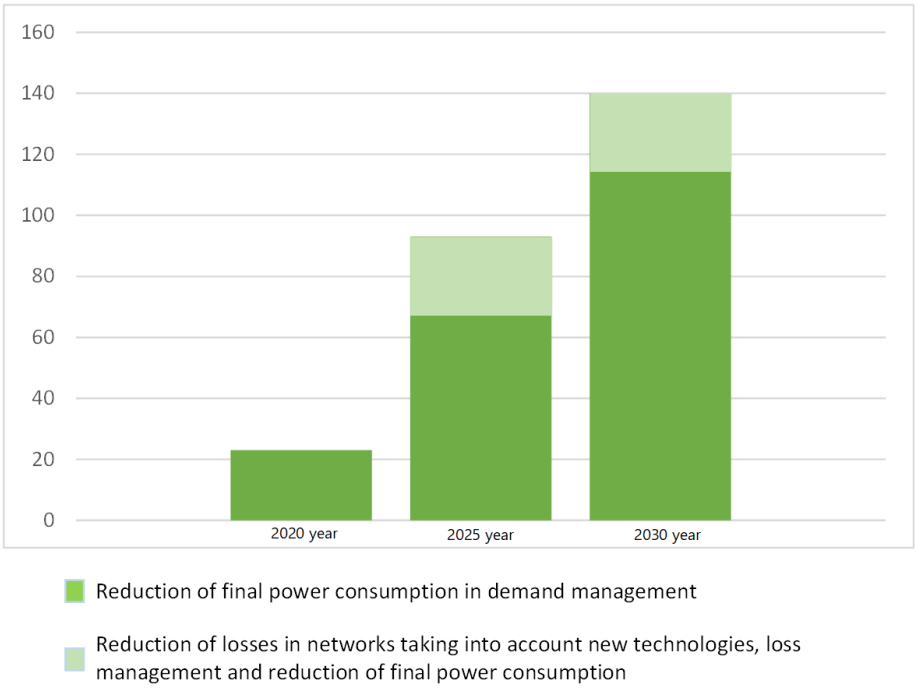

*Fig. 5. Diagram of reduction in electricity demand, billion*kWh*

Conclusion

The creation of a Smart Grid system in cottage settlements is a promising direction for energy, since with the use of new technology, a village can exist as an autonomous unit, generating energy through microgeneration using renewable energy sources, and a source of additional power given to the grid to improve the efficiency of the country's electricity grid as a whole. The smart grid system requires no small investments to create two-way power transmission lines, data processing servers, and the construction of digital substations, but also this system has a noticeable payback due to the sale of electricity to the network and an increase in the period of trouble-free operation of the network. The creation of a Smart Grid in cottage settlements will reduce costs aimed at increasing the capacity of the country's power grid. In the long term, the creation of such systems is a profitable investment. Quite an important factor is that the Smart Grid system using renewable energy sources allows you to reduce carbon emissions, reduce the use of non-renewable energy sources and, as a consequence, reduce the human impact on the environment.

References

1. "Cybersecurity in intelligent networks: an overview and problems. Computer Networks" Wenye Wang, Zhuo Lu , ying, 2013

2. STO 56947007-29.240.10.302-2020 "Standard technical requirements for the organization and performance of technological LAN in the automated control system of the PS ENES" – https://www.fsk-ees.ru/upload/docs/STO_56947007-29.240.10.302-2020.pdf

3. I.N. Pashchenko V.I. Vasiliev, M.B. Guzairov "Information protection in networks based on intelligent technologies: designing a rule base"

4. Federal Law No. 149-FZ of July 27, 2006 "On Information, Information Technologies and Information Protection"

5. Requirements for the protection of personal data during their processing in personal data information systems approved by Decree of the Government of the Russian Federation No. 1119 of November 1, 2012

6. Requirements for the protection of information that does not constitute a state secret contained in state information systems (approved by Order of the FSTEC of Russia No. 17 of February 11, 2013)

7. The composition and content of organizational and technical measures to ensure the security of personal data during their processing in personal data information systems (approved by the Order of the FSTEC of Russia No. 21 dated February 18, 2013)

8. "The main provisions of the concept of an intelligent power system with an active adaptive network" developed in 2011 by order of JSC FGC UES of JSC STC of Electric Power Industry.

CONSTRUCTION OF A PHYSICALLY RELEVANT MODEL OF BEHAVIOR OF COMPOSITE MATERIALS

Rassykhaeva Maria
Saint Petersburg State University of Aerospace Instrumentation
E-mail: mitschiru@gmail. com

Abstract. *In the context of constantly ongoing work on the creation of new structural materials, the task of developing ideas about the mechanisms of formation of mechanical and, in particular, strength properties of such materials remains relevant. Given that most promising materials are composites, of particular importance is the study of the influence of the reinforcement structure of these materials on the formation of their mechanical properties. The presence of the structure formed by the reinforcement elements of the composite leads, among other things, to the appearance of multiple stress concentrators in the volume of the material, in the area of action of which localized processes of damage accumulation can actively develop, ultimately leading to the appearance of macrocracks and the destruction of the material. The conditions for the development of these processes can be significantly influenced by the mechanical characteristics and configuration of the interphase layers formed along the contact boundaries of the reinforcing elements and the composite matrix. It is also interesting to study the influence of the random nature of the placement of reinforcing elements in the volume of real composite materials on the mechanisms of formation of their mechanical properties.*

A composite is an inhomogeneous (heterogeneous) material consisting of two or more mutually insoluble components (phases). According to this definition, composites include dispersion-strengthened alloys, concretes, coated metals, etc. Polycrystalline bodies consisting of one substance can also be attributed to this class of materials, considering granules with different orientations as different phases. Finally, this can include homogeneous materials with voids (the latter can be interpreted as inclusions with an elastic modulus equal to zero).

Composites reinforced with such elements, in which all sizes are quantities of the same order, are called granular. The materials that can be classified as granular composites are very diverse in nature. Composites reinforced with such elements, the two dimensions of which are much larger than the third, are called flat-textured. And, finally, we note the fibrous composites that are most common in modern power structures. They consist of a comparatively pliable matrix reinforced with high-strength fibers with high values of modulus of elasticity E and tensile strength σ in . There are two main types here: composites with continuous fibers and composites with short (torn) fibers. In turn, in the first of these types, long fibers can either be arranged strictly parallel to each other, or woven into a fabric impregnated with a polymer binder. However, textile processing significantly reduces the strength and rigidity of the material.

The mechanics of composite materials is one of the main sections of modern mechanics of deformable solids. The subject of the mechanics of composites is, firstly, the development of models and methods for predicting the properties of the composite by the known properties of its components in order to design the best composite for the task, secondly, the study of the processes of deformation and destruction of products made of composite materials and the development of methods for calculating and optimal design of such products. These two directions of mechanics of composites are closely related to each other, especially since, as a rule, a composite material is designed and created simultaneously with the product. A significant place in the mechanics of composites belongs to technological problems. Unlike the properties of traditional materials, the technology of which is well developed and stable, the properties of composites are quite sensitive to small changes in the technological regime, and the technological techniques themselves are very diverse. In principle, the design of the material, product and technological process should constitute a single whole.

A distinctive feature of composites is the heterogeneity of their structure. As a result, the physical and mechanical properties of composites depend not only on the properties of the components, but also on the structure of the filling, namely, geometry, laying density and volume content of reinforcing elements. The presence of a random structure and its role in the formation of the effective properties of the composite determine the practical significance of the development of methods for modeling the mechanical behavior of such materials.

At the micro level, elementary volumes of material belonging entirely to one of the components of the composite are considered. As the characteristic size of such volumes, the size L1 is chosen, the value of which is less than the characteristic dimensions of the structural components of the composite Fig. 1.

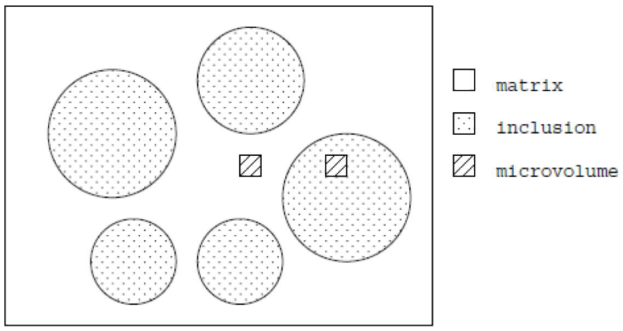

Fig. 1. Structure of composite material modeling

In accordance with this, three levels of manifestation of the properties of the composite are considered: the level of composite components (microlevel), the level of the reinforcement structure (mesou level) and the level of effective properties (macro level). Each level is assigned to the volumes of the composite, which have the dimensions characteristic of this level. As a unit of measurement of the dimensions of each of the levels, a certain value Li (i = 1,2,3) is taken, which characterizes the typical linear size of the elements of the reinforcement structure of the L0 composite (for example, the diameter of the reinforcing elements, the average thickness of the layers of the matrix material, etc.) Fig. 2.

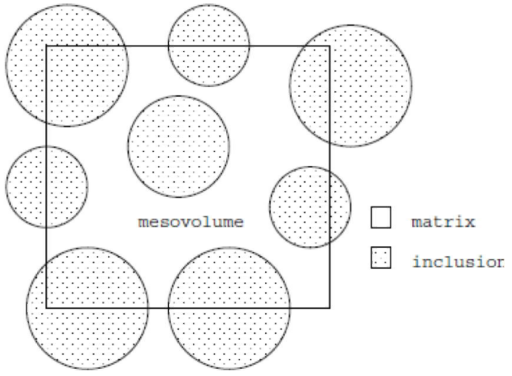

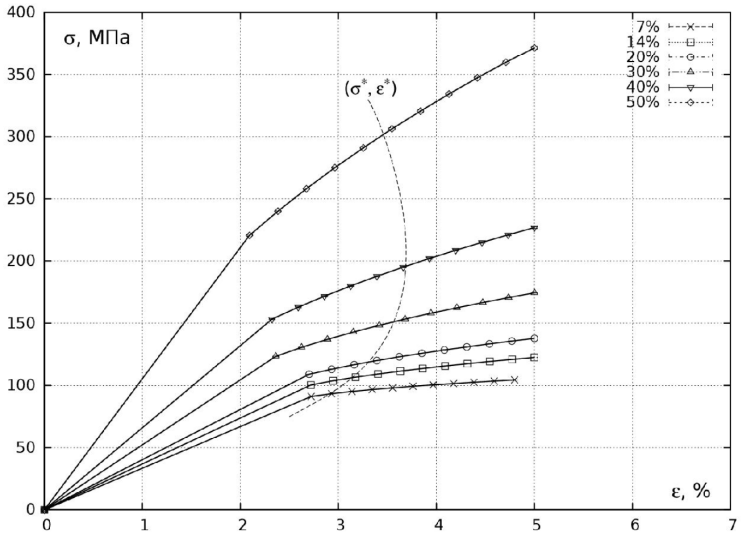

Fig. 2. Composite Material Load Modeling to Automate Assessment

In composite materials, an important role is given to the matrix, which ensures the monolithic nature of the composite, fixes the shape of the product and the mutual arrangement of reinforcing fibers, distributes the acting stresses over the volume of the material, ensuring a uniform load on the fiber and its redistribution during the destruction of part of the fibers.

The requirements for matrix materials can also be divided into operational and technological.

The first include requirements related to the mechanical and physicochemical properties of the matrix material, which ensure the performance of the composition under the action of various operational factors.

The mechanical properties of the matrix should ensure the effective joint operation of the fibers under different types of loads.

It is believed that for such a microvolume the provisions of continuum mechanics are valid, i.e. the hypotheses of continuity and homogeneity are fulfilled. The mechanical properties of such volumes are assumed to coincide with the properties of the components. When describing the state of each of the microvolumes at the microscale level, the usual relations of the theory of small elastic deformations are assumed to be valid. The system of equations describing the behavior of a microvolume of material includes a system of equilibrium equations.

Examples of equipment printing polymers Fig. 3.

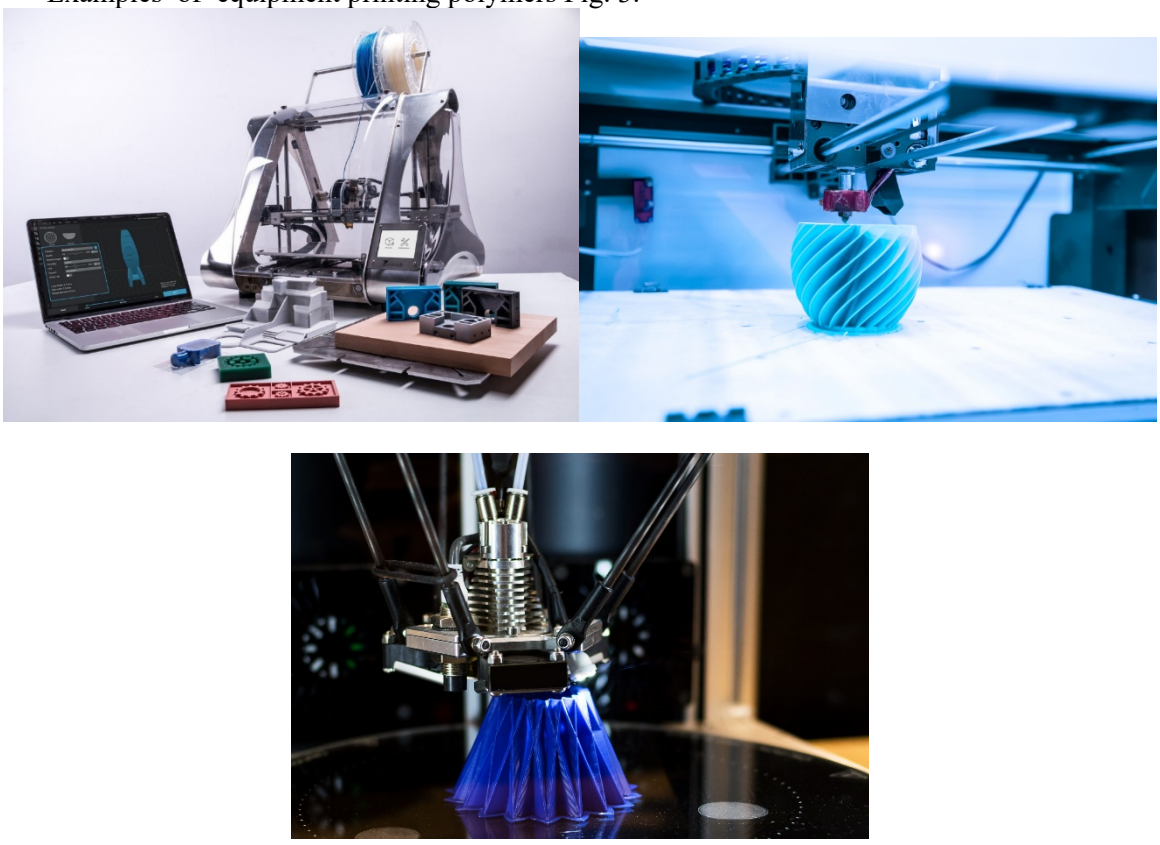

Fig. 3. Additive installations

Direct calculation of the field of parameters of the tense-deformed state of the entire model structure is a complex computational task. The complexity of the reinforcement structure makes it impossible to obtain an accurate analytical solution. The study by numerical methods requires a high degree of sampling, which leads to a large number of equations, the solution of which requires large computational resources, and, as a result, can lead to an uncontrolled increase in the error of calculations.

Conclusion

Interest in these materials is due to the fact that their inherent complex of properties and features significantly distinguishes them from traditional structural materials. This is primarily high strength and low density, as well as the ability to control the mechanical and physical characteristics when creating the material of the structure. The properties of composites depend primarily on the properties of the initial components: reinforcing elements and the matrix. In addition, their combination gives a synergistic effect

associated with the appearance of properties in the composition that are not characteristic of isolated initial components. Composites are distinguished by a wide range of useful, and in some respects unique properties, and their rational combination makes it possible to obtain effective structures with a high degree of weight perfection and a given anisotropy of the physical and mechanical characteristics of the material. The issue of implementing properties is associated with the management of the characteristics of composites in the process of manufacturing the structure by changing the orientation of the fibers and combining layers of different materials. This makes it possible to obtain materials with the necessary properties and characteristics. In principle, for each structure, a material can be developed that most fully corresponds to its purpose, field of operating loads and operating conditions. In this respect, composites are similar to natural materials, the rational combination of properties of which was formed in the process of long evolution. The directional nature of the properties of composites simultaneously means that, along with high performance in some directions, they have low characteristics in others. Therefore, making an arbitrarily bad design from an arbitrarily good composite is much easier than making it out of metal. However, the correct consideration of the features of composites makes it possible to obtain structures with a high degree of weight perfection, which is not achievable when using traditional materials.

References

1. Chabanenko A V, Kurlov A V 2021 Control the quality of polymers based on the model of Dzeno Journal of Physics: Conference Series

2. Chabanenko A V, Kurlov A V and Tour A C 2020 Model to improve the quality of additive production by forming competencies in training for high-tech industries *J. Phys.: Conf. Ser.* 1515 052065.

3. Chabanenko A V and Yastrebov A P 2018 Quality Assurance of Hull Elements of Radio-Electronic Equipment by Means of Control System *J. Phys.: Conf. Ser.* 1515 052065.

4. Chabanenko A V, Kurlov A V 2019 Construction of mathematical model of training and professional development of personnel support of additive production of REA IOP Conference Series: Materials Science and Engineering

5. Quality management of additive products / A. V. Chabanenko // RIA: Journal.: «Standards and quality». 2018. №2. S. 90-94.

6. Implementation of the PLM information system in the organization of Rassykhaeva M.D., Chabanenko A.V. In the collection: Selected scientific works of the twentieth International Scientific and Practical Conference "Quality Management". Moscow, 2021. S. 285-289.

7. Assessment of plasticity with combined hardening for the study of deformation processes of structural materials under various modes of low-cycle loads Chabanenko Alexander Valeryevich, Rassykhaeva Maria Dmitrievna Certificate of registration of the computer program 2021619545, 11.06.2021. Application No. 2021618914 dated 11.06.2021.

DEVELOPMENT OF A MATHEMATICAL MODEL FOR EVALUATION OF WORK PARAMETERS OF ADDITIVE PRODUCTION CELL

Shchukina Daria
Saint Petersburg State University of Aerospace Instrumentation
E- mail: shchukinadaria00@gmail.com

Abstract. *The paper presents a full-cycle management model for an additive manufacturing line based on a quadratic arrangement of printers, the complete exclusion of the human factor, and the use of video recording of deviation control in manufactured products. To assess the quality of the system, a model for estimating parameters based on a comprehensive assessment of individual parameters of the presented system has been developed.*
Keywords*: additive technologies, layer-by-layer synthesis, quality assessment, production cell, organization of production.*

The relevance of the research topic is due to the unattainability of a sufficient level of automation in traditional injection molding industries and the impossibility of managing the human factor, which entails all sorts of costs. Conceptual development of a remotely controlled layered synthesis system and a parameter estimation model for evaluating the performance of this system will not only provide a suffi-cient level of automation, but also reduce maintenance time and resource overruns for the production pro-cess.

Fig. 1 shows a scheme for organizing the space of a production cell. The principle of operation of the system is a cyclical and waste-free process of additive manufacturing with remote control and the ex-clusion of the human factor. [1]. The remote control point gives a command to print the product and downloads data on permissible errors. The control point starts the printing process on 3D printers located around the manipulator, and also performs the preparatory process. During the printing process, there is constant monitoring by an X-ray separator located on a robotic arm and, if a discrepancy is detected with the pre-set parameters of the product, the printing process is stopped to move the defective part for pro-cessing by using a conveyor belt [2].

The advantage of this system is the absence of jobs with operators replaced by workstations, according to the principle of unification. To control the quality of the process of operation of the additive installations of the production line, an X-ray separator was installed for the process of continuous moni-toring of the quality level of the filamentized product in the process of layer-by-layer synthesis [3].

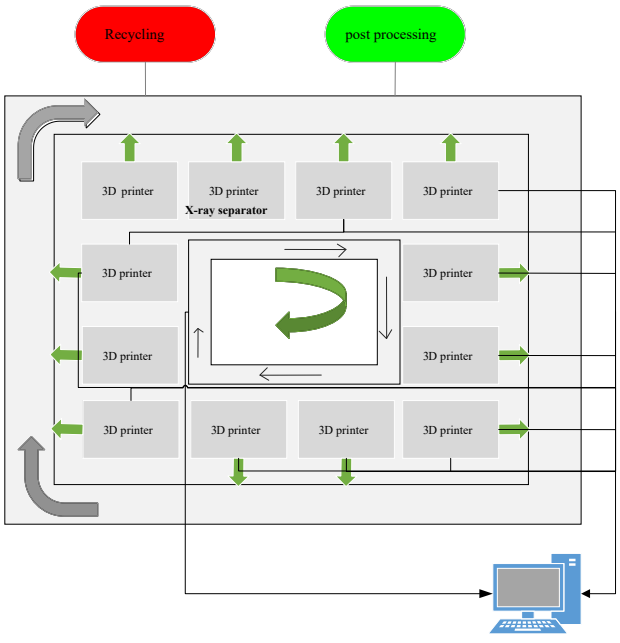

Fig. 1. Organization of the production cell space

To assess the quality of the system, the main quality indicators were identified, on which the operation of the system depends (formula 1).

$$Q_c = \{Q_к; Q_t; P_x; D_I\} \quad (1)$$

Q_k - product quality level; Q_t – system speed; P_t – probability of a defect; D_I – number of defects.

The quality level of the system will be defined as the arithmetic mean of all indicators taken into account in the evaluation (2).

$$Q_c = \frac{1}{n}\sum_{i-1}^{n} S_i \cdot k_i \quad (2)$$

where Q_c – the quality level of the system, S_i – the level of parameters taken into account, k_i – the weighting factor.

Table 1

Gradation of the assessment of the quality of the system

Percentage	Point scale	Gradation of system operation levels	Qualitative characteristics of the system
90% <Q_c ≤ 100%	5	Superior system performance	The system works non-stop and identifies 95% of non-conformities, high level of product quality, compliance with the time of the system, and with a minimum probability of failure, the presence of the operator is not required.
75% <Q_c ≤ 90%	4	High level of system performance	The system works non-stop and identifies 90% of discrepancies, high quality products, there may be delays in system operation time, the presence of an operator is not required
50% <Q_c ≤ 75%	3	Average level of system operation	The system works non-stop, the product characteristics correspond to the specification, the system operation time increases slightly, at least 85% of inconsistencies are identified, the presence of an operator is not required
25% <Q_c ≤ 50%	2	Unsatisfactory level of system performance	The system works intermittently, the characteristics of the products differ slightly from the TOR, the operating time of the system increases, less than 80% of inconsistencies are identified, the presence of an operator is required.
Q_c ≤ 25%	1	Low system performance	The system works with constant interruptions, needs maintenance by the operator, the level of product quality is low, there are deviations from the TOR, the operating time differs significantly from the reference, less than 80% of discrepancies are detected, the presence of the operator is required.

The assessment of the quality level of the product will be determined using a comprehensive quality assessment. To assess the quality of a product, it is necessary to determine the set of product properties that will adequately characterize its quality, determine the numerical values of these properties, and compare the obtained data with the reference ones.

In accordance with GOST R 57586-2017 “Products obtained by the method of additive technological processes [4]. General requirements” the main requirements for the parameters, composition and properties of the product are established depending on the purpose of the products manufactured by prototyping. There are 3 types of destination. General requirements include appearance, geometric dimensions, chemical composition (material), porosity.

To assess the quality of the proposed system, the main properties of the product were identified, according to which the level of product quality will be determined (3):

$$Q_k = \{F; S; G\} \quad (3)$$

F – Construction accuracy; S – Layer thickness; G – Compliance with the dimensions of the product TK.

All parameters of the evaluated objects must be brought to the form when it is possible to compare them, that is, to such values, using which you can get the value of the quality level of the evaluated object [5].

To do this, it is necessary to carry out the procedure of formalization (normalization) of heterogeneous information into dimensionless relative values in order to be able to compare the analyzed objects. As a result, we get scores from 1 to 5.

The evaluation of the quality of products must be calculated by the complex method (4), which takes into account the weight coefficients.

$$Q_k = \frac{1}{n}\sum_{i-1}^{n} Q_i \cdot k_i \tag{4}$$

Q_k – the quality level of the product; Q_i – level of properties taken into account K_i – weighting factor

The weight coefficient will be calculated using the following formula (5):

$$k_i = \frac{A_i}{\sum A_i}, \text{ при } \sum k_i = 1 \tag{5}$$

k_i – the weight coefficient, A_i – the measured value of the importance of the product property, ΣA_i – the total value of all the importance of the product properties.

The weight coefficient is determined by the main method – expert. From the entered indicators, a table is built by groups in percentage terms using the percentile approach, based on the minimum and maximum values of the i-th object of the j-th property. To assess the speed of the system, the main parameters were also determined (formula 6).

$$Q_t = \{t_n; t_{пл}; t_{печ}; t_c\} \tag{6}$$

t_n - preparation time; $t_{пл}$ – planned time for processing the model to the required format; $t_{печ}$ - product printing time; t_c - removal time.

Estimation of system operation time will be determined by a differentiated method. (formula 7)

$$Q_t = \frac{1}{n}\sum_{i-1}^{n} \frac{Q_i}{Q_{баз}} \tag{7}$$

The differential method for assessing the quality of products is carried out by comparing the indicators of each property of the evaluated indicator with the corresponding reference indicators. With the differential method of quality assessment, all indicators are considered equivalent [6].

The probability of occurrence of a defect will depend on the failure rate, the average time for the appearance of a nonconformity, as well as the operating time of the installation. (formula 8)

$$P(x) = \{\lambda; T_x; t\} \tag{8}$$

λ- failure rate; T_x – average time of occurrence of nonconformity; t – plant operating time.

To calculate the probability of occurrence of defects, Poisson's law is applied formula 9.

$$P(t) = \frac{\lambda^m \cdot e^{-\lambda}}{m!} \tag{9}$$

m – total number of printed products; λ – average number of defects in printing.

The probability of a defect occurring is calculated as the difference between all outcomes and the probability of failure-free operation (10)

$$P(x) = 1 - P(t) \tag{10}$$

The number of defects will be calculated as the arithmetic mean of the number of defects that appeared during the operation of the system.

$$D_I = \{D_{I1}; D_{I2}; D_{I3}; D_{I4}; D_{I5}\} \tag{11}$$

D_{I1} – number of nonconformities in a product series; D_{I2} – number of discrepancies in the part planning process; D_{I3} – number of inconsistencies in the print preparation process; D_{I4} – number of inconsistencies in the printing process; D_{I5} – number of inconsistencies in the final process.

In this work, a model for assessing the quality parameters of the system of an automated production cell for layer-by-layer synthesis with remote control and full-cycle control using an X-ray separator has been developed. The next stage of the study is testing the presented model on the basis of the laboratory of additive technologies of the SUAI FPTI.

Библиографический список

1. Назаревич, С. А. Модели и методики мониторинга процессов оценки новизны и конкурентоспособности продукции: дис. канд. тех. наук: защищена 19.02.2015: утв. 24.02.2015 / Назаревич Станислав Анатольевич. Спб., 2015. 211 с.

2. Щукина Д.С., Разработка модели производственной ячейки аддитивных технологий с применением робота-манипулятора, «Будущее сильной России – в высоких технологиях» сборник тезисов XV Открытой юношеской научно-практической конференции, ГБОНОУ «СПб ГДТЮ», – СПб, 2021, Секция «Техника», стр. 7-9

3. Щукина Д.С., Концепция системы послойного синтеза с удаленным управлением, Метрологическое обеспечение инновационных технологий: III Междунар.форум: сб./под ред. академика РАН В.В. Окрепилова. – СПб.: ГУАП, 2021. Стр. 451-452

4. ГОСТ Р 57556-2017. Материалы для аддитивных технологических процессов. Методы контроля и испытаний. М.: Стандартинформ, 2017.

5. Ларссен, Я. Аддитивное и гибридное производство с применением 3D-печати / Я. Ларссен // CAD/CAM/CAE Observer. 2015. № 3 (95). С. 26-28.

6. А.В. Богачева СОВРЕМЕННЫЕ ИННОВАЦИИ В ПРОФЕССИОНАЛЬНОМ ОБРАЗОВАНИИ – АДДИТИВНЫЕ ТЕХНОЛОГИИ // ПРОФЕССИОНАЛЬНОЕ ОБРАЗОВАНИЕ В СОВРЕМЕННОМ МИРЕ: ТРАДИЦИИ И ИННОВАЦИИ. – Выборг: Государственный институт экономики, финансов, права и технологий, 2019. – С. 14-19.

7. А. В. Минчева РИСК – ОРИЕНТАЦИОННЫЙ ПОДХОД К ОПРЕДЕЛЕНИЮ КОНТРОЛЬНЫХ ТОЧЕК ПРИ ОРГАНИЗАЦИИ АДДИТИВНОГО ПРОИЗВОДСТВА ПРОДУКЦИИ // Сборник статей Всероссийской научно-практической конференции «3D технологии в решении научно-практических задач».. – СПб: 2021. – С. 109-112.

8. Нефедова Л.А. Организация и проведение проектов внедрения архитектурных решений по управлению аддитивными производствами // Научный журнал НИУ ИТМО. Серия Экономика и экологический менеджмент. – СПб: 2019. – С. 184-189.

9. Орлов А.И. О ЧЕТЫРЕХ НАПРАВЛЕНИЯХ ИССЛЕДОВАНИЙ В ОБЛАСТИ ТЕОРИИ И ПРАКТИКИ УПРАВЛЕНИЯ ПРОИЗВОДСТВЕННЫМИ СИСТЕМАМИ // Научный журнал КубГАУ. – М: 2022

10. Орлов А.И. Искусственный интеллект: статистические методы анализа данных. – М.: Ай Пи Ар Медиа, 2022. – 843 с.

IR-CAMERA IN PCB MALFUNCTION DETECTING

Sokolova Ksenia
Saint Petersburg State University of Aerospace Instrumentation
E-mail: ksusha.so-va@yandex.ru

Abstract. *This article describes the main methods of non-destructive electronic products testing, the features of using a thermal imager to detect circuit board malfunctions. It also presents the infrared image noise rejection experiment results.*
Keywords: *thermal imager, printed circuit board, flaw detection, infrared photography.*

There are numerous systems of electronic products quality control nowadays. Visual inspection allows to identify significant technology violations, printed circuit board (PCB) defects and solder joints. However, this method is not perfect and does not allow detecting minor defects.

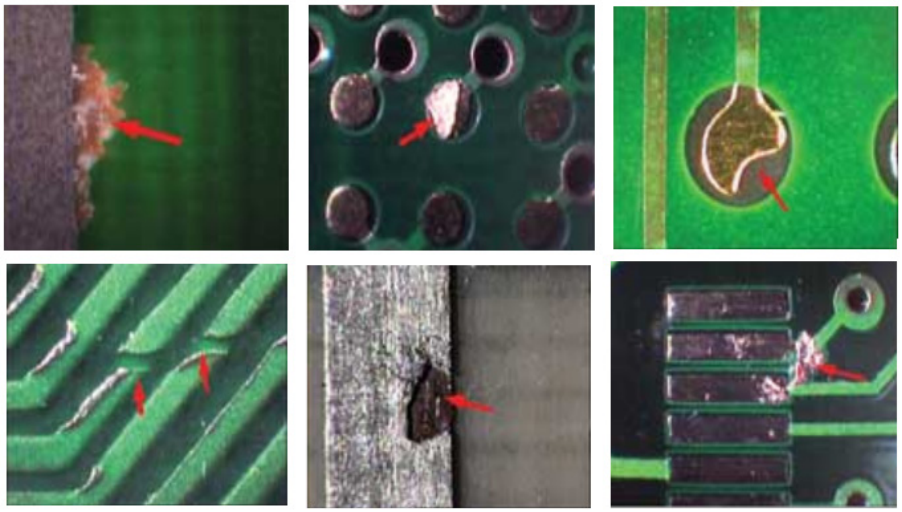

Fig. 1 – Examples of visible PCB defects [1]

Various optical devices (for example microscopes and endoscopes) are used to increase the effectiveness of this method. X-ray control helps to detect soldering defects invisible to the human eye. This is especially important for BGA components, which are inaccessible for visual analysis because of their location. This method also makes it possible to detect various types of material inhomogeneities indicating concealed defects. PCB inner layers microfracture and defects could be detected with X-ray control.

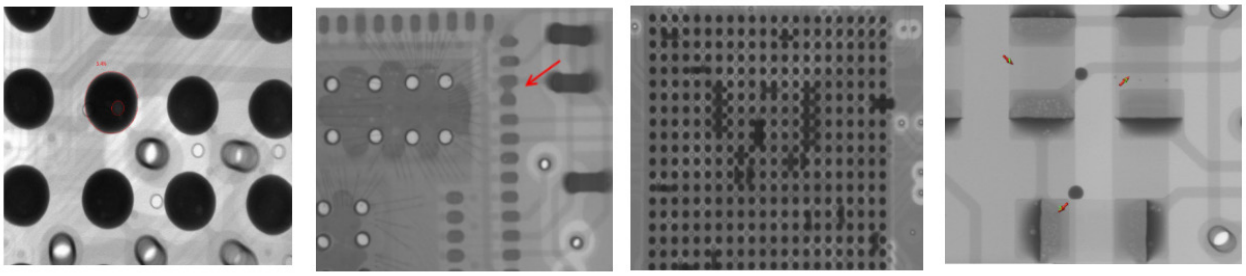

Fig. 2 – Examples of concealed PCB defects [2]

Electrical circuit malfunctions could be detected implementing boundary scan (over JTAG interface). It allows to detect signal delays, open contacts, short circuits and digital microchip malfunctions. Boundary scanning is based on IEEE 1149.1 group of standards [3].

Special high reliability equipment that can operate in high humidity, extreme temperature, high radiation conditions and under other radical environmental factors influence is required for some tasks, such as providing space flights, polar and oceanographic expeditions. Such products are subjected to particularly thorough control, aimed not only at finding existing defects, but also factors that can affect its operation in the future. For example, exceeding the rated current by 1% will not affect equipment operation, but may shorten component service life, which could reduce system reliability. It is necessary to identify such factors at the production stage to extend the service life of the equipment and increase its reliability. Another task of production output control is to identify design features that can affect further operation of the device. Non-destructive output control systems and methods are being developed and improved in order to solve such problems. Thermal imaging (or thermo photometric) control allows identify increased heat generation areas on the board. Information about a faulty component or assembly can be obtained through thermal image analysis.

Thermal imaging systems are widely used in medicine, mechanical engineering, power electrics, thermal engineering and many other industries. They are used to prevent various electromechanical systems and installations malfunctions, to detect composite material defects, for equipment testing, and identifying heat losses.

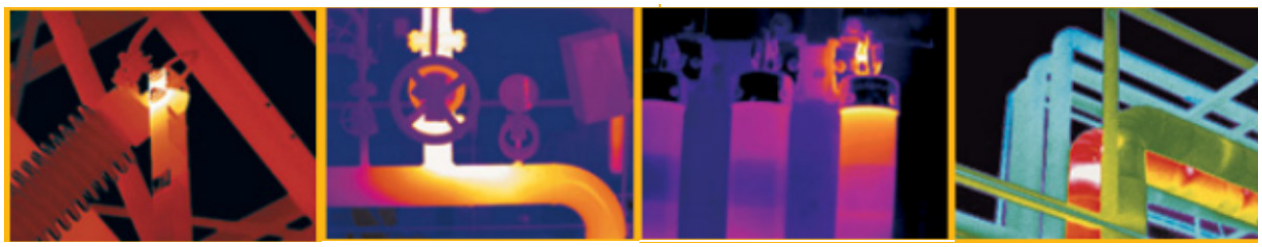

Fig. 3 – Thermal imager application for various industrial system troubleshooting [4]

However, at large electronic production enterprises, thermal photographic output control systems are steel rarely used. The development of such a system is extremely relevant in this regard.

A prototype of a thermal photographic system is being developed for the electronic products output control implementation. The layout of the developed system is shown in Fig. 4

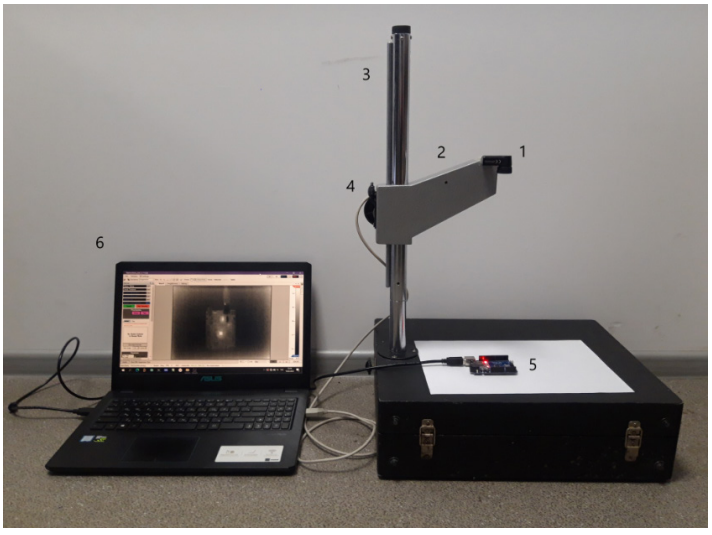

Fig. 3 – System layout: 1 – IR camera Seek Thermal Compact Pro.; 2 – holder; 3 – tripod; 4 – regulator; 5 – test sample; 6 – computer

The Seek Thermal Compact Pro infrared camera is used to obtain visual data. The computer performs data processing and display.

Electronic components generate some heat during normal operation. If the product malfunctions, some areas of the board may heat up more than usual, and some, on the contrary, generate less heat than during normal operation.

It is necessary to outline some features of thermal image analysis. Different objects having the same temperature may have different emissivity. This indicator is responsible for the object ability to give off heat and depends on the material properties. Fig. 5 shows an illustrative example. There is hot water in a porcelain cup. The whole cup surface has the same temperature however the gold paint has a lower emissivity in the infrared spectrum. Therefore, in the image, the areas of the surface covered with this paint appear colder, but they are not.

а)  *б)* 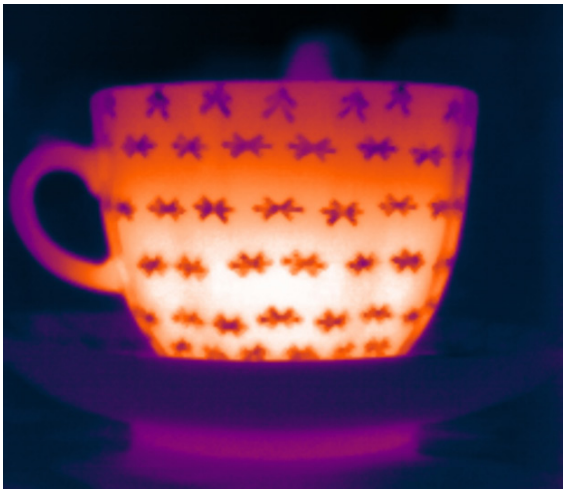

Fig. 5 – Image of a porcelain cup with a pattern:
a) – in the visible spectrum, b) – in the infrared spectrum

It is worth noting that the temperature in the room where the tests are carried out can vary within a few degrees. This factor should not affect diagnostic result.

It is not necessary to accurately determine the temperature of all objects in the image to identify a malfunction. It is enough to compare the thermal picture of a fully serviceable device (gauge) with the thermal picture of the sample under study and identify differences to localize the problem.

It is not always possible to carry out such an analysis visually. If the values of some parameters do not differ much from the nominal ones, the differences in thermal patterns will not be noticeable. Another problem is these differences are difficult to distinguish against the noise background. In this regard, there is a question of increasing the dynamic range of a thermal photographic system using digital processing of the obtained images.

It is possible to identify areas whose temperature differs by obtaining high resolution thermal images of the gauge and the test sample.

Consider some types of noise in the image and methods of dealing with them. When obtaining a thermal picture, two main types of noise can be distinguished: photon-shot and thermal.

Photon shot noise arises as a result of a change in the number of captured photons at a given exposure level. Each cell of the matrix receives a certain number of photons. Photons hitting the matrix are converted into electrons. Thus, a certain charge accumulates in each cell. The data on the charge in each cell (which is equivalent to the number of received photons) is then passed through the ADC, after which the normalized charge of each cell can be obtained. The process of conversion of the photon flux is discrete. Photon shot noise depends on the radiation intensity and does not depend on temperature.

Thermal noise arises as a result of the chaotic movement of atoms, the intensity of which depends on temperature.

Both noises considered above (thermal and shot) represent a statistically probabilistic structure that satisfies the Poisson distribution [4]. At a relatively low noise intensity, it approaches the Gaussian distribution.

The influence of noise can be reduced by the signal accumulation method, which is widely used to compensate for noise in communication systems [5]. This method is also applicable to image processing, provided that the noise is random variables that have one distribution law and are not correlated with the signal. In this case, the noise is proportional to the square root of the intensity of infrared radiation (useful signal).

It should be noted that all images must be taken when the system is in thermodynamic equilibrium.

Fig. 6 shows the result of adding 100 images.

а)

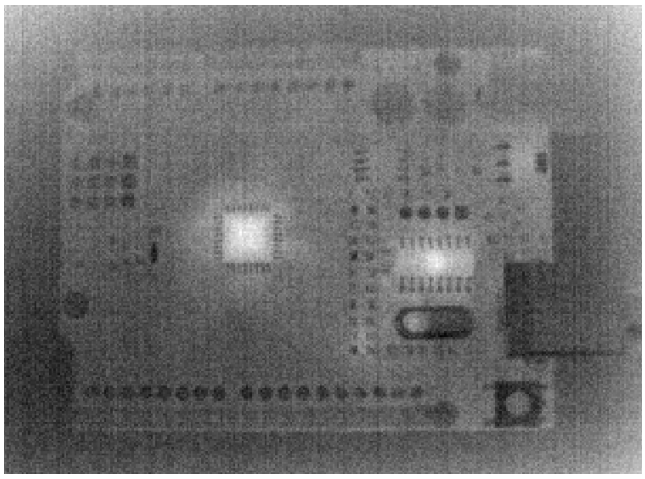

б)

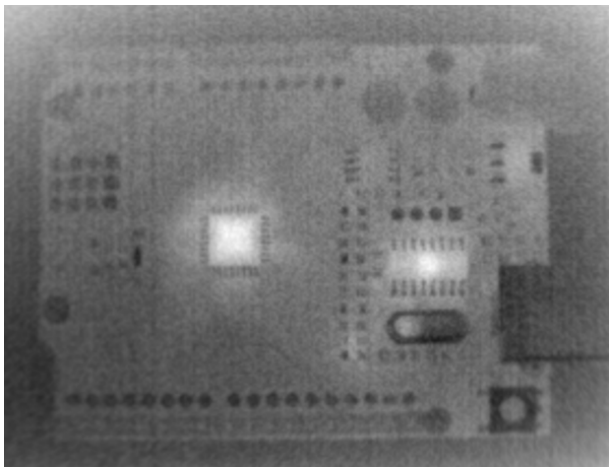

Fig. 6 – PCB thermal image obtained using the Seek Thermal Compact PRO infrared camera with a resolution of 320×240: a) – one frame without processing; b) – 100 frames summed

In conclusion, it should be noted that the use of infrared cameras in the electronic industry for the output control of products has great prospects, as they are of little use in large enterprises nowadays. But there is a significant need for such technologies for the electronic industries. In this regard, it is necessary to develop this area of technology and improve existing systems.

The prototype considered in this article can be the next step in the development of the output electronic products control technology.

This system needs to be improved. However, already at this stage it can be used to test printed circuit boards produced in small batches.

References

1 Input control – the most important stage of production preparation – URL:// https://russianelectronics.ru/vhodnoj-kontrol-vazhnejshij-etap-podgotovki-proizvodstva / (accessed 2023-18-02).

2 Examples of images of printed circuit boards from the Dage X–ray control system – URL:// http://www.pse-m.noolab.ru/293 / (accessed 2023-18-02).

3 IEEE Standard for Test Access Port and Boundary-Scan Architecture – URL:// https://standards.ieee.org/ieee/1149.1/4484 / (accessed 2023-18-02).

4 Application of thermal imaging technologies in preventive maintenance //Reference guide for the use of thermal imaging cameras in industry// © FLIR Systems AB – 2011. – 48 p.

THE CHALLENGES OF ORGANISING ADDITIVE MANUFACTURING

Sozdateleva Maria
Saint Petersburg State University of Aerospace Instrumentation,
Saint Petersburg, Russia
E-mail: macreatoor@yandex.ru

Abstract: *Additive technologies open up the possibility of reproducing products, objects, engineering structures and mechanisms manufactured from digital CAD model data. The use of such technologies in industry, significantly accelerate the production process, and allow working with models of manufactured parts.*
The diversity of additive manufacturing relies on the automatic conversion of digital models into solid material forms using specific fabricators – sets of mutually integrated tools for collaborative, efficient development.

Introduction

The production of one complex part using traditional production methods can require a relatively extensive multi-stage manufacturing cycle requiring a certain amount of equipment, which in turn requires a large number of qualified personnel, then resorting to additive manufacturing has the possibility to replace an entire production line with a single 3D printing system.

However, despite the fact that additive manufacturing has some advantages over traditional methods, there are problems that complicate its organization.

Depending on the additive technology used for the task at hand, the material is selected which is transformed by an external energy source, such as heat, light, laser light or other forms of energy.

At present there is no clearly established classification of AT, but they are represented by a number of printing methods which vary depending on the material used as well as the method of application. Source materials are divided into polymers, metals, ceramics and composites.

Source materials are divided into polymers, metals, ceramics and composites.

Polymers can be divided into:

- high-performance – these materials have exceptional environmental resistance, are durable, in some cases reach the level of mechanical properties normally found in metals, and can work under extreme conditions at elevated temperatures.

Polymers such as PEEK, PEKK (polyetheretherketones), Ultem (polyesterimide) fall into this category and are often used in the mechanical engineering, aerospace and defence industries.

The disadvantages of this material are its relative high cost as well as the need for postprocessing in strictly controlled conditions which can only be provided by industrial-grade 3D printers.

– Engineering – materials which are characterised by resistance to chemicals, temperature, mechanical and shock loads. This category includes PC-ABS (polycarbonate/acrylonitrile butadiene styrene), PA (polyamide), PC (polycarbonate), PET (polyethylene terephthalate).

- Consumer grade is a category of the cheapest polymers, whose resistance to external conditions is limited and which have comparatively low mechanical properties. Polymers in this category have been used successfully for rapid prototyping. These include PLA (polylactide), PP (polypropylene), HIPS (polystyrene).

Metal for use in 3D machines is used in the form of fine granules, and the grain size and composition are determined during its creation, at this stage it is important to maintain the ratio of coarse to fine grains, as this determines the fluidity of the material.

In general, the grain size ranges from 4 to 80 microns, this value determines the thickness of the future 3D printed product.

Metals include all kinds of alloys, aluminium, nickel, titanium, cobalt, copper as well as tool steel and stainless steel.

During the development of AT, photopolymers, in particular resins that change their properties when exposed to UV rays, have emerged. This material can be used in both industrial and professional applications. The large number of varieties makes the material suitable for a wide range of applications, from shoe making to the development of aerospace devices.

The cost, rather small market or inaccessibility of the necessary materials, in some cases limit the introduction or expansion of additive manufacturing.

In order to manufacture any part using 3D printing, the material must be selected based on the characteristics of the part.

For example, to select the right material for a moving part with bearing seats that will be exposed to friction on one side during rotation, consider ABS plastic (a), nylon (b), PETG – polyethylene terephthalate (c), PLA – polylactide (d).

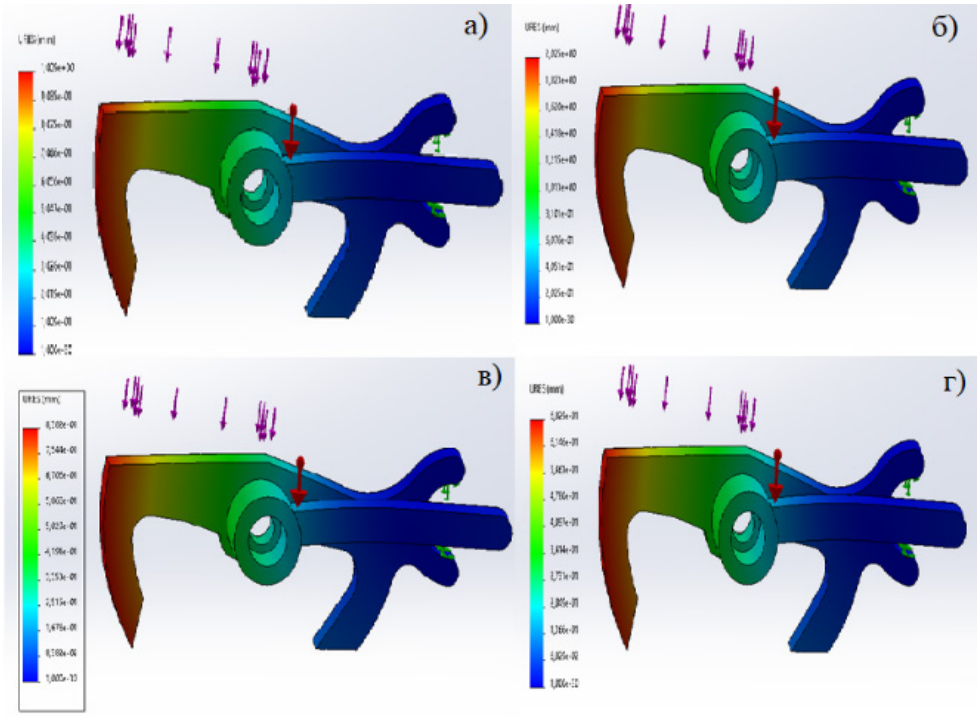

Fig. 1. Shoulder loads when making a product in a) ABS b) Nylon c) PETG d) PLA

Nylon has the lowest coefficient of friction (k=0.17), but it is not suitable due to insufficient rigidity and strength. Next in friction is PETG (k=0.22).

PETG part deformation is insignificant in comparison with other materials, so we select this material.

If a required material is not available or its cost is unsatisfactory, manufacturers have to resort to traditional methods, which incurs financial as well as time costs.

With regard to the materials used in additive manufacturing, there are special requirements for the premises in which the production takes place, such as

- depending on the hazard class of the substance in accordance with GOST 12.1.007 the room must be equipped with ventilation;
- depending on the characteristics of the material a certain level of lighting, humidity, temperature must be maintained in the room.

In view of the various stages of additive manufacturing, the staff needs to have specific competences for analyzing the technical specifications, creating a 3D model, carrying out various analyses, such as static or aerodynamic, setting the print quality, creating supports, post-processing the finished product and setting up the additive machine.

The operator must be sufficiently qualified to carry out the calculations before programming the machine, e.g:

The rate of production of the part will only depend on the volume consumption of the plastic, as the small size of the part will not allow the motors to be accelerated to their maximum speed. The volumetric consumption of plastic depends on the heating element from the filament diameter and the feed rate.

$$Vp = \pi R^2 * \upsilon ,$$

where R – radius of filament, mm = D/2, where D – diameter of filament, mm; υ speed of filament feeding into heating block, mm\s.

By experimental way it was found that the maximum possible volume flow rate of filament, diameter 1.75 mm, without loss of quality, is in the range from 12 to 15 mm3 / s.

For further increase, it is necessary to raise the temperature of the heating unit, which is not recommended by the manufacturer. At a volumetric flow of 15mm3/s, select the nozzle on which the printing speed will depend,

$$V = \frac{Vp}{\left(\pi\left(\frac{d}{2}\right)2\right)},$$

where d is the diameter of the nozzle, mm.

Parts of extremely simple geometry should not be manufactured using additive manufacturing methods due to time and energy costs, especially in the case of multi-batch production and without full utilization of the additive manufacturing facility.

Conclusion.

To date, the problems of organization of additive manufacturing, discussed in the article, are the most relevant and act as a problem to be solved for specialists.

Each year the rate of development of additive manufacturing means and methods is increasing, representatives of different industries adopt additive technologies and popularize them among their colleagues.

By solving the abovementioned challenges, it will be possible to increase the pace and volume of additive manufacturing in a short time, as well as improve the quality of the products produced, which will increase the profit margins and efficiency of many industries.

[1] Additive Technologies – dynamically developing production / O.N. Goncharova, Yu.M. Berezhnoi, E.N. Bessarabov, E.A. Kadamov // Vestnik Don. – 2016. №4.

[2] GOST R 57558-2017/ISO/ASTM 52900:2015, Additive manufacturing processes. basic principles. – M., 2020. – 12 c.

[3] Application of polymeric materials as coatings / S.B. Genel, V.A. White, V.Y. Bulgakov, G.A. Gehtman // – M.: Chemistry, 1968. – 238 c.

[4] Zlenko, M.A., Popovich, A.A., Mutylina, I.N. Additive technologies in mechanical engineering // – St. Petersburg: Polytechnic University Press, 2013. – 222 c.

[5] Technology of additive manufacturing // – M.: Technosphere, 2016. – 656 c.

[6] Occupational safety standards system harmful substances classification and general safety requirements

MODEL OF USER MICROMOBILITY BASED ON MARKOV CHAINS FOR THE THZ RANGE

Stepanov Nikita
Saint Petersburg State University of Aerospace Instrumentation,
Saint Petersburg, Russia
E-mail: Leos29-07@yandex.ru

Abstract. *The work measures and statistically characterizes the process of micromobility of various applications, including video viewing, phone calls, virtual reality viewing and racing games. For these, the occupancy distribution and first-pass time (FPT) to disconnection are characterized for various THz band antenna configurations.*
Keywords: *micromobility, HPBW, FTP, TTų, Markov model.*

INTRODUCTION

Cellular networks of the new generation 6G allow the use of the terahertz frequency range (0.3 – 3 THz) [1], [2]. We assume a radiation pattern of a conical antenna [3], with a non-zero main-lobe gain, of a circular shape with a half-power beamwidth (HPBW) approximated by $102^{o}/N_B$ and $102^{o}/N_U$ [4]. Where N_B and N_U are the dimensions of the BS and UE lattices, respectively. There is a direct connection between the fixed base station (BS) of the THz band and the mobile user equipment (UE).

In this use case, the system enters the off state when the UE's beam center leaves the circular coverage area corresponding to the HPBW BS for THz antennas, as shown in Fig. 1.

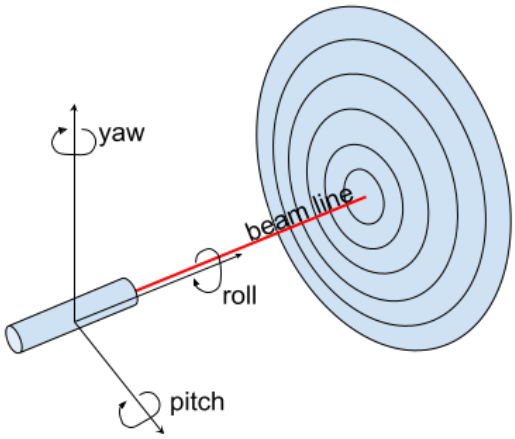

Fig. 1. *Used measuring setup and medium*

The work [5] measures stochastic patterns of user micromobility for four different classes of applications: (i) video viewing, (ii) phone calls, (iii) virtual reality (VR) viewing, and (iv) racing game.

We perform an analysis of the measured mobility patterns, including the first transit time (FPT) to the circular boundary characterizing the continuous connection time interval. In addition, setting the goal of mathematical modeling of micromobility to assess the performance of communication systems in the THz range, as in [6]. This paper describes the main idea of the approach to implementing the micromobility model based on the construction of Markov chains. Further results of these studies were obtained in [5], [6].

To conduct analytical and simulation studies of THz systems with micromobility, we develop reference Markov models for all considered applications and show that they serve as a good approximation for applications that do not directly control the user's micromobility pattern in the THz range [7],[8].

Data post-processing

The following method was used to obtain the laser trajectory from video recordings. The laser dot is separated from the image using the background difference method [9]. Following this approach, by subtracting two adjacent frames and combining the resulting values in the range 0 to 255, you can get a

background with zero pixel values and non-zero pixels where the laser moved. For a more accurate estimate of the position of the laser, not only adjacent frames are subtracted, but also frames with a certain time step, so that the laser can change its position at a distance exceeding the radius of the laser spot itself on the screen. To determine the center of the laser spot, among the pixels detected by the frame difference method, there is a pixel that has the highest non-zero value. Thus, it is possible to accurately determine the trajectory of the laser spot on the screen in the video stream.

Note that sometimes, due to the micromobility of the UE, part of the trajectory lies outside the space captured by the camera, i.e. the visible frame of the camera. In this case, it is assumed that the trajectory is tied to the boundary of the captured frame.

Due to camera limitations, the internal time resolution is 1/30 s. To obtain traces with arbitrary temporal detail, we used the method of linear spatial interpolation by determining the coordinates of the trajectory between the measured points.

Statistical data analysis

In this section, we present a statistical analysis of the resulting micromobility patterns. First, derive the extended metrics of interest to us, suitable for further stochastic modeling of micromobility processes in THz systems.

Before proceeding to the simulation analysis, we first draw the reader's attention to a critical metric of interest for THz communications. For purposes of illustration, we consider a simple cone antenna model, assuming that the boundary of interest is a circle centered at the starting point. Note that we further assume that the beam search procedure is ideal, i.e. each time a beam search is performed, the beams of the UE and BS are perfectly aligned.

To increase the number of samples to be used in the average FPT calculations, we use the following interpretation. Note that, according to the direct approach, only one FPT observation can be obtained from one experiment, following the following assumption: at the beginning of the experiment, the connection is established, i.e., the THz radiation patterns of BS and UE are perfectly matched to each of them. Another with HPBW centers lying on the same axis. FPT occurs once per experiment if, due to micromobility, the beam goes outside the circle with a certain radius specified by the THz BS HPBW antenna. However, in order to increase the number of FPT observations and obtain reliable statistics, we assume that as soon as antenna mismatch occurs, a beam search is performed to align them back. Following this approach, the number of FPT observations in one 10 s experiment can be more than one. To remove the residual correlation in the micromobility pattern, we also skip exactly 1 second from the moment the beam shift was detected.

The average FPT value increases as the radius increases, i.e. an antenna with fewer elements is used or the distance between the THz BS and the UE increases. The shortest time on average is observed in the VR viewing application, and the most in the video viewing application [5]. Of particular note is that for the latter application, no transit times were observed for radii greater than 18 cm. We also provide the projection radius of the HPBW in a plane orthogonal to the line-of-sight (LoS) trajectory between BS THz and UE, where the HPBW is estimated to be $102^{o}/N_B$ and the radius is found using conventional geometry. When watching video, application crashes rarely happen within a radius of more than 20 cm, which corresponds to using, for example, a 100X100 antenna array at a distance of just under 50 m [5]. By increasing the number of beamforming antenna elements, it can be ensured that the application rarely suffers from micromobility effects. Similarly, other antenna configurations and associated communication distances can be derived that result in little impact from micromobility patterns, as well as average link active time.

Markov model

To parameterize a Markov model, we need to determine the number of states and estimate the transition probabilities. A number of general fitting algorithms have been developed for Markov models, for example, algorithms based on the expectation minimization (EM) method [10] or adaptation of the maximum likelihood estimate [11]. However, these methods are only useful when the internal structure is not clearly observable or the number of states cannot be inferred from the physical parameters. In our case, we can use simpler methods.

Before we proceed to estimate the transition probabilities, two critical parameters must be defined. These are the temporal and spatial resolution of the model, Δs and Δt. Please note that although we can work with any temporal resolution through the use of interpolation techniques, we use a native resolu-

tion of 1/30 s to avoid additional errors. Thus, the choice of the spatial resolution Δs, which implicitly determines the number of states of the Markov chain, is a matter of trade-off between the amount of statistics available and the capabilities of the model. to accurately predict the main FPT metric of interest. For the latter to be possible, Δs must be at least five times smaller than the considered HPBW radius [12], [13]. For typical terahertz communication distances (up to 50 m) and modern design options for antenna arrays, radii from 10 to 50 cm are primarily of interest. On the other hand, an increase in spatial resolution reduces the amount of available statistics for model parameterization. Thus, in what follows we will use two values of Δs, equal to 2 and 5 cm, corresponding to 50X50 and 100X100. Since micromobility is concentrated in the center of the grid, this number of cells is sufficient. Note that the corresponding number of states is 50^2 and 100^2 respectively.

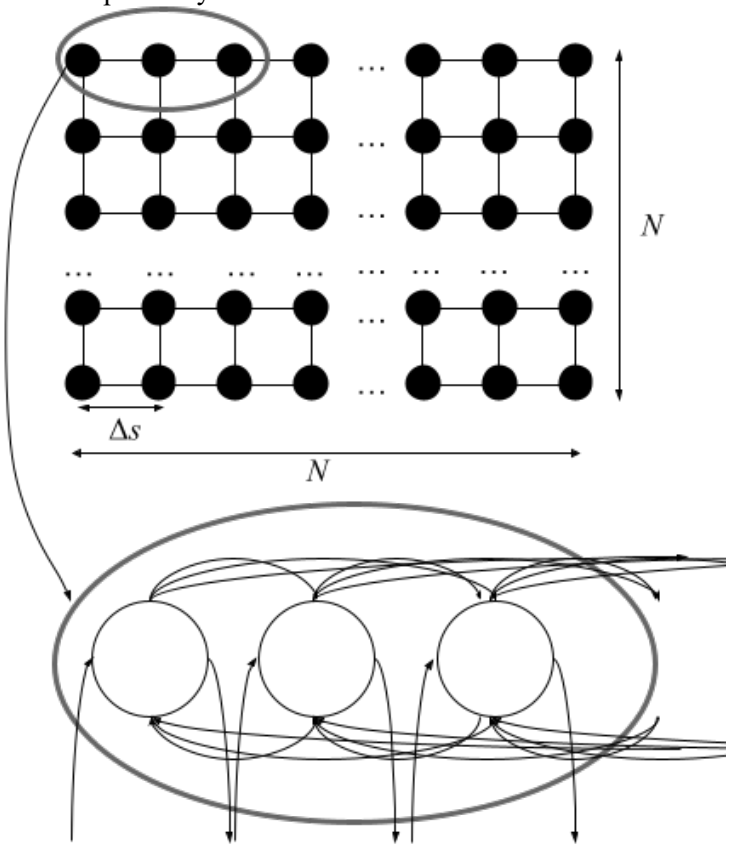

Fig. 2. *Markov chain*

After the number of states N is chosen, we proceed to determine the transition probabilities p_{ij}, i, j = 1, 2, …, N, using the usual statistical methodology. We first determine the state boundaries between states, and then calculate the number of state changes for specific values of i and j between the previous and current value in the trace, and divide it by the number of samples in the trace. To determine the probability matrix of transitions from cell to cell, the statistics of such transitions is collected and recorded in the matrix. Such a matrix has the same number of rows and columns, which correspond to the coordinate of the point at any time t and t+1, respectively.

The dimension of such a matrix corresponds to the square of the grid dimension, i.e., for example, if the quantization grid is equal to NXN (see Fig. 2), then the transition probability matrix is equal to N^2XN^2. Due to the fact that the probabilities of transitions over long distances are unlikely, part of the data of the transition probability matrix is not used. For this reason, to save memory for storing the transition probability matrix, a list is used that stores only non-zero transition probabilities. In this case, non-zero probabilities are significantly less than zero probabilities.

CONCLUSION

In order to develop terahertz beam steering algorithms, in this paper, we have comprehensively characterized the UE micromobility process for various applications. We looked at modern applications, including video and VR viewing, phone calls, and racing games, and characterized first and second order

statistical properties such as sampling trajectories, bivariate occupancy distribution, and FPT time. The latter is of decisive importance, since it characterizes the time before a trip in THz range communication systems.

Having set ourselves the task of stochastic mathematical modeling of the UE micromobility process, we also revealed the consequences of modeling the UE micromobility patterns of the considered applications. We have shown that none of the considered applications is characterized by radial symmetry. Moreover, both the speed of random mobility patterns and the drift are distance dependent by nature. Thus, in order to accurately map the stochastic properties of UE micromobility patterns, these properties require complex modeling approaches involving 2D random walks with independent increments.

Finally, we developed Markov models and demonstrated that they are only suitable for applications with low and purely random dynamics, such as video viewing and phone calls. When the user is guided by an application, as is the case with games, such models are generally not applicable to THz communication systems.

REFERENCES

[1] Polese, Michele, et al. "Toward end-to-end, full-stack 6G terahertz networks." IEEE Communications Magazine 58.11 (2020): 48-54.

[2] Petrov, Vitaly, et al. "Last meter indoor terahertz wireless access: Performance insights and implementation roadmap." IEEE Communications Magazine 56.6 (2018): 158-165.

[3] Petrov, Vitaly, et al. "Interference and SINR in millimeter wave and terahertz communication systems with blocking and directional antennas." IEEE Transactions on Wireless Communications 16.3 (2017): 1791-1808.

[4] Constantine, A. Balanis. Antenna theory: analysis and design. Wiley-Interscience, 2005.

[5] Stusek, Martin, et al. "Performance Assessment of Reinforcement Learning Policies for Battery Lifetime Extension in Mobile Multi-RAT LPWAN Scenarios." IEEE Internet of Things Journal 9.24 (2022): 25581-25595.

[6] Stepanov, Nikita, et al. "Accuracy assessment of user micromobility models for thz cellular systems." Proceedings of the 5th ACM Workshop on Millimeter-Wave and Terahertz Networks and Sensing Systems. 2021.

[7] Mokrov, Evgeni, and Konstantin Samouylov. "Performance Assessment and Comparison of Deployment Options for 5G Millimeter Wave Systems." Future Internet 15.2 (2023): 60.

[8] Lyubchak, A. N., A. N. Prikhodko, and V. S. Andreev. "A mmWave rod antenna array compatible with a PCB prototyping technology."

[9] Liu, Yaxin, et al. "Laser point detection based on improved target matching method for application in home environment human-robot interaction." 2018 11th International Workshop on Human Friendly Robotics (HFR). IEEE, 2018.

[10] Khreich, Wael, et al. "A survey of techniques for incremental learning of HMM parameters." Information Sciences 197 (2012): 105-130.

[11] Gales, Mark JF. "Maximum likelihood linear transformations for HMM-based speech recognition." Computer speech & language 12.2 (1998): 75-98.

[12] Redner, Sidney. A guide to first-passage processes. Cambridge university press, 2001.

[13] Krapivsky, Pavel L., Sidney Redner, and Eli Ben-Naim. A kinetic view of statistical physics. Cambridge University Press, 2010.

ISSUES OF OPTIMIZING THE PROCESS OF COLLECTING AND PROCESSING PLASTIC GARBAGE IN THE OCEAN

Suslov Pavel
Saint Petersburg State University of Aerospace Instrumentation,
Saint Petersburg, Russia
E-mail: suslovpasha@yandex.ru

Abstract. *The paper discusses issues related to the solution of an urgent problem – the processing of accumulations of plastic garbage in the ocean. It is proposed to organize the plastic recycling process directly in the ocean on recycling vessels. At the same time, the processed products can be used to support the construction, road construction, and electric power industries of coastal developing countries in Africa and Latin America. It is proposed to use for sorting and identification both systems with artificial intelligence trained to recognize and identify plastic by shape, and systems based on spectral analysis of the composition of plastic.*
Keywords*: plastic garbage, microplastics, plastic recycling in the ocean, plastic products*

Introduction

Today, in the era of consumption, goods largely acquire a commercially attractive appearance due to packaging, which allows not only to preserve the marketable appearance of products, but also to complement its external design. At the same time, the packaging itself becomes unnecessary after purchase and becomes garbage.

In addition, a huge number of plastic products become garbage every year in the world: containers, household items, toys, parts and constructs of mechanisms and household appliances, computers, etc. In total, according to experts, over 400 million tons of plastic waste are generated per year [1]. Some plastic is recycled, some is stored in landfills, but up to 80% of all existing plastics accumulate in the environment – on earth and in the ocean. It is obvious that the contribution of industrialized countries is the most significant. According to a study published in The Guardian newspaper [2], Australia tops the list of countries producing the largest amount of single-use plastic waste per capita. It is followed by the United States, South Korea and the United Kingdom. Nevertheless, in the generation of household garbage in kg per person in countries with different levels of consumption, plastic makes up at least 10%.

The largest producers of disposable plastic waste in the world are ExxonMobil (5.9 million tons), the largest American chemical company Dow (5.5 million tons), the Chinese oil and gas company Sinopec (5.3 million tons).

The classification of plastics [3] contains the main six names, referring all the others to a separate group, including very toxic plastics based on bisphenol A. Plastics of the LDPE and HDPE (polyethylene) and PP (polypropylene) groups are subject to repeated use as the safest (with reservations), plastics of the PET, PCV and PS groups are less safe and not recommended for secondary use.

However, it is not only the toxicity/non-toxicity of plastics that determines the need to combat their accumulation and recycling. Unlike food products, paper, cardboard, and iron, some types of plastics decompose in places of disposal for at least 300 years.

Unauthorized landfills with plastic in forests, fields, and water pose a particularly great danger to the environment. At domestic waste processing plants, there is a possibility of organizing technological chains focused on separate processing, and there are no such opportunities in places of unauthorized waste storage.

The aim of the work is to analyze the possible optimization of the functioning of modern systems for collecting and processing plastic in places of accumulation in the ocean and the prospects for the use of its processed products.

Collection and recycling of plastic garbage in the ocean

Environmentalists and governments of many states are particularly concerned about the accumulation of plastic garbage in the ocean, where, turning into microplastics, it accumulates in fish and other ocean biological resources. Subsequently, microplastics with them in the form of food enters the human body, causing significant damage to health. According to the rate of plastic accumulation in the oceans of the planet, it is predicted that by 2050 the mass of plastic in the world's oceans will exceed the mass of all fish living there [4].

Estimates of the structure of plastic garbage in the ocean show that only 18% of it is directly related to fishing, and the rest is household plastic garbage thrown out from ships in the ocean, and, to a much larger extent, carried out by rivers from continents.

Picked up by ocean currents, this plastic garbage is concentrated in several places in the Pacific, Atlantic and Indian Oceans, although plastic is found everywhere – from the North Pole to the South. The places of the greatest concentration of garbage, according to the BBC [5], are shown in Fig. 1.

Recycling plastic that is located and concentrated in the ocean is difficult.

Catching garbage with its delivery to processing plants on land is very costly. Therefore, the task of sorting and processing plastic directly in the ocean with the transportation of processed products, in much smaller volumes, to land and use in economic activities is urgent. At the same time, the natural aquatic environment is convenient for sorting and identifying plastic garbage. Specially create pools with water as on land, usually fresh, for sorting in the ocean is not required.

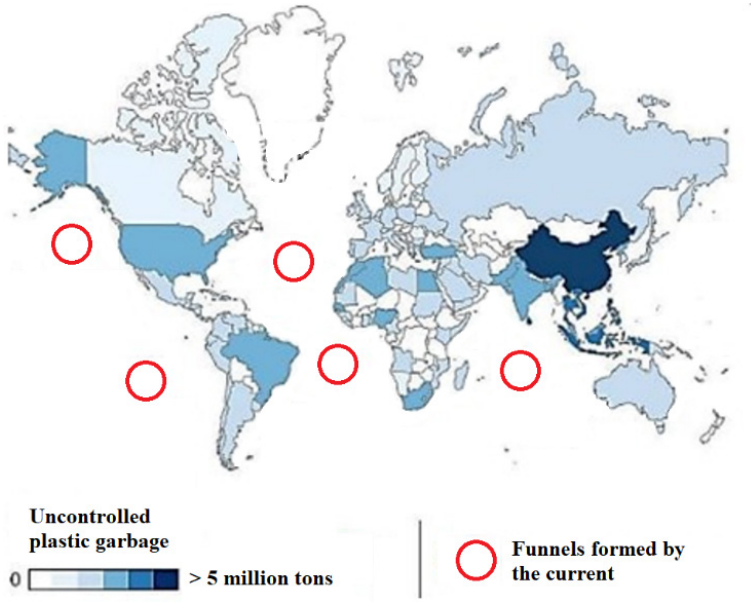

Fig. 1. Places of concentration of plastic garbage in the oceans

The organization of the proposed production process assumes the presence of:

– processing ship with technological lines for catching, identification and sorting, processing of plastic garbage on board;

– support ships, which are assigned the tasks of:

– supply of life support systems of the processing vessel;

– delivery of reagents and other consumables;

– transportation of processed products for use on land.

Below we will consider the organization of systems on board the main vessel.

Plastic type recognition

For recognition (identification) and, consequently, sorting of plastic at the present stage of technology development, the following are used:

– video cameras operating in the visible range;

– multispectral cameras, spectroscopes.

The first ones are designed for recognition systems based on the appearance and shape of plastic waste. Such systems are implemented today using convolutional neural networks trained, for example, on the external types of containers, bottles of various sizes, packages of a standardized type.

The second, identifying plastics by their spectra, as a rule [6] are equipped with a complete database of polymer spectra: any plastic can be identified, including with the involvement of artificial intelligence in the identification process. An example of the difference in the spectra obtained during the study and identification of microplastics extracted from surface waters [7] is shown in Fig. 2.

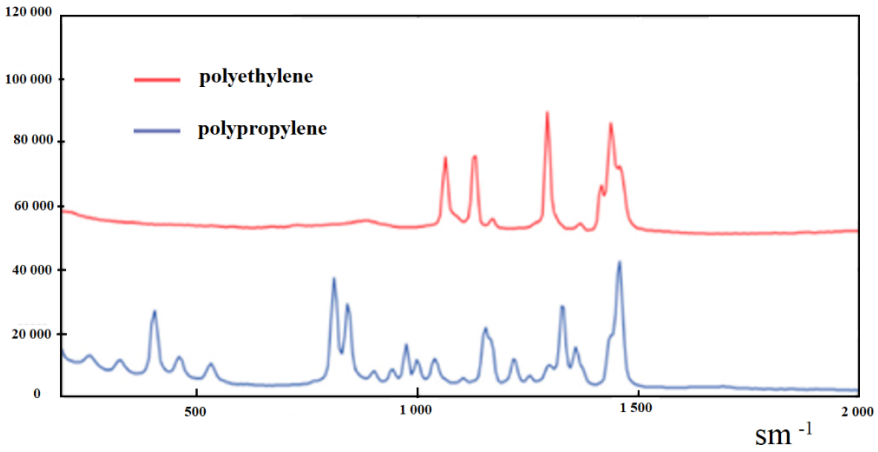

Fig. 2. Spectra of microplastics made of polyethylene and polypropylene

Plastic recycling

The fight against the accumulation of plastic garbage in the ocean can be carried out as:

– recycling using pyrolysis (decomposition of plastic);

– production of products and giving them new properties without changing the composition and condition of plastic.

Pyrolysis systems, in which plastics chemically disintegrate, allows them to produce fuel oil, heating oil, combustible gas, gasoline, waxes, etc. Thus, when processing 1 ton of plastic garbage, up to 10% of combustible gas, about 85% of liquid components and up to 5% of incinerated ash can be obtained [8]. Pyrolysis is a compromise between an energy–efficient and environmentally friendly way of recycling plastic waste. Up to 90% of harmful substances are destroyed by decomposition.

Production lines can be used as industrial processing lines for plastic processing located on processing ships.

These are production lines for:

– production of building blocks from plastic bags made of LDPE-type plastic can be used as industrial processing lines for plastic processing on processing vessels [9];

– production of polymer from plastics for use in asphalt mixture instead of bitumen [10];

– production of additives to asphalt mixture [11];

– production of fuel oil and heating oil [8].

Use of plastic processing products

The processing ship and the support ships have the opportunity to use the produced fuel oil and gas for their own consumption, supporting their livelihoods through the processing technologies being implemented. However, the problem is a disproportionately larger volume of processed products that should be used effectively.

Fig. 1 shows that the two main places of accumulation of plastic garbage in the Atlantic Ocean are close to the African continent. Accordingly, a proposal should be formulated for the Governments of the coastal countries of Africa for the supply of products for the development of road networks, building blocks for the construction of buildings and structures, fuel oil and heating oil for electric generating enterprises, etc.

Plastic recycling in its other accumulations in the Pacific and Indian Oceans can contribute to the same goals for developing countries in South America and East Africa.

It is obvious that the successful and operational implementation of the proposed structure for processing plastic in the ocean and the coordinated use of processed products on land should be supported of international organizations of the relevant profile. This are Organizations:

– the United Nations Industrial Development Organization (UNIDO);

– the World Health Organization (WHO);

– the International Maritime Organization (IMO);

– the International Union for the Conservation of Nature and Natural Resources (IUCN);

– many other international structures focused on helping developing countries.

Conclusions

Accumulations of plastic in the ocean, catastrophic in volume, require urgent human intervention with modern technologies for recycling and reuse of plastics.

The ocean is a convenient environment for sorting plastic garbage, since it already partially sorts this garbage from glass and metal, and in places of long–term accumulation – from paper, cardboard, food waste.

Recycling of plastic garbage in the ocean can become the basis for the creation of production facilities for the use and support of industrial development of developing coastal countries in Africa and Latin America.

Gratitude

The authors thank Associate Professor Sergeev A.M. for guidance in the preparation of this work and valuable advice.

References

1. Sadovskaya A.V., Ilyutchik I.V. Sorting and recycling of plastic household waste is the way to responsible consumption and production / In: Geographical and economic studies in the context of sustainable development of the state and the region. Materials of the III International Scientific and Practical Conference. Under the general editorship of E.G. Kosheleva. Donetsk, 2021. P. 37-39. (In Russian)

2. Twenty firms produce 55% of world's plastic waste, report reveals. URL: theguardian.com/environment/2021/may/18/twenty-firms-produce-55-of-worlds-plastic-waste-report-reveals (accessed 28.01.2023)

3. All about recyclables. Dangerous plastic. URL: makulaturu.ru/articles/opasniy-plastik (accessed 28.01.2023)

4. Belova M.K., Kondratenko L.N. Migration of plastic into the world ocean / In the collection: Ecology of river landscapes. Collection of articles based on the materials of the IV International Scientific Ecological Conference. Krasnodar, 2020. P. 8-11. (In Russian)

5. Seven Graphs Explaining Why Plastic in the Ocean is Bad. URL: bbc.com/russian/features-42307854 (accessed 28.01.2023)

6. Company «Spectr-M». URL: enspectr.ru/about/ (accessed 28.01.2023)

7. Identification of microplastics using raman microscopy. URL: czl.ru/blog/raman-spectroscopy/identification-of-microplastics-with-portable-raman-microscopy.html (accessed 28.01.2023)

8. Pyrolysis of plastics as a method of obtaining fuel. URL: rcycle.net/plastmassy/piroliz-plastikov-kak-sposob-polucheniya-topliva (accessed 28.01.2023)

9. Remizova V.M. Composites from garbage // University Science. 2018. № 1 (5). P. 79-82 (In Russian)

10. Asphalt from recycled plastic in the UK. URL: dtech.su/bitumen-plastic (accessed 28.01.2023)

11. KK Plastic Waste Management Ltd. URL: kkplasticroads.com/ (accessed 28.01.2023)

ALGORITHM MODELING OF TRAPEZOIDAL DISTRIBUTION

Tyurinova Violetta
Saint Petersburg State University of Aerospace Instrumentation,
Saint Petersburg, Russia
E-mail: viletteee@yanbdex.ru

Abstract. *The paper presents an algorithm for modeling random numerical sequences whose distribution follows a trapezoidal distribution. This distribution is the core of the distribution polygon used to construct the empirical probability distribution density of parameters of input data streams of complex systems.*
Keywords: *complex system, information flow of data, modeling algorithm, statistical equivalent, histogram, distribution polygon.*

Simulation modeling methods are actually the main methods of studying the characteristics of complex systems throughout their entire life cycle [1]. Modeling is preferably carried out using real recordings of input signals, which brings the results obtained during modeling closer to the results obtained during field tests. In the case, when there are not enough records, you can use the method of statistical equivalents [2,3,4], which allows you to expand the ensemble of records that do not contradict real experiments. The method of statistical equivalents usually uses histograms and polygons of records [5,6].

When using histograms, a rectangle acts as the core of approximation of the empirical distribution density, and when using a polygon of records, the core is a trapezoid. It allows more accurately reproducing the characteristics of the simulated initial input signal [5]. If the source statistical material is a histogram of the distribution, then it can be recalculated into a polygon. The recalculation algorithm depends on the availability of reliable information about the general characteristics of the simulated distribution. The example is that the modeled distribution is finite, or unlimited, or non-negatively determined, etc. In the absence of such information, which is of a general nature, one of the possible methods for converting a histogram into a polygon is considered in [4].

The probability distribution density of a random variable distributed according to the trapezoidal law is shown in Fig. 1 [7].

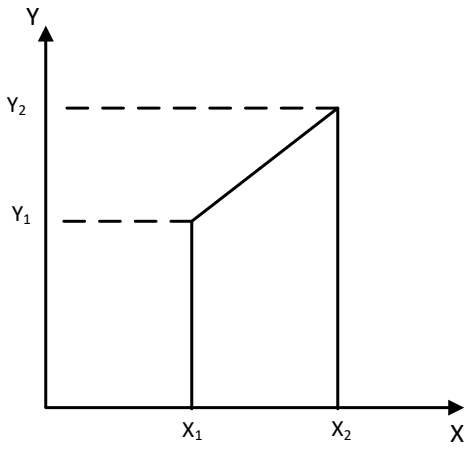

Fig.1. The density of the trapezoidal distribution

Indeed, we need to take a look at a step-by-step algorithm for modeling random numerical sequences distributed according to a trapezoidal law. To simulate a random sequence η_i, i=1,2,…k,…, we will use the inverse function method [5] and the random number sensor r_i, i=1,2,…k,…, the probability distribution density of which obeys the standard uniform distribution law, that is $r_i \sim RAV(0,1)$

$$f_r(x) = RAV(0,1) = \begin{cases} 0, x \le 0, \\ 1, 0 \le x \le 1, \\ 0, x \ge 1. \end{cases} \quad (1)$$

The density of the trapezoidal distribution $f_\eta(x)$ random variable η, as follows from Fig.1, in general form it can be written as [8]

$$f_\eta(x)=\begin{cases}0, x<x_1,\\ \dfrac{y_2-y_1}{x_2-x_1}\cdot x+\dfrac{y_1x_2-y_2x_1}{x_2-x_1}, x_1\le x\le x_2,\\ 0, x>x_2,\end{cases} \tag{2}$$

at the same time, of course, equality must be fulfilled $0.5\cdot(y_1+y_2)\cdot(x_2-x_1)=1$. In the particular case when $y_1=y_2=y_0$, expression (2) is written as

$$f_\eta(x)=RAV(x_1,x_2)=\begin{cases}0, x<x_1,\\ y_0=\dfrac{1}{x_2-x_1}, x_1\le x\le x_2,\\ 0, x>x_2,\end{cases} \tag{3}$$

that is, it goes, as expected, into a uniform distribution $\eta\sim RAV(x_1,x_2)$.

Integrating expression (2), we obtain the distribution function $F_\eta(x)$ random variable η

$$F_\eta(x)=\int_{-\infty}^{x}f_\eta(t)dt=\begin{cases}0, x<x_1,\\ \dfrac{1}{2}\cdot\dfrac{y_2-y_1}{x_2-x_1}x^2+\dfrac{y_1x_2-y_2x_1}{x_2-x_1}x+\dfrac{x_1^2}{2}\cdot\dfrac{y_2+y_1}{x_2-x_1}, x_1\le x\le x_2,\\ 1, x>x_2.\end{cases} \tag{4}$$

Using the inverse function method, namely, calculating the inverse function $F_\eta^{-1}(x)$, substituting numbers of a random sequence into it r_i, i=1,2,…k,…, we obtain an algorithm for modeling a random sequence η_i, i=1,2,…k,…, distributed according to the trapezoidal law

$$\eta_i=\begin{cases}x_1-\dfrac{y_1\cdot(x_2-x_1)}{y_2-y_1}+\sqrt{\left(\dfrac{y_1\cdot(x_2-x_1)}{y_2-y_1}\right)^2+\dfrac{2\cdot(x_2-x_1)}{y_2-y_1}\cdot r_i}, y_1<y_2,\\ x_1+(x_2-x_1)\cdot r_i, y_1=y_2,\\ x_1+\dfrac{y_1\cdot(x_2-x_1)}{y_1-y_2}-\sqrt{\left(\dfrac{y_1\cdot(x_2-x_1)}{y_1-y_2}\right)^2-\dfrac{2\cdot(x_2-x_1)}{y_1-y_2}\cdot r_i}, y_1>y_2.\end{cases} \tag{5}$$

The second expression in formula (5) can be obtained directly from expression (3), or by limiting the transition $y_1\to y_2\to y_0=1/(x_2-x_1)$ from formula (5). For example, from the first expression of formula (5) follows

$$\begin{aligned}\eta_i&=x_1-\frac{y_1\cdot(x_2-x_1)}{y_2-y_1}+\sqrt{\left(\frac{y_1\cdot(x_2-x_1)}{y_2-y_1}\right)^2+\frac{2\cdot(x_2-x_1)}{y_2-y_1}\cdot r_i}=\\ &=x_1-\frac{y_1\cdot(x_2-x_1)}{y_2-y_1}+\frac{y_1\cdot(x_2-x_1)}{y_2-y_1}\sqrt{1+\frac{2\cdot(y_2-y_1)}{y_1(x_2-x_1)}\cdot r_i}=\\ &=x_1-\frac{y_1\cdot(x_2-x_1)}{y_2-y_1}+\frac{y_1\cdot(x_2-x_1)}{y_2-y_1}\cdot\left(1+\frac{(y_2-y_1)}{y_1(x_2-x_1)}\cdot r_i+R\right),\end{aligned} \tag{6}$$

where R=R(y_2-y_1) – the remainder of the alternating series is equal to

$$R(y_2-y_1)=-\frac{1\cdot 1}{2\cdot 4}\left(\frac{(y_2-y_1)}{y_1(x_2-x_1)}\cdot r\right)^2+\frac{1\cdot 1\cdot 3}{2\cdot 4\cdot 6}\left(\frac{(y_2-y_1)}{y_1(x_2-x_1)}\cdot r\right)^3-\ldots, \tag{7}$$

substituting which into expression (6) and going to the limit $y_1 \to y_2 \to y_0 = 1/(x_2-x_1)$, expression (6) is reduced to the form

$$\begin{aligned}\eta_i &= \lim_{(y_2-y_1)\to 0}\left[x_1-\frac{y_1\cdot(x_2-x_1)}{y_2-y_1}+\frac{y_1\cdot(x_2-x_1)}{y_2-y_1}\cdot\left(1+\frac{(y_2-y_1)}{y_1(x_2-x_1)}\cdot r_i+R(y_2-y_1)\right)\right]= \\ &= \lim_{(y_2-y_1)\to 0}\left[x_1+\frac{1}{(x_2-x_1)}\cdot r_i-\frac{1\cdot 1}{2\cdot 4}\frac{(y_2-y_1)}{y_1^2(x_2-x_1)}\cdot r_i^2+\frac{1\cdot 1\cdot 3}{2\cdot 4\cdot 6}\left(\frac{(y_2-y_1)}{y_1(x_2-x_1)}\right)^2\frac{r_i^3}{y_1^2}-\ldots\right]= \\ &= x_1+\frac{1}{y_1}\cdot r_i = x_1+\frac{1}{y_0}\cdot r_i = x_1+(x_2-x_1)\cdot r,\end{aligned} \tag{8}$$

which coincides with the expression (5).

The algorithm for generating the trapezoidal distribution is shown in Fig.2.

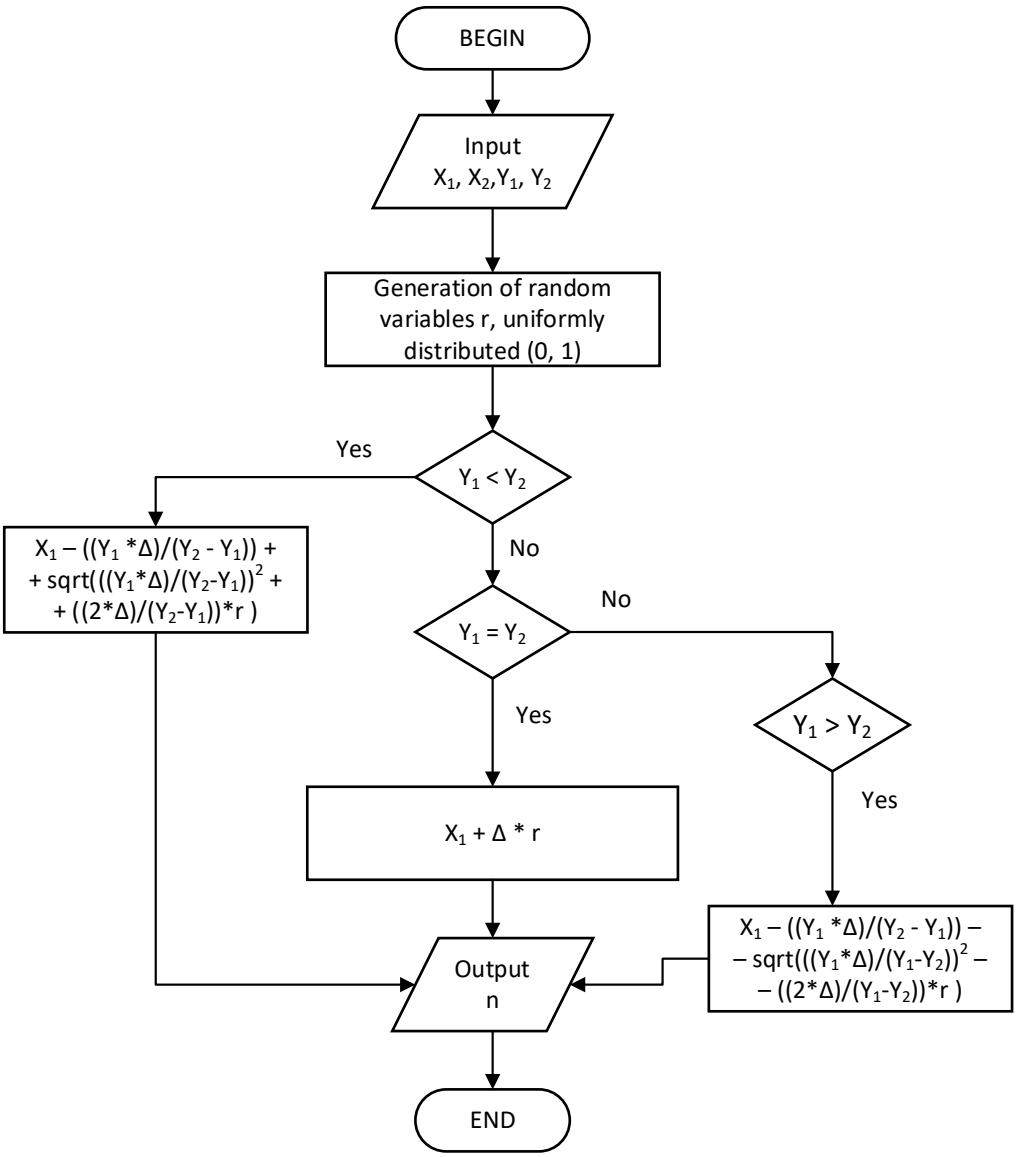

Fig.2. Trapezoidal distribution generation algorithm

Fig. 3 shows a histogram of the distribution obtained using the algorithm shown in Fig. 1, with the following parameters x_1=1, x_2=2, y_1=0.5, y_2=1.5.

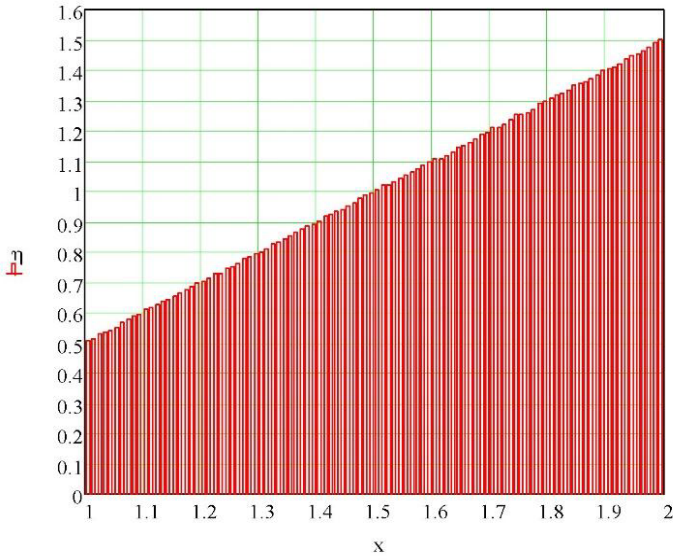

Fig.3. Histogram of trapezoidal distribution

The presented trapezoidal distribution algorithm can be directly used to simulate random numerical sequences that are empirical equivalents of real recordings of input signals of complex systems. At the same time, unlike the algorithms for generating empirical equivalents considered in [2,3,4], the presented algorithm is based not on histograms of records, but on polygons of distributions, which allows more accurately reproducing the statistical characteristics of input signals.

References

1. Izrantsev V.V., Shepeta D.A. Modeling of external signals of onboard instrument complexes of fifth-generation aircraft. Scientific instrumentation. 2000. Vol. 10. No. 2. pp. 14-19.

2. Ivanova M.S. Synthesis of algorithms for statistical equivalents of input signals of information processing systems based on empirical data. Bulletin of the UNESCO department “Distance education in engineering” of the SUAI: Collection of the papers. St. Petersburg, Issue 5.– SPb.: SUAI, 2020, pp. 77-81.

3. Ivanova M.S., Isakov V.I., Shepeta D.A. Simulation Models of Input Signals of Information Processing Systems Synthesized from Empirical DATA. В сборнике: 2020 Wave Electronics and its Application in Information and Telecommunication Systems, WECONF 2020. 2020. С. 9131164.

4. Ivanova M.S., Shepeta A.P. Algorithms for modeling information flows of information processing systems synthesized from empirical data. In the book: Processing, transmission and protection of information in computer systems 21 International Scientific Conference: collection of reports. Saint Petersburg, 2021. pp.20-24.

5. Shalygin A.S., Palagin Yu.I. Applied methods of statistical modeling- L.: Mechanical Engineering. Leningr. department, 1986. – 320 p.

6. Kobzar A.I. Applied mathematical statistics. For engineers and researchers. – M. Fizmatlit. 2006 -816 p .

7. Tyurinova, V. A. Algorithms for input signals simulation of complex systems synthesized based on empirical data / V. A. Tyurinova, G. M. Wattimena, D. A. Shepeta // Wave Electronics and Its Application in Information and Telecommunication Systems. – 2022. – Vol. 5. – No 1. – P. 506-510. – EDN OOXSVU.

SOLVING THE PROBLEM OF SELECTING CONNECTED AREAS IN A BINARY IMAGE

Vinogradov Dmitry
Saint Petersburg State University of Aerospace Instrumentation,
Saint Petersburg, Russia
E-mail: vinmitya@gmail.com

Abstract. *The paper considers a methodology of identifying connected contours on a binary image with implementation in various computer programs.*
Keywords: *image processing, connected contours, binary image, Python*

The problem of identifying connected contours in an image is closely related to the problem of pattern recognition, which is currently one of the most important and significant problems in the field of image processing. The tasks of selecting graphic objects from the background are acute, for example, in the analysis of biomedical images, location images, etc. The simplest subtask is the selection of connected contours in binary images. It is assumed that the original image in grayscale is subjected to primary binarization, for example, using a threshold level (everything below the threshold in the brightness gradation is considered a background, everything above is an image). In this case, great importance (taking into account interference of various properties) is given to the differentiation of extended objects (consisting of at least a given number of pixels) from single objects, which are various kinds of artifacts that should not be taken into account, and counting their number. For this kind of identification, it is advisable to use modern algorithms for identifying connections.

For simplicity, we will further assume that the objects of interest to us after binarization are black (conditional "1" in the matrix entry), and the background is "colored" in white (conditional "0" in the matrix entry).

To select objects in the image, it is necessary to select groups of black pixels that are “neighbors” of each other. In other words, the objects on a given binary image are connected components of this image.

Generally speaking, a connected component is a set of "single" pixels P, such that for each pair of pixels Pi and Pj from the set P, every 2 pixels that are adjacent in a sequence are "neighbors".

What is meant by the term "neighbours"? If we consider a single pixel as a square, then we can distinguish the following situations: these squares have a common edge, vertex, or have nothing in common. Each square has 8 adjacent square pixels that share a common vertex with it; such pixels constitute the "Moore neighborhood" of the given square. Is it right to consider them "neighbors" of a given pixel if they have only a common vertex with the given pixel? Or do two pixels need to have a common edge to do this?

To answer this question, we need to consider two types of connections.

4-connectedness (direct connection)

The concept of 4-connectivity implies that each of the black pixels from the set under consideration has at least one common edge with potential neighbors. This type of connectivity is illustrated in Fig. 1.

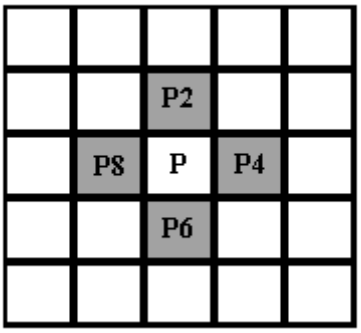

Fig. 1 – 4-neighbors of pixel P

Fig. 2 below shows examples of 4-connected regions in images.

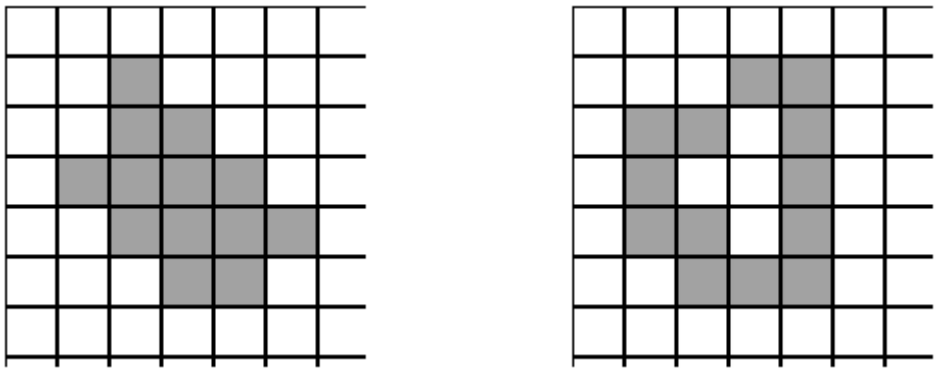

Fig. 2 – Examples of 4-connected areas

8-connection (indirect connection)

The concept of 8-connectivity is related to the presence of neighbors from the Moore neighborhood for the considered black pixel. This type of connectivity is shown in Fig. 3.

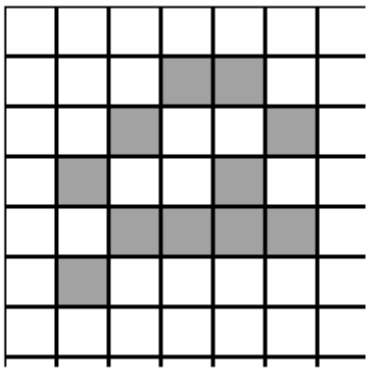

Fig. 3 – An example of an 8-connected area

It should be noted that any 4-connected area is also 8-connected, the converse, in turn, is not true (see the example in Fig. 3 – this area is not 4-connected).

To solve the problems of extracting connected biomedical images, as a rule, the concept of 4-neighborhood is used. There are many different algorithms for identifying such "neighbors", they are analyzed in sufficient detail, indicating all the pros and cons, in electronic sources and printed publications [1].

Let us dwell in more detail on the algorithm of the one-pass non-recursive labeling algorithm using the ABC-mask [2].

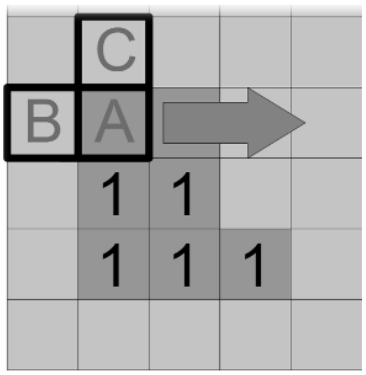

Fig. 4 – ABC-mask and the direction of sequential scanning of the image

The passage through the image with such a mask is carried out from left to right and from top to bottom. We will assume that there are no objects outside the image boundary, therefore, if B or C get there, no additional check is required. Fig. 5 shows five (from 0 to 4) possible mask positions in the image.

Position 0 – no pixel matches the mask – skip a pixel.

Position 1 – only pixel A is marked – create a new object.

Position 2 – element B is marked – we give the pixel with the current label A the value located in B.

Position 3 – the element C is marked – we give the pixel with the current label A the value located in C.

Position 4 – we will assume that B and C are connected – that is, they are equivalent. Then pixel A can be labeled either as B or as C. In some algorithms, in this case, an equivalence graph of such labels is compiled and then parsed. In general, in the event that B is not equal to C, then it is advisable to renumber all already processed pixels marked as C to label B.

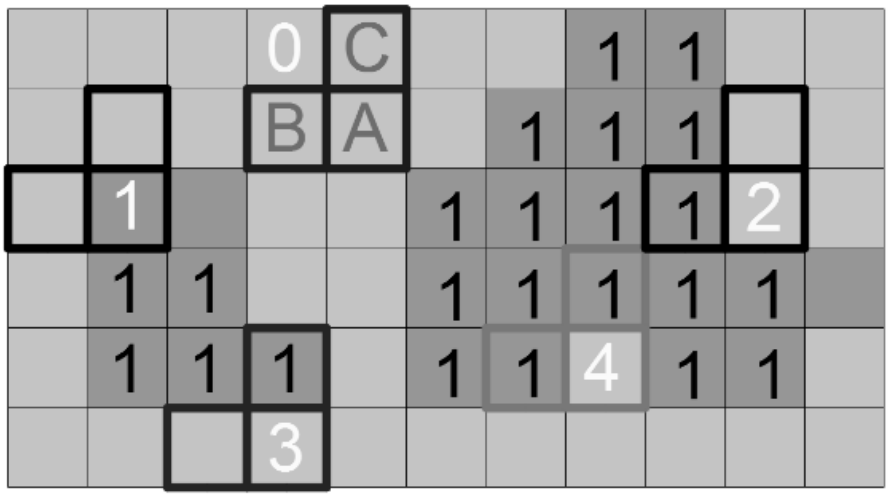

Fig. 5 – Five possible positions of the ABC mask

Let Image be a binary array of the original image. Here is a fragment of the listing of the processing algorithm implemented in the Scilab environment.

```
        [m,n]=size(Image);
km = 0; kn = 0;
cur = 1;
        for i = 1:1:m
 for j = 1:1:n
  kn = j – 1;
  if kn <= 0 then
   kn = 1;
   B = 0;
  else
   B = Image(i,kn);
  end
  km = i – 1;
  if km <= 0 then
   km = 1;
   C = 0;
  else
   C = Image(km,j);
  end
  A = Image(i,j);
  if A == 0 then
  elseif B == 0 & C == 0 then
```

```
      cur = cur + 1;
      Image(i,j) = cur;
    elseif B ~=0 & C == 0 then
      Image(i,j) = B;
    elseif B == 0 & C ~= 0 then
      Image(i,j) = C;
    elseif B ~= 0 & C ~= 0 then
      if B == C then
        Image(i,j) = B;
      else
        Image(i,j) = B;
        Image(Image == C) = B;
      end
    end
  end
end
```

Listing 1 – The algorithm of the non-recursive method of counting connected objects

It should also be noted that in modern programming environments, in particular, in the Python language, there are built-in libraries that greatly facilitate the implementation of this non-recursive method for selecting connected objects in an image. An example of the implementation of such a Python program [3] is shown below in Fig. 6-8.

```
 9    print(map)
10    labeled_array, num_features = ndimage.label(map, np.ones((3,3)))
11    koll=num_features
12    map=labeled_array
13    print()
14    print(map)
```

Fig. 6 – A fragment of a program that implements a non-recursive algorithm in the Python environment

```
[[0 0 0 0 0 0 0 0 0 0 0 0 0 0 0 0 0 0 0 0]
 [0 0 0 0 0 0 0 0 0 0 0 0 0 0 0 0 0 0 0 0]
 [0 0 0 0 0 0 0 0 0 0 0 0 0 0 0 0 0 0 0 0]
 [1 1 1 0 1 1 1 0 1 1 1 0 1 1 1 0 1 1 1 0]
 [1 1 1 0 1 1 1 0 1 1 1 0 1 1 1 0 1 1 1 0]
 [1 1 1 0 1 1 1 0 1 1 1 0 1 1 1 0 1 1 1 0]
 [1 1 1 0 0 0 0 0 0 0 0 0 0 0 0 0 0 0 0 0]
 [0 0 0 0 0 0 0 0 0 0 0 0 0 0 0 0 0 0 0 0]
 [0 0 0 0 1 1 1 0 1 1 1 0 1 1 1 0 1 1 1 0]
 [1 1 1 0 1 1 1 0 1 1 1 0 0 0 0 0 0 0 0 0]
 [0 0 0 0 0 0 0 0 0 0 0 0 0 0 0 0 0 0 0 0]
 [0 0 0 0 0 0 0 0 0 0 0 0 0 0 0 0 0 0 0 0]
 [0 0 0 0 0 0 0 0 0 0 0 0 0 0 0 0 0 0 0 0]
 [0 0 0 0 1 1 1 0 1 1 1 0 1 1 1 0 1 1 1 0]
 [1 1 1 0 1 1 1 0 1 1 1 0 1 1 1 0 1 1 1 0]
 [1 1 1 0 1 1 1 0 1 1 1 0 1 1 1 0 1 1 1 0]
 [1 1 1 0 1 1 1 0 1 1 1 0 0 0 0 0 0 0 0 0]
 [0 0 0 0 0 0 0 0 0 0 0 0 0 0 0 0 0 0 0 0]
 [0 0 0 0 0 0 0 0 0 0 0 0 0 0 0 0 0 0 0 0]
 [0 0 0 0 0 0 0 0 0 0 0 0 0 0 0 0 0 0 0 0]]
```

Fig. 7 – An example of the program – the original array

```
[[ 0  0  0  0  0  0  0  0  0  0  0  0  0  0  0  0  0  0  0  0]
 [ 0  0  0  0  0  0  0  0  0  0  0  0  0  0  0  0  0  0  0  0]
 [ 0  0  0  0  0  0  0  0  0  0  0  0  0  0  0  0  0  0  0  0]
 [ 1  1  1  0  2  2  2  0  3  3  3  0  4  4  4  0  5  5  5  0]
 [ 1  1  1  0  2  2  2  0  3  3  3  0  4  4  4  0  5  5  5  0]
 [ 1  1  1  0  2  2  2  0  3  3  3  0  4  4  4  0  5  5  5  0]
 [ 1  1  1  0  0  0  0  0  0  0  0  0  0  0  0  0  0  0  0  0]
 [ 0  0  0  0  0  0  0  0  0  0  0  0  0  0  0  0  0  0  0  0]
 [ 0  0  0  0  6  6  6  0  7  7  7  0  8  8  8  0  9  9  9  0]
 [10 10 10  0  6  6  6  0  7  7  7  0  0  0  0  0  0  0  0  0]
 [ 0  0  0  0  0  0  0  0  0  0  0  0  0  0  0  0  0  0  0  0]
 [ 0  0  0  0  0  0  0  0  0  0  0  0  0  0  0  0  0  0  0  0]
 [ 0  0  0  0  0  0  0  0  0  0  0  0  0  0  0  0  0  0  0  0]
 [ 0  0  0  0 11 11 11  0 12 12 12  0 13 13 13  0 14 14 14  0]
 [15 15 15  0 11 11 11  0 12 12 12  0 13 13 13  0 14 14 14  0]
 [15 15 15  0 11 11 11  0 12 12 12  0 13 13 13  0 14 14 14  0]
 [15 15 15  0 11 11 11  0 12 12 12  0  0  0  0  0  0  0  0  0]
 [ 0  0  0  0  0  0  0  0  0  0  0  0  0  0  0  0  0  0  0  0]
 [ 0  0  0  0  0  0  0  0  0  0  0  0  0  0  0  0  0  0  0  0]
 [ 0  0  0  0  0  0  0  0  0  0  0  0  0  0  0  0  0  0  0  0]]
```

Fig. 8 – An example of the program's operation – the resulting array

From the material discussed above, it is clearly seen that modern image processing tools make it possible to successfully solve the problem of selecting and counting connected objects in binary images.

References

1. W. Prett. Digital image processing. In 2 volumes.—M.: Mir, 1982.

2. Review of the main image contours detection algorithms. URL: https://newtechaudit.ru/obzor-osnovnyh-algoritmov-vydeleniya-konturov-izobrazheniya/ (accessed 09/14/2022).

3. Computer vision lessons in Python. URL: https://itnan.ru/post.php?c=1&p=654663 (accessed 09/14/2022).

CALCULATION OF THE POWER OF THE SEA SURFACE ECHO SIGNAL OBSERVED IN THE ELEMENT OF RESOLUTION OF THE AIRBORNE LOCATION COMPLEX

Yudin Ivan
Saint Petersburg State University of Aerospace Instrumentation,
Saint Petersburg, Russia
E-mail: ivan-yudin@mail.ru

Abstract. *The paper presents analytical expressions for calculating the power of the radar signal reflected from the sea surface, observed in the resolution elements of the onboard complex of an aircraft that detects marine objects in distress.*
Keywords: *sea surface, resolution element, detection, echo signal, airborne complex, aircraft.*

Recently, due to the warming of the Earth's climate, natural disasters – earthquakes, tsunamis, hurricanes, etc. – have become more frequent and significantly intensified. These phenomena pose the greatest danger to marine vessels, since they most often lead to all kinds of disasters. Therefore, the search for ships in distress far from land is a very important task, in solving which the greatest attention is paid to minimizing the search time for a ship in distress in order to provide it with timely assistance [1,2].

Algorithms for minimizing the search time for sea vessels use information about the probabilistic map of the vessel's location in a certain area, called the search area [3,4]. This information allows optimizing the configuration of the search area and minimizing the search time by viewing the resolution el-ements of the airborne radar complex performing the search, in which the probability of the presence of the desired physical object is maximum [5,6].

With such a view of the resolution elements, the problem is solved only about the presence of the desired marine object in a given element. However, the search task is the object detection problem [7]. The main criterion for detecting an object is the probability of correct detection $P_{по}$ at a fixed false alarm probability $P_{лт}$.

The probability of correct object detection $P_{по}$ depends on the detection algorithm and on the signal-to-noise ratio, and the false alarm probability depends on the detection algorithm, search area configuration, the number of resolution elements in this area, the power level of the inherent noise of the receiving equipment of the airborne radar complex and the power of echo signals underlying surface, in this case, the underlying surface of the sea [7,8]. In this paper, we also analyze analytical relationships that allow us to calculate the power of sea surface echo signals taking into account the generalized characteristics of the onboard equipment, the conditions for observing the sea surface, and the characteristics of sea waves.

When considering the problem posed, we confine ourselves to analyzing the powers of the sea surface echo signals observed at the receiver input in the range strobe of the onboard equipment [8], which is illustrated in Fig. 1 showing: range strobe and sea-reflected view.

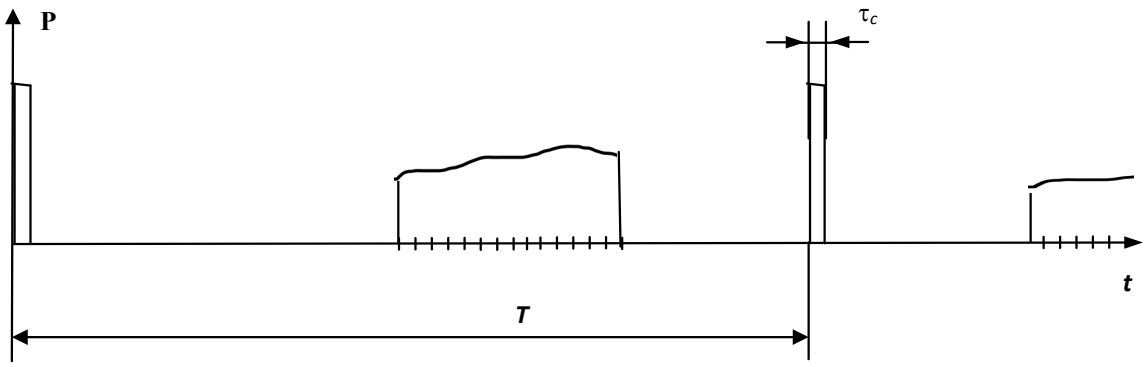

Fig. 1. Receiver range strobe

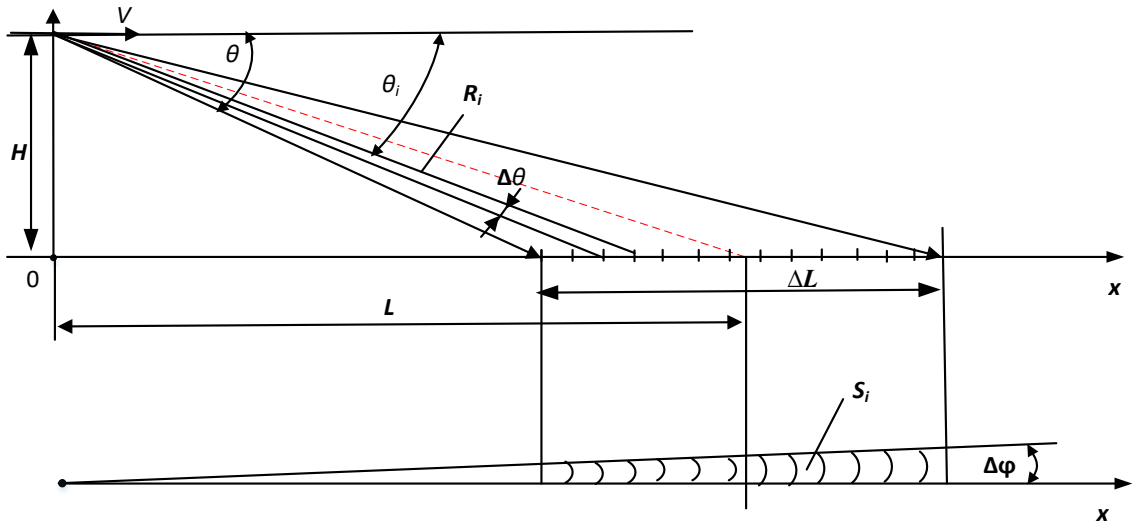

Fig. 2. Range track

The following designations are adopted in Fig. 2: H – the flight altitude of the aircraft; L – the distance to the center of the search area in the polar coordinate system, which, due to the condition $H << L$, practically coincides with the slant range R_i; (ΔL) – the dimensions of the search area along the range coordinate ΔL; $\Delta\varphi$ – the width of the needle pattern of the onboard radar antenna system in both planes.

The average power $\tilde{P}_i$ of the probing radar signal reflected from the sea surface, limited by the i-th resolution element of the onboard radio-electronic complex, can be represented by the expression [8]

$$\tilde{P}_i = \frac{G_i^2 P_{\text{прд}} \lambda^2 \eta}{(4\pi)^3 R_i^4} \cdot S_i, \tag{1}$$

where $P_{\text{прд}}$ – the transmitter power, λ – the wavelength of the probing radar pulse, η – the loss factor, Ri – the slant distance to the i-th resolution element of the sea surface in the range strobe of the receiving device, G_i – the gain of the radiation pattern in the direction during radiation and reception on one antenna, S_i – the effective reflecting surface of the i-th resolution element of the sea surface.

The effective reflective surface S_i depends on its area s_i and the specific effective reflective surface of the i-th resolution element σ_i^0, $S_i = s_i \cdot \sigma_i^0$ [8,9].

The area of the sea surface area illuminated by the radar s_i is equal to

$$s_i = \frac{c\tau_c}{2\cos\theta_i} \Delta\varphi R_i, \tag{2}$$

where τ_c – the duration of the probing pulse, c – the speed of light, $\Delta\varphi$ – the width of the radiation pattern of the antenna system of the onboard radio-electronic complex in the horizontal plane, – the viewing angle in the vertical plane of the i-th surface element.

Substituting expression (2) and σ_i^0 into formula (1), we obtain

$$\tilde{P}_i = \frac{G_i^2 P_{\text{прд}} \lambda^2 \eta}{(4\pi)^3 R_i^3} \cdot \frac{c\tau_c}{2\cos\theta_i} \Delta\varphi \sigma_i^0. \tag{3}$$

The specific effective reflective surface of the resolution element σ_i^0 in different scientific sources is represented by different empirical expressions [10,11,12] obtained by the authors when processing the results of field experiments. The analysis of these sources shows that the expressions give similar results, differing by no more than three decibels, which fits into the error accepted when using mathematical models in engineering calculations.

The most convenient expression for calculations in decibels for σ_i^0 is given in [12]

$$\sigma_i^* = \sigma_i^*\left(\lambda, W, \psi, \theta_i\right) = 10\left[1,6\lg\left(\theta_i + 0,5\right) + \frac{0,9}{\lambda}\left(W - \frac{\psi_i}{\pi} - \sin\psi_i\right) - 5\right], \quad (4)$$

where, ψ_i – in radians, λ – wavelength in centimeters, W – sea waves in points, ψ – view of the direction of movement of sea waves in radians, $\square$ – viewing angle of the i-th resolution element in degrees, – in decibels per square meter. Expression (4) is given for vertical polarization; for horizontal polarization σ_i^* the value must be reduced by approximately 7-12 decibels.

The expression for in times, used in the above formulas, is written as

$$\begin{aligned}\sigma_i^0 &= \sigma_i^0\left(\lambda, W, \psi, \theta_i\right) = 10^{0.1\sigma_i^*(\lambda, W, \psi, \theta_i)} = \exp\left(0.23 \cdot \sigma_i^*\left(\lambda, W, \psi, \theta_i\right)\right) = \\ &= \exp\left(0.23 \cdot \left(1,6\lg\left(\theta_i + 0,5\right) + \frac{0,9}{\lambda}\left(W - \frac{\psi_i}{\pi} - \sin\psi_i\right) - 5\right)\right).\end{aligned} \quad (5)$$

Expression (5), which is valid for vertical polarization, is the final expression that can be used to calculate the power of radar signals reflected from a sea surface area, the area of which is limited by the resolution element area of the onboard equipment.

REFERENCES

1. Shepeta A.P. Determination of the search area for a surface object according to preliminary target designation data. Information and control systems. 2012. No. 4 (59). pp. 98-99

2. Yudin I., Grigoriev E., Zhuravlev A.**,** Method of Determining the Size of the Search Area a Moving Object on a Priori Information to Meet the Challenges of Modern Search Ministry for Emergency Situations Disaster Zones Structure. Bulletin of the UNESCO department “Distance education in engineering” of the SUAI: Collection of the papers. St. Petersburg, Issue 5.– SPb.:SUAI, 2016, pp. 35-36.

3. Shepeta A.P., Nenashev V.A. Optimization the size of the search area for moving physical objects based on preliminary target designation data // В сборнике: 2021 Wave Electronics and its Application in Information and Tel-ecommunication Systems, WECONF 2021 – Conference Proceedings. 2021. С. 9470590.

4. Podoplekin Yu.F., Shepeta D.A., Ivanova M.S. Calculation of the search area for physical objects, taking into account a priori information about their movement // Marine Radio Electronics No. 3 (77) September 2021, pp. 30-33.

5. Podoplekin Yu.F., Shepeta D.A., Ivanova M.S. Probabilistic map of the location of an object in the resolution elements of an onboard radar // Marine Radioelectronics No. 4 (78) December 2021, pp. 30-33.

6. Podoplekin Yu.F., Shepeta A.P., Ivanova M.S. Optimization of the search mode for marine objects in the far field of view // Marine radio electronics No. 3 (81) September 2022, pp. 39-40.

7. Izrantsev V.V., Shepeta D.A. Modeling of external signals of onboard instrument complexes of fifth-generation aircraft. Scientific instrumentation. 2000. Vol. 10. No. 2. pp. 14-19.

8. Blaunstein N. S., Sergeev M. B., Shepeta A. P. Prikladnye aspekty elektrodinamiki [Applied Aspects of Electrodynamics]. Saint Petersburg, Agraf+ Publ., 2016. 272 p. (In Russian).

9. Isakov V.I., Modeling location signals. reflected from the edge of the land-sea/ D.A. Shepeta., V.I. Isakov // Information management systems. 2017. No5 (90). P. 89-94.

10. hepeta D.A. Development of mathematical models and synthesis of algorithms for modeling input signals of on-board information processing and control systems. Dissertation for the degree of Candidate of Technical Sciences / St. Petersburg, 2000.

11. Sesin A.E., Shepeta D.A. Mathematical model of echo signals of the sea surface observed by onboard locators of aircraft // Information–control systems. 2010. No. 2(45). pp. 21-25.

12. Tverskoy G.N., Terentyev G.K., Kharchenko I.P. Simulators of echo signals of ship radar stations, Publishing House "Shipbuilding", 1973. p. 224.

ROBUST STUDY OF PARAMETER ESTIMATES REGRESSION CURVE

Zakharova Alexandra
Ivangorod branch of Saint Petersburg State University of Aerospace Instrumentation,
Saint Petersburg, Russia,
E-mail: zaharova.psk@mail.ru

Abstract. *The paper proposes a method for estimating the robustness of the parameters of regression dependencies constructed using the least squares method. The parameters are estimated by the method of mathematical modeling of non-Gaussian distributions with weighted tails used as contaminating distributions of Tukki and Huber mathematical models.*
Keywords: *robustness, least squares method, regression dependence, clogging distribution, weighted tails of distributions, Tukki's model, Huber's model.*

The design of complex systems necessarily involves a forecast of the assessment of their quality characteristics, which must be achieved by the time they are put into operation [1]. One of the most common and effective forecasting methods is a forecast based on regression dependencies. When using regression curves, it is assumed that the original data on which this forecast is based contains some errors, and these errors follow a normal distribution. Therefore, to estimate the parameters of the regression curves, the least squares method is used, which is the best among all estimates with a normal distribution of errors. In the case when the errors are distributed according to a law different from normal, all conclusions regarding the accuracy of the estimates obtained may not correspond to reality [2]. Therefore, the assessment of the stability of the estimates obtained under these conditions needs to be verified.

The stability of estimates to changes in the conditions that were adopted during their synthesis is assessed by the “deterioration” of the characteristics of the estimates with corresponding deviations from the accepted conditions and assumptions. At present, in relation to our problem, it is necessary to change, within certain limits, the assumptions about the distribution of errors in the initial data. This resistance to changes in the statistical characteristics of errors is called the robustness of estimates [3]. The study of robustness, most often, is carried out by changing the statistical characteristics of the distribution of errors, which are reduced to the study of characteristics when the tails of distributions are weighted.

At the same time, the Tukki and Huber models are most often used, which use as the main distribution the distribution adopted in the synthesis of algorithms for estimating the parameters of distributions, in our case this is a normal distribution, and the so-called clogging distribution is added to this main distribution [3]. However, this is not the only approach to the study of robustness. Another approach is to replace the original distribution with another distribution, usually with a weighted tail [4,5], since such a replacement puts the work of the algorithms under test in conditions that approach the worst conditions, which is well known from practice.

n this paper, the above approaches to the study of robustness are considered and the corresponding clogging distributions and distributions with weighted tails are proposed. Verification of robustness for non-Gaussian distributions is possible, as a rule, only by simulation methods [6], therefore, in the work, we limited ourselves to describing the algorithms for generating the proposed distributions. These algorithms are considered in relation to pairwise regression, since this is not fundamental, since it does not limit the generality of the consideration and practical applicability of the proposed algorithms.

Consider the problem statement. There is a dataset

$$\begin{pmatrix} x_1 & x_2 & \dots & x_n \\ y_1 & y_2 & \dots & y_n \end{pmatrix}, \tag{1}$$

in which under xi in our case we mean time readings, not necessarily equally spaced, and under y_i – indicators that require a forecast, $i=1,2,...n$. It is required to find a dependence, which, without loss of generality, for simplicity, we assume to be linear

$$y=\varphi(x, b_0, b_1,\dots b_m)= b_{0+} b_1 x. \tag{2}$$

In fact, it is necessary to find the "best" values b_0 and b_1. To do this, we use the least squares method, that is, we minimize the quadratic form

$$S(b_0,b_1)=\sum_{i=1}^{n}(b_0+b_1x_i-y_i)^2\to\min_{b_0,b_1}S(b_0,b_1), \tag{3}$$

the minimum of which is determined by the roots of the system of equations [7]

$$\begin{cases}\dfrac{\partial S(b_0,b_1)}{db_0}=\dfrac{\partial}{db_0}\sum\limits_{i=1}^{n}(b_0+b_1x_i-y_i)^2=2\sum\limits_{i=1}^{n}(b_0+b_1x_i-y_i)=0,\\ \dfrac{\partial S(b_0,b_1)}{db_1}=\dfrac{\partial}{db_1}\sum\limits_{i=1}^{n}(b_0+b_1x_i-y_i)^2=2\sum\limits_{i=1}^{n}(b_0+b_1x_i-y_i)x=0.\end{cases} \tag{4}$$

Transforming system (4) to the form

$$\begin{cases}b_0+b_1\overline{x}=\overline{y}\ ,\\ b_0\overline{x}+b_1k_{xx}=k_{xy},\end{cases} \tag{5}$$

find its solution

$$\begin{cases}b_1=\dfrac{k_{xy}-\overline{x}\cdot\overline{y}}{k_{xx}-\overline{x}^2}=\dfrac{\operatorname{cov}(x,y)}{s_x^2},\\ b_0=\overline{y}-b_1\overline{x}=\overline{y}-\dfrac{k_{xy}-\overline{x}\cdot\overline{y}}{k_{xx}-\overline{x}^2}\overline{x}=\overline{y}-\dfrac{\operatorname{cov}(x,y)}{s_x^2}\overline{x},\end{cases} \tag{6}$$

$$\overline{x}=\frac{1}{n}\sum_{i=1}^{n}x_i,\quad \overline{y}=\frac{1}{n}\sum_{i=1}^{n}y_i\quad k_{xx}=\frac{1}{n}\sum_{i=1}^{n}x^2{}_i\qquad k_{xy}=\frac{1}{n}\sum_{i=1}^{n}x_iy_i. \tag{7}$$

Let's move on to algorithms. So, let the true dependence of y on x be determined by a linear function $y=b_0^*+b_1^*x$, where b_0^* and b_1^* the true coefficients of this dependence, which the least squares method should determine. We observe *y* values with errors ε distributed according to some law *f(x)*, so the data set y_i, is a set of random variables $y_i=b_0^*+b_1^*x_i+\varepsilon_i, i=1,2,\ldots n.$. We consider random variables εi to be equally distributed and independent in the aggregate. In the classical regression model, these quantities have a normal distribution with zero mean and variance σ^2 [7]. Under these assumptions, the estimates defined by expressions (6) are the best.

In the study of robustness, $x_i, i=1,2,\ldots n,$ the quantities can be considered constant deterministic quantities, physically these can be, for example, time readings in which the quantities $y_i, i=1,2,\ldots n.$ are determined. Therefore, in expressions (7), the quantities $\overline{x}=\frac{1}{n}\sum_{i=1}^{n}x_i,\ k_{xx}=\frac{1}{n}\sum_{i=1}^{n}x^2{}_i$ remain constant throughout the entire simulation process, although the study of robustness can be extended to these quantities, introducing temporary fluctuations.

Under the above conditions, under the accepted restrictions, the simulation algorithm for studying the robustness of estimates (6) in steps can be described as follows:

1)

the true values b_0^* and b_1^* of the coefficients and are set;

2)

the law of distribution of random errors $f_\varepsilon(x)$ is set;

3) a sample of random variables is formed for given values $y_i=b_0^*+b_1^*x_i+\varepsilon_i, i=1,2,\ldots n,$, which we consider to be constant deterministic variables $x_i, i=1,2,\ldots n,$;

4) according to expression (6), estimates b_0 and b_1 are calculated;

5) return to point 3), repeat the calculations of points 3) and 4), repeating this process m times;

6)) after the completion of the collection of statistics, we obtain a sample of m values of the evaluation vectors $(b_0, b_1)^T$;

7) we process the received sample, extracting the information we need – distribution laws, confidence intervals, variances of estimates, etc. [8].

8) draw conclusions about the stability of estimates with respect to the introduced deviations from the classical regression model.

As a universal mathematical model of the distributions $f_\varepsilon(x)$, one can use the Huber model [3], from which, as special cases, one can obtain both the Tukki model and models with weighted distribution tails.

The Huber model is written as

$$f_\varepsilon(x) = (1-\gamma)\cdot f_0(x) + \gamma \cdot f_з(x) \tag{8}$$

where $f_0(x)$ the main error distribution is ε , $f_з(x)$ the "clogging" distribution, and γ is the clogging coefficient.

For the Tukki model, $f_0(x)$ and $f_з(x)$ the distributions and are normal with zero means, but the variance of the polluting distribution is much larger than the variance of the main one, which leads to the appearance of "tails" of the distribution $f_з(x)$.

For the Huber model, in our case, we should take the normal distribution as the main distribution $f_0(x)$, as well as for the Tukki model, and use non-Gaussian distribution densities that are symmetric with respect to zero as a clogging one. The most acceptable are the Laplace distribution – double exponential, and symmetric logarithmic-normal distribution, proposed and considered in [9].

The third option, in our opinion, the most difficult one, is to set the clogging coefficient equal to unity γ=1 in expression (8), and use the Laplace distribution and the symmetric log-normal distribution as clogging distributions.

In the case when γ=0, when using the Tukki model, we get a classic version of the study of estimates of the parameters of regression curves with a normal distribution of errors, but this study is performed using simulation modeling. This, in particular, makes it possible to study nonlinear dependencies and introduce error correlation [10] when forming y values.

Bibliographic list

1. Izrantsev V.V., Shepeta D.A. Simulation of external signals of on-board instrumentation complexes of aircraft of the fifth generation. Scientific instrumentation. 2000. V.10. No. 2. pp. 14-19.

2. Zakharova A. Yu., Tyurinova V. A., Shepeta A. P. Evaluation of regression curve parameters using the Huber model // Young scientist. – 2022. – No. S47-1 (442-1). – S. 52-54. – EDN CXQGWX.

3. Huber J.P. Robustness in statistics / Per. from English-M.: Mir, 1984.- 304 p., ill.

4. Ivanova M.S., Isakov V.I., Shepeta D.A. Simulation Models of Input Signals of Information Processing Systems Synthesized from Empirical DATA. In the collection: 2020 Wave Electronics and its Application in Information and Telecommunication Systems, WECONF 2020. 2020. P. 9131164.

5. Ivanova M.S., Shepeta A.P. Algorithms for modeling information flows of information processing systems, synthesized from empirical data. In the book: Processing, transmission and protection of information in computer systems 21st International scientific conference: collection of reports. St. Petersburg, 2021. P.20-24.

6. Shalygin A.S., Palagin Yu.I. Applied Methods of Statistical Modeling – L.: Mashinostroenie. Leningrad. department, 1986. – 320 p.

7. Ayvazyan S., Mkhitaryan V., Applied statistics, Fundamentals of econometrics (in 2 volumes), M.: UNITY-DANA, 2001 – 2nd ed., Rev., p. 656+432.

8. Kobzar A.I. Applied mathematical statistics. For engineers and scientists. – M. Fizmatlit. 2006 -816 p.

9. Tyurinova V.A., Shepeta D.A., Isakov V.I. Direct method for modeling the log-normal distribution // In the book: Wave electronics and infocommunication systems. Collection of articles of the XXV International Scientific Conference. In 3 parts. St. Petersburg, 2022, pp. 135-139.

10. Shepeta D.A. Development of mathematical models and synthesis of algorithms for modeling input signals of onboard information processing and control systems. Thesis for the degree of candidate of technical sciences / St. Petersburg, 2000.

DEVELOPMENT OF SOFTWARE FOR CLASSIFICATION AND RECOGNITION OF MOVING OBJECTS IN A STREAM OF VIDEO FRAMES BASED ON A NEURAL NETWORK METHOD AND THEIR MAPPING ON A DIGITAL TERRAIN MODEL

Zalishchuk Aleksandr
Saint Petersburg State University of Aerospace Instrumentation
Saint Petersburg, Russia
E-mail: sacha1501@yandex.ru

Abstract. *This article talks about a way to efficiently track road transport in a video stream. Neural network methods are presented for embedding in a complex transport management system. Also presented is a method for creating a digital terrain model using image segmentation with transport overlay on the finished model. This method will contribute to the rapid processing of data on the current state of the road flow without extraneous factors and will allow faster processing of information about each vehicle by ignoring the processing of a static background in the video stream.*
Keywords*:video stream, image segmentation, digital terrain model, tracking, recognition system, vehicle detection, machine learning, vehicle counting.*

Introduction

The importance of the theme of accurate classification and recognition of transport objects in the stream of video frames [1] is growing significantly in the field of traffic management. Every year the size of road traffic increases and resources to process this data also increase.

An extensive installation of traffic cameras is used to cover all highways, because vehicle detection and statistics in the video stream are of great importance for intelligent traffic management and highway control.

However, to analyze the dynamics of objects in the considered space in real time additional computational costs and a special approach to the distribution of resources between the components of the computer system would be required [2].

To solve this problem we need to use a classification and recognition system for transport moving objects based on computer vision with neural network methods. The system also uses the method of analyzing video frames with mapping information on a digital terrain model. That is, based on the video stream, the system generates a digital terrain model and uses it to map the data received from the neural network architecture without unnecessary information about the static background.

To test the proposed system we use video recordings from road surveillance cameras on the highway.

Using Neural Network Methods for Real-Time Detection

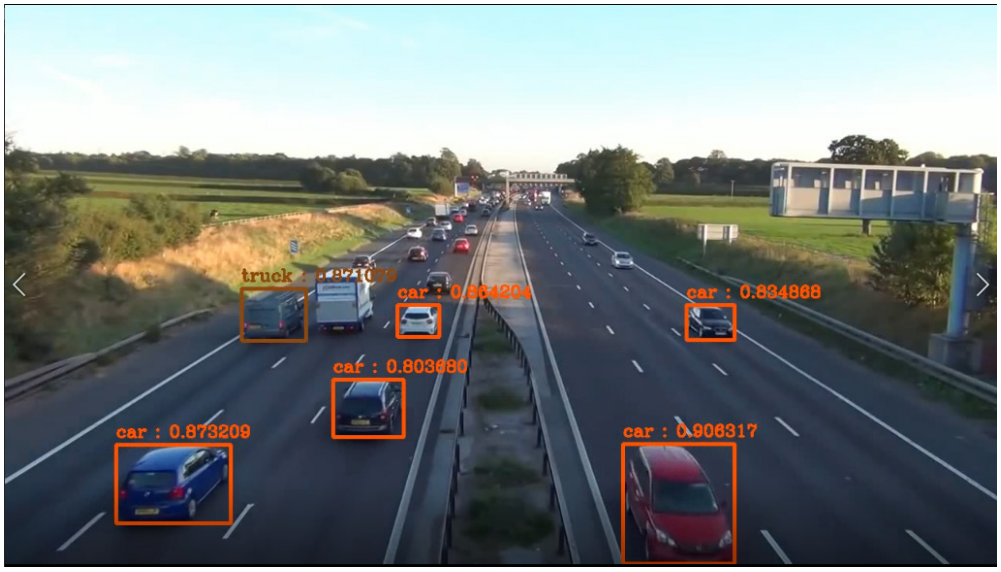

Fig. 1 – Recognition of vehicles using the developed system

In computer vision, real-time object detection is a very important problem that is often a key component of computer vision systems. An object detector [3] is an algorithm that performs recognition tasks by taking an image as input and then predicting the bounding boxes and class probabilities for each object in the image (Fig. 1).

Most of the algorithms use a Convolutional Neural Network (CNN) [4] to extract features from an image in order to predict the probability of learned classes.

As such a detector, the system uses the model of the detection algorithm " YOLOv7" [2], pre-trained on one of the largest datasets "MS COCO" [6]. The official documentation demonstrates how this improved model outperforms all previous versions of YOLO as well as all other object detection models in terms of speed and accuracy on the "MS COCO" dataset (achieving this performance was obtained without using any pre-trained weights, which shows excellent coherence of architecture).

This model detects and classifies objects in a real-time video frame stream with good accuracy, showing high speed visual information processing capabilities, which puts it in an honorable place as one of the best models for solving transport problems.

Description of composition of the system and the principle of its operation

For the system to work, an analysis was made of connecting and activating the model on video recordings from road cameras. All libraries for work were installed and were organized in a virtual environment [7] – to avoid intersections with other programs, which can later be used when deployed on another server.

At the beginning of work, the system analyzes the first 500 video frames and, using the median filter [8], removes all moving objects in the picture – getting a “clean” road (Fig. 2)

Fig. 2 – Preparing the background for generating a digital terrain model

Then, a Gaussian blur and a Canny edge detector [9] are applied to the resulting image to search for “road markings” (Fig. 3).

Fig. 3 – Highlighting the boundaries of the road

After that, a “manually” mask is created to determine the area with road markings [10], and which will later determine the vehicle detection area (Fig. 4). For each camera, this area can be adjusted through its points in the image, which can be set during the initial system setup.

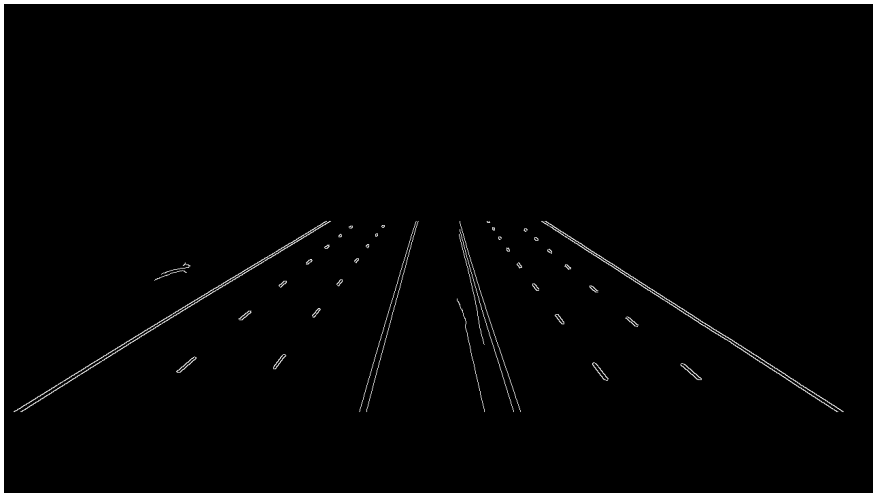

Fig. 4 – Determination of the area of road markings

And now the resulting image is analyzed for the presence of lines using the Hough transform [11] and the resulting lines are averaged into two bands through polynomials (Fig. 5).

Fig. 5 – The result of the search for highway markings

Based on the received marking data, a digital terrain model is created, which displays the results of the detection and classification of vehicles (Fig. 6).

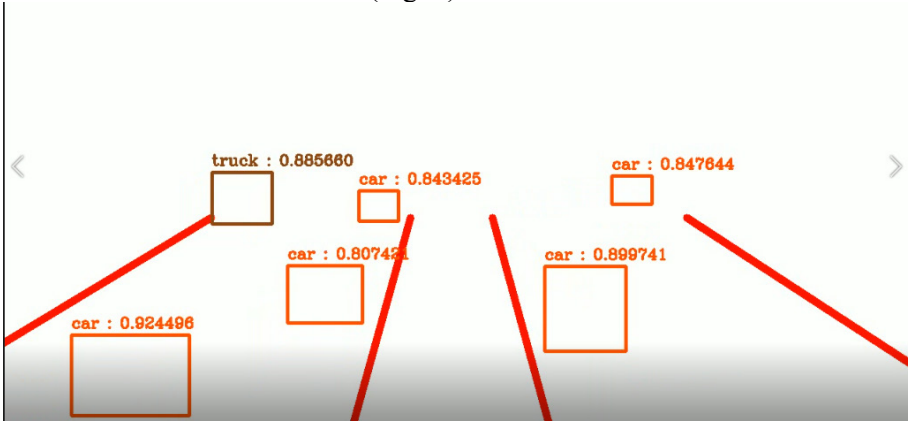

Fig. 6 – Displaying the results of recognition and classification on a digital terrain model

It is worth noting that the system was limited to detecting objects only near the camera and this was done in order to improve the efficiency of tracking and recognition of objects, because. technically, models of the " YOLO "[12] family cannot process a huge number of objects at once.

However, the system manages the task of finding and recognizing transport in a given area quickly and efficiently.

Gratitude

The author expresses his sincere gratitude to his supervisor, Associate Professor V. A. Nenashev for his help and valuable advice in the preparation of this article.

Conclusion

The result of the development of the application is a comprehensive system of software video processing in real time for the detection and classification of moving objects.

The system copes with the task of identifying and recognizing transport in a given area quickly and efficiently. This system improves the accuracy of object detection from the point of view of video surveillance on the road and builds a plan for tracking detection and collecting traffic information within the field of view of the camera.

Reference

1. Polischukov R.M. Vehicle recognition in streaming video with machine learning // Actual research. 2020. No. 8 (11). pp. 20-24. URL: https://apni.ru/article/607-raspoznavanie-transportnikh-sredstv-v-potokov (Date of access: 02/05/2023)

2. Dushkin, R. V. Intelligent transport systems: monograph / R. V. Dushkin. – Moscow: DMK Press, 2020. – 280 p.

3. Christopher M. Bishop, Pattern Recognition and Machine Learning, Springer, 2006.

4. Ross Girshick, Jeff Donahue, Trevor Darrell, and Jitendra Malik. Rich feature hierarchies for accurate object detection and semantic segmentation. In Proceedings of the IEEE Conference on Computer Vision and Pattern Recognition (CVPR), pages 580–587, 201

5. WongKinYiu / yolov 7 // GitHub URL : https :// github . com / WongKinYiu / yolov 7 (accessed 02/07/2022).

6. Lin T.Y. et al. Microsoft COCO: Common objects in context // Lect. Note Comput. sci. (including Subser. Lect. Notes Artif. Intel. Lect. Notes Bioinformatics). 2014. Vol. 8693 LNCS, no. PART 5, pp. 740–755.

7. Virtual Environments and Packages // Python.org URL: https://docs.python.org/3/tutorial/venv.html (accessed 2/8/2023).

8. Lizhe Tan, Jean Jiang Digital Signal Processing. – Academic Press, 02.10.2018. – 920 p.

9. Canni border detector // Sudo Null IT News URL : https :// habr . com / ru / post /114589/ (date of access: 02/08/2023).

10. Image Masking with OpenCV // PyImageSearch URL: https://pyimagesearch.com/2021/01/19/image-masking-with-opencv/ (date of access: 02/12/2023).

11. Hough Algorithm for Detecting Arbitrary Curves in Images // Sudo Null IT News URL : https :// habr . com / ru / post /102948/ (date of access: 02/10/2023).

MUSCLE MOTION ANALYSIS DEVICE

Zyryanov Dmitry
Saint Petersburg State University of Aerospace Instrumentation,
Saint Petersburg, Russia
E-mail: zyrikdima@gmail.com

Abstract. *Muscle motion analysis devices have great potential for use in all areas of human activity. Such devices can be used to control robots, computers, phones, cars, can be used in prostheses and medical devices. However, at the moment there are many problems that do not allow their use in a wide range of devices. The article describes the problems associated with the development, operation, adjustment and calibration of the device and offers possible solutions with a practical example. The article also describes the potential of using muscle motion analysis devices.*

Theoretical summary

Every day there are more and more devices that interact with human bioelectrical signals. In addition, the capabilities of these devices are expanding, if previously they were represented only by bionic prostheses, now there are gesture recognition devices for the deaf-mute, devices for remote diagnostics of cardiovascular diseases, muscle and brain diseases, etc. All this clearly shows the feasibility of introducing bioelectrical signal acquisition technology in other areas, including everyday life. But at the same time there is a need to develop new, small-sized devices. Let us consider the tasks that a device for analyzing muscle movements can perform.

One of the most important advantages of devices that interact directly with bioelectrical signals is the ability to recognize gestures in people with amputations. This makes it possible not only to significantly expand the functionality of modern prostheses, but also to enable a person to interact with the world indirectly. For example, in 2019, students at Novosibirsk State University developed software solutions that allow gesture recognition and translation from sign language through a camera [1]. A similar device in the form of a glove was developed by scientists from the University of California, San Diego. However, all of these devices interact with existing limbs, and the muscle recognition device allows giving such functionality to people with disabilities as well. In addition, it will be mobile and easy to use.

Another application of muscle movement recognition devices is virtual reality. Thanks to bioelectric signal sensors, primitive input devices can be dispensed with. This will not only expand functionality and improve immersion in virtual reality, but also enable people with disabilities to interact with virtual reality. In turn, this opens up new opportunities not only in the gaming field, but also in industry. In some software working with digital twins, simulation models, it is possible to interact with the simulation and the model through virtual reality. For example, Visual Components software packages have such functionality (Fig. 1). This gives a person the opportunity to participate in the development of models, in the study of the future behavior of the enterprise, identifying development errors [2]. In addition, when using this product or another one aimed at working with robots, such as Delfoi Robotic, it is possible to remotely configure, commissioning robots in the enterprise, writing control programs, testing operation, checking collisions and compliance with safety zones.

As mentioned earlier, the muscle analyzer can be used as an input device. This makes it possible to work remotely with some objects. For example, it will be useful for speakers or speakers using special consoles to control presentations, artists, for remote control of lighting, the stage, directors and cinematographers, to control cameras, objects on stage, workers with a robot cell to control the positions of the robot. However, it facilitates the work of not only narrowly focused specialists, but also ordinary people: remote control of computers, TVs, smart homes. These solutions can already be seen in the form of voice commands in smart houses, smart music speakers, but at the same time the potential of gestures is not less huge. In addition, this technology allows people who are deprived of the ability to interact with computers and other devices to regain this ability.

Modern technological solutions in the field of everyday activities significantly expand human capabilities. So, for example, a smart watch, originally necessary for getting information about the time, now allows performing routine actions faster: viewing messages, quick search for information on the Internet, getting data about the body [3, 4]. And the last point is especially important for consideration of the problem of diagnosing human health without visiting medical personnel. According to a study conducted by the Journal of Biomedical Informatics in 2016 [5], the theory is confirmed that with the help of

smart watches it is possible to volumetrically monitor the human condition at a distance from doctors. This makes it possible not only to detect diseases such as epilepsy, Parkinson's disease, but also to monitor patients with cardiovascular diseases, obesity, etc. Along with this, the need for modern people to get relevant information about their heart rate, caloric intake, and health in general is being met. However, other studies in the U.S. confirm the discrepancy between the figures obtained from the watch and the indicators of special medical devices by more than 27%, which confirms the idea that even with remote diagnostics requires consultation with specialists. However, because of the increasing trust in the Internet, in particular in forums, where laypeople often write, as confirmed by research by the Public Opinion Foundation in 2019, there is the opposite danger of improper self-medication.

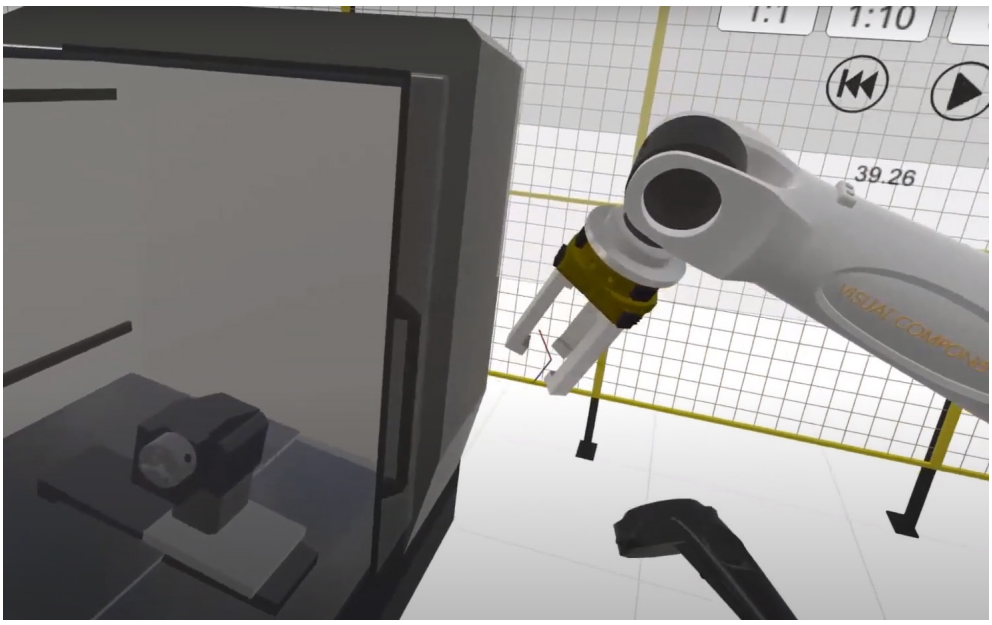

Fig. 1 – Visual Components

All this confirms the usefulness of introducing background diagnostics by devices interacting with humans. And hence, it is reasonable to implement diagnostics of diseases and pathologies of nerves and muscles, such as: polyneuropathy, mononeuropathy, tunnel syndrome, vitamin B, E, C deficiency, into the device of muscle movement analysis as well. To perform this task, it is necessary to implement background data accumulation in the device, as well as background analysis of these data on the basis of standard techniques of electromyographic study. This is possible with volumetric interaction with medical workers during device development.

It is also worth noting the possibility of interaction of the muscle motion analysis device with other sensors. For example, a gyroscope and accelerometer may allow receiving not only gestures, but also their location in space; pulse sensors may give a more complete picture of a person's health status; additional interfaces, for example a watch, may extend the functionality for everyday use.

Existing devices. There are two types of muscle movement analysis devices at the moment: medical EMG devices, bionic prostheses. The first group of devices does not have mobility. Most often the electrodes for EMG devices are needle-like (invasive), which makes it impossible to use them for a long time. Bionic prostheses are more interesting as a representative of an everyday mobile device. At their core they have myographic sensors, which are connected to the prosthesis microcontroller [6]. All over the world there are many companies producing bionic prostheses: "Touch Bionics", "Frost & Sullivan", MeHandA and many others. However, at the moment there are no bright representatives of prostheses with gesture recognition and individual finger movements, many prostheses do not have separated fingers, but move synchronously. Gestures are implemented using pre-recorded commands. Today, there are no generally accepted solutions to this problem, but there are developments that rely on the introduction of new data processing algorithms, such as neural networks. Prosthetic companies also distribute individual myographic sensors that can be connected to a computer, smartphone or other device [7]. For example: MYOstack, MYO, Myoware. The functionality of these sensors is determined by the user. Often a person requires extensive skills and knowledge. There are no universal ready-made devices now. It speaks about the relevance of development of such devices.

Existing devices

There are two types of muscle movement analysis devices at the moment: medical EMG devices, bionic prostheses. The first group of devices does not have mobility. Most often the electrodes for EMG devices are needle-like (invasive), which makes it impossible to use them for a long time. Bionic prostheses are more interesting as a representative of an everyday mobile device. At their core they have myographic sensors, which are connected to the prosthesis microcontroller [6]. All over the world there are many companies producing bionic prostheses: "Touch Bionics", "Frost & Sullivan", MeHandA and many others. However, at the moment there are no bright representatives of prostheses with gesture recognition and individual finger movements, many prostheses do not have separated fingers, but move synchronously. Gestures are implemented using pre-recorded commands. Today, there are no generally accepted solutions to this problem, but there are developments that rely on the introduction of new data processing algorithms, such as neural networks. Prosthetic companies also distribute individual myographic sensors that can be connected to a computer, smartphone or other device [7]. For example: MYOstack, MYO, Myoware. The functionality of these sensors is determined by the user. Often a person requires extensive skills and knowledge. There are no universal ready-made devices now. It speaks about the relevance of development of such devices.

Development Challenges. The development of muscle movement analysis devices has the following problems:

- weak bioelectric signal;
- strong attenuation of the signal when recording it;
- strong drift of the signal due to the constant change of resistance of the electrode-skin contact;
- complicated analysis of the signal from the muscles;
- impossibility of accurate and permanent installation of the sensors on the muscle.

The first three problems can be solved during the circuit design of the device. The other problems are solved programmatically.

General scheme of the device. The muscle motion analysis device has several features that differ from other information input devices and devices that interact with humans. The first and the main one is the presence of a special electrode.

The electrode allows taking a bioelectric signal from the human skin. There is a large variety of electrode types, but when designing a universal reusable device, it is worth stopping at the dry surface electrode. Dry surface electrode is such an electrode, which interacts with the body through direct contact of conductive material and skin [8]. The peculiarity of dry contact from wet contact is the absence of auxiliary humidification during contact, which significantly increases the skin resistance, in humans the resistance increases from about 100 kOhm to 1 MOhm. This makes it difficult to transmit the signal directly from the electrode to the next transducer. The solution to this is to use an active electrode.

The active electrode, in general, should consist of a current collector plate, a low-pass filter, an impedance converter (aka voltage repeater), a high-pass filter, a matching resistance, an active screen (Fig. 2).

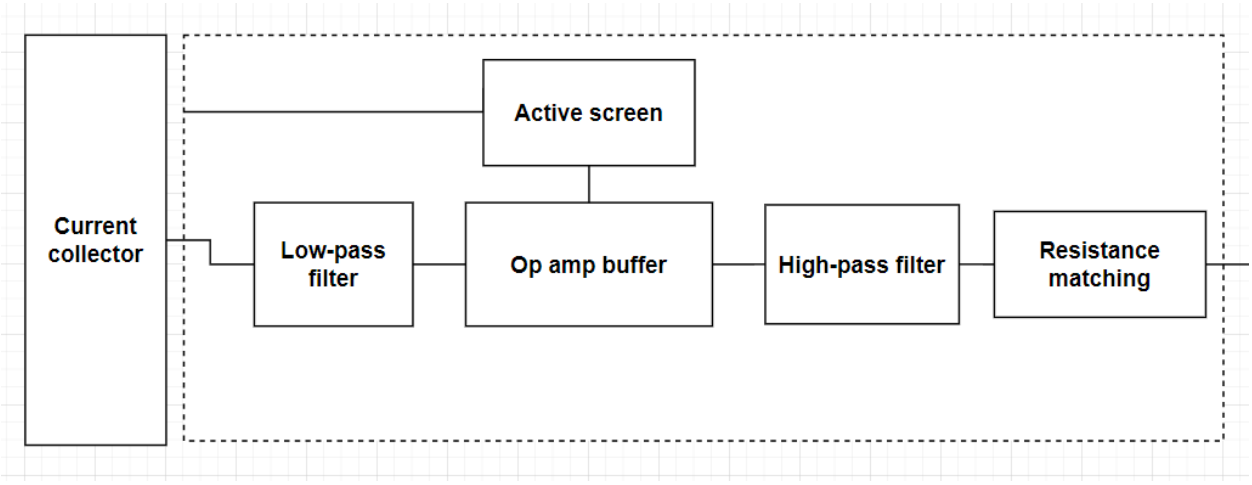

Fig. 2 – active electrode arrangement

High-pass and low-pass filters are necessary to filter out signals outside the 0.05 – 500 Hz range. Only the signals within this narrow range are of interest for analysis and diagnostics, they are the ones most often taken during medical procedures.

The impedance converter is the most important part of the circuit. It allows you to amplify the signal by current. This allows the signal to be transmitted through the wires over a sufficient distance without distortion. They are most often made with operational amplifiers (Fig. 3). This is due to the small values of current and voltage source, the high frequency fluctuations of the signal, the small required size of the device, the requirements for the installation of negative feedback. Since the components of the circuit are not perfect, a resistance is introduced into the feedback circuit, the value of which is comparable with the source resistance (about 1 MOhm).

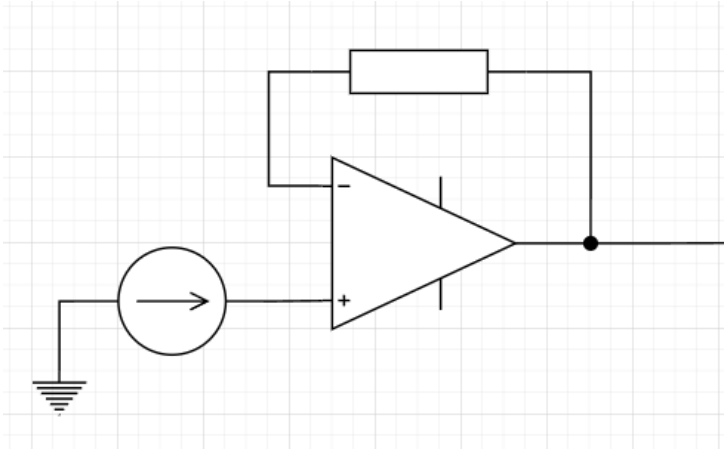

Fig. 3 – Op-Amp voltage repeater

The active shield is necessary to reduce interference and to avoid pickup of external signals. It must be connected to the negative feedback of the drive for proper operation. It is also recommended to connect it to the slip-ring plate via capacitance.

Resistance matching is necessary for connection to the following converter devices. Here the voltage and current input parameters of the following inverters must be taken into account.

The current collector plate must be made of materials with low resistance and low polarizability. Chloro-silver or silver plating is most commonly used. At this stage it is also necessary to consider the toxicity of the material and its effect on the human body.

According to these criteria, an active electrode was designed with the following circuit (Fig. 4, 5): filters on RC circuits, voltage repeater on Op-Amp.

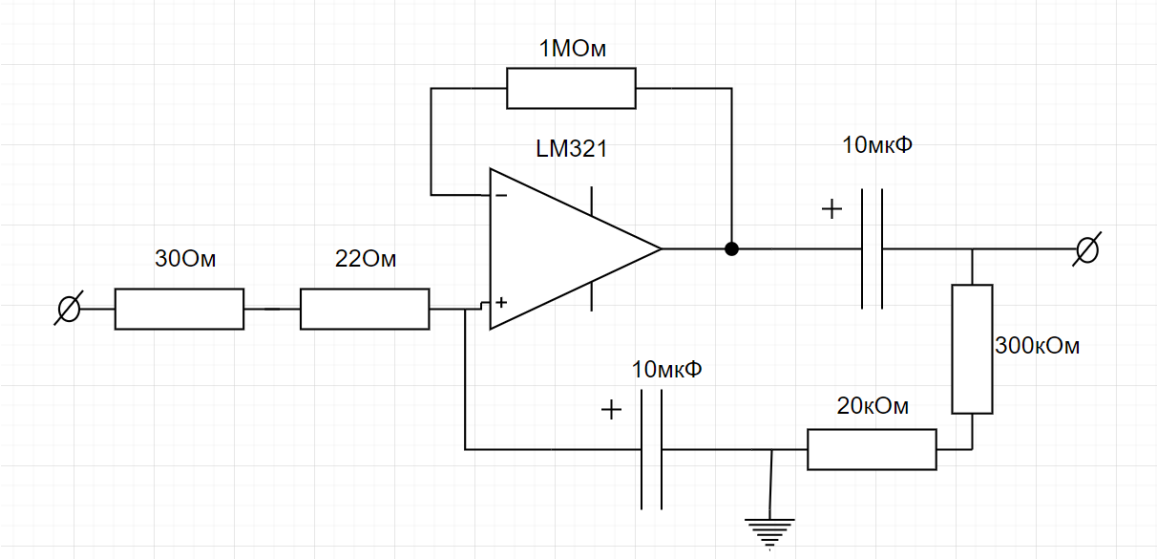

Fig. 4 – scheme of the active electrode

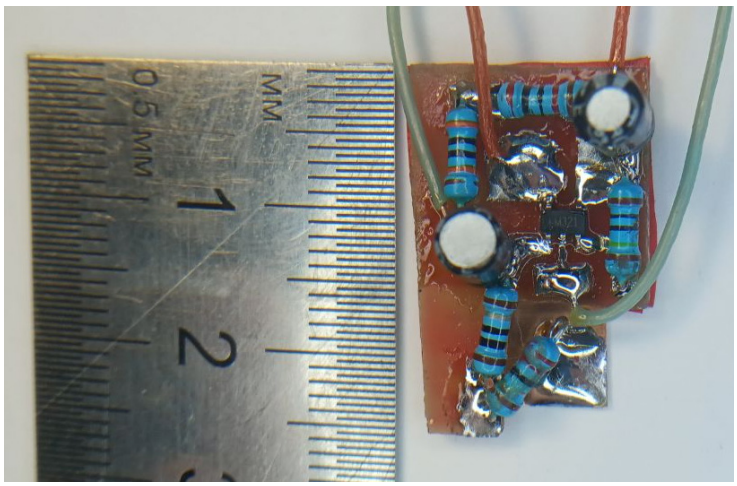

Fig. 5 – active electrode

To reduce the size of the device it is advisable to use Op-Amp filters.

The next stage of signal conversion is amplification. The signal obtained by EMG is taken along a nerve or muscle (Fig. 6). Therefore, 2 sources of signals come to the amplifier. To study the signals it is necessary to use differential amplifiers, most often built on Op-Amps.

Fig. 6 – electrode connection

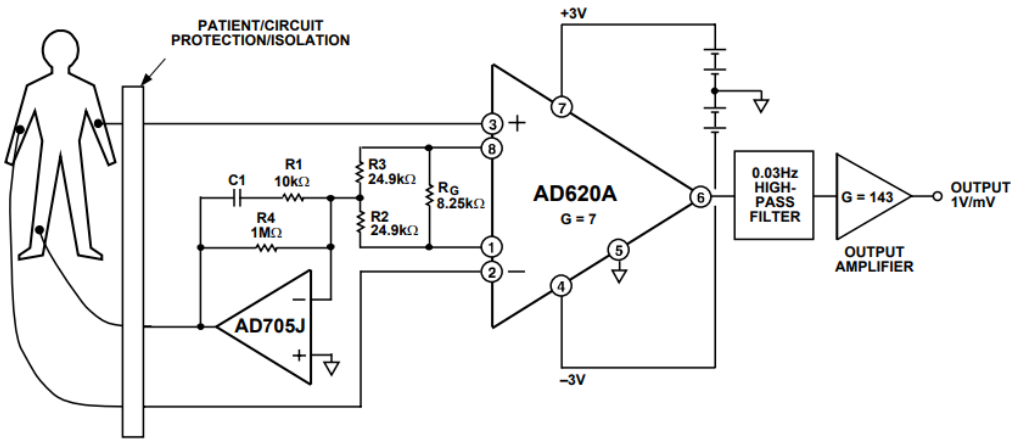

Fig. 7 – amplifier on AD620

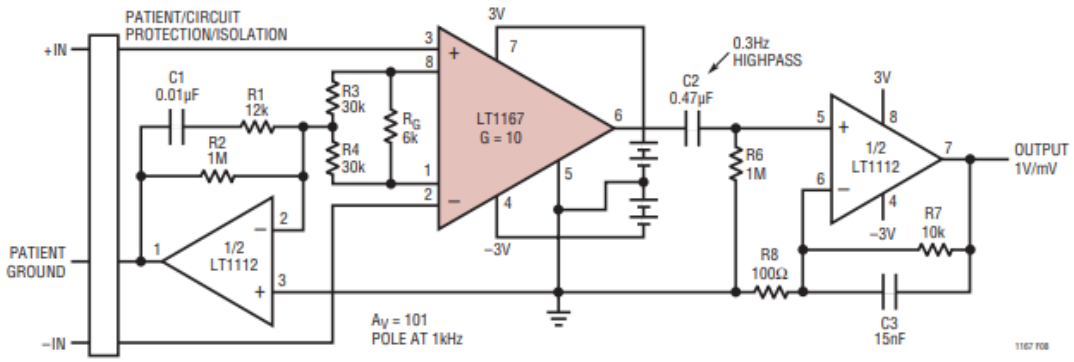

Fig. 8 – amplifier on TL1167

Specialized instrumental amplifiers with a small signal drift, designed specifically for ECG, EMG, EEG: AD620 (Fig. 7), TL1167 (Fig. 8) are good at this task. In all cases in the schemes there are: protective insulation (to protect a person from a large electric current flowing through him when the equipment breaks – the power supply of the equipment is usually 110/220 volts), low-pass and high-pass filters (in these devices there are no active electrodes, also it allows to remove interference caused by operational amplifiers), preamplifier stages on Op-Amp.

For the final device was chosen a module with adjustable resistors R7 and R6 – they allow to adjust zero and gain. In addition to AD620 op-amp there is a 7660 reverse voltage generator in the circuit, gain stages on LM358 (Fig. 9).

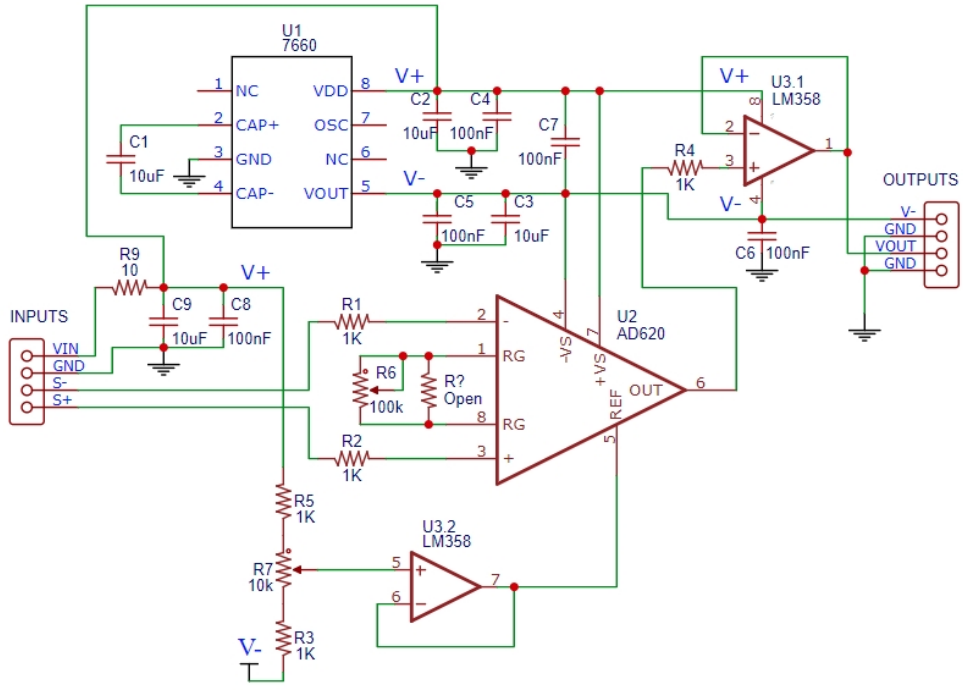

Fig. 9 – schematic of the amplifier module

The next stage of conversion is the most complex – ADC. At this stage the received analog signal must be converted and decoded. The simplest solution here is to perform sampling and send the signal further. However, when using this method, a lot of information about the signal is lost. Another option is to decompose the signal into harmonic components. In this case, the accuracy of further processing will depend on the ADC capabilities. It is also worth noting that when using microcontrollers as ADCs, it is possible to analyze the signal already at this stage, as well as to connect several modules simultaneously. Connecting several modules is necessary for volumetric analysis of the whole limb movement. For example, on the forearm it will allow to get information about gestures, which is the purpose of the device.

After converting the signal into a digital form, we can move on to information processing. At the moment the task of EMG signal decoding is a complicated and in many cases non-linear task, complicated by signal drift due to the change of skin-electrode contact resistance, this can be compensated by introducing additional resistance from the electrode, as well as due to inconstancy of sensors location. Standard methods of amplitude-frequency analysis can be used for EMG signal interpretation. This increases the speed of information processing, simplifies interaction with control programs, and does not require expensive complex processors. However, this analysis will not be accurate. And the device will require constant long manual calibration. Another way to decode the EMG signal is to connect a neural network. Of the disadvantages of this method it is worth noting – it is difficult to create a database for training, floating inaccurate results, requiring additional processing. However, when the database is prepared in advance on the device, it solves the calibration problems and increases the final accuracy of the device. An already computed and trained neural network also does not require a lot of power. However, it is worth considering that it will require a strong processor and training time.

The next step is to connect the executive device. Here the functionality of the device will be limited only by the imagination and goals of the person. As previously described, this can also be a virtual reality interface,

In general, the diagram of the muscle movement analysis device is shown in Fig. 10.

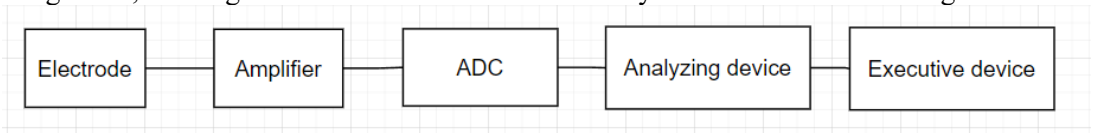

Fig. 10 – general device

Software signal processing

Normal cutaneous EMG (Fig. 11) represents oscillations of different harmonics coming from several sources (depending on the point of electrode overlap).

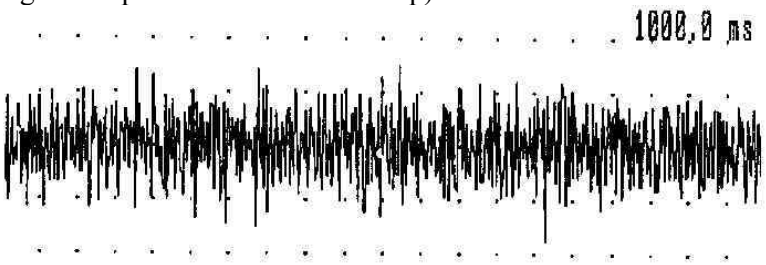

Fig. 11 – normal cutaneous EMG

The output of our device produced a similar signal (Fig. 12).

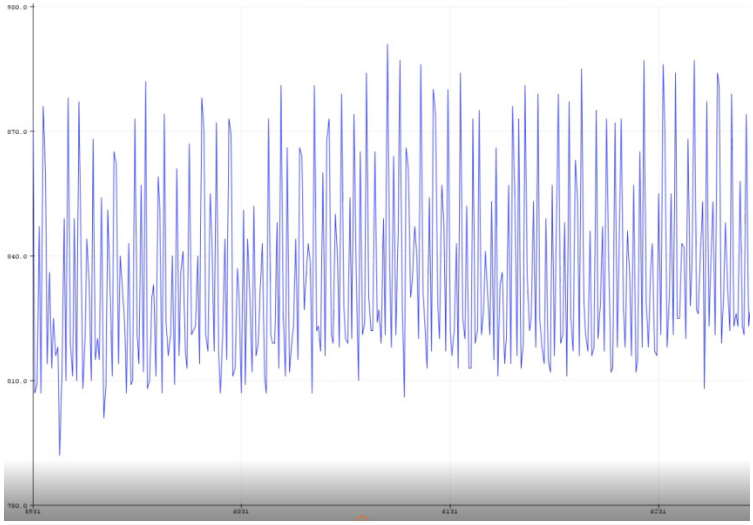

Fig. 12 – the signal of the device

In our circuit, only 1 module was used, placed on the forearm. This does not allow us to collect a database for training the neural network, but at this stage we can already analyze flexion-extension of the muscles. To do this we need to process the signal in the program: introduce sampling, process the signal with a filter to reduce the high-frequency component, reflect the signal relative to its middle. The output will be a signal that changes its amplitude in response to muscle movements. In this experiment, increase of amplitude corresponded to muscle flexion, and decrease corresponded to muscle extension (Fig. 13).

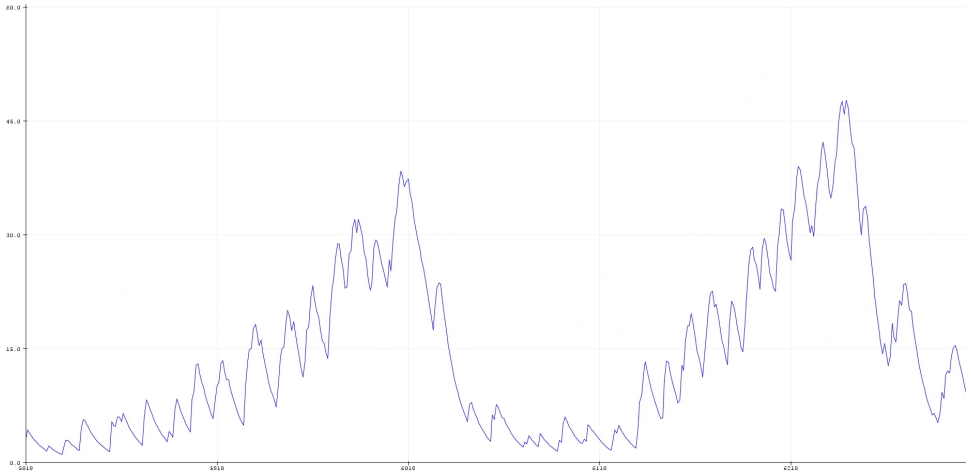

Fig. 13 – transformed signal

This signal can be fed to external devices, but before that it is worth introducing some more filters into the program, in order to reduce the oscillatory signal. Even at this stage you can see that it is difficult to isolate separate components for each muscle from the EMG. The oscillation and complex composition of harmonics also become obstacles to signal processing.

Conclusion

The muscle motion analysis device is a complex multicomponent device. Each component of this device is represented by complex electrical transducers that have their own nuances of design. However, there are now many off-the-shelf solutions that can simplify the creation of the final device. And with the expansion of information technology to all areas of human life, the potential of the device is only becoming greater every day. However, there are also unresolved problems, demonstrated in this article:

- inaccuracy of registration of cutaneous EMG (there are no circuits that give a perfect signal without interference yet);
- complexity of signal processing – separation of individual muscle signals from the total EMG.

Solving these problems will give a strong impetus to the development of muscle movement analysis devices and associated: bionic prostheses, EMG devices.

References

1. Grief Mikhail Gennadyevich, Elakkiya R., Prikhodko Alexey Leonidovich, Bakaev Maxim Aleksandrovich, Rajalakshmi E. The Recognition of Russian and Indian LANGUAGE LANGUAGES BASED ON MACHINE LEARNING // Data Analysis and Processing Systems. 2021. №3 (83). URL: https://cyberleninka.ru/article/n/raspoznavanie-russkogo-i-indiyskogo-zhestovyh-yazykov-na-osnove-mashinnogo-obucheniya (accessed 18.02.2023).

2. Zyryanov D.A., Badika E.M., Istomina Y.P., Tspilev V.S. The Advantages of Using Digital Twin Producers as an Example of a Model in DELFOI ROBOTICS // "Actual Issues of Scientific Research". – Saratov: NOP "Digital Science", 2023. – P. 153-163.

3. Kravchenko S.A., Rakova K.V. "Smart Watches". As a Factor of Hybrid Communication between a Physician and a Patient // Communicology. 2021. №3. URL: https://cyberleninka.ru/article/n/umnye-chasy-kak-faktor-stanovleniya-gibridnoy-kommunikatsii-mezhdu-vrachom-i-patsientom (date of reference: 05.02.2023).

4. Patarkatsishvili Nikolay Yurievich, Zavyalov Dmitriy Aleksandrovich, Bliznevsky Andrey Aleksandrovich, Tashchyan Arshak Andranikovich, Matonina Olga Gennadyevna, Masloboeva Natalia Anatolievna Justification of Efficacy of Application of Modern Electronic Technologies for Monitoring

of Students' Health Parameters // Lesgaft University Scientific Notes. 2021. №3 (193). URL: https://cyberleninka.ru/article/n/obosnovanie-effektivnosti-primeneniya-sovremennyh-elektronnyh-tehnologiy-kontrolya-pokazateley-zdorovya-u-studentov (date of reference: 05.02.2023).

5. Reeder, B. and David, A., 2016. Health at hand: A systematic review of smart watch uses for health and wellness. Journal of biomedical informatics, 63, pp.269-276.

6. Urazbakhtina Y.O. Bionic prostheses of the upper extremities: A comparative analysis and the prospects of use / Y.O. Urazbakhtina, K.R. Kamalova, E.S. Morozova // International Scientific Research Journal. – №1 (115). – URL: https://research-journal.org/archive/1-115-2022-january/bionicheskie-protezy-verxnix-konechnostej-sravnitelnyj-analiz-i-perspektivy-ispolzovaniya (date of reference: 12.02.2023). – doi: 10.23670/IRJ.2022.115.1.063

7. Patent No. 2683859 C1 Russian Federation, IPC A61B 5/0488, A61F 4/00. Method and system for controlling electronic devices by means of an electromyographic reading device : No. 2017146206 : application. 27.12.2017 : publ. 02.04.2019 / V. R. Karimov, N. M. Ivanyuk, Z. A. Ponimash [et al.] ; applicant OOO LIMITED LIABILITY "B-ON EMG". – EDN ODHVMK.

8. Zyryanov D.A., Badika E.M., Istomina Yu.P., Tspilev V.S. The Selection of Dry Contact Electrode Materials for Production of Bioelectronic Signals // "Actual Questions of Scientific Investigations". – Saratov: NOP "Digital Science", 2023. – P. 143-152.

CONTENTS

The scientific edition

ИЗВЕСТИЯ КАФЕДРЫ UNESCO ГУАП «ДИСТАНЦИОННОЕ ИНЖЕНЕРНОЕ ОБРАЗОВАНИЕ»

Сборник статей

Выпуск 8

BULLETIN OF THE UNESCO DEPARTMENT “DISTANCE EDUCATION IN ENGINEERING” OF THE SUAI

Collection of the papers

Issue 8

ISBN: 978-5-8088-1825-5

9 785808 818255

Computer imposition A. N. Koleshko
Papers are publish in author’s edition

Подписано в печать 07.04.2023. Дата выхода в свет: 12.04.2023.
Формат 60×84 1\8. Усл. печ. л. 25,2. Тираж 150 экз. Заказ № 106.

Редакционно-издательский центр ГУАП
190000, г. Санкт-Петербург, ул. Большая Морская, 67, лит. А
Распространяется бесплатно

Submitted for publication 07.04.2023. Passed for printing 12.04.2023.
Format 60×84 1/8.

Department of operative polygraphy SUAI
67A, B. Morskaia, 190000, Saint Petersburg, Russia
Free distribution